Journal of Nuclear Materials 521 (2019) 167–244

Contents lists available at ScienceDirect

Journal of Nuclear Materials

journal homepage: www.elsevier.com/locate/jnucmat

Irradiation creep and growth of zirconium alloys: A critical review

Ronald B. Adamson [a], Christopher E. Coleman [b], Malcolm Griffiths [c, *]

[a] Zircology Plus, Freemont, California, USA
[b] Canadian Nuclear Laboratories, Chalk River, Ontario, Canada
[c] Queens University, Kingston, Ontario, Canada

ARTICLE INFO

Article history:
Received 29 October 2018
Received in revised form
22 March 2019
Accepted 15 April 2019
Available online 14 May 2019

ABSTRACT

The fuel channels and fuel assemblies of all conventional nuclear reactors that generate power from the fission of uranium by thermal neutrons are made from zirconium alloys because of their low thermal neutron absorption cross-section. The dimensional stability, and the ability to predict dimensional changes, of components made from zirconium alloys is important to designers and operators of such reactors because deformation has a consequence for the operability or life of the reactor core. The dimensional changes in zirconium alloys due to neutron irradiation has been the subject of intense study since the inception of the thermal nuclear power reactor. During irradiation zirconium alloys behave differently from most other engineering alloys in that they resist swelling. They do exhibit anisotropic dimensional changes in the absence of an applied stress that depend on the microstructure; this process is called irradiation growth. Like any other material they also exhibit a dimensional response to an applied stress; this process is called irradiation creep. In this review the evolution in measurement methodologies (either from controlled experiments in materials test reactors or gauging of power reactor components) is described together with the results gleaned from such measurements. As measurements have improved and the amount of experimental and operational data has increased, the theoretical basis for modelling creep and growth has also evolved. The history of the evolution in understanding and the ability to predict dimensional changes in zirconium alloys over the past 60–70 years is described and discussed.

Contents

* Corresponding author.
E-mail address: malcolm.griffiths@queensu.ca (M. Griffiths).

https://doi.org/10.1016/j.jnucmat.2019.04.021
0022-3115/

1. Introduction

Dimensional stability of the core components of a nuclear reactor is critical to safe and efficient operation. Primary structural materials are Zr-based alloys, originally chosen because of a low capture cross-section for thermal neutrons and adequate strength and corrosion resistance in about 300 °C ± 50 °C (573 K ± 50 K) water; consequentially this review will be mostly limited to this temperature range. Although it was known that materials in general deformed under the influence of stress, at the time of first use (about 1955), almost nothing was known about the dimensional stability of zirconium, in-or-out of a radiation field. Another unknown was the influence on all the anisotropic properties induced by the hexagonal close packed (HCP) structure of Zr. Even at the time of the successful demonstrations of the Naval Reactor prototype core (Mark, I, 1953) using un-alloyed Zr, and the Nautilus submarine core (1955) [1,2] using Zircaloy-2, almost nothing was known about the topics of this review – irradiation growth (henceforth called “growth”) and irradiation creep (henceforth called “creep”) of zirconium alloys.

Irradiation growth is a change in the dimensions of a zirconium alloy reactor component even though the applied stress is nominally zero. It is considered to be a constant volume process, so if there is, for example, an increase in the length of a component, then the width, or thickness, or both, must decrease to maintain constant volume. Understanding of the detailed mechanism is still evolving, see Section 4; however, a clear correlation of growth to microstructure evolution exists, and many empirical observations have revealed key mechanistic aspects. The inherent anisotropy of the Zr crystallographic structure and the texture induced during fabrication play strong roles in the mechanism, as materials with cubic crystal structure (like stainless steel, copper and Inconel) do not undergo irradiation growth. Growth is not to be confused with irradiation swelling (primarily induced by microscopic voids or gas bubbles in the matrix) which does not conserve volume and does not occur in zirconium alloys under normal reactor operating conditions.

Creep is defined as a time dependent change in dimension of a reactor component (or any material) under a stress. Creep is deformation occurring as a constant volume process, normally at low stresses below the usual yield strength, which is usually measured at strain rates 10^6 to 10^7 times greater than creep rates [3]. During normal reactor operation, failure of components by creep rupture is unlikely because large safety margins are included

by design. For pressure bearing structures, specifications usually require that the material has a certain strength that is several times that of the design stress. For example, pressure-retaining components may follow the principles of Section III of the American Society of Mechanical Engineers (ASME) Boiler and Pressure Vessel Code; at the maximum operating temperature the imposed stress must not exceed the lowest of:

- 1/3 of the ultimate tensile strength (UTS),
- 2/3 of the yield strength,
- 3/5 of the stress to produce rupture within 100 000 h, or
- the stress to provide a creep rate of 10^{-7} per hour. The creep strain is sometimes restricted to 1%.

As with the early applications of Zircaloy-2, this code was applied to components before information on in-reactor effects were known. Fig. 1–1 shows schematically the temperature regimes where short-term and long-term mechanical properties control the design stress. Early in an irradiation, short term strength determines the design stress below about 350 °C; the lines intersect at lower temperatures after irradiation.

For materials in an irradiation field, the most important for purposes of this review being the neutron environment of a nuclear reactor. The deformation occurs by the motion of dislocations and irradiation-produced defects under the influence of stress. Neutron irradiation produces large quantities of point defects – vacancies (V) and self-interstitial atoms (SIA) – that migrate to and collect at various sinks. Due to the anisotropy of the zirconium crystal lattice, motion of both dislocations and irradiation-produced defects is anisotropic, with SIAs preferring to diffuse parallel to the basal plane in the <a>-directions of the lattice and V more randomly. Dislocations are sinks for both vacancies and SIAs, but an edge dislocation attracts SIAs more than vacancies. In addition, an important factor is the concept that anisotropic diffusion is enhanced by stress. Many mechanisms of irradiation creep have been proposed, as discussed in detail later in this review.

Irradiation creep is distinguishable from creep without irradiation in the shape of the creep curve: at moderate temperatures, e.g. 300 °C, after a small amount of strain with no irradiation the strain rate declines rapidly while during irradiation the strain rate does not decline and, after the same time, can appear to be much larger than that with no irradiation.

Growth occurs simultaneously with creep if there is an applied stress, as is almost always the case with any reactor component. The two processes are often assumed to be independent and additive, even though mechanistically they compete for the same radiation-produced defects. The subject of "independency" is examined in detail in Sections 4 and 5 of this review.

Design and operational issues can arise when allowances for dimensional change are insufficient or not possible because of the component's configuration; for example, BWR channels or PWR guide tubes that are subjected to large gradients in neutron fluence, may result in gradients in creep and growth. BWR flow channels are susceptible to bowing that may restrict control blade motion, an issue described in detail in Refs. [4–6]. Issues can also arise when growth or creep allowances depend on the behaviour of different materials, or components that operate at different temperatures, or neutron flux or both. For example, pressure tubes in CANDU reactors operate for decades rather than years and have gradients of temperature, pressure, flux and microstructure along their lengths of 6 m. In CANDU reactors, axial and differential axial elongation may cause interference between fuel channel components, as described in Ref. [7].

Schematic diagrams of two types of fuel assemblies are given in Figs. 1–2.

1.1. Measure of irradiation damage to zirconium alloy microstructure

Most of the "irradiation damage" in-reactor components is caused by neutrons. The energy of neutrons produced by fission ranges up to about 10 MeV. Common terms for energy ranges are: thermal (up to 0.03 eV), epithermal (up to 100 eV) and fast (>about 0.1 MeV, although often classed as >1.0 MeV). The amount of energy required to displace an atom of Zr from its normal lattice position is about 40 eV, and from straight forward energy transfer theory (see, for example [8]) it is seen that any "fast" neutron can easily transfer enough energy to displace a Zr atom (the "primary knock-on"), which in turn can displace additional atoms. For purposes of this review, the immediate results are small clusters of vacancies (depleted zones), individual vacancies, individual interstitials[1] (although interstitials are often thought to cluster in pairs) and, after some short time ($<10^{-10}$ s), vacancy and interstitial dislocation loops form. Collectively this rearrangement of the crystal lattice is termed "irradiation damage". Only 1–10% of the individual defects survive their original creation.

The absolute amount of irradiation damage produced in a reactor component depends on the neutron energy spectra within a specific reactor. The energy spectra vary with reactor type, and for the location within the reactor. Typical pressurized (PWR/VVER) and boiling (BWR) water reactors have similar energy spectra, but in a BWR they vary along the core length depending on local void fraction. CANDU reactors differ from both PWR and BWRs, and test reactors (particularly fast or sodium cooled reactors) can have quite different neutron energy spectra across their volume. Therefore, it is useful to use a parameter more closely related to "irradiation damage" than the conventional fluence, n/m^2 >1 MeV or >0.1 MeV. If the complete energy spectrum is considered and a consistent estimate of the energy needed to "knock" an atom from its normal lattice position is used (40 eV is standard, but 25 eV is sometimes used), it is helpful to use displacement per atom, dpa, as a measure of irradiation damage. Dpa refers to the average number of times an individual atom is displaced from its normal lattice position during a given reactor exposure.

Reactor engineers frequently use a measure of irradiation damage or component exposure called fuel burnup, usually expressed as:

$$\text{Burnup} \equiv \text{GWd/MT or MWd/kgU}$$

Burnup is a measure of the amount of energy produced by fission in a given amount of fuel. The conversion of burnup to neutron fluence is complex, depending on neutron energy spectrum, fuel enrichment, void fraction, and other factors. But for a rule of thumb (approximated by calculation for a VVER, [9]) and PWR it is close to:

$$50\ \text{GWd/MT} = 1 \times 10^{26}\ \text{n/m}^2\ (\text{E} > 1\ \text{MeV}) = 15.4\ \text{dpa}$$

For the current review, wherever it is possible "dpa" is used as the measure of damage, making it possible to compare growth and creep as a function of damage from a variety of reactors.

Conversion factors have been calculated by Walters et al. [10]. An abbreviated conversion chart, (in this case for neutron energies

[1] "Interstitials" in this report will often be called SIAs (self-interstitial atoms) to distinguish them from impurities or alloying elements that occupy interstitial lattice sites, for example, hydrogen, oxygen, nitrogen and carbon.

[2] Units of the variables must be consistent, preferably in the International System of Units (SI).

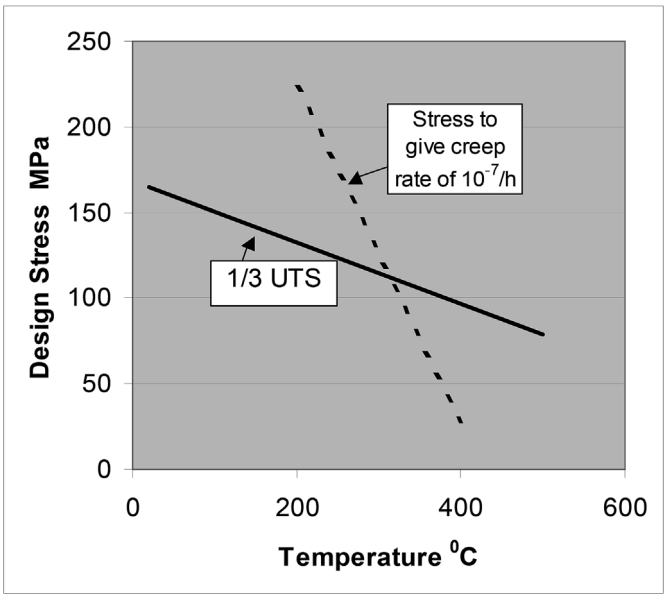

Fig. 1–1. Schematic diagram showing temperature regimes where the design stress of a hypothetical zirconium alloy pressure vessel is controlled by short-term and long-term mechanical properties of unirradiated material.

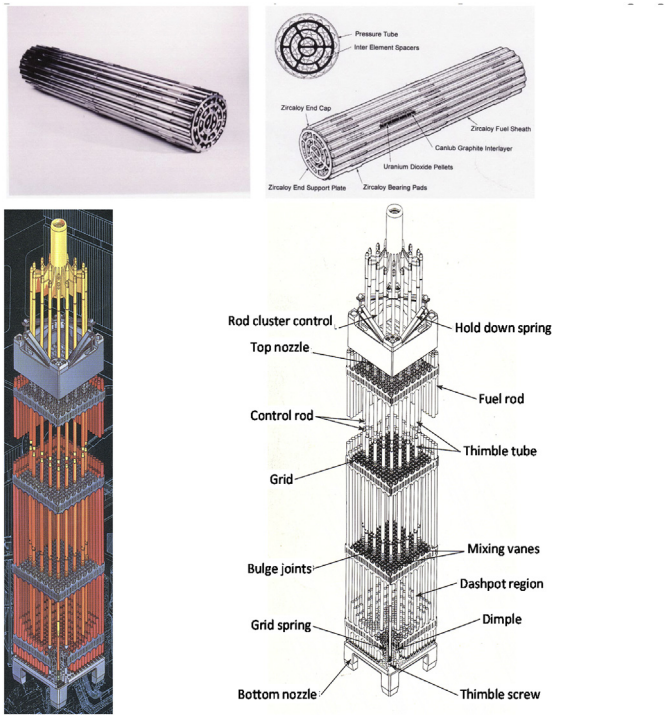

Fig. 1–2. Typical fuel assemblies: upper, CANDU; lower PWR.

>1 MeV, but also available for E > 0.1 MeV in Ref. [10], is given in Tables 1–1.

Tables 1–2 gives typical damage rates for different types of reactors.

1.2. Texture and crystallography

At 863 °C zirconium has a transformation from the hexagonal-close-packed (hcp) structure, called the α-phase, to a body-centred cubic (bcc) structure, called the β-phase. Alloys containing α-stabilizers, (e.g. oxygen, tin) can have a transformation temperature >863 °C while those containing β-stabilizers (e.g. Nb, H) can have a transformation temperature <863 °C. In commercial alloys the majority of the microstructure contains the α-phase. Important planes in the hcp structure are shown in Figs. 1–3 [11]; basal plane, prism plane and pyramidal plane.

Fabrication of components from polycrystalline zirconium alloys results in marked preferred crystallographic orientation or texture, with a resulting prominent anisotropy of properties. These properties include irradiation growth and creep, mechanical strength and ductility, hydride orientation and corrosion.

Texture is often characterised by f-parameters [12] that are commonly designated as f_r, f_t and f_l, for the average volume fraction of a given pole in the radial or normal (r or n), transverse or circumferential (t or c) and longitudinal or axial (l or a) directions. In practice the poles are distributed about those directions. The f-parameters for typical LWR cladding for the (0002) basal poles are:

$$f_r = 0.636\ f_l = 0.047,\ f_t = 0.317 \quad (1.1)$$

This texture is developed mostly by extensive cold working and annealing cycles during the pilger fabrication process.

For typical CANDU pressure tubes the texture parameters are:

$$f_r = 0.33\ f_l = 0.06,\ f_t = 0.61. \quad (1.2)$$

This texture is developed during extrusion in the (α + β)-phase field and is little changed by the subsequent small amount of cold-work, usually <30%.

These two types of tubes represent the majority of the zirconium alloy components that are stressed in-reactor and are therefore used as examples. In both types of tubes f_l is very low while f_r in cladding is large and similar to f_t in pressure tubes, and f_t in cladding is similar to f_r in pressure tubes with both being about half f_r and f_t respectively.

Tables 1–1
Comparison of radiation damage for zirconium in different reactors for E > 1 MeV [10].

Neutron Fluence, $10^{24}/m^2$, E > 1 MeV	
Reactor	per 1 dpa
CANDU (pressure tube)	5.8
BWR core	6.2
PWR core	6.5
ATR	7.0
DIDO	5.9
BOR-60 (6th row)	4.9
OSIR15	6.5
EBR2	3.2
Halden 13 w/o booster fuel	5.6
NRU (fast neutron rod)	6.1
HFIR (peripheral target)	6.6
HFIR (removable Beryllium)	6.0
SM2 (C4W)	5.8
RBMK (site 33, H = 1.9 m)	5.1

Tables 1–2
Approximate typical damage rates for different types of reactors.

Reactor	Peak neutron flux, $n/m^2/s$ E > 1 MeV	Damage rates, dpa/s
BOR-60	43×10^{17}	8.9×10^{-7}
BWR	6.0×10^{17}	1.0×10^{-7}
PWR	8.1×10^{17}	1.3×10^{-7}
CANDU	4.0×10^{17}	6.4×10^{-8}

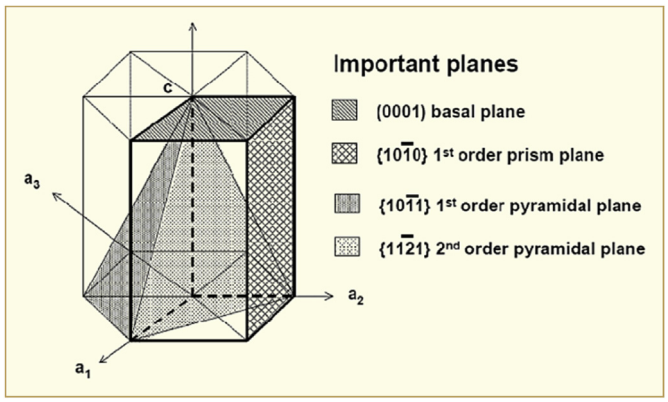

Fig. 1–3. Crystallographic characterizations of the hcp elementary cell [11].

When a component is loaded in several directions and its material has a distinct preferred orientation, the creep rates responding to the stresses, σ_i, in each principal direction, transverse, t, axial, a, or radial, r, are described in Ref. [13] based on plasticity theory through:

$$\dot{\varepsilon}_t/[G(\sigma_t - \sigma_r) - F(\sigma_a - \sigma_t)] = \dot{\varepsilon}_a/[F(\sigma_a - \sigma_t) - H(\sigma_r - \sigma_a)] = \dot{\varepsilon}_r/[H(\sigma_r - \sigma_a) - G(\sigma_t - \sigma_r)] = \text{constant} \quad (1.3)$$

where F, G, H characterise anisotropy, as introduced in Ref. [14]. These characteristics have been evaluated from uniaxial tests and biaxial tests with the arbitrary assumption that they sum to 1.5 [15]. For example, in Zr-2.5Nb pressure tubes F = 0.58, G = 0.04 and H = 0.88. When a tube is internally pressurised, the loading is biaxial; $\sigma_t = 2\sigma_a$ and $\sigma_r \cong 0$. Using the anisotropy constants the transverse strain rate in the tube is predicted to be 2.2 times faster than the axial strain rate. The analysis also indicates that an internally pressurized tube should elongate when it deforms. If F = G = H, the material is isotropic and elongation is absent with internal pressurization. For more details see section 2.4.1.

It has been proposed [16–18], that the growth strain in any given direction of a polycrystalline zirconium alloy can be related to the crystallographic texture and is proportional to a growth anisotropy factor G_d given by:

$$G_d = 1 - 3f_d^c \quad (1.4)$$

where f_d^c is the resolved volume fraction of basal poles, f^c, in the d-direction. The factor depends on the assumption that each grain behaves as an independent single crystal and that the volume change due to irradiation growth is zero. It further assumes that sinks for irradiation-produced defects are on basal planes and prism planes only and that there is a net flux of vacancies to basal sinks and a net flux of interstitials to prism planes. Applying the texture factors of Eqs. (1.1) and (1.2) indicates growth in the axial direction of tubes, $G_a = 0.82$ to 0.86, whereas in cladding $G_t = 0.05$ and in pressure tubes $G_t = -0.83$.

For growth, if $f_d^c = 0.33$, growth is absent. For details see section 3.4.1. An isotropic texture may be attained by quenching the material from the β-phase, see page 2–22 in Ref. [19] and in Ref. [20].

2. Irradiation creep

2.1. Creep curves

Since creep without irradiation tends to have a relatively high initial rate, and since irradiation damage builds up with time, the creep curve (strain versus time or fluence) is usually divided into primary and secondary stages, as shown in Figs. 2–1 and Figs. 2–2. High burnup implies long times, but for in-reactor service the third stage (tertiary or unstable) creep is not reached except in very rare, high stress cases [6,21]. Generally, the secondary (steady state) creep stage is approached with little decline in rate, Figs. 2–. Whether or not true time "steady state" creep rate is obtained in-reactor is problematic, but in many cases, it is assumed for the analysis of the important parameters (see Fig. 3).

Primary creep rates are influenced by the rate of buildup of radiation hardening of the material, as will be described in Section 2.4.

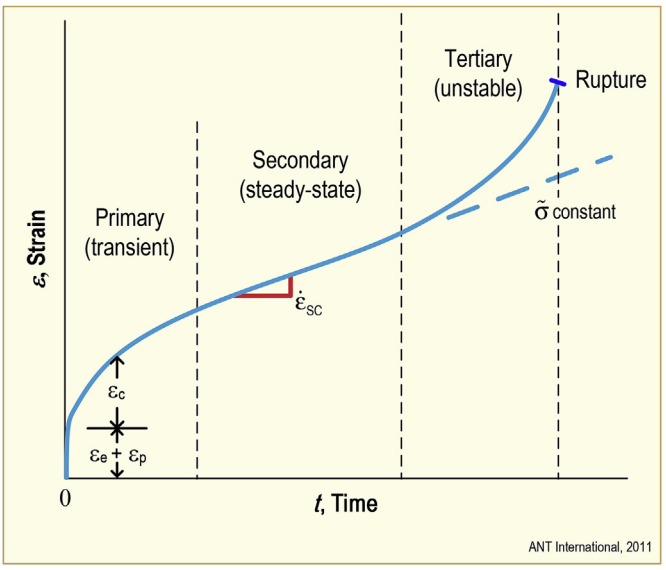

Fig. 2–1. Idealized strain vs. time behaviour during creep of unirradiated material under constant load, and the three stages of creep. ε_e = elastic, $\varepsilon_{p\ =plastic}$ (high stress), ε_c = transient, $\dot{\varepsilon}_{sc}$ = steady state rate, σ = stress, [22].

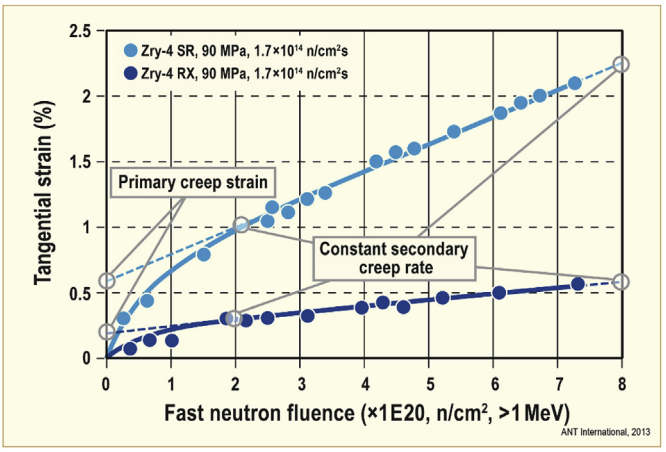

Fig. 2–2. In-reactor creep curves of RX and SR Zircaloy-4 under biaxial stress conditions at 350 °C, data [23] and re-plotted, Garzarolli in Ref. [24].

2.2. Previous creep reviews

Very little information on irradiation creep of zirconium alloys was known before the start-up of the Nautilus in 1955, the first power reactor, Shippingport, in 1957 and the first commercial power reactors in the early 1960s. The first comprehensive review of

Tables 2–1
Significant reviews of irradiation creep and growth.

1968	Fidleris [25]
1975	Rickover [2]
1975	Fidleris [29]
1979	Lustman [1]
1980	Carpenter, Coleman and MacEwen [27]
1983	Franklin, Lucas and Bement [30]
1987	Nichols [31]
1988	Woo and McElroy [28]
1988	Fidleris [18]
1996	Garzarolli, Stehle and Steinberg [32]
2000	Adamson [33]
2007	Griffiths [35]
2008	Holt [34]
2009	Adamson, Garzarolli and Patterson [24]
2010	Adamson [36]
2010	Shishov [37]
2010	Cheadle [38]
2017	Adamson, Griffiths and Patterson [39]

creep data was in 1968 by Fidleris [25] and more followed regularly, as listed in Tables 2–1 In addition to the reviews listed in Tables 2–1, three major conferences were held to discuss irradiation growth and creep:

M.R. Cundy, P. von der Hardt and R.H. Loelgen, Proceedings of International Conference on Measurement of Irradiation-Enhanced Creep in Nuclear Materials, Petten May 1976 [26].

- G.J.C. Carpenter, C.E. Coleman, S.R. MacEwen, Proceedings of the International Conference on Fundamental Mechanisms of Radiation Induced Creep and Growth, Chalk River, May 8–10, 1979 [27].
- C.H. Woo and R.J. McElroy, Proceedings of the International Conference on Fundamental Mechanisms of Radiation-Induced Creep and Growth, Hecla Island, Manitoba, Canada, June 22–25, 1987, [28].

2.3. *In-reactor creep testing techniques*

In-reactor creep testing requires measurement of strain as a function of time or fluence when a constant load or stress is applied to a sample of material at a temperature of interest. The simplest procedure is to apply force to the specimen either in tension, compression or both, induced by the application of the equivalent to a simple weight, or bending or, in the case of a tube, by internal or external pressure. The ASTM standard for creep testing, E139-11, provides helpful descriptions for various basic creep techniques for use in a laboratory but no guidance is given for in-reactor testing. The uniaxial tension arrangement usually used in a laboratory [22] is too cumbersome to use in a reactor. The two main sources of information on in-reactor creep are measurements of dimensions of components during or after service in power reactors, or with small representative specimens tested in either power or research reactors. Information from the power reactors is important because its application does not require extrapolation to operating conditions.

The evaluation of deformation of components from power reactors is often complicated by gradients in temperature and neutron flux, by temporal changes in reactor operation, and by the changes in various sources of stress, for example, cladding is surrounded by pressurized water, contains an internal gas pressure and sustains interactions with fuel. Separating effects can be difficult. These types of estimates are based on initial values of dimensions from the fabricators and from similar measurements of the components in water pools after the irradiation; thereafter interpretation is based on knowledge gleaned from previous measurements and testing of small specimens. Pre- and post-irradiation measurements are ideally conducted with the same equipment. Errors in strain are typically about 0.01% in power reactors, based on a measurement accuracy of 1 μm for a 10 mm diameter tube.

Early in the development of reactors in which the pressure vessels were a series of tubes passing through the core of the reactor, it was recognized that the tubes could change shape during service; their diameter and length could increase and, if horizontal, they could sag. Inspection indicated that irradiation could increase these changes in dimensions in unexpected amounts. The tubes were designed to operate for 30 years or longer and thus knowledge of the irradiation-induced strains was of vital importance. Programs were initiated to measure tubes during service and to develop techniques to study in detail the variables important for in-reactor deformation using small specimens. Gauging pressure tubes in power or research reactors provides a clearer picture of the effect of variables on deformation than measurements on cladding because the environment is less complicated. Typically, the tube internal diameter, D, is between about 80 and 103 mm, the wall thickness, t, is around 4 mm and the differential pressures between the inside and outside, P, are in the range 8–11 MPa. When the ends are closed the resulting hoop stresses, σ_H, are between 84 and 115 MPa, based on the thin wall approximation, $\sigma_H = P(D + t)/2t$; the axial stresses are half the hoop stresses. The temperature of the heat-transport water varies along the length of the tube from 260 to 312 °C while the flux of neutrons passes through a maximum value in the centre of the reactor. Diametral creep is estimated at time intervals with a probe, typically comprising Linear Variable Differential Transformers (LVDTs), Figs. 2–3 [40] or ultrasonic transducers [41,42], that travels along the full length of the tube and deliver a continuous measurement of the internal diameter with an accuracy of about 0.1%, Figs. 2–4 [43].

Such a measurement in CANDU reactors provides information on the effects of profiles of temperature and neutron flux as well as details of flux suppressions causing less deformation in the pressure tube corresponding to the ends of fuel bundles. Similar effects are observed in the pressure tubes in RBMK reactors in the centre of the reactor, where the two fuel assemblies meet, and in a small ripple corresponding to the ends of graphite bricks used as a moderator [42]. In research reactors the effect of stress may be obtained by varying the tube wall thickness [15,40]. Examples of this type of measurement on pressure tubes made from various alloys in various reactors include:

- *Zircaloy-2*: NRU [15,40], NPD [44].
- *Cold-worked Zr-2.*5Nb: NRU [15,40]; Pickering G.S., Bruce G.S., Point Lepreau G.S., WR1 and NRU [45,46]; Qinshan [47].
- *Heat-treated Zr-2.*5Nb: Fugen [41]; NPD [48].
- *Zr-2.*5Nb *with Annealed, TMT-1 or TMT-2 heat-treatments*: RBMK [42,47].

Alternatively, lengths of Zr-2.5Nb tubing with inside diameter of 23 mm were formed into a U-shaped assembly and placed inside a research reactor, Figs. 2–5 [49,50]. The assembly was stressed with water at 300 ± 3 °C and 10.4 MPa. In a central zone the outside surface was machined to reduce the tube wall thickness and provide a range of hoop stress from 104 to 313 MPa. During shutdowns the inside diameter of specimen lengths was measured with an air-gauge with a resolution between 1 and 3.6% [51].

Biaxial loading may also be achieved by using sealed, pressurized capsules, typically illustrated with Figs. 2–6 [52]. These specimens provide tests close to constant stress rather than

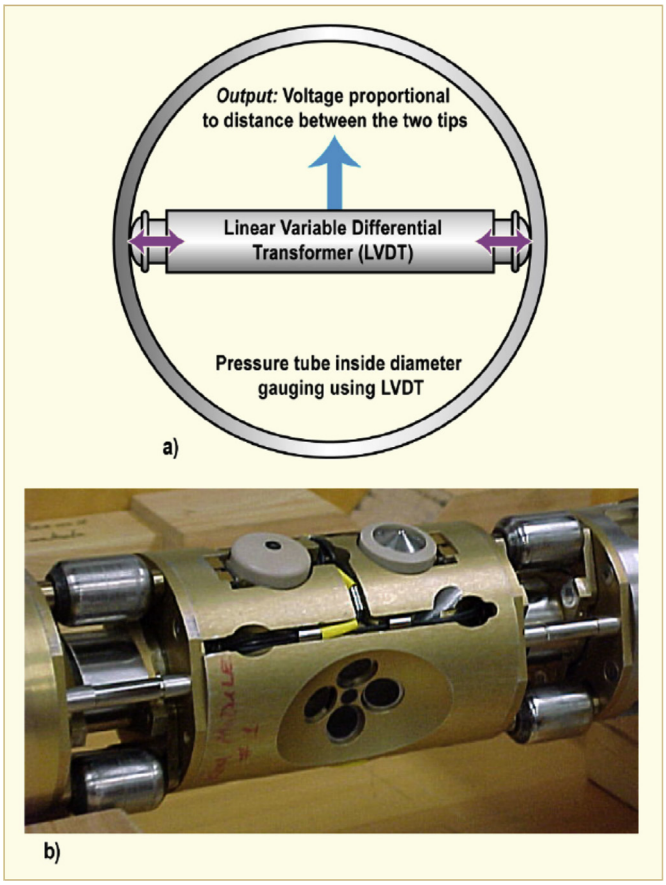

Fig. 2–3. a) Schematic diagram of instrumented probe and b) photograph of probe to evaluated pressure tubes. The shiny metallic tip is the LVDT (on the right) to measure the inside diameter, and the dull gray plastic head is an eddy current probe (on the left) to detect surface flaws. Based on Ross-Ross and Hunt [40].

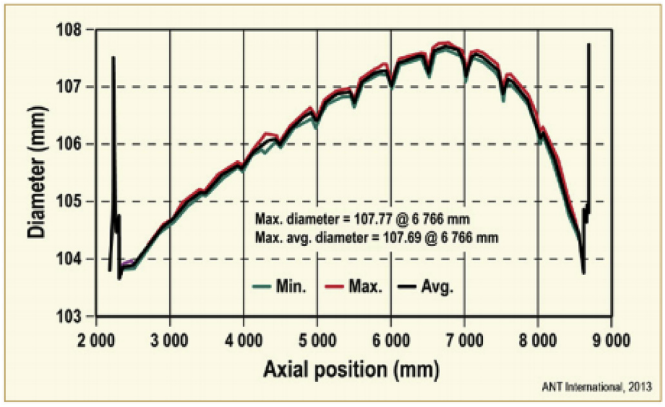

Fig. 2–4. Typical axial profile of internal diameter of Zr-2.5Nb pressure tube. Although the maximum flux is in the center of the tube, the profile is displaced towards the hotter, outlet end of the fuel channel at 8500 mm. The regular dips in the diameter correspond to the ends of each fuel bundle where there is a small reduction in neutron flux. Based on Gunn et al. [43].

constant load, so the results may appear optimistic for application in a power reactor but useful for storage of spent fuel when no new fission gasses are being generated. In capsule specimens the diameters were smaller and microstructures different from pressure tubes used in power reactors, so the results require care in their application whereas this concern is avoided when applying this

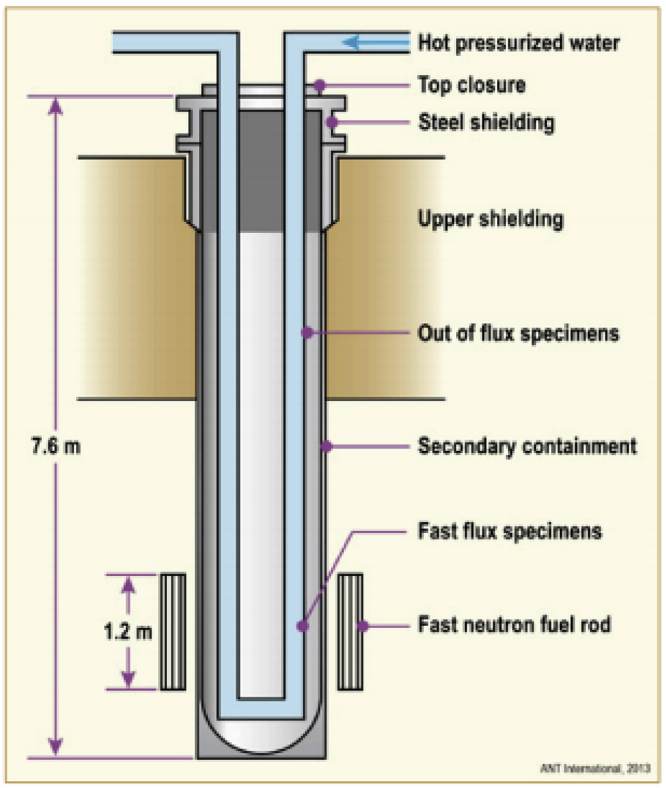

Fig. 2–5. . In-reactor assembly for constant pressure creep tests on Zr-2.5Nb, after [49,50]. Individual specimens were 200 mm long with an inside diameter of 23 mm. They were brazed together to form a continuous U-tube. Hot, pressurized water passed through the tube subjecting the specimens to similar temperature, about 300 °C, and internal pressure, about 10.4 MPa. The outside surface of the central 100 mm of each specimen was machined to reduce the wall thickness to provide hoop stresses in the range 104–313 MPa. The inside diameter was measured at intervals using an air-gauge.

technique to fuel cladding. Specimens of Zircaloy-2, Zr-2.5Nb, ZIRLO, M4, M5 were irradiated in pressurized water or NaK at temperatures in the range 270–350 °C with hoop stresses in the range −60 MPa up to 500 MPa. To avoid end effects the specimen length to diameter ratio was usually about four or greater. Creep strain was estimated from measurements of the outside diameter of the tubes using various techniques during reactor shutdowns, listed below, with measurement uncertainty, where available, indicated within parentheses.

- [53], micrometer;
- [53], neutron radiography of dysprosium markers [54];
- [52,55], dial gauge (3 μm);
- [41] ultrasonics (20 μm);
- [23,56–58] comparator using LVDT's, (±(2–7) μm);
- [59–61] laser micrometer (±0.11 to ± 0.37 μm);
- [58] non-contact silhouette system, (±1 μm).

Uniaxial creep tests have been done on dog-bone specimens of zirconium alloys with gauge lengths of about 50 mm and small cross-sections in research reactors [62]. Such tests require clever design:

- Usually the entry holes in the reactors have a small diameter;
- The region of high flux is several metres from the access point;
- Control of temperature gradients from gamma heating is a challenge;
- Application of large stresses can be difficult;

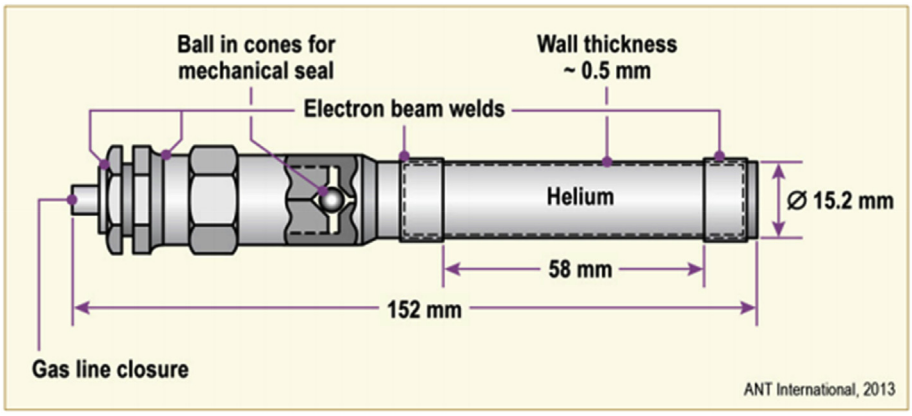

Fig. 2–6. Typical creep capsule; tube pressurized at room temperature and sealed. Dimensions measured during reactor shut-downs, after [52].

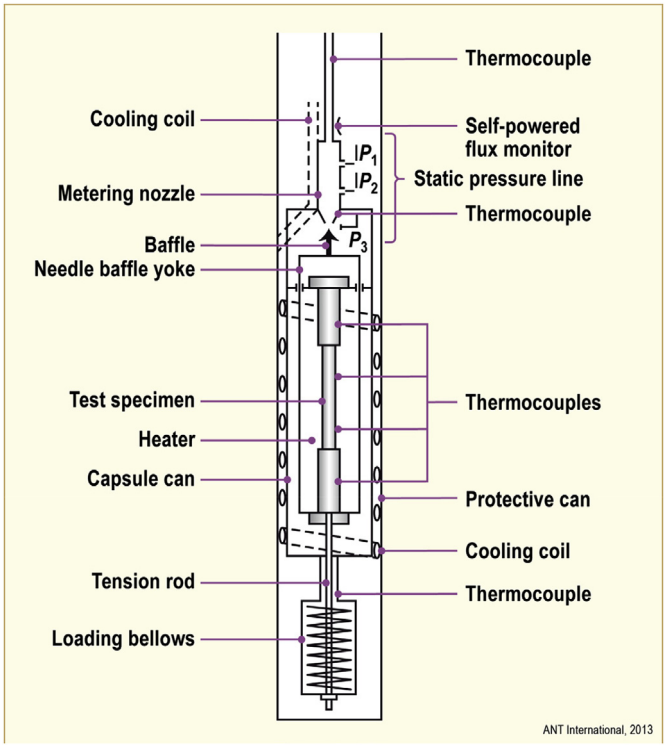

Fig. 2–7. Schematic diagram of in-reactor uniaxial creep machine, after [63]. The test specimen is machined from a zirconium alloy component and loaded in tension by a bellows. The elongation is measured by a gas gauge. The temperature is controlled by balancing gamma and electrical heating within a helium atmosphere. Instrumentation includes thermocouples, pressure gauges and flux monitors. The whole assembly fits into a 35 mm-diameter, 3.7 m long hole in the reactor.

- Measuring deformation with good resolution requires much care.

Fidleris et al. [63] solved these issues, Figs. 2–7, by balancing the gamma heating with both cooling coils and heaters, the tensile load was imposed by expanding a bellows and changes in specimen length were measured using an air-gauge with a sensitivity of about 0.020% [64]. Corrosion was minimized by testing in a helium atmosphere. If the proposed tensile stress for the test was large, >200 MPa, to avoid premature rupture, the test specimen was pre-hardened by irradiating to between 10^{23} and 10^{24} n/m^2 under a small stress. Early similar test techniques were used by Fidleris [25,65,66] and Wood and Watkins [67, 68]. Similar designs have been developed at Halden for testing in a water environment with capability for both tensile [69] and compressive stresses, Figs. 2–8 [70]. Length changes were measured with an LVDT. These methods have the additional complications of:

- The effect of irradiation and environment on LVDT's, with occasional failures (e.g. 2 out of 12 [69])
- Corrosion and hydrogen pick-up on the specimens;
- Loop pressure variation;
- Effect on all test parameters by reactor start-up and shutdown.

In these studies, useful data have been obtained on Zircaloy-2, Zircaloy-2 + 1 %Nb, Zircaloy-4, Zr-2.5Nb at temperatures in the range 288–343 °C and stresses in the range to −40 to 455 MPa. Tensile creep testing of stainless steels successfully used the same techniques [71].

Information on in-reactor deformation may also be obtained from stress relaxation tests. In these tests the total strain of the specimen is kept constant and stress relaxes with time as the elastic strain converts to plastic strain through creep. If the creep rate, $\dot{\varepsilon}_p$, follows behaviour like:

$$\dot{\varepsilon}_p = K\sigma^n t^m \tag{2.1}$$

where K is a constant for constant temperature.

σis the stress,
t is time, and
n and m are constants,

then, if n = 1, the initial stress, σ_0, declines to a value, σ_f, at time t given, through Hooke's law, by:

$$\ln(\sigma_f/\sigma_0) = -\{KEt^{(m+1)}\}/m+1 \tag{2.2}$$

where E is Young's modulus.

Therefore, by measuring the change in stress with time, the contribution from creep with time can be calculated. (The creep law with n = 1 provides a good approximation when σ_0 is low, < 240 MPa) A simplification follows from the observations that the unrelaxed stress ratio is independent of σ_0 and $\ln(\sigma_f/\sigma_0)$ decreases approximately linearly with time after an initial rapid drop. The data can then be represented in Ref. [72]:

$$\sigma_f/\sigma_0 = D \exp(-Rt) \tag{2.3}$$

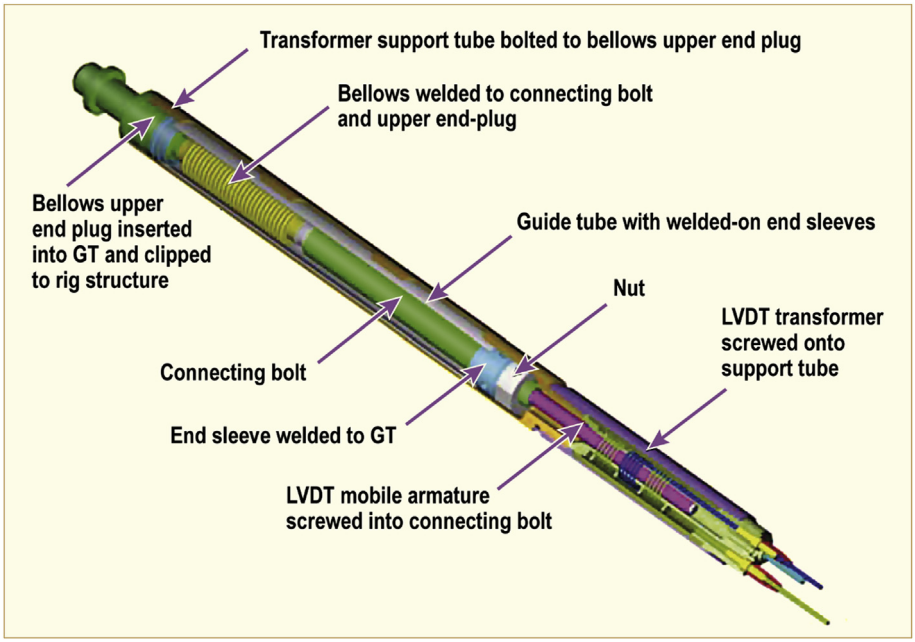

Fig. 2–8. . Isometric drawing of PWR guide tube (GT) specimen assembly with bellows loading unit and.LVDT measurement system; note that the specimen is loaded in compression [70].

where D is unrelaxed stress ratio after an initial rapid drop, and R is a relaxation constant, i.e. slope of $\ln(\sigma_f/\sigma_0)$ vs time.

The stress is evaluated from the change in outer fiber stress during bending of a simple beam of thickness c by clamping it to a holder of known radius of curvature:

$$\sigma_f - \sigma_0 = \tfrac{1}{2}Ec(1/R_1 - 1/R_2) \quad (2.4)$$

where R_1 is the beam radius with σ_0 and R_2 is the beam radius with σ_f.

The radii were variously measured with a microscope [74] and a profile projector [73,75]. The error in stress was about 5% and for the stress ratio the error was about $\pm 0.1\ \sigma_f/\sigma_0$. Irradiations were done on holders containing several specimens, typically six, thus providing an estimate of experimental error, Figs. 2–9. Example of data in Figs. 2–10. Such data can be used to either:

- Compare different materials, metallurgical variables, test temperatures, qualitatively (e.g., which material relaxes faster?)
- Evaluate many alloys or metallurgical conditions at once, if a multi-specimen holder is used
- Calculate the creep strain for the test conditions quantitatively if the relevant creep law is chosen with simple exponents; as indicated above, values may be derived at low stresses if the creep rate is independent of time and the exponent on stress is close to 1.0.

Useful information on creep and relaxation are found in Refs.[72-83]. The ASTM Standard, (E328-02, 2010) recommends 4-point bending, which produces a constant bending moment in the

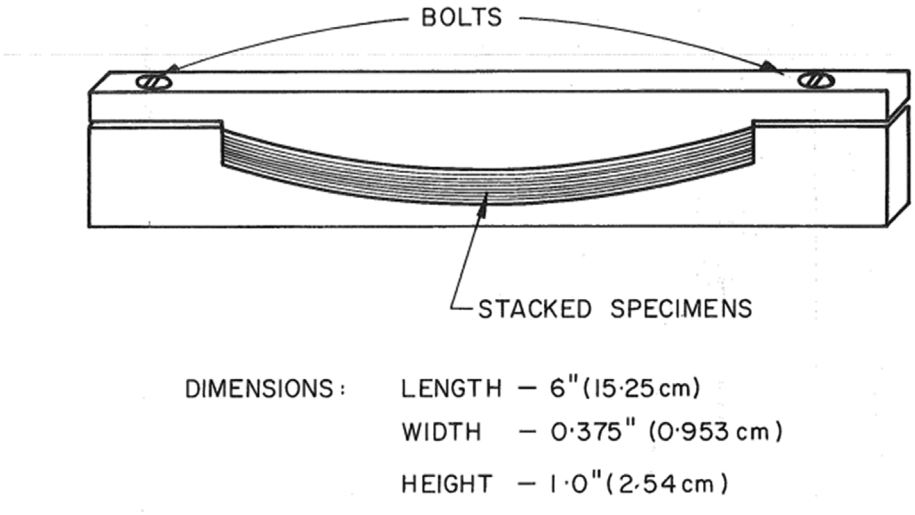

Fig. 2–9. Schematic diagram of specimen holder containing specimens for stress relaxation [73].

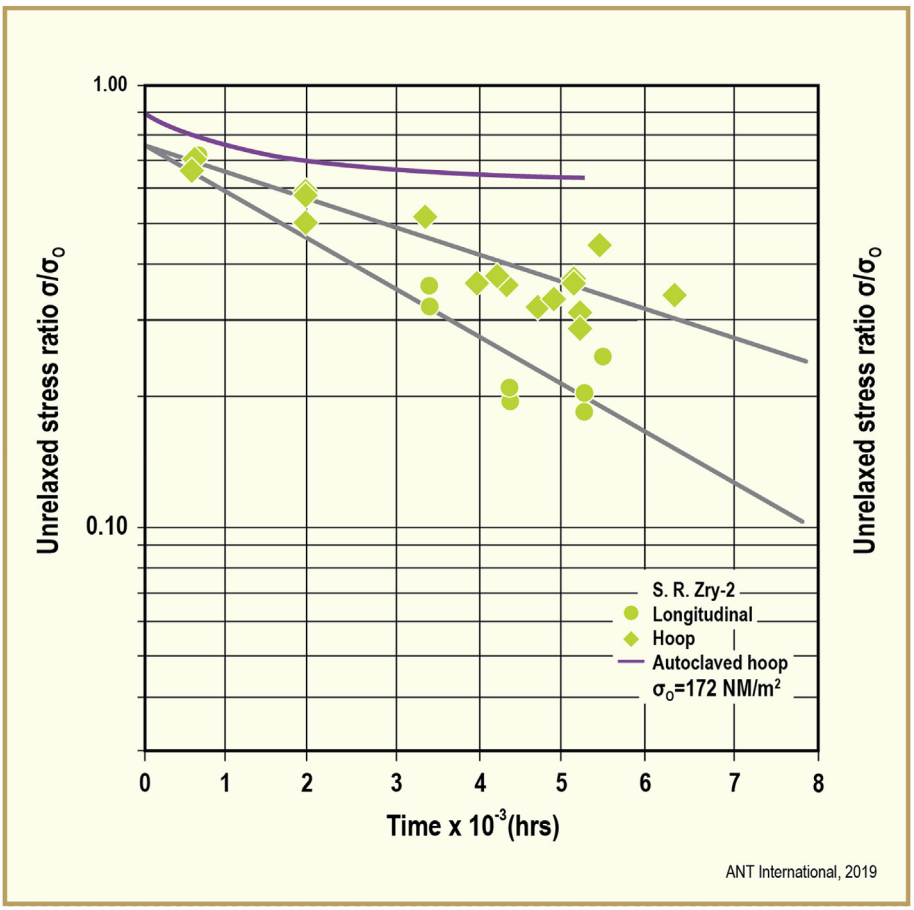

Fig. 2–10. Unrelaxed stress ratio as a function of time for stress-relieved Zircaloy-2, in-reactor at 566 K (293 °C). "Unrelaxed stress ratio" is the stress at time t divided by the stress at time 0. "Autoclaved hoop" is unirradiated material tested out-of-reactor [75].

test section as illustrated in Figs. 2–11. Standard Test Method C-2 states that the stress can be determined by measuring (before and after relaxation) the force P required to lift the specimen just free of one or more of the constraints during the test. This technique has been used in an EPRI-directed NFIR programme on in-reactor stress relaxation (abstract accepted for presentation at ASTM Zirconium in the Nuclear Industry, Manchester, 2019).

There are several requirements, cautions and advantages of the various stress relaxation testing techniques:

- Measurements in-reactor and in hot-cells are difficult and laborious. Great care must be taken when handling specimens.
- Reproducibility in best conditions is ±10% [ASTM E328-02, 2010, Section 38.],
- Clever design can allow many specimens to be tested at once.
- Testing environment, particularly in-reactor, may affect results. For example, corrosion, shadow corrosion, absorption of hydrogen, variable gamma heating, must be anticipated and minimized.
- Calculations involve using Young's Modulus, E, so it must be known for all temperatures used - usually cell temperature for measurements and elevated temperature for testing; it is assumed that irradiation at normal reactor operating temperatures does not change E.
- The applied stress-strain must be in the elastic range. One cannot expect recovered strain to exceed the initial applied strain.

2.4. Creep data (not including spent fuel storage and LOCA related)

In reactor deformation is often thought of as comprising four strain components driven by an applied stress:

$$\varepsilon_{total} = \varepsilon_{thermal} + \varepsilon_{irradiated\ thermal} + \varepsilon_{irradiation} + \varepsilon_{growth} \quad (2.5)$$

where:

$\varepsilon_{thermal} \equiv \varepsilon_t$ = creep strain of unirradiated material in the absence of a neutron flux

$\varepsilon_{irradiation\ thermal} \equiv \varepsilon_{i\text{-}thermal}$ = creep strain of irradiated material in the absence of a neutron flux

$\varepsilon_{irradiation} \equiv \varepsilon_{irr}$ = creep strain of irradiated material in the presence of a neutron flux

$\varepsilon_{growth} \equiv \varepsilon_g$ = strain due to irradiation growth (with zero applied stress)

It is assumed that each component is independent of the other three. Note that there is also a strain component resulting from volume expansion due to hydrogen and hydrides.

True ***thermal creep*** can occur only in the absence of irradiation damage sufficient to harden the material. For irradiation temperature near 300 °C (573 K) significant hardening is shown to occur at less than 3×10^{23} n/m^2 (E > 1 MeV), [83]. For a typical Light Water Reactor (LWR) neutron flux of 7×10^{17} n/m.^{2}s, E > 1 MeV, "significant hardening" would occur in less than three days and therefore thermal creep would have little effect on overall strain. For a very

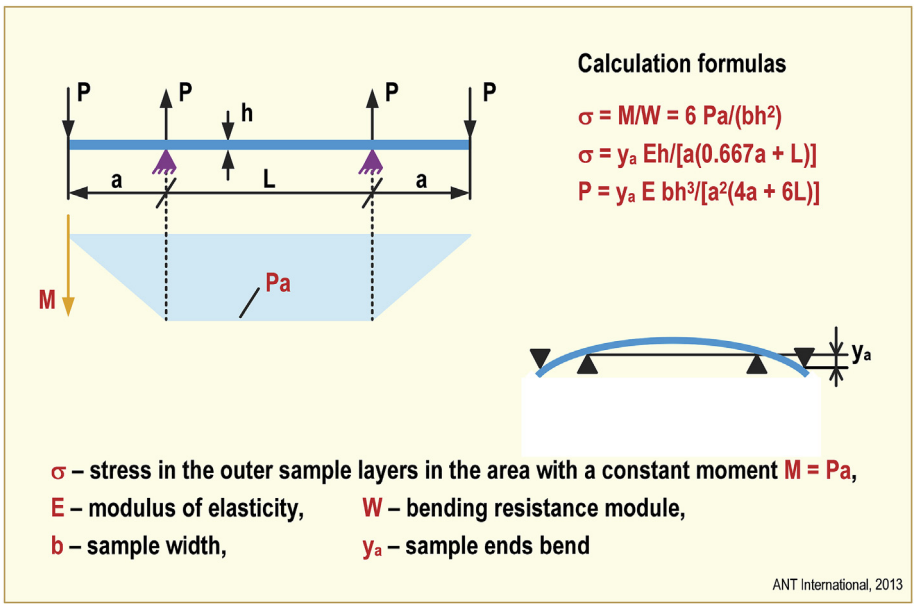

Fig. 2–11. Schematic diagram of 4-point bend experimental setup and appropriate equations, [ASTM E328-02, 2010], Section 35.

low flux of 5×10^{16} n/m^2 which might occur at the ends of fuel rods, and particularly at the inlet and outlet ends of a pressure tube in a CANDU reactor, the time during which thermal creep is significant would be on the order of 100 days. In that case, strain due to thermal creep would be important, depending on the stress and temperature.

Likewise, $\varepsilon_{irradiation\ thermal}$ is very small and can be neglected, except at temperatures where vacancies become very mobile and irradiation damage is becoming unstable (about 400 °C [673 K], see Section 3.4.10). The effect of irradiation hardening (fluence or dpa) on thermal creep is illustrated by Figs. 2–12, where it is seen that pre-creep test fluence above about 21×10^{24} n/m^2 is enough to significantly lower both the creep strain and creep rate. Another example is for creep in a CANDU environment, Figs. 2–13. The 4th term, $\varepsilon_{irradiation\ growth}$, is without applied stress and is considered to be independent of creep. In most creep experiments, the growth strain is ignored, but for thorough analysis, such as provided by Garzarolli in Ref. [24], it is subtracted from the creep strain.

$\varepsilon_{irradiation} \equiv \varepsilon_{irr}$ = creep strain of irradiated material in the presence of a neutron flux is the primary topic of his review.

In the U.S., the first reactors (Nautilus, 1954; Shippingport, 1957; Dresden, 1960; Yankee Rowe, 1960) all used either Zircaloy-2 or Zircaloy-4 for structural components of these PWR or BWR designs. For pressure tube designs (Hanford N, 1963; SGHWR, 1967; CANDU, 1968), the choice was between Zircaloy-2 and Zr-2.5Nb. In the USSR at the time, various Zr–Nb were under development.

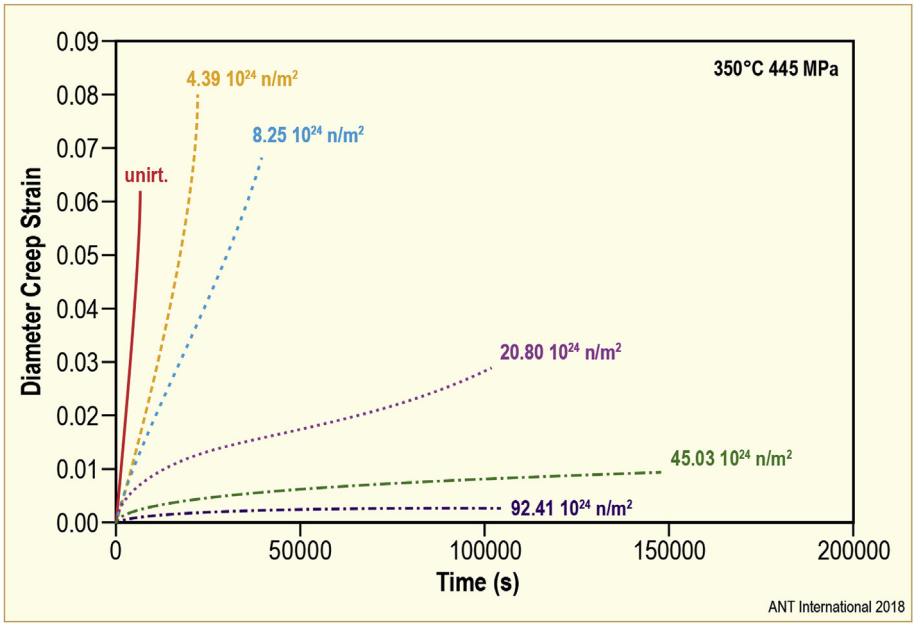

Fig. 2–12. Effect of fluence on thermal (post-irradiation, zero flux) creep behaviour at 350 °C (623 K) of irradiated SRA Zircaloy-4 cladding tubes.

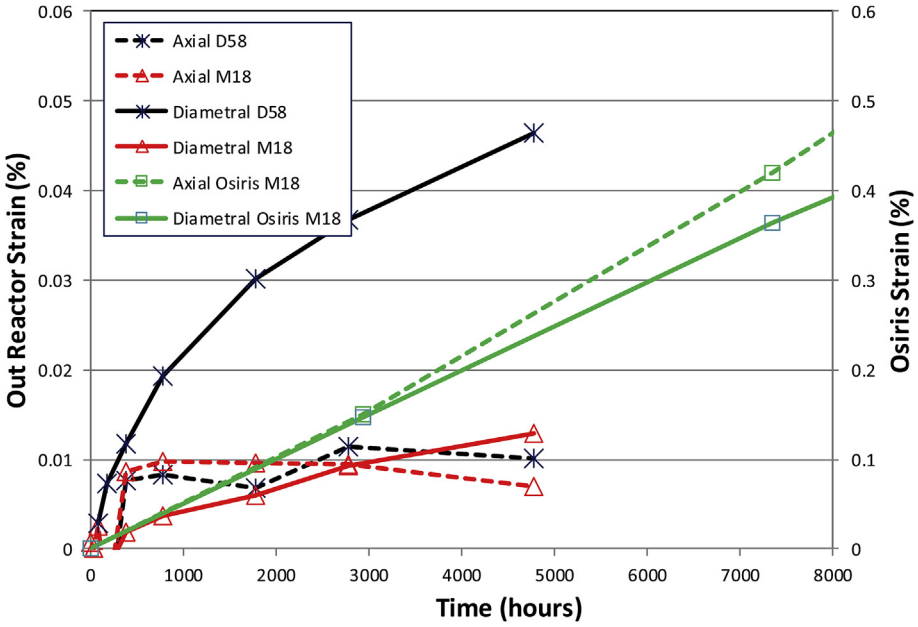

Fig. 2–13. Creep strain as a function of time for laboratory tests of unirradiated Zr-2.5Nb (D58) and Zr-2.5Nb irradiated in the Osiris reactor (M18) and then further creep tested in the laboratory after irradiation. Temperature = 280 °C, hoop stress = 125 MPa and cold work = 27%, [61].

Since no creep data were available, it was assumed that creep behaviour was the same in-or-out of reactor, and the ASME codes[2] were used for design (for examples, Watkins and Wood [67] and Coleman [84]). It was known that orthorhombic alpha-uranium was dimensionally unstable in a neutron or fission fragment environment (Roberts and Cottrell [85] and Hesketh et al. [86], creating some anxiety for core designers [1]. An additional complication was that some early reports indicated no effect of neutrons on creep of Zircaloy-2 [87], reported by Nichols [88]. Also, the high temperature (377 °C) results of Holmes et al. [89] reported no significant effect of irradiation.

Therefore, the early work on creep of zirconium alloys centered on two important questions: 1) did neutron flux affect creep strains and strain rates and, if so; 2) which zirconium alloys and microstructures had the lowest creep rate?

By 1969, both questions were answered with qualifications depending on test and material conditions. Chosen for its higher strength than RXA Zircaloy, cold worked (CW) Zircaloy-2 was found to have creep rates higher by a factor of 10 in-reactor when compared to out-of-reactor rates, Fidleris [29], Ross-Ross and Hunt [40], Watkins and Wood [67]. Figs. 2–14 shows an example.

Under the same parameters of temperature, stress and neutron flux (relevant to CANDU pressure tube operation), CW Zr-2.5Nb was shown to have a creep rate of about one-third that of CW Zircaloy-2, [15, 40]. And for the uniaxial tests of [29], similar, although smaller reductions were found. As a result, the higher-tensile-strength Zr-2.5Nb was chosen, after about 1970, as the pressure tube material of choice for CANDU reactors: higher strength, smaller wall thickness, less neutron absorption. Earlier, CW Zircaloy-2 was chosen for the Hanford N Reactor [17,90].

2.4.1. Anisotropy and texture

One indication of a texture effect in tubes is observed with uniaxial loading in-reactor in two orthogonal directions, for example, in the axial, a, and transverse, t, directions. From equation (1.3) the strain rates in each direction at the same temperature, neutron fluence and applied stress are related through the anisotropic parameters [14]:

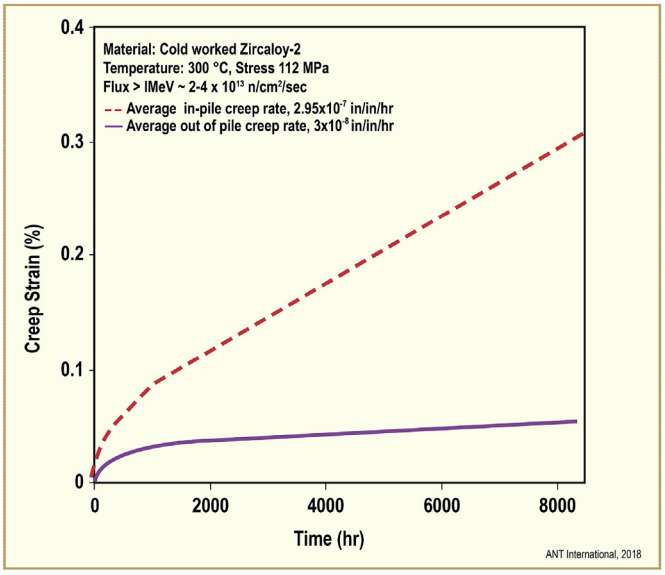

Fig. 2–14. Effect of irradiation on the uniaxial creep behaviour of cold-worked Zircaloy-2. Testing for 8000 h results in a fluence of 7×10^{24} n/m^2, E > 1 MeV; after Watkins and Wood [67].

$$\dot{\varepsilon}_a / \dot{\varepsilon}_t = (F+H)/(F+G) \tag{2.6}$$

When these parameters are equal the material is isotropic and the strain rate ratio is 1.

In small tensile specimens or bent beams machined from pressure tubes made from Zircaloy-2 and Zr-2.5Nb with the textures of equation (1.2), creep rates and stress relaxation are 1.7–2.5 times faster in the axial direction than in the transverse direction [15,76]. Figs. 2–10 provides an example from stress relaxation where the samples bent in the axial direction of a pressure tube relax faster than those bent in the transverse direction. This conclusion applies for materials with a low resolved fraction of

basal plane normals in the axial direction, f_l of ≤0.1. In Zr-2.5Nb pressure tubes the resolved volume fraction of prism planes in the axial direction is 1.5–1.8 times that in the transverse direction. The general observation is that creep resistance in the <c>-direction is high and therefore plastic deformation is more difficult compared with easier options of slip in the orthogonal <a>– or pyramidal <a + c>-directions.

The ratio between the transverse creep rate in a uniaxial test and hoop creep rate in a biaxial test with.

($\sigma_a = \sigma_t/2$) is:

$$\dot{\varepsilon}_{t,biaxial} \,/\, \dot{\varepsilon}_{t,uniaxial} = (0.5F + G)/(F + G) \tag{2.7}$$

For an isotropic material this ratio is 0.75. With the texture of fuel cladding and pressure tubes the hoop creep rate of a thin wall tube under a differential pressure should be less than that estimated for a uniaxial stress in the transverse direction confirming that results of uniaxial tests are not reliable indicators of the behaviour of pressurised tubes.

During internal pressurising of a tube, the ratio between axial and transverse creep strain rate is:

$$\dot{\varepsilon}_a \,/\, \dot{\varepsilon}_t = (H - F)/(2G + F) \tag{2.8}$$

This ratio is zero in an isotropic material therefore internally pressurised tubes do not change length during creep. With anisotropic material the strain rates can be correlated with the texture through the difference (f_t - f_r) [91, 92, **93**]. Here the quantity (f_t - f_r) is used as a measure of the texture since f_a is small for the materials considered. When f_r values are large, which are typical for thin wall cold-worked cladding tubes, equation (1.1), and rolled sheet components, (f_t - f_r) can be as low as −0.4 consequently negative axial creep strain rates are predicted under biaxial conditions. Such negative axial strain rates have been reported with internally pressurised capsules of recrystallized Zircaloy-4 and M – 5 fuel cladding [57]. When f_t values are large, which are typical for cold-drawn CANDU pressure tubes, (f_t - f_r) can be as high as 0.35 and positive axial strain rates are predicted under biaxial test condition. Thus during reactor service and experimental irradiations, pressure tubes are predicted to elongate. Such elongation is observed in power reactors:

- The Zircaloy-2 pressure tubes in the N-reactor elongated up to 0.4% mm in 5.7 years [17**]** These tubes had four types of fabrication schedule all producing a low preferred orientation of (0002) in the axial direction, f-values of 0.07–0.09, and a range of f-values of either 0.44 to 0.46 or 0.54 to 0.58 in the transverse direction. Consequently the contributions from growth to the elongation were similar for each type of tube but the creep contributions were negative in the transverse direction for the material with the lower f-values. These differences in creep contribution to the strain explained the observed differences in elongation and transverse strain.
- The Zircaloy-2 pressure tubes in NPD had a texture with low f_a, and f_t and f_t of about 0.45. After 140 000 h of operation a typical tube had elongated 7 mm, corresponding to a strain over the whole length of the tube of 0.17%, while the diameter had increased by 0.38% [44**]**.
- In CANDU reactors the cold-worked Zr-2.5Nb tubes have the texture described by Equation (1.2) and they also exhibit elongation and diametral expansion. For example, Zr-2.5Nb pressure tubes in Pickering Unit 3 elongated linearly with time nearly 45 mm in 12 years of operation and the diameter increased at strain rates between 8 and 10×10^{-8} h^{-1} [45**]**. Elongations of 76 and 110 mm were reported after neutron fluences of 8 and 12×10^{25} n/m^2 (averaged over the length of the tube) [93,94].

Evaluating axial strain rates from elongation of pressure tubes is fraught with error because the neutron flux, the inside temperature, internal pressure and microstructure all vary along the 4–6 m of the tube. Short, internally pressurized capsules of small diameter tubes, Figs. 2–6, allow both axial and transverse strain rates to be measured. For example Zr-2.5Nb tubes, that had textures either similar to fuel cladding or to pressure tubes, were irradiated in NRU and Osiris up to 6.5×10^{25} n/m^2 between 280 and 340 °C with hoop stresses between 0 and 500 MPa [52,58,61,92]. From the results of strain as a function of fluence, creep compliances, C_d (strain/(fluence x stress)) for each direction in each material and at each temperature were obtained. Care has to be taken to subtract any contribution to the creep strain from growth strain attained at zero stress. Most reliable results are obtained after the neutron fluence has exceeded about 2×10^{24} n/m^2 to allow saturation of irradiation damage. For example, for "fuel cladding" $C_t = 1.9 \times 10^{-30}$ and $C_l = -0.2 \times 10^{-30}$ m^2/n.MPa. The ratio, C_l/C_t, is −0.1. For "pressure tubes", $C_t = 0.92 \times 10^{-30}$ and $C_l = 0.55 \times 10^{-30}$ m^2/n.MPa. The ratio, C_l/C_t, is 0.6. The values from several experiments were related to the texture parameters of the tubes and represented by $f_t - f_r$. The results are summarised in Figs. 2–15 where they are compared with a self-consistent model developed in Refs. [46,91]. The data representing the texture of pressure tubes, "micro-pressure tubes" (MPT) and similar earlier tests, are arrayed about the line of the model indicating that the model may describe the effect of texture on biaxial creep of pressure tube-type material. The results of one set of experiments at 340 °C suggest that the anisotropy of irradiation creep diminishes as the temperature for annealing irradiation damage is approached. With textures where $f_t - f_r < 0$ and more representative of "fuel sheathing" (FS or cladding), the creep anisotropy is not well described by the model indicating that other microstructural features are contributing to the anisotropy (This discrepancy will be discussed in Sections 4 and 5.). Now the axial strains lead to small negative changes in length that are less of a problem for fuel assemblies made from cold-worked cladding than in pressure tubes.

In summary, the crystallographic texture developed during tube fabrication of zirconium alloy tubes leads to anisotropy of in-reactor creep when driven by internal pressure around 300 °C. Pressure tubes with high concentrations of basal plane normals in the transverse direction tend to elongate during irradiation. The tendency to elongate is much less in cold-worked fuel cladding where this concentration is high in the radial direction.

2.5. Variables

The in-reactor strain rate, $\dot{\varepsilon}$, is usually expressed in empirical equations employing a number of variables [2]:

$$\dot{\varepsilon} = \mathrm{f}\left(\sigma^n, D, \frac{1}{B}, \Phi^p, T, f, A\right) \tag{2.9}$$

where.

$\sigma$is the applied stress
D is the density of mobile dislocations
B is density of barriers to dislocation motion (where B has different strength depending on the nature of the barrier, e.g. dislocations, dislocation loops, solutes, precipitates.)
$\Phi$is the neutron flux
T is irradiation temperature
f is the texture factor
A is a metallurgical factor related to a specific alloy
n and p are constants

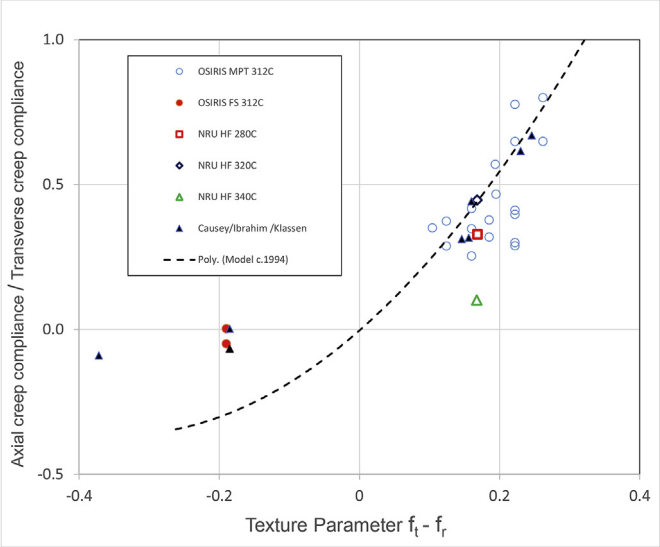

Fig. 2–15. Dependence of the ratio of biaxial in-reactor creep compliance in the transverse and axial directions of zirconium alloys on the texture parameter, $f_t - f_r$, and comparison with theory (dotted line) [52,58,61,92].

In-reactor strain is often expressed by the equation

$$\varepsilon = A(\Phi t)^m \sigma^n e^{\frac{-Q}{RT}} \quad (2.10)$$

where.

$\varepsilon$is strain
Φt is fluence
R is the gas constant
m is a constant
Q is the temperature activation energy (note that when Q is positive, an increase in temperature results in an increase in strain)
A, T, n as above

2.5.1. Stress

The stress dependency of in-reactor creep is complicated. The older review of literature provided by Franklin et al., 1983 indicated that

$n \approx 10–100$ for $400 < \sigma \leq 600$ MPa (58–87 ksi) – (post-irradiation)

$n \approx 4–10$ for $205 < \sigma \leq 400$ MPa (30–58 ksi) – (thermal)

$n \approx 1$ for $138 < \sigma \leq 205$ MPa (20–58 ksi) – (irradiation creep)

$n \approx 0–1$ for $\sigma \leq 138$ MPa (0–20 ksi) – (irradiation growth/creep)

In practice, the stress exponent "n" also depends on variables including, e.g. stress magnitude (Figs. 2–16, [95]), and temperature (Figs. 2–17, [18]).

Using equation (2.10), Soniak et al. [23] determined that "n" ranged between 0.8 and 2.0 depending on flux and temperature, with an average of about 1.6.

Results of extensive data analyses by Garzarolli [24] indicated that the stress dependency is linear in the most interesting stress range at <100–200 MPa and temperature range 275–390 °C independent of the direction of creep, neutron flux, material composition or material condition, for example, Figs. 2–18 and Figs. 2–19.

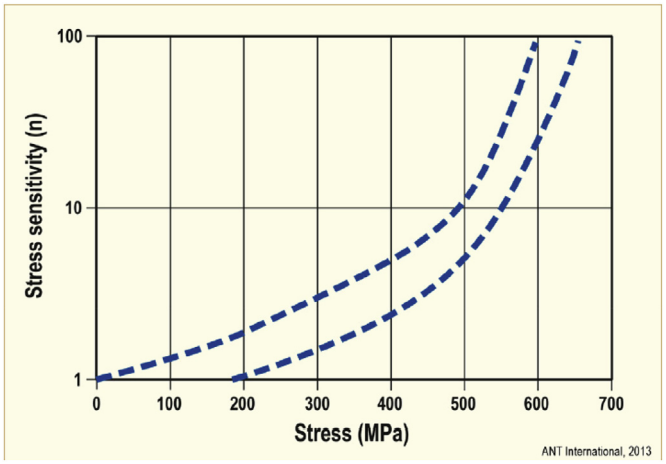

Fig. 2–16. Stress dependence of in reactor stress exponent for Zr-2.5Nb at 570 K and a fast flux of 1×10^{17} n/m^{2}s (E > 1 MeV), [95].

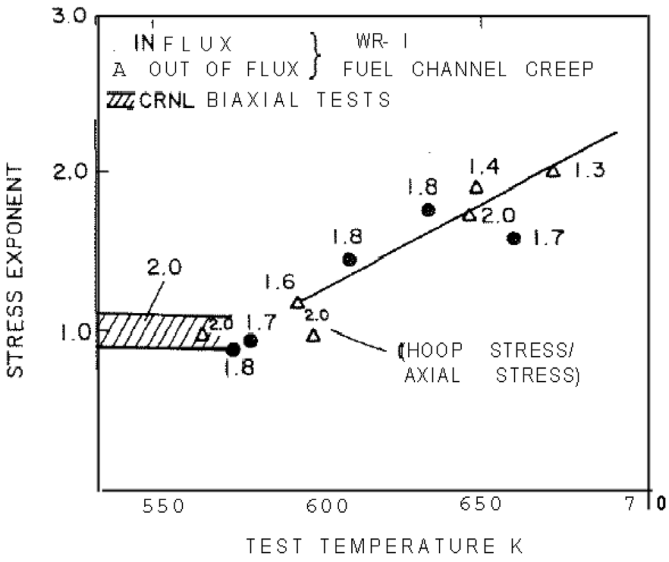

Fig. 2–17. Effect of temperature on the stress dependence of creep for Zr-2.5Nb pressure tubes, [18].

2.5.2. Flux

The theory proposed by Dollins [96], indicates that the flux dependency increases with flux as a power dependence with exponent p; the "constant" p ranges between 0.25 and 1.0 in the span of fluxes appropriate for light water reactors, Figs. 2–20. Two factors may cause the fast flux dependency to be less than unity. First, at temperatures in the upper range of reactor component temperature (roughly, 340 °C (513 K)) irradiation-thermal creep may be occurring that has no dependency on neutron flux. This contribution to the strain would cause the overall flux dependence and the associated exponent to decrease. Second, at low values of fast flux (in combination with temperature) the defect production rate may be insufficient to build up the microstructure needed to eliminate significant thermal creep. In most situations, then, from a mechanistic view the flux dependency is expected to be near or slightly below unity.

Griffiths et al. [97] and DeAbreu et al. [61], presented data indicating that for Zr-2.5Nb in a CANDU reactor the flux

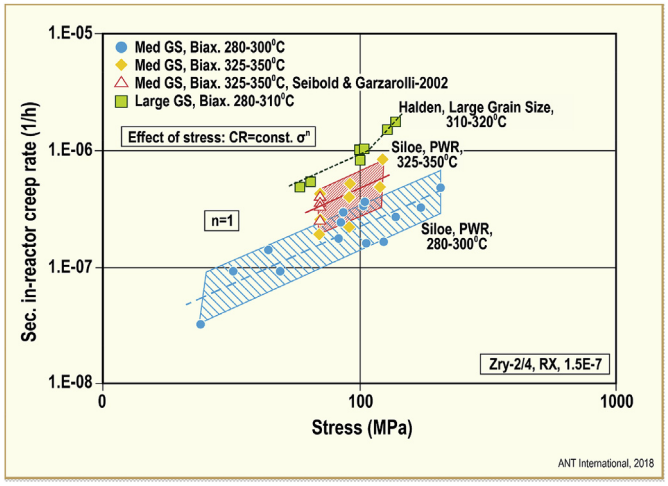

Fig. 2–18. Effect of stress on in-reactor creep of fully recrystallized Zry-2/4. The reported creep rates were normalized to a damage rate of 1.5×10^{-7} dpa/s (≈fast flux of 1×10^{18} n/m.^{2}s in LWRs).

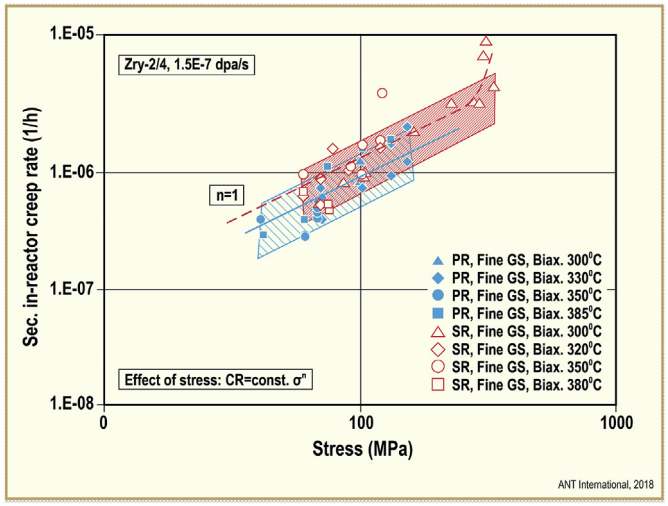

Fig. 2–19. Effect of stress on in-reactor creep of PR and SR Zry-2/4. The reported creep rates are predominantly from tests in Siloe and PWR and were normalized to a damage rate of 1.5×10^{-7} dpa/s (≈fast flux of 1×10^{18} n/m.^{2}s in LWRs).

dependency is non-linear ($p < 1$) at low flux and becomes linear ($p \approx 1$) at fluxes greater than about 4×10^{16} n/m.^{2}s ($E > 1$ MeV), Figs. 2–21.

Data from test on cold-worked Zircaloy indicate the flux dependency becomes linear above about 5×10^{17} n/m^{2}s, Figs. 2–22, [98]. These latter data are for fluences less than 1×10^{24} n/m^2 where the irradiation-damage structure and mechanical properties have not yet saturated and steady state creep is unlikely to have been achieved.

Proton irradiation experiments, although having the disadvantage of requiring very thin (about 50 μm thick) specimens have the distinct advantage, compared to in-reactor experiments, of control of the damage rate. Thereby, individual parameters like flux dependency can be assessed. In an experiment at a temperature low enough to eliminate thermal creep, it was shown that under proton bombardment conditions (which simulate but do not duplicate neutron irradiation) low stress creep and irradiation growth deformation of zirconium occurred only when the proton beam was "on". The flux dependency (in this case the defect-production

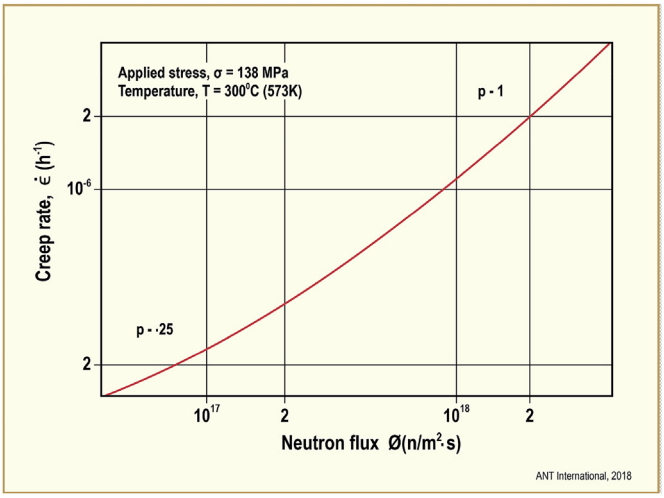

Fig. 2–20. Calculation of the variation of in-reactor creep rate with neutron flux in zirconium, [96]. 20 ksi = 138 MPa.

rate dependency) was very near unity [99], Figs. 2–23. The dose rate (ϕ) was changed several times during the test; the smooth curve indicated that the strain rate is only a weak function of dose rate.

Earlier proton irradiation experiments on large grained RXA Zircaloy-2 at temperatures (300 °C (553 K)) and stresses between (100 and 267 MPa) in the higher range of reactor interest have conclusively shown a linear damage rate dependency in the range of 0.1 to 10×10^{-7} dpa/sec, equivalent to a PWR flux range of about $0.7–70 \times 10^{17}$ n/m^2/s, $E > 1$ MeV [100], Figs. 2–24. For additional comparison between of the Chow/Chapman experiments, see Adamson, [24].

To estimate the creep-flux dependency, independent of the various literature conclusions based on particular data sets, a large data base, listed in Adamson et al. [24], was evaluated. The evaluation is shown in Figs. 2–25, which shows the in-reactor creep behaviour of different experiments of similar materials tested under comparable conditions versus the damage rate in the temperature range of 270–380 °C either at the given stress or in the stress range of 60–130 MPa and normalized to 100 MPa, applying a linear creep rate - stress dependency. The figure indicates:

- a nearly linear creep rate - damage rate dependency,
- a flux exponent of 0.85, for axial, tangential (transverse in rolled plate) and diametral (in tubing) creep under a differential pressure (between inside and outside of the tubular samples) in the fast flux range of 5×10^{16} to 5×10^{18} n/m.^{2}s (>1 MeV),
- at low fluxes, the apparent flux exponent decreases to zero at about 1×10^{16} n/m.^{2}s and apparently becomes negative. Irradiation hardening is insufficient to suppress thermal creep and the strain rate becomes higher than the minimum value.

The sum of the available data indicates that the flux dependency, *p*, varies between about 0.5 and 1.0 in the range of fluxes of most interest for power reactors.

In most experiments it is not possible to separate flux and fluence; the practical expression becomes equation (2.10).

An extensive creep program at 350 °C (623 K), [23], has provided data like those shown Figs. 2–26 for SRA Zircaloy-4. No growth was observed at zero stress as expected from the texture. Therefore, the creep data are "pure irradiation creep". However, there is likely to be a component of thermal creep occurring in addition to

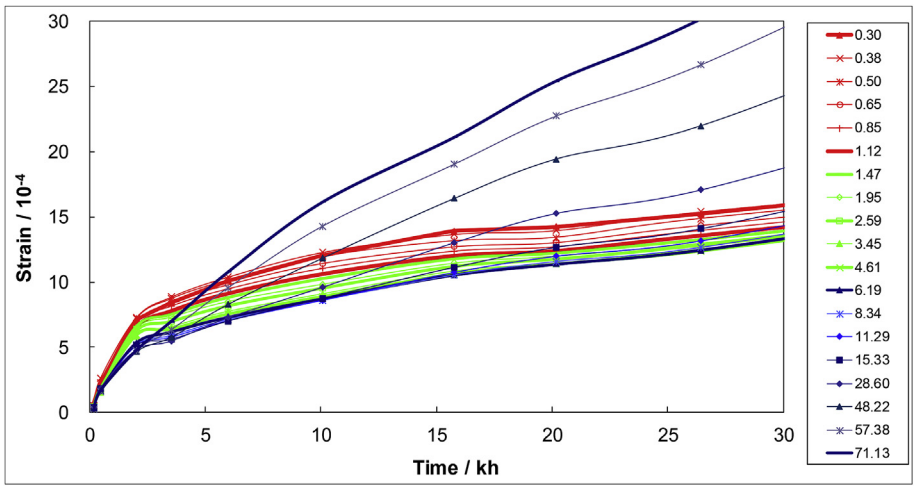

Fig. 2–21. Effect of flux on diametral strains for a Zr-2.5Nb pressure tube. Fast neutron fluxes for each curve are displayed in the legend (units of 10^{15} n/m^2·s), [97].

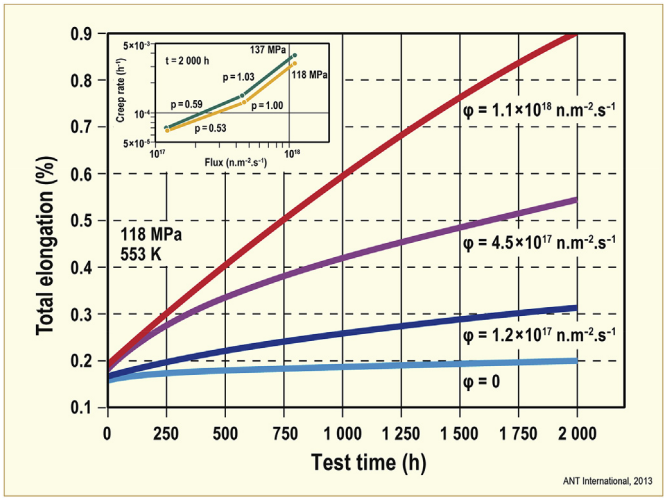

Fig. 2–22. Flux dependence of in-reactor uniaxial creep of cold-worked Zircaloy-2, data modified from Tinti, [98].

irradiation creep.

Values of the constants in equation (2-10) depend on test conditions, but these studies have given what appear to be reasonable values for low burnup at 350 °C (623 K):

m ≈ 0.5, n ≈ 1.6, (Q > 0, from additional data)

At high burnups (>4 × 10^{25} n/m^2) the creep curves tend to become linear with fluence, so the value of *m* becomes 1.0 [58], for Zr-2.5Nb, also showed that for fluence above 1.5 × 10^{25} n/m^2 creep appears to be linear with fluence.

2.5.3. *Effect of cold work (CW)*

The effect of recrystallization or cold work is shown in Figs. 2–27, where the "annealing parameter" is the metric describing the metallurgical state. The trends are clear – in-reactor, cold-worked or stress relieved Zircaloy-4 has higher creep strain than recrystallized material. The opposite occurs for out-of-reactor testing.

$$A = t\ exp\left(\frac{-Q}{RT}\right) \qquad (2-11)$$

where *t* = annealing time.

T = annealing temperature, K
Q/R = 40 000 K

All creep mechanisms depend in some way on the presence or absence of cold-work-induced (as-fabricated) dislocations. Using stress relaxation experiments with no contribution from irradiation growth or thermal creep [101] obtained a creep rate dependence on dislocation density of about $\rho^{0.2}$ at 300 °C (573 K) in Zircaloy. The

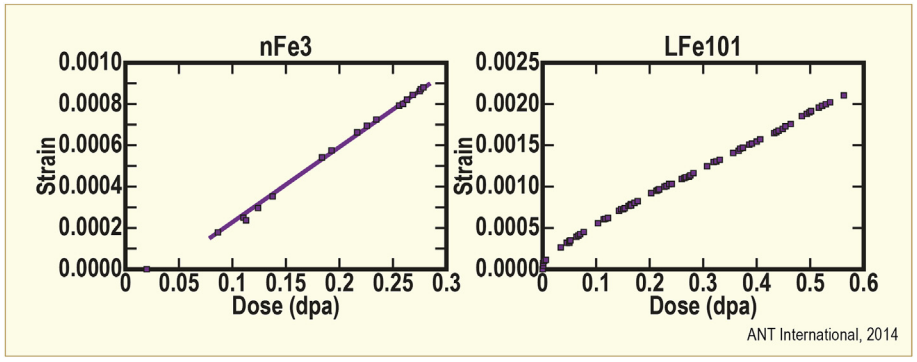

Fig. 2–23. Strain as a function of dose for specimens of different Fe concentration. (nFe3 = 70 ppm; LFe101 = 3 ppm), after [99].

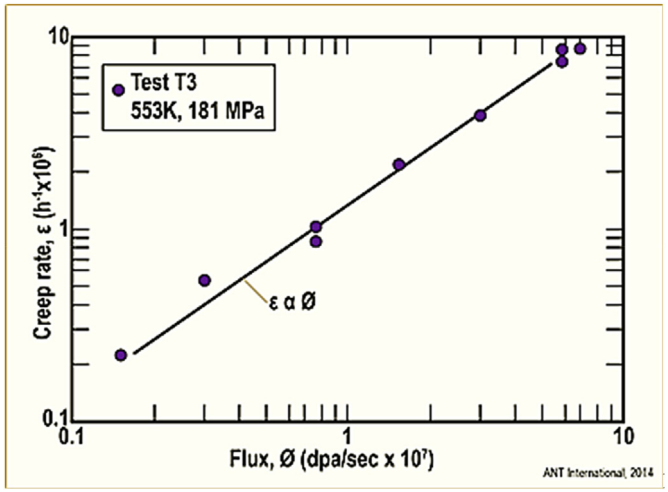

Fig. 2–24. Flux (damage rate) dependence of irradiation creep of Zircaloy-2 during proton bombardment, 91 MPa, 553 K (280 °C), after [100].

experimental data are very limited and are confounded by texture factors. As will be shown later, for irradiation growth, the dependency is more like $\rho^{0.8}$.

The in-reactor relaxation experiments of [74] showed that in-reactor relaxation rates for Zircaloy-4 were much higher than rates out-of-reactor and that relaxation was faster at 310 °C (583 K) than at 60 °C (333 K), Figs. 2–28 and Figs. 2–29. The raw data indicated that cold-worked material relaxed faster than RXA material, and calculations based on a linear stress dependence indicated that 79% cold work increased the low fluence (about 1×10^{25} n/m^2 E > 1 MeV) relaxation rate by a factor of three. At that fluence, the <a> dislocation loop structure would have been well formed, but <c> component loops would not have yet formed in the RXA material. (See mechanism Section 4).

A more definitive effect of cold-work on creep behaviour is shown by the tests of internally pressurized tubes at 350 °C (623 K) in CEA test reactors, [23].

Figs. 2–30 Zircaloy-4 SRA material (presumably about 70% cold work followed by a low temperature anneal) has a higher initial and final creep rate than RXA Zircaloy-4. It is not clear whether or not a steady-state creep rate was reached. For the textures of specimens in this experiment, no diametral irradiation growth would be expected. In this experiment, the RXA M5 (Zr–1Nb) alloy has about the same behaviour as RXA Zircaloy-4.(see.figs2-31)

2.5.3.1. Effect of dislocation density. Cold-work induces dislocations into the material. Dislocation density, ρ, for an RXA zirconium alloy is near 5×10^{13}/m^2 and for fully cold-worked is near 10×10^{14}/m^2. The effect of dislocation density on creep in the range of $1–10 \times 10^{14}$/m^2 appears to be weak: taking creep rate = $K\rho^x$ at 510 K (297 °C), x ≈ 0.23 for Zr-2.5Nb [101], and x ≈ 0.16 for Zircaloy-2 [102], Figs. 2–33. It is noted that for irradiation growth, strain is almost linear, with ρ. In all cases, data are limited and are confounded by texture and microstructure factors.

2.5.4. Effect of temperature

The temperature dependence of in-reactor creep has components based on thermal and irradiation processes. It is generally considered the pure irradiation creep has only a weak temperature dependence (often the process is called "athermal") but thermal processes play an increasingly large role above about 300 °C (573 K). Above about 350 °C (623 K), thermally produced vacancies compete with irradiation-produced defects, and by 400 °C (673 K) thermal processes dominate in-reactor creep. In all cases, increasing temperature, increases creep rates. Analysis of a large amount of data [24], indicates that temperature dependency in the range of 270–400 °C, which encompasses most commercial reactor temperatures, varies and depends on several variables, including cold work, alloy element concentration and fabrication history.

Schematic illustration of the temperature effect is given in Figs. 2–34, after Fidleris [18]. The strong strain aging regime around 350 °C (623 K) observed for unirradiated zirconium alloys does not appear to be present in the in-reactor case. Several specific examples are given here.

The effect of temperature on creep strain of RXA Zircaloy-4 is shown in Figs. 2–35. Trends are the same for 91 and 120 MPa hoop stress. Strain increases as temperature is increased from 320 to 350-380 °C.

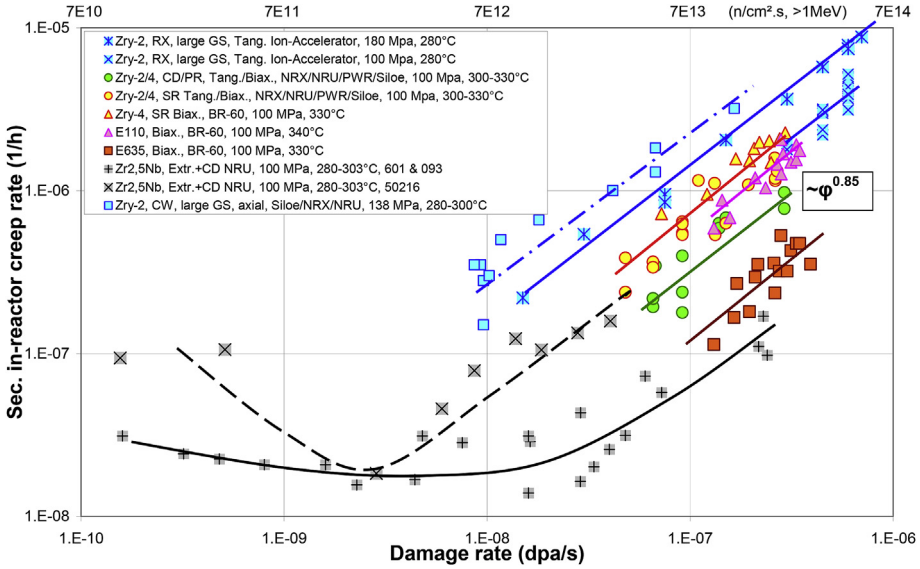

Fig. 2–25. Correlation between in-reactor creep rate and damage rate (≈ fast flux, in-PWR: 1×10^{-7} dpa/s ≈ 6.7×10^{17} n/m.^{2}s, >1 MeV) for certain test conditions and materials at either the given stress or at a stress between 60 and 130 MPa and normalized to 100 MPa (applying a linear stress dependency), based on data in Adamson et al., [24].

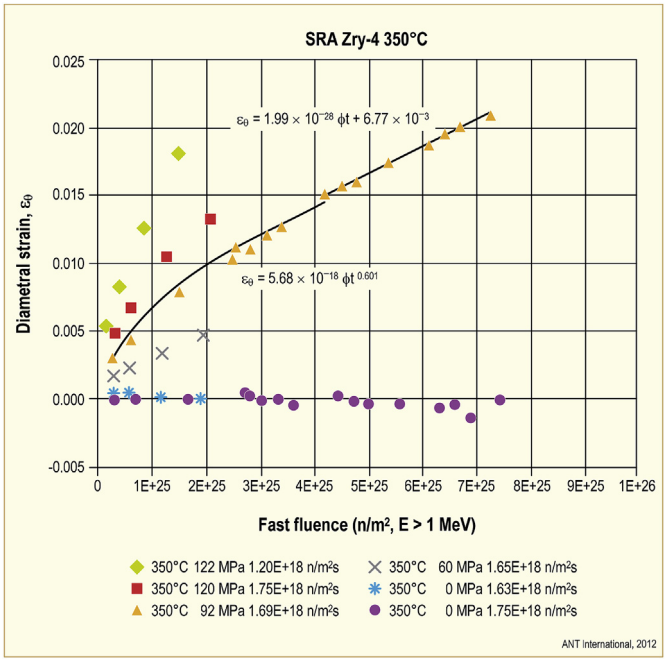

Fig. 2–26. Hoop (diametral,θ) strains vs. fluence for SRA Zircaloy-4 at 350 °C (623 K) in the stress range 0–120 MPa, modified figure according to Ref. [23], (5×10^{25} n/m^2 = 8 dpa).

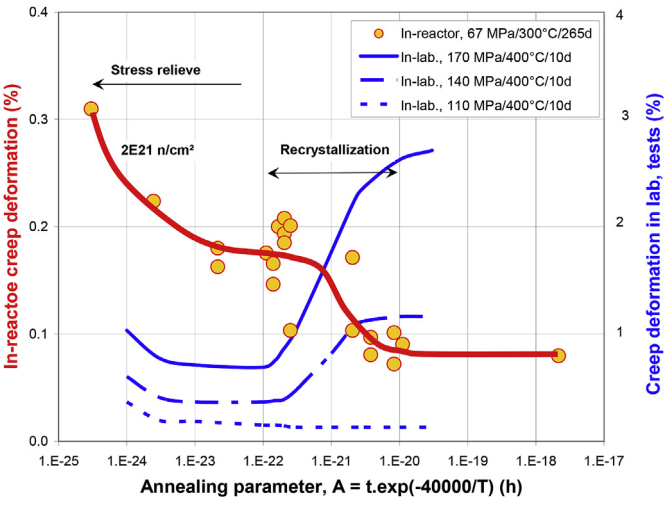

Fig. 2–27. Correlation between final annealing and creep behaviour of about 65% cold-worked Zircaloy-4 fuel cladding for both in-reactor and unirradiated out-of-reactor testing. Recrystallization begins at about A = 1×10^{-22} [24].

The effect of temperature is larger for RXA than for SRA Zircaloy-4. The activation temperature Q/R (equations (2–10)) for RXA is 7200 K and for SRA is 4200 K in these experiments, [23].

An effect of flux is noted at both 320 and 350 °C (623 K), Figs. 2–36, where it is seen that creep strains are lower at the higher flux. For a given attained fluence, higher flux requires less time to reach the fluence; therefore, the contribution of thermal creep to the total would be smaller. It is speculated that thermal creep has a significant contribution to the strain at 320 and 350 °C (623 K) in these experiments.

Another specific example for cold-worked Zircaloy-2, Figs. 2–37, indicate low temperature sensitivity below about 300 °C (573 K) with Q/R between 2000 and 5000 K. At higher temperatures,

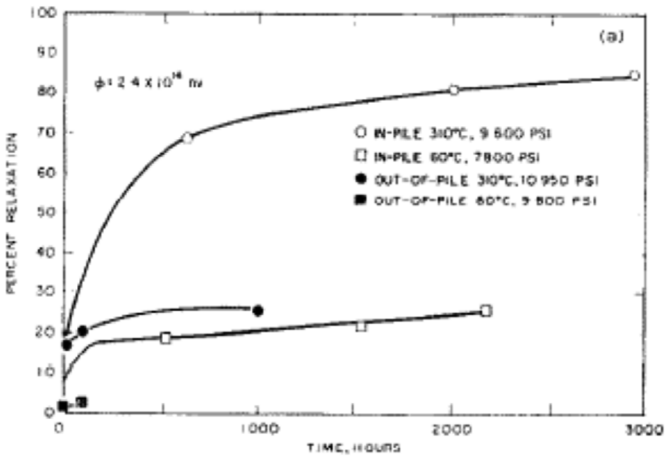

Fig. 2–28. Stress relaxation of RXA Zircaloy-4 [74].

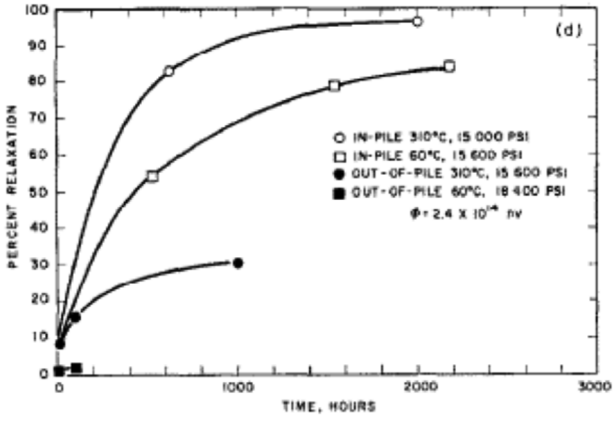

Fig. 2–29. Stress relaxation of 79% cold worked Zircaloy-4 [74].

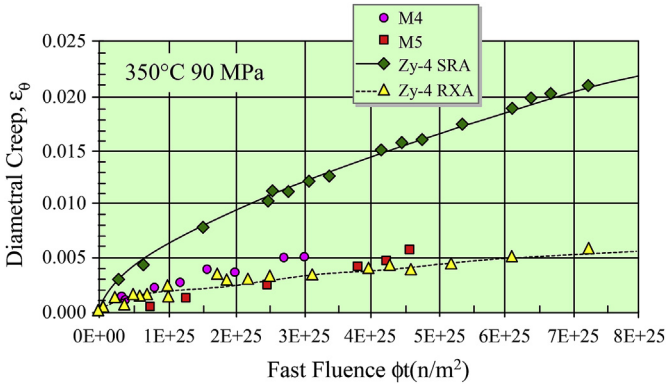

Fig. 2–30. In-reactor diametral creep behaviour of SRA Zircaloy-4 and RXA Zircaloy-4 internally pressurized tubes at 350 °C (623 K), [23]. (M5 is a Zr–1Nb alloy; M4 is a ZrSnFeV alloy). (5×10^{25} n/m^2 = 8 dpa).

sensitivity increases rapidly with Q/R approaching 25 000 K similar to that of tests on unirradiated material in the laboratory.

For cold-worked Zr-2.5Nb, the data indicate similar trends – low sensitivity below 300 °C (573 K), with Q/R rapidly increasing to above 17 000 K [93], Figs. 2–38. Note that CANDU Zr-2.5Nb pressure tubes normally operate between 275 and 315 °C (508 and 590 K).

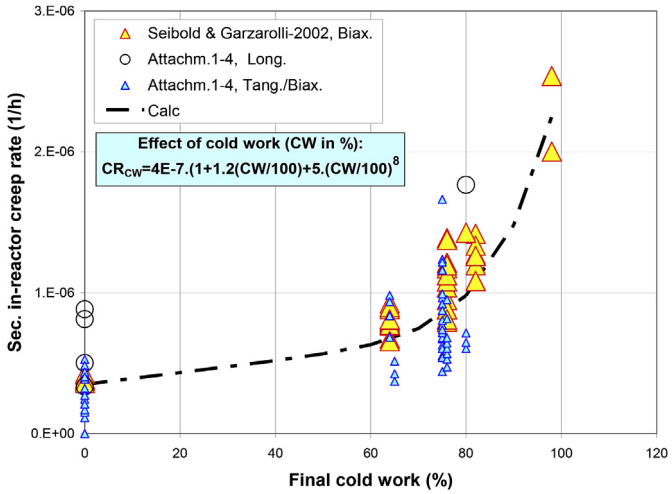

Fig. 2–31. Effect of CW on in-reactor creep behaviour of Zircaloy-2 and -4 applying a large database after conversion to a secondary in-reactor creep rate at a hoop stress of 100 MPa, test flux of 1×10^{18} n/m.^{2}s, temperature about 300 °C (573 K) [24]. The shape of the curve is similar to more restricted data presented by Causey [72], Figs. 2–32, obtained by stress relaxation of bent beams.

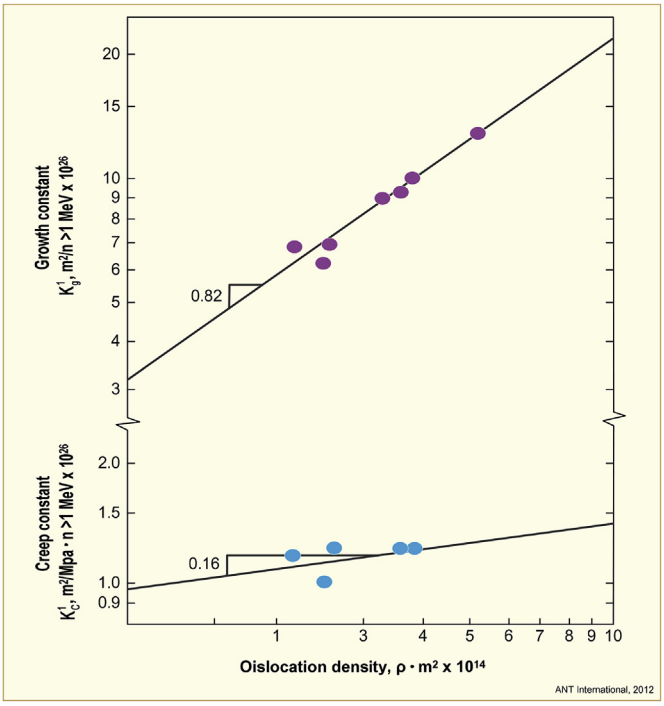

Fig. 2–33. In-reactor creep as a function of dislocation density in cold-worked Zircaloy-2 pressure tubes, [102].

It is noted [58], that temperature sensitivity in the axial direction of tubing is as expected, but in the transverse (hoop) direction appears to have little temperature dependence, Figs. 2–39.

Garzarolli in Ref. [24] plotted data from several materials and conditions, Figs. 2–40 and Figs. 2–41.

For in-reactor creep in the temperature range (275–390 °C), Garzarolli in Ref. [24], surmised:

- The temperature dependency of in-reactor creep of Zry-2/4 depends on the cold deformation.
- RX Zry-2/4 has a moderate temperature dependency with an Activation Temperature (Q/R) of 3500 K under biaxial stress conditions at least up to 380 °C.
- 15–40% CW Zry-2/4 shows a higher temperature dependency with an Activation Temperature (Q/R) of 5500 K under biaxial and uniaxial longitudinal stresses.
- High CW (≥65% CW) Zry-2/4 exhibits an in-reactor creep behaviour that is independent of temperature at least in the temperature range 280–380 °C.
- Zr-2.5Nb CANDU pressure tubes has a high temperature dependency with an Activation temperature (Q/R) of 5500–12

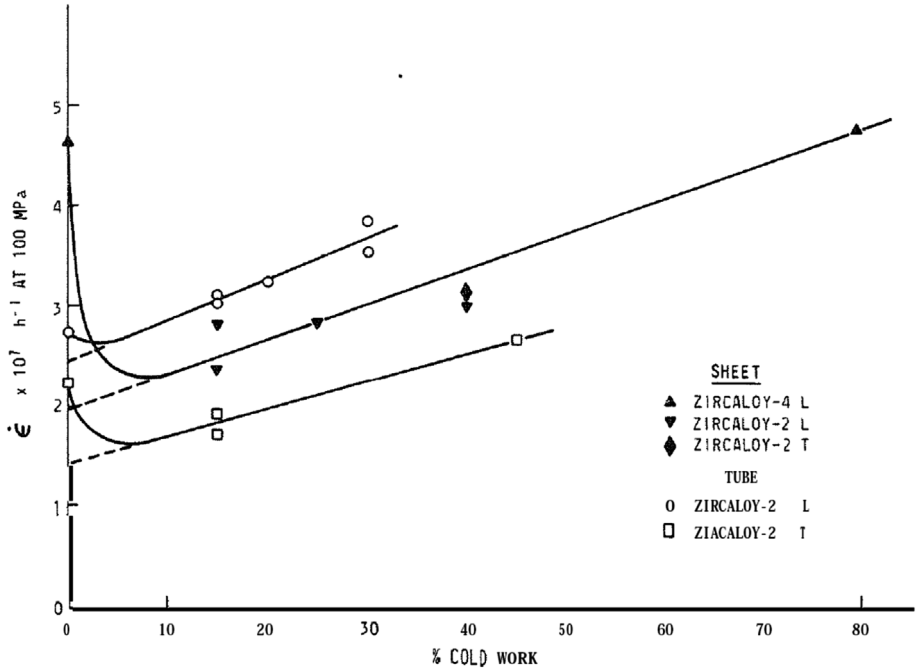

Fig. 2–32. Effect of cold-work on creep rate of Zircaloy [72].

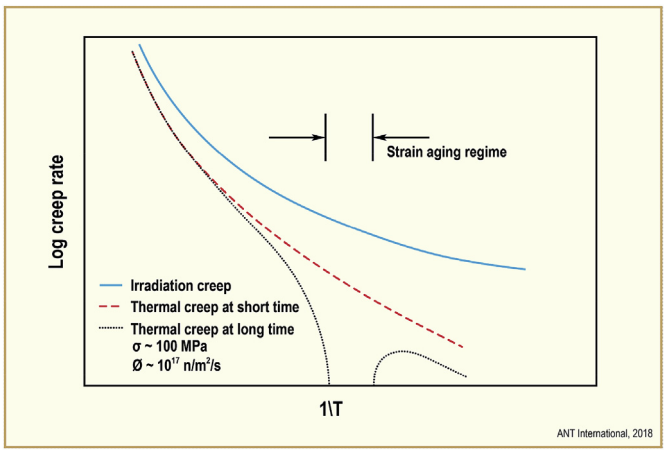

Fig. 2–34. Schematic representation of the temperature dependence of in-reactor creep of cold-worked Zircaloy-2, after Fidleris [18].

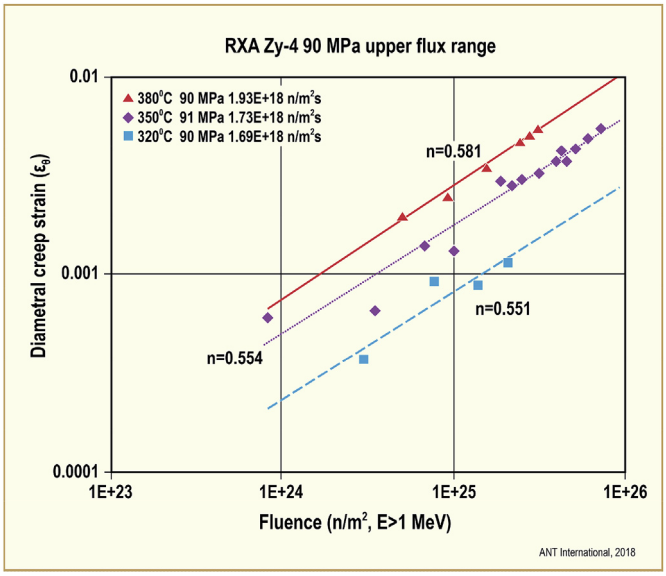

Fig. 2–35. Effect of irradiation temperature on hoop creep strain versus fluence for RXA Zircaloy-4 specimen, in the flux range $\geq 1.59 \times 10^{18}$ n/m^2/s. "n" the exponent on fluence in $\varepsilon = K\,(\phi t)^n$ [23].

000 K, independent of material and stress condition. Zr-2.5Nb with an equiaxed grain structure seems to have a lower activation temperature, similar to that of RX Zry-4.

- M5 under biaxial conditions probably has a similar temperature dependency as RX Zry-4 but E110 exhibits, at least at high axial stresses, a much higher temperature dependency.

The data presented in this Section 2.5.4 indicate that the temperature response appears to depend on specifics of the alloy, material and material conditions, and temperature magnitude. Cold worked (CW, SRA) material has less dependence on irradiation temperature than does recrystallized (RXA) material. Overall, the higher the irradiation temperature, the higher the creep rate.

2.5.5. Metallurgical effects

2.5.5.1. Metallurgical effects – alloying. Early stress relaxation experiments gave insight to both macro- and micro-effects of alloying, [81]. Tables 2–2 compares different alloys with different

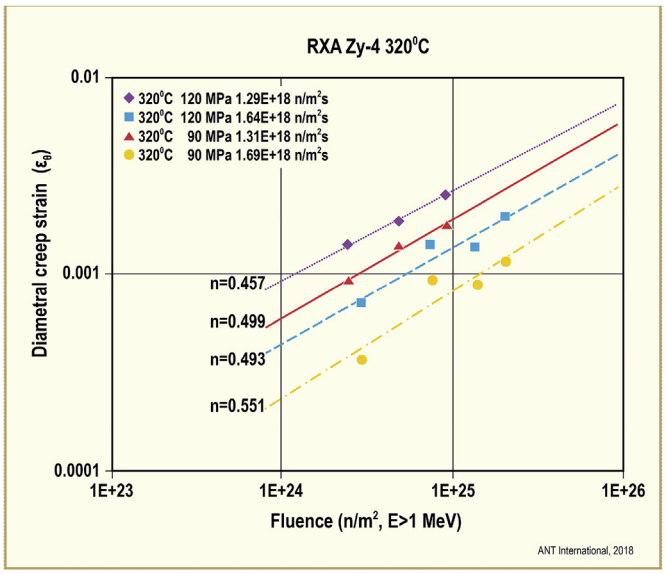

Fig. 2–36. Effect of neutron flux on hoop strain versus fluence for RXA Zircaloy-4 specimens at 90 or 120 MPa [23].

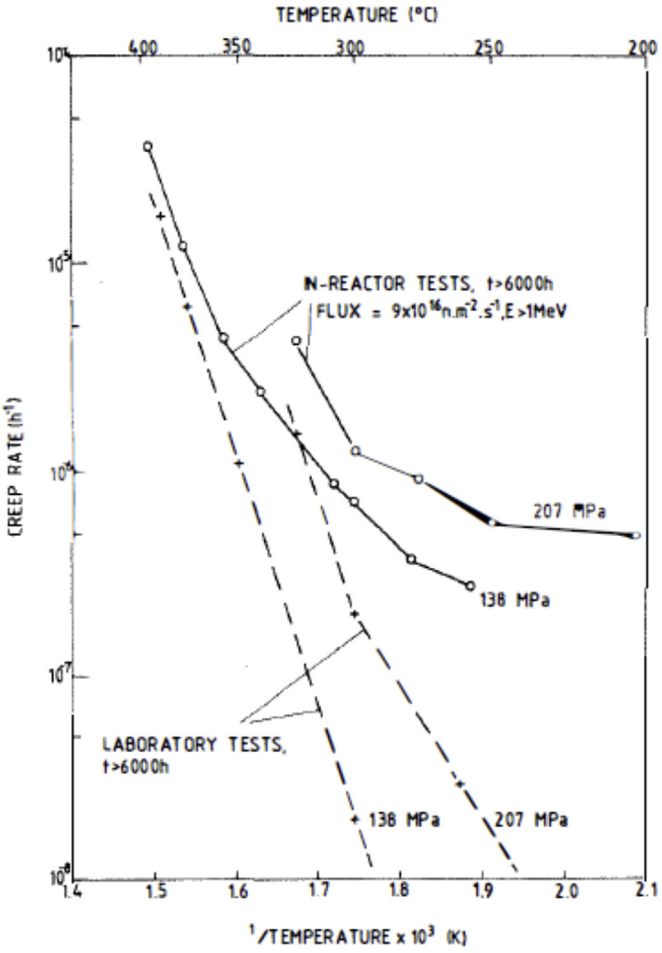

Fig. 2–37. Temperature dependence of laboratory and in-reactor creep rates of cold-worked Zircaloy-2, [18].

microstructures. The Nb-containing alloys having ($\alpha + \beta$)-phases creep less than the α-phase-plus-precipitates Zircaloy. Tables 2–3

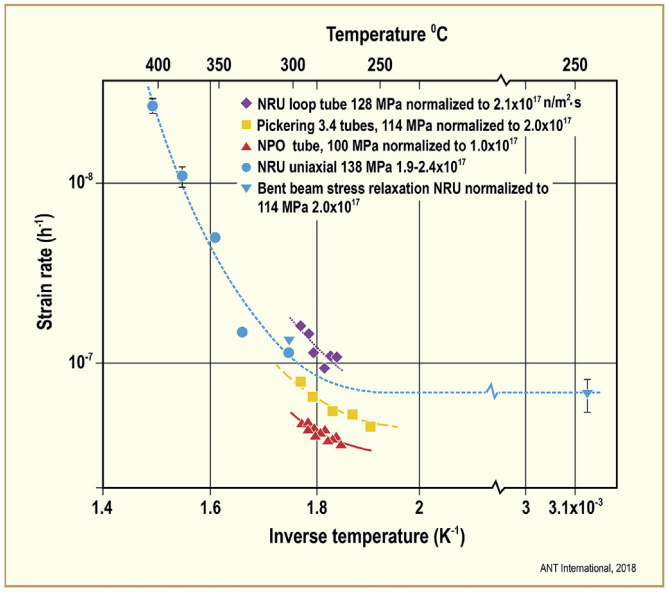

Fig. 2–38. Temperature dependence of the transverse creep rate of cold-worked Zr-2.5Nb pressure tubes and pressure tube material, [33].

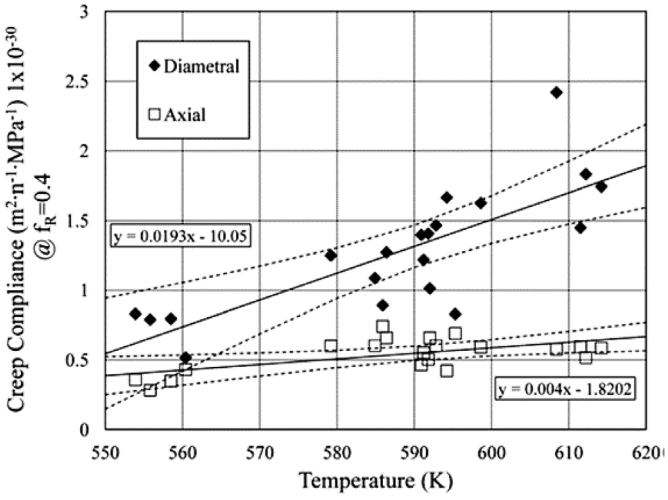

Fig. 2–39. Creep compliance normalized to $f_r = 0.4$ versus temperature. Dashed lines are the 95% confidence interval on the mean value [58].

indicates that solutes in the binary alloys lower the creep rate up to the solubility limit, but have little additional effect above the solubility limit.

A potentially useful quantification of the effect of solutes on creep was proposed by Seibold and Garzarolli [103] and refined by Garzarolli in Ref. [24]. For alloys without extensive beta-phases, which include Zircaloy, Zr–1Nb and Zr–1Sn–1Nb but not Zr-2.5Nb and Excel, the SNO parameter can help predict creep rates. The SNO parameter depends on the assumption (not entirely proven) that solid solution hardening increases creep strength and that up to the appropriate solubility limits, Nb is twice as effective as Sn, and oxygen (O) six times as effective as Sn. Figs. 2–42 illustrates the effect for a variety of alloys. Figs. 2–43 is for a broad range of alloys and separates the data for recrystallized (RXA) (lower solid line) and CW, CWSR (upper solid line) materials. For reference, SNO parameters for various materials, using approximate solubility limits and compositions, are: Zircaloy (2.0), M5 (1.6), ZIRLO™ (2.6),

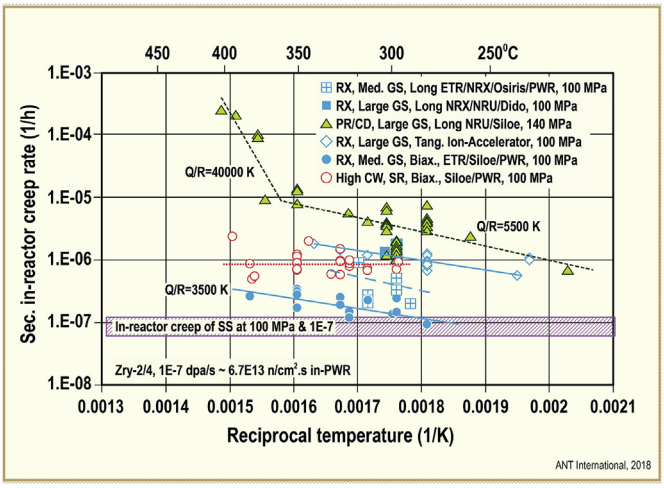

Fig. 2–40. Temperature dependence of steady state in-reactor creep rate of Zircaloy-2 and -4 under biaxial and uniaxial stresses for the given stress normalized to 100 MPa and a damage rate of 10^{-7} dpa/s [24].

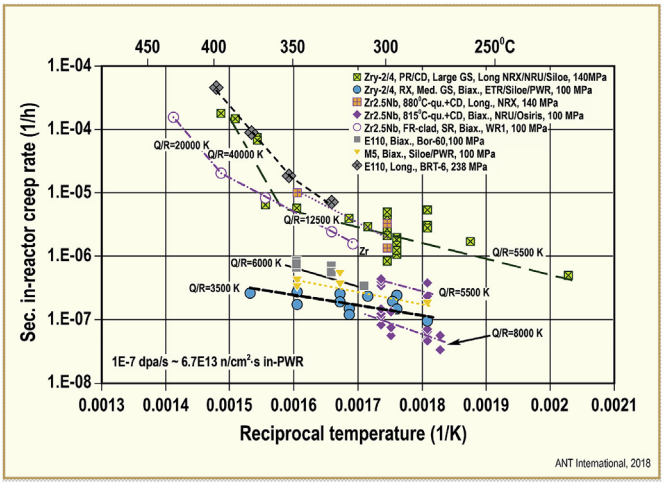

Fig. 2–41. Temperature dependence of steady state in-reactor creep rate of Zr-2.5Nb, M5 and E110 under biaxial and uniaxial.

Tables 2–2
Creep rates of zirconium alloy pressure tubes, by relaxation tests at 570 K (297 °C) and flux 2×10^{17} n/m.^{2}s [81].

Material	Creep rate relative to CW Zr-2.5Nb
CW Zr-2.5Nb	1.0
CW Zircaloy-2	1.1
CW Excel*	0.6
Annealed Excel*	0.4

* Zr-3.5Sn-0.8Mo-0.8Nb.

Excel (4.5). The alloying or impurity elements Fe, Cr, Ni, V, and Cu, are considered to be insoluble and not influential on creep behaviour in this SNO-approach.

2.5.5.2. Metallurgical effects – sulphur. For RXA Zr–1Nb, it appears that small concentrations of S (sulphur) affect the creep behaviour. The solubility limit of S in Zr is about 20 ppm. Creep tests on unirradiated material indicate a substantial increase in creep rate for 1 ppm S compared with 31 ppm S [104, 105, 106]. The mechanism is unclear but is thought to be related to sulphur-dislocation core

Tables 2–3
Creep rates of binary Zr alloys, stress relaxation at 320 K (47 °C), flux 1.6×10^{17} n/m.^{2}s [81].

Solute conc. w/o	Creep rate x 10^{-10} (h^{-1} MPa^{-1})	
	Annealed	CW
Sponge Zr	1.0	2.0
0.15 Nb	0.3	0.6
0.6 Nb*	0.4	
1.0 Nb	0.5	
20.0 Nb	0.4	
0.2 Sn	0.6	1.5
1.5 Sn*	0.1	0.4
5.0 Sn	0.2	0.4

* Lower limit of solubility limit in Zr.

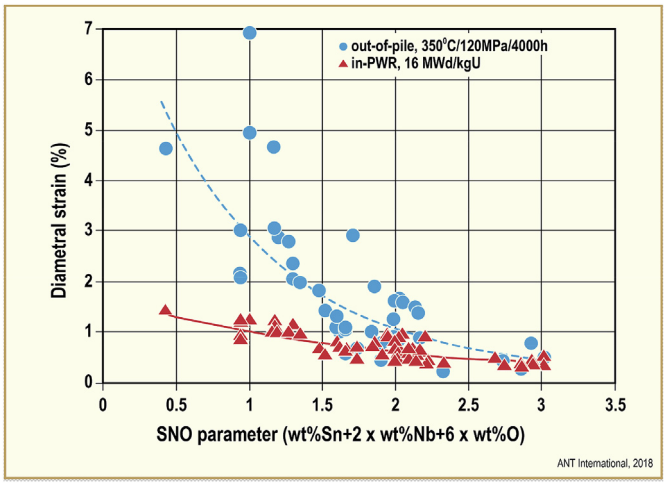

Fig. 2–42. Influence of Sn, Nb and O concentrations on laboratory and in-PWR creep-down of CW experimental Zr-alloy cladding tubes [103], (16 MWd/kgU ≈ 5 dpa).

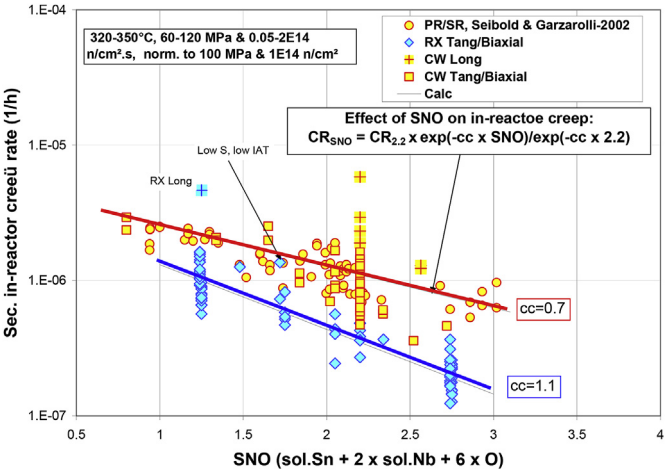

Fig. 2–43. Correlation between SNO and secondary in-reactor creep rates. All data normalized as indicated. Upper solid line (red) for CW and SRA materials, lower solid line (blue) for RXA materials. Details by Garzarolli in Ref. [24].

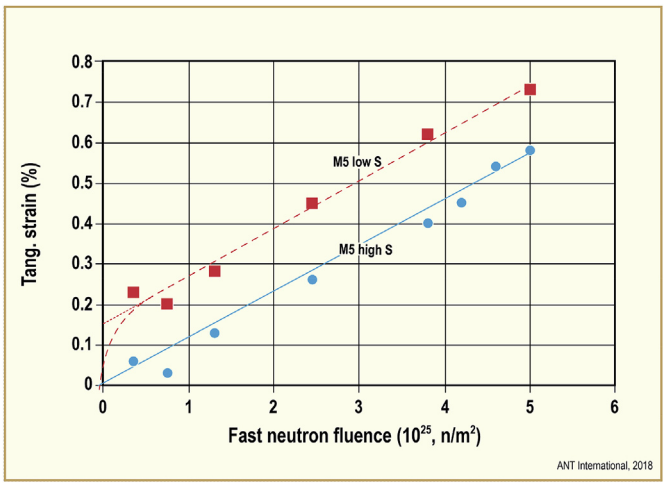

Fig. 2–44. In-reactor creep curves of M5 with high (33 ppm) or low (≈0 ppm) sulphur concentration under biaxial creep, 90 MPa, 350 °C (623 K), and flux of ≈2×10^{18} n/m.^{2}s, E > 1 MeV, updated data from Ref. [23], (5 = 7.5 dpa).

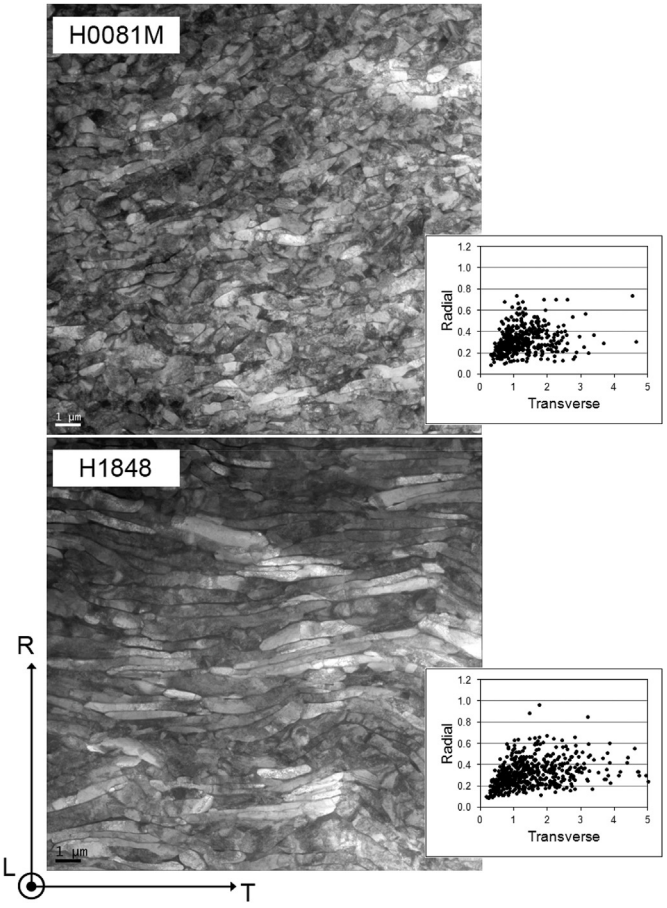

Fig. 2–45. TEM micrographs of Zr-2.5Nb pressure tube cross sections. The inserts are plots of the major and minor axes dimensions in units of μm [58].

interaction that slows dislocation glide and climb [104]. In-reactor, it was observed that the cladding-fuel pellet gap closure occurs earlier for the low sulphur alloy. Data from Ref. [23] replotted in Figs. 2–44, indicates the effect is mainly due to an increased primary creep strain with no effect on secondary creep. Conventional zirconium used for reactor components normally contains low concentrations of S (<1 ppm), but the range for M5™ has been raised to ≈ 20–35 ppm.

2.5.5.3. Grain size and shape. Grain boundaries are important because they can serve as sinks for irradiation-produced defects,

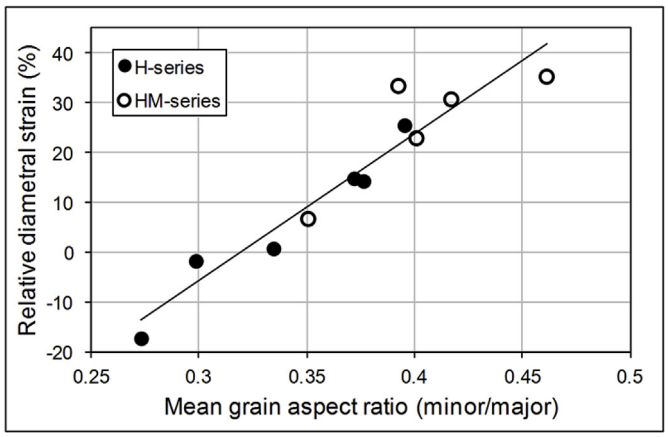

Fig. 2–46. Mean measured aspect ratio and relative diametral strain in Zr-2.5Nb pressure tube material for microstructures such as shown in Figs. 2–45 [58].

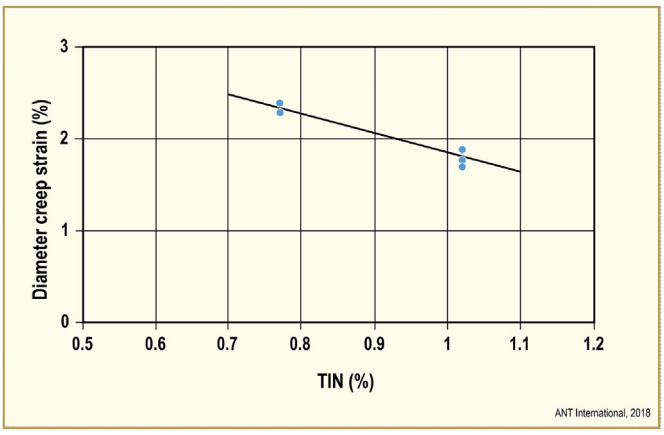

Fig. 2–48. SRA-ZIRLO™ in-reactor creep in biaxial compression as a function of Sn. The ZIRLO™ processing was the same for all materials. The samples were tested in the temperature range of 306–316 °C at hoop stresses - 61 MPa for one cycle of irradiation [110].

thereby influencing the mechanisms of both creep and growth. However, isolating them as an independent variable is difficult due to the variety of thermo-mechanical processes that affect both size and shape of grains. For Zircaloy**,** Franklin et al. [30] and Holt [102], report only small effects on creep, with grain shape being more important than size**.** Kreyns and Burkhart [74] report larger relaxation creep rates in Zircaloy for fine grained, cold-worked and recrystallized microstructure than for larger grained hot-rolled microstructures, but the influence of fabrication variables is not clear. For Zr-2.5Nb pressure tubes, Griffith et al., **[**106, 108] found grain width to be an important variable, with creep rate increasing with increasing width. Walters et al. [58**]** reported the same effect. Figs. 2–45 shows microstructures of two pressure tubes having similar operation histories, texture and dislocation density. Figs. 2–46 illustrates more creep with larger grain widths and high ratio of width/thickness.

Garzarolli in Ref. [109] has analyzed a large amount of data on Zircaloy, with some results given in Figs. 2–47. There appears to be a minimum creep rate in the grain size range 5–10 μm. Grain size of most commercial Zircaloy products are in this range.

2.5.5.4. Metallurgical effects – Sn. The effect of Sn concentration on in-reactor creep is particularly important in that lowered Sn is thought to decrease corrosion.

Lowering Sn concentration increased out-of-reactor creep rates in CW Zircaloy-4 at 399 °C [110**]** and in ZIRLO™ [111] at 380 °C. Foster et al. [111], conducted in-reactor compression creep tests, relevant to creep-down of fuel cladding, on SRA ZIRLO™ cladding tubes whose only difference was Sn concentration. Results indicate a significant increase in creep-down for Sn concentration of 0.77% (wt) compared with 1.02% (wt), Figs. 2–48.

To prevent the loss of creep strength, the heat treatment can be changed from SRA to partially recrystallized (PRX), which is shown to restore the desired creep strength. Figs. 2–49, Garde et al. [111], illustrates the increase in in-reactor creep strength during and after transition of the microstructure from CW Zircaloy-4 (normalized annealing time (A) = 10^{-22}) to fully RXA (A = 10^{-20}), where

$$A = t\ exp\left(\frac{-Q}{RT}\right) \qquad (2-11)$$

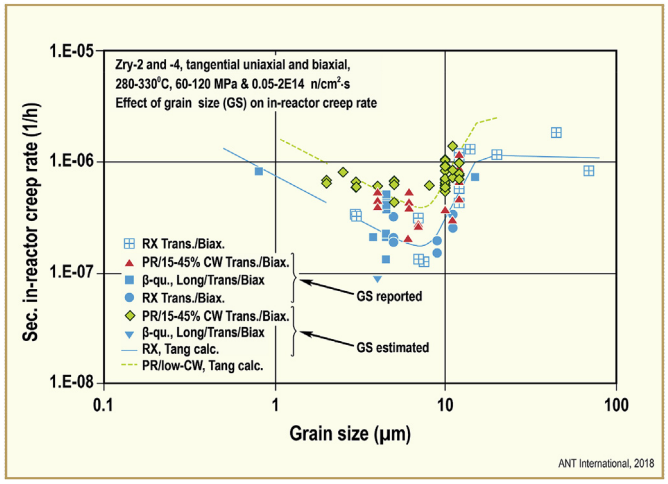

Fig. 2–47. Effect of GS on the tangential uniaxial and biaxial secondary in-reactor creep rate of Zry-2 and -4 at 280–330 °C, 60–120 MPa and 0.05–2 x 10^{14} n/cm.^{2}s, normalized to 100 MPa and 1 × 10^{14} n/cm^2 in an LWR [109].

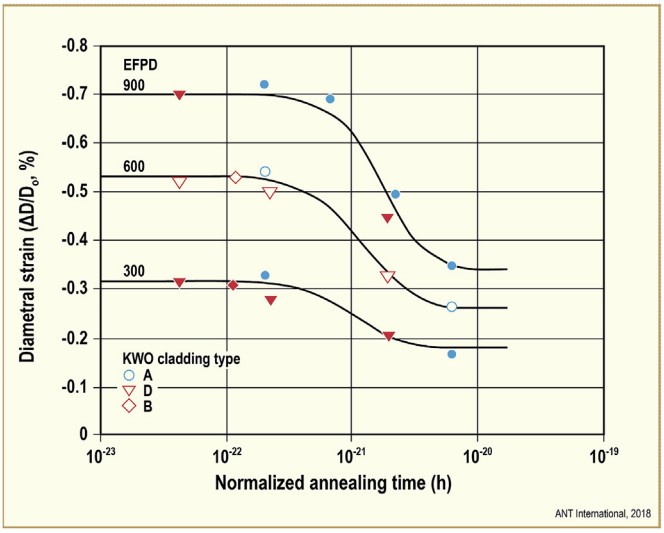

Fig. 2–49. Effect of normalized annealing time on in-reactor diametral creep-down strain of Zircaloy-4 fuel cladding for different resident times (EFPD). Stress is 70 N/mm^2 (MPa), [119].

and.

t = annealing time
T = annealing temperature, K
Q/R = 40 000 K

2.5.5.5. Metallurgical effects – hydrogen. Although it is known that hydrogen (H) concentration above the solubility limit (about 70 ppm at 300 °C (573 K) increases irradiation growth [112], and H in unirradiated Zircaloy does affect creep, H does not appear to affect in-reactor creep.

McGrath and Yagnik [70], conducted axial creep and growth experiments in the Halden Reactor, using pre-irradiated RXA Zircaloy-4 guide tube segments. Individual specimens had hydrogen concentrations between 135 and 700 ppm, applied uniaxial compressive stress was 40 MP, temperature was about 320 °C (593 K) and >1 MeV flux was 3×10^{17} n/m.^{2}s. It was deduced that there was little or no effect of H concentration on the irradiation creep rates.

Foster et al., 2018, conducted in-reactor biaxial creep and growth tests on tube specimens prehydrided with 160–170 ppm H. Irradiation was in a commercial reactor out to a fluence of 16×10^{25} n/m^2 (E > 1 MeV) at about 300 °C (573 K). Hydrogen had no effect on axial or diametral creep of SRA ZIRLO or Zr–1Nb cladding. Effects on growth were mixed, to be discussed in a later section.

2.6. Summary (creep data)

Knowledge of irradiation creep (and irradiation growth) of zirconium alloys, absent at the time of the first naval (1955) and naval/commercial (1957) reactors, has steadily advanced such that today dimensional stability of reactor cores can be accurately predicted. Early in-reactor dimensional measurements were difficult to perform, and still are very difficult, but today experiments can be conducted with dimensional accuracies in the micrometer (μm) range.

Experiments have determined that irradiation creep of reactor components depend on reactor parameters neutron flux (ϕ) and temperature (T), on stress (σ), and on material and fabrication parameters such as texture, dislocation density, cold work and elemental composition. In the ranges most applicable to commercial reactors, effects of the various parameters on creep strain rate have been determined experimentally to be functions of:

- Stress: expressed as σ^n: n is in the range 1–2
- Temperature: for Zircaloy and dilute alloys increases with increasing temperature; for Zr-2.5Nb CANDU alloys, decreases with increasing temperature
- Flux: expressed as ϕ^p:p is between 0.85 and 1.00 for the steady state, decreasing as temperature increases
- Cold-work: generally increases with increasing cold work, but sensitive to texture
- Dislocation density expressed ρ^x: small dependency, x ≈ 0.2
- Composition: decreases with increasing concentrations of solutes Nb, Sn and O, and perhaps, with low concentration of S
- Grain size: for Zircaloys with grain size in the normal range (5–10 μm), only a small effect; for Zr-2.5Nb CANDU pressure tubes decreases with decreasing grain width.

Predictions of creep behaviour are made by either fitting empirical models to creep data or by developing models based on fundamental principles. Both approaches are described in the mechanisms sections in this report.

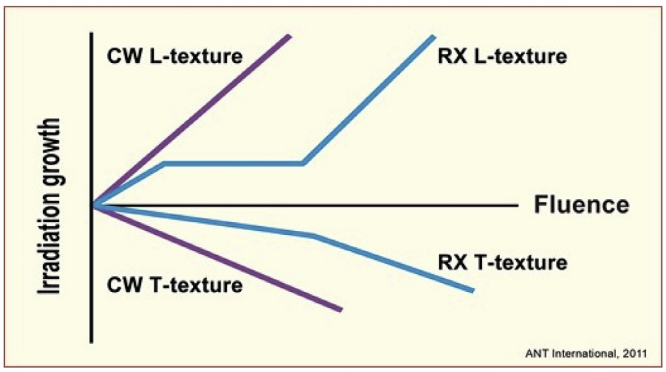

Fig. 3–1. Schematic curves for irradiation growth as a function of fluence (dpa) for tubes made from recrystallized (RXA) and cold worked (CW) zirconium alloys having textures characterized as L (f ≈ 0.1) and T (f ≈ 0.4) and irradiation temperature near 300 °C (573 K).

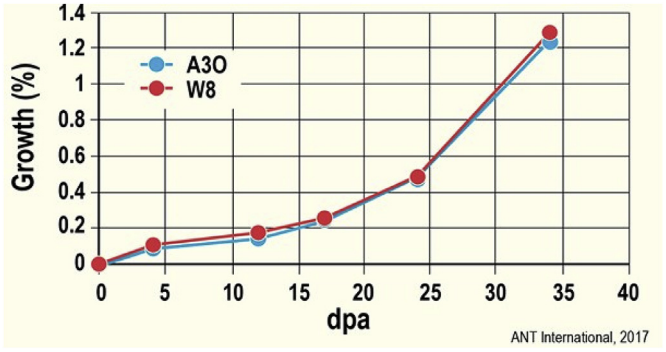

Fig. 3–2. Irradiation growth of RXA Zircaloy-2 at 320 °C (593 K) in BOR60 reactor. Data from Yagnik et al. [113] in Adamson et al., [39].

3. Growth

3.1. Growth curves - generic[3]

Curves of irradiation growth versus fluence (dpa) have the generic shape shown schematically in Figs. 3–1. Throughout this paper the source of the data enabling this summary will be exhibited in a similar format to highlight the contribution of several variables appropriate for operation of power reactors. For recrystallization annealed (RXA) material, growth begins rapidly (stage 1, transient), levels out toward a constant value (stage 2, pre-breakaway), transitions at some critical fluence (dpa) to a high rate (stage 3, breakaway) and at very high fluence (dpa) not shown, to an even higher rate., indicative of a non-linear growth on fluence. For cold worked (CW) material, the rate is high even at low fluence (dpa) and remains high out to high fluence. The various stages relate to radiation-induced microstructural changes (such as <a> and <c>-component dislocation loops) are described in Section 4.1.1. The influence of crystallographic texture is indicated by L, representing the longitudinal or axial direction in fuel cladding and very low Kearns' factor for basal plane normals and "T" representing the transverse or hoop direction in fuel cladding and moderate Kearns' factor for basal plane normals (see Fig. 4).

For RXA Zircaloys, the typical growth curves are shown in Figs. 3–2. For RXA Nb-containing alloys, Figs. 3–3, it is seen that the

[3] Whenever possible, irradiation dose will be expressed as dpa, converted from a fluence, n/m^2, E > 1 MeV, by the factors given in Tables 1–1

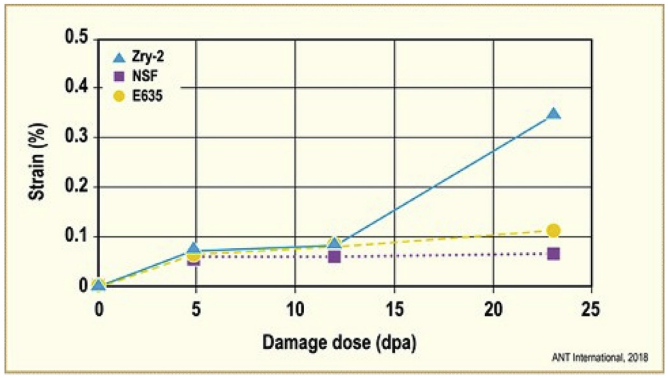

Fig. 3–3. Irradiation growth RXA Zircaloy-2, NSF(Zr–1Sn–1Nb-0.35Fe) and E635 (1.2Sn-1.0Nb-0.34Fe) at 320 °C (593 K) for longitudinal specimens, f ≈ 0.1, Kobylyansky et al., [114].

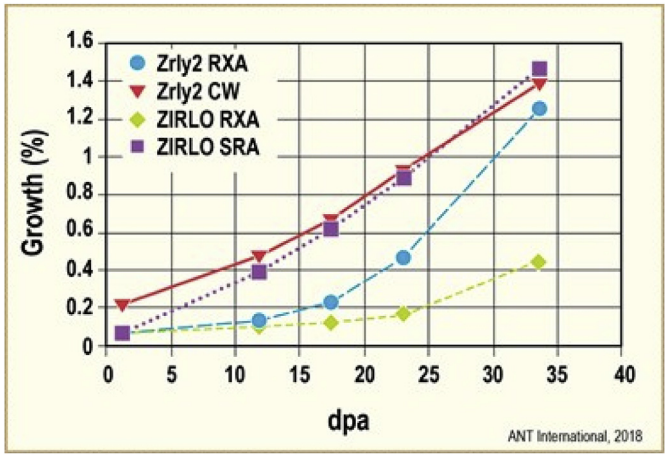

Fig. 3–4. Irradiation growth as a function of dpa for SRA and RXA Zircaloy-2 and ZIRLO™ (Zr–1Nb–1Sn-0.1Fe). Temperature = 320 °C (593 K), f ≈ 0.1. Data from Data from Yagnik et al. [113] in Adamson et al., [39].

pre-breakaway plateau extends to higher fluence (dpa) than in Zircaloy. Note that the pre-breakaway growth strains are about the same for the two types of alloys, ≈ 0.1%. For CW or stress-relieved (SRA) materials, the growth strain is nearly linear with fluence (dpa) and is higher than for RXA out to high fluence (dpa), Figs. 3–4.

Compositions of various alloys used in light water reactors are given in Tables 3–1.

3.2. Previous growth reviews

Many of the creep reviews listed in Section 2.2 also apply to growth. Additional growth reviews are listed in Tables 3–2.

Tables 3–2
Irradiation growth reviews.

1987	[117]	V. Fidleris, R.P Tucker, R.B. Adamson, An Overview of Microstructural and Experimental Factors that Affect the Irradiation Growth Behaviour of Zirconium Alloys, Zirconium in the Nuclear Industry: 7th International Symposium, Adamson, R. B. and Van Swam, L.F.P., Eds., ASTM Spec. Techn. Publ. STP 939, ASTM, pp. 49–85, 1987.
1988	[118]	A. Rogerson, Irradiation Growth in Zirconium and its Alloys, J. Nucl. Mater. 159, pp. 43–61, 1988.(a)
2000	[33]	R.B. Adamson, Effects of Neutron Irradiation on Microstructure and Properties of Zircaloy, Zirconium in the Nuclear Industry: Twelfth International Symposium, ASTM STP 1354. G. P. Sabol and G. D. Moan, Eds., American Society for Testing and Materials, West Conshohocken, PA, 2000, pp.15–31.
2013	[119]	S.I. Choi, J.H. Kim, Radiation-Induced Dislocation and Growth Behaviour of Zirconium and Zirconium Alloys – A Review, Nuclear Engineering and Technology, Vol. 45 (June 2013), 385-392
2018	[120]	A. Rogerson and R.A. Murgatroyd, Long-Term Irradiation Growth in Zirconium Alloys, Zirconium in the Nuclear Industry: 18th International Symposium, ASTM STP 1597, R.J. Comstock and A.T. Motta, Eds., ASTM International, West Conshohocken, PA, 2018, pp. 1–18, https://doi.org/10.1520/stp159720160034.
2018	[24]	R. Adamson, M. Griffiths and C. Patterson, Irradiation Growth of Zirconium Alloys – A Review, ZIRAT Special Topic Report, Advanced Nuclear Technology International, Tollered, Sweden, December 2017.

3.3. In-reactor testing technique

Poolside measurements or visual inspection of core components after service in a power reactor are often used to assess dimensional changes due to all causes.

Length of fuel bundle components (for example, fuel rods, guide tubes, instrument tubes, fuel channels in LWRs) are measured by means of in-pool devices that range from tape measures to calliper-like gages equipped with LVDTs or similar sensors. The length, channel bow and lateral growth of BWR fuel channels, can be measured with appropriate sensors, see Ref. [121].

A non-growth or creep-related dimensional change is induced by hydrides in components. A concentration of 1000 ppm hydrogen (all as hydrides at reactor pool temperature) can cause a dimensional change of about 0.2%, due to the larger specific volume of hydrides compared with that of the zirconium matrix. Hydrogen and hydrides also cause an increase in irradiation growth, to be discussed in Section 3.4.6.1.

In addition to hydrogen effects, the length of a fuel rod is influenced by a combination of irradiation growth, anisotropic creep and creep due to PCMI (pellet-cladding mechanical interaction): in the CW-SRA condition, length change is dominated by irradiation growth, while RXA materials lengthen by both growth and PCMI, [111,122].

Tables 3–1
Nominal compositions of various zirconium alloys used in LWR (light water reactor) experimental programs.

Paper	Composition wt. %						
	Alloy	Sn	Fe	Nb	Cr	Ni	O
[Kobylyansky et al. [114], Yagnik, et al. [113]	Zircaloy-2	1.34	0.17	<0.002	0.1	0.07	0.12
[Kobylyansky et al. [114]	NSF	1.05	0.35	1.05	<0.005	<0.003	≈0.12
[Kobylyansky et al. [114]	E635	1.20	0.34	1.0	<0.003	<0.003	≈0.12
[Bossis et al., [115]]	M5	–	≈0.04	1.0	–	–	0.12
[Bossis et al., [115]] [Yagnik et al., [113]]	Zircaloy-4	1.3–1.5	0.20	–	0.11	–	0.13
[Garde et al. [116]	ZIRLO™	1.02	0.10	1.01	–	–	0.11
	X5A	0.5	0.35	1.0	0.25	–	0.15
	ZIRLO	1.0	0.10	1.0	–	–	0.13

Testing a reactor component provides the opportunity to compare laboratory data and theory with data for power reactor conditions. For example, Mahmood et al. [121], used length measurements taken over many years on a PWR control rod follower plate. To isolate variables, most growth data have been obtained on test specimens irradiated in commercial or test reactors.

As for creep testing, precautions must be taken to control and measure temperature, flux, corrosion and hydrogen pick-up, and absorptions of H from the coolant. Specimens are usually short (<100 mm) and ends must be protected from wear during irradiation. Surface condition must resist hydrogen pickup from the environment, either water, gas or liquid metal. Capsules used to hold specimens must be rugged enough to withstand multiple removals from the reactor. Key components of the measurement device (usually in a hot cell) must be thermally stable relative to the specimen to ensure consistency and reproducibility. The use of proper, dimensionally stable standards is mandatory to insure reliable measurements.

Examples:

- Bossis et al. [115]: Small diameter tube inserted into an empty PWR guide tube. Tube 1200 mm long, with holes in wall each 400 mm, allowing water to flow inside and outside. Hole spacing measured at reactor shutdowns to obtain growth data. Hydriding of tubing material possible.
- Rogerson [118] and Carpenter et al. [123]: Specimens 127 mm long plates inserted into a rigid case, to "prevent bowing" during irradiation and damage to specimen during measurement. Length changes measured by comparing (with two LVDTs) to a master specimen made from an alloy having similar thermal expansion properties as Zr. Maximum measurement error <1 μm, that is 0.001% strain. In-reactor water environment with corrosion and hydrogen pick-up possible.
- Fleck et al., [124]; Holt et al. [125]: Specimens cut from CANDU Zr-2.5Nb pressure tubes (PT): Dimensions 38.1 mm long, 6.4 mm wide and 1.5 or 2.5 mm thick, e.g., rugged specimens. Radiation rig is inserted in-reactor, with water outside and NaK inside. Rig heated by reactor power and by external furnace. Some hydrogen (<50 ppm) picked up during irradiation. Length measurement by a computer-controlled system with two LVDTs. Accuracy was 0.5 μm (0.0013% strain).
- Yagnik et al., [113]; Kobylyansky et al. [114]: Specimens 35 × 6.5 × 0.8 mm plates fabricated from many different alloys. Precision machined irradiation-rig-specimen holder with specimens distributed 360° around the circumference. Heating and temperature control provided by the BOR60 sodium (Na) coolant that flowed inside and outside the specimen holder. Specimens pre-oxidized to prevent hydrogen pickup from the Na. Specimen length measurement compared to a reference gauge by a specially designed device using two opposing sensors (LDT, linear displacement transducers) with overall resolution of 2 μm which is 0.006% strain. No oxidation or hydrogen pick-up during irradiation at 320 °C (593 K).

3.4. Data

3.4.1. Texture effects

Section 1.2 briefly discusses texture effects in zirconium alloys. As indicated in Section 1.2, the growth strain in any given direction of a poly-crystalline zirconium alloy can be related to the crystallographic texture and is proportional to a growth anisotropy factor G_d given by Equation (1.4):

$$G_d \propto 1\text{-}3f^c_d$$

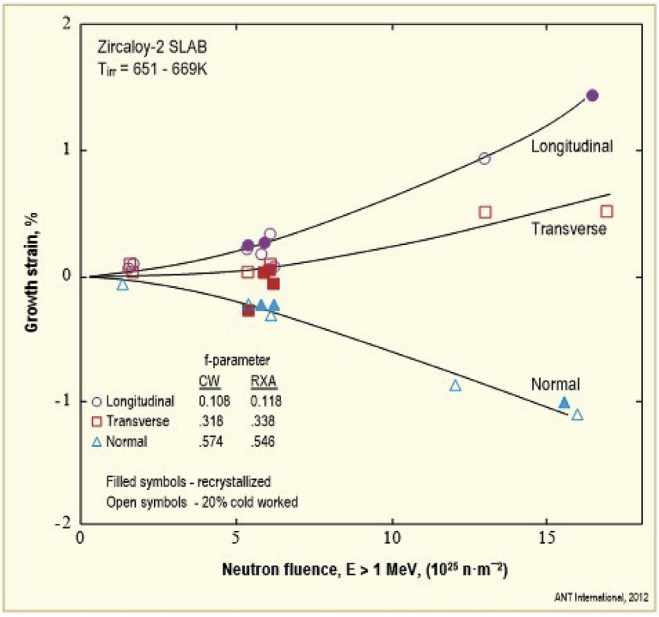

Fig. 3–5. Dependence of growth on neutron fluence in three orthogonal directions at irradiation temperatures in the range 651–669 K, after [Tucker et al., [126]], (10×10^{25} n/m^2 ≈ 30 dpa).

The trend was demonstrated by the early high temperature (387 °C [660 K]) experiments of **Tucker et al.,** [126], Figs. 3–5. For "low" f-values (f ≈ 0.1) growth is positive and large; for "high" f-factors (f ≈ 0.6), growth is negative and large.

Note that for $f_d = 0.333$, $G_d = 0$. For a beta-quenched zirconium alloy, ideally $f_d = 0.333$ in all directions, giving zero growth in all directions out to very high fluence (dpa) in the absence of specimen hydriding (Figs. 3–6 and Figs. 3–7). Also, for typical fuel tubes, texture in the hoop direction is close to $f_t = 0.333$, giving very little growth, Figs. 3–5.

Other data at 320 °C (593 K) are given in Section 3.4.8, where it is shown that experimentally measured volume change is very nearly zero.

3.4.2. Zircaloy

For similar metallurgical structures, growth of Zircaloy-2 and Zircaloy-4 are expected to be similar. Tables 3–3 lists some experiments that provide data for evaluations. In Figs. 3–8, the two Zircaloys are seen to provide similar results. There are exceptions: in Tucker et al. [126] at high temperature and in Yagnik et al. [113], for Zircaloy-4 with non-standard (high carbon) compositions.

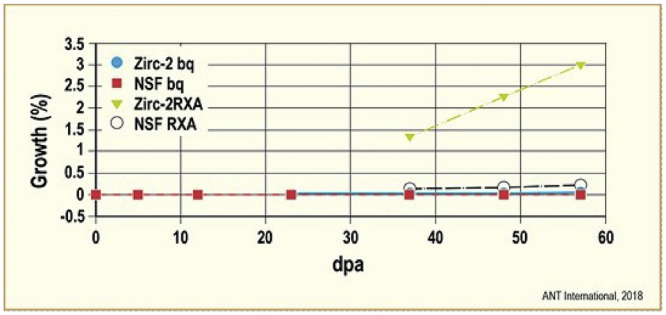

Fig. 3–6. Growth of longitudinal specimens of Zircaloy-2 and NSF having been beta quenched (f ≈ 0.33) or recrystallized (RXA) (f ≈ 0.1). Irradiation temperature was 320 °C (593 K) [Kobylyansky et al., [114]]. and [Yagnik et al., [113]].

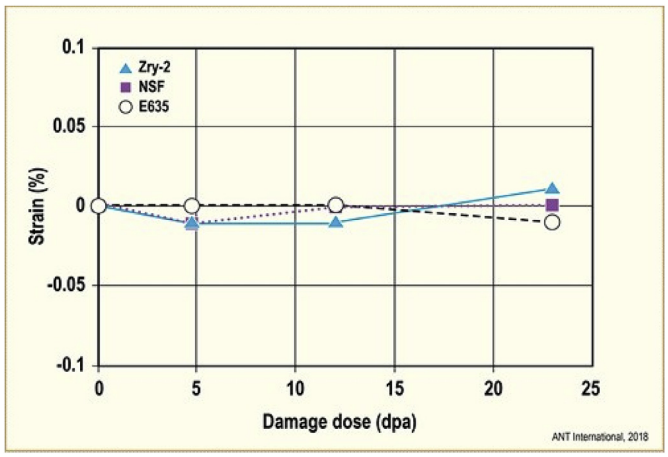

Fig. 3–7. Growth of longitudinal beta-quenched samples ($f_l \approx 0.33$). Irradiation temperature 320 °C (593 K), Kobylyansky et al., [114].

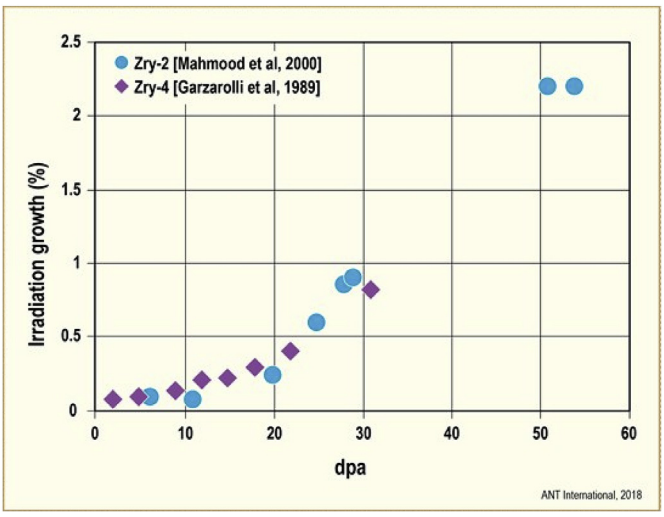

Fig. 3–8. Irradiation growth comparison between RXA Zircaloy-2 and Zircaloy-4 from experiments in Tables 3–3.tbl3c

Data on Zircaloy-4 are shown in Figs. 3–9, [130]. Among the features to note are:

1. The fluence is low, only about 3 dpa;
2. Growth is negative for high texture factor (f) and positive for a low texture factor;
3. there is a complicated temperature dependence
4. the growth appears to saturate with fluence.

Feature 4 extrapolated to high fluence would be very misleading for component design application. Newer data from Rogerson [118], showed that a "breakaway" occurred at a moderate fluence (≈10 dpa in this case), but if the Rogerson data were extrapolated, they fall below the even newer data given in Figs. 3–10 and the RXA Zircaloy-4 data of Garzarolli [127], Figs. 3–8.

Data plotted to the highest fluences obtained, and fitted with a polynomial, Figs. 3–11, give a reasonable expectation of growth of RXA Zircaloy over a wide range of fluences. In Figs. 3–11, however, the effect of hydrogen is seen to be detectable, to be discussed in Section 4.3.6.1.

For calibration to commercial reactors, a typical maximum fluence for a light water reactor fuel assembly (LWR) is about 2×10^{26} n/m^2 E > 1 MeV, or 31 dpa.

3.4.3. Alloying elements

3.4.3.1. Nb-containing alloys. PWRs have mainly switched from SRA Zircaloy-4 to an Nb-containing alloy for fuel cladding because of concerns for corrosion at high burnup, for example, Bossis et al., [115]. Typical alloys are listed in Tables 3–4. As shown in Figs. 3–12, adding Nb dramatically reduces growth relative to Zircaloy, primarily by delaying the transition to the breakaway growth region. One other consideration is that Nb results in a lower defect production efficiency than for Zircaloy, see Section 4. For these particular materials, TEM (transmission electron microscopy) shows that the density of radiation-induced <c>-component dislocation is also reduced relative to Zircaloy at a given fluence.

Growth of the M5 alloy, having no Sn, is also reduced relative to Zircaloy-4, Figs. 3–13. In this case, specimens were irradiated in BWR water, and hydrogen pickup (HPU) in the Zircaloy-4 increased growth a small amount (see Section 3.4.6.1). Bossis et al. [115], also found a low density of <c>-component dislocation in M5 at 18 dpa, 10X lower than for Zircaloy-4.

In an inert environment, the Yagnik et al. [113] experiments, comparison were made between Zircaloy-2 and various Nb-containing alloys. Nb-additions appear to delay breakaway to above 15 dpa and to reduce the post-breakaway growth rate relative to Zircaloy. An example is shown in Figs. 3–12 for data extracted from Yagnik et al., [113]. The main differences in growth rate between alloys occurs after the breakaway initiation, and that differences become larger as fluence (dpa) increases.

3.4.3.2. Tin (Sn). In light water reactors (LWR), Sn is often added, as an alloying element, in the range 0.5–1.5% (by weight). As noted in the creep section of this review, increased Sn results in increased creep strength. Effects on growth are not as clear as they are for creep.

Early data indicated that higher Sn resulted in higher growth for Zr1.5%Sn compared with Zr0.1%Sn, the difference mainly is due to increased initial transient growth for the higher Sn alloy, Figs. 3–14. Also, breakaway appeared at about 4×10^{25} n/m^2 with the higher concentration of Sn. These alloys had very low Fe and O (oxygen) concentrations and unknown concentrations of other impurities,

Tables 3–3
Irradiation growth experiments and data for Zircaloy (RXA).

Reference	Material, (Sn, w/o)	Reactor	Temp, °C	Grain size, microns (μm)	Texture (fL)	H	Environment
[Garzarolli et al. [127]	Zirc-4, (1.5)	PWR	300	3–7	0.045	?	Water
[Rogerson [118]	Zirc-2, (1.5)	DIDO	280	20	0.100	10	Inert gas
[Mahmood et al., [128]]	Zirc-2, (1.5)	PWR	290	15	0.060	50–85	Water
[Morize et al. [129]	Zirc-4 (1.5)	PWR	315	?	0.190	<50	NaK
[Bossis et al., [115]]	Zirc-4 (1.3–1.5)	PWR	315	?	0.065	<1600	Water
GNF [Kobylyansky et al., [114]]	Zirc-2, (1.3)	Fast BOR60	320	6	0.090	<50	Na
A30 [Yagnik et al. [113]	Zirc-2 (1.3)	Fast BOR60	320	6	0.100	<50	Na

ANT International, 2017.

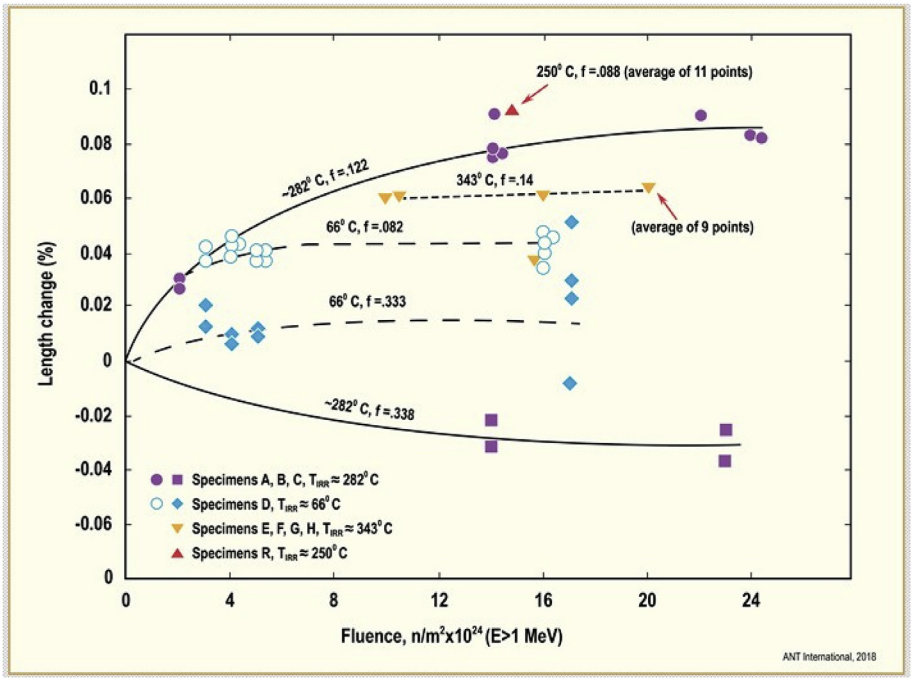

Fig. 3–9. Growth of Zircaloy-4 as functions of fluence, texture (f) and irradiation temperature [130], (20×10^{25} n/m^2 ≈ 3 dpa).

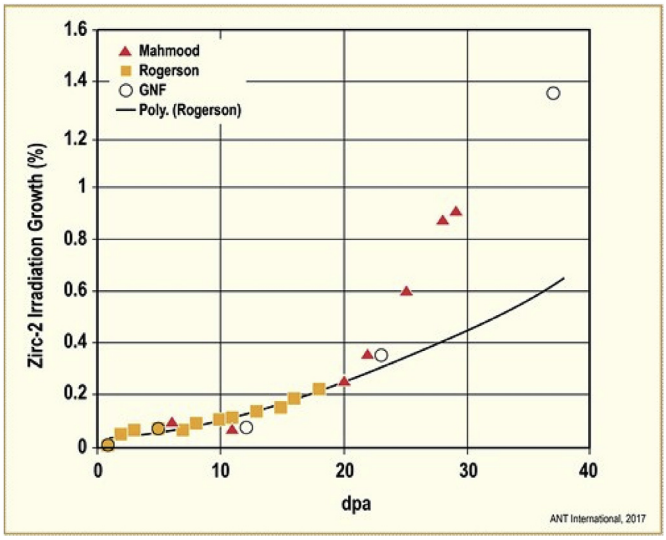

Fig. 3–10. Irradiation growth of Zircaloy-2 from experiments listed in Tables 3–3

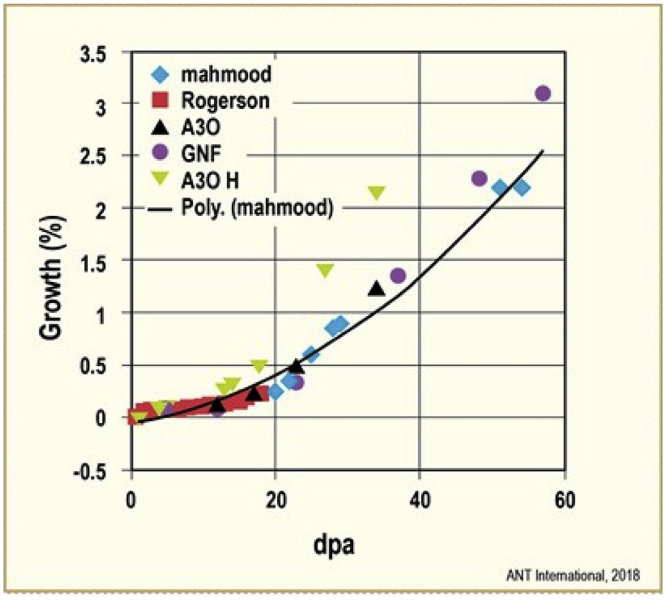

Fig. 3–11. Irradiation growth of Zircaloy-2 between 290 and 320 °C from experiments listed in Tables 3–3 Specimen A3OH has high hydrogen.

including carbon (C) and had grains about 2–10 times larger than most fuel cladding. It is not clear how, or if, those metallurgical factors influenced the results.

An extensive set of data on length change of SRA PWR fuel rods [103] also indicated that higher Sn results in higher length change. Figs. 3–15 reveals a large difference in length change for rods having 0.25%Sn compared with 1.55%Sn, with the differences starting after low burnup (15 MWd/kgU or about 5 dpa) at breakaway. Without knowing more details (power history, corrosion and hydriding, anisotropic creep, pellet-cladding interaction (PCMI), it is not possible to ascribe all the length change to growth. In support of the data, **Baty et al.,** [122]**,** have shown that for SRA rods with biaxial compressive stresses, like fuel rods before pellet-cladding contact, axial strain is primarily due to irradiation growth; whereas for RXA rods axial strain is primarily due to anisotropic creep, Figs. 3–16. See Figs. 3–23 for stress-free growth of these rods.

More recent experiments explored the effect of Sn and Fe on growth at 320 °C (593 K) of ZrNbSnFe alloy coupons with well controlled chemistry, Figs. 3–17 and Figs. 3–18, [113]. In every case, the higher Sn alloy had the lower growth. The effect is small, and is observable only at high fluences, > about 20 dpa, after breakaway. In the measurement direction, $f_d \approx 0.1$.

In summary, the available data are conflicting, but decreasing Sn in ternary and quaternary alloys has a small effect on increasing growth.

Tables 3–5
Recovery of irradiation growth by post-irradiation thermal annealing.

Reference	Material condition	Growth, %	Growth recovery, %	Approximate fluence, 10^{21} n/cm^2	Temperature, °C	
					Irradiation	Annealing temperature for time, hr
[Adamson, 1977]	RXA	0.09	0.09	2.2	260	510/30
	RXA	0.06	0.06	1.4	343	510/30
	20% CW	0.10	0.06	1.4	343	510/30
	20% CW	0.18	0.08	2.5	283	510/30
	78% CW*	0.14	0.06	1.0	278	510/30
	78% CW	0.22	0.10	1.3	239	510/30
	78% CW*	0.50	0.09	3.3	244	510/30
[Garzarolli et al., 1989]	RXA	0.11	0.08	4	295	500/24-48
	RXA	0.19	0.08	8	295	500/24-48
	RXA	0.38	0.08	16	295	500/24-48
						ANT International, 2012

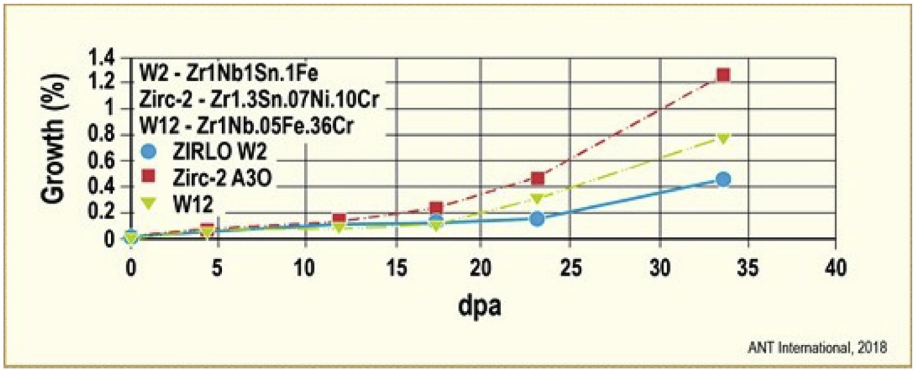

Fig. 3–12. Comparison of growth for RXA alloys with and without Nb additions. Irradiation is at 320 °C (593 K) in an inert environment. Data extracted from [Yagnik et al., [113]].

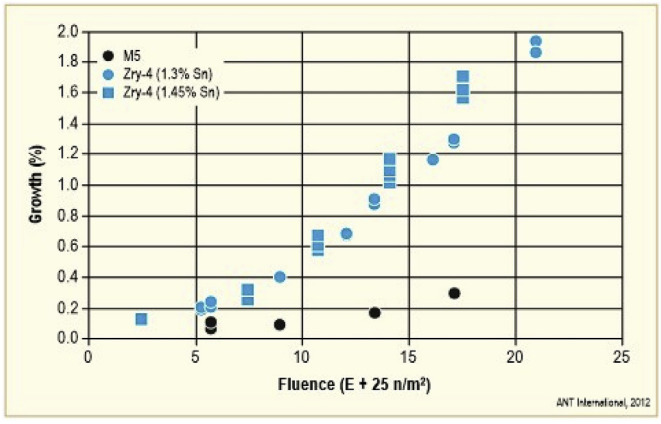

Fig. 3–13. Axial growth of RXA Zircaloy-4 and M5 tubing at 315 °C (578 K) [115], (10×10^{25} n/m^2 ≈ 15 dpa).

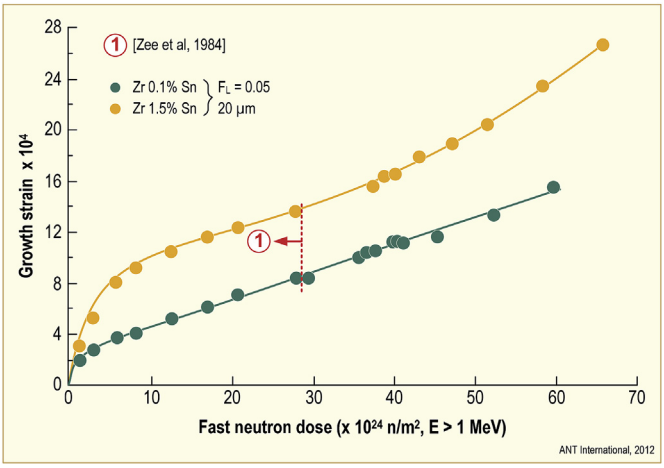

Fig. 3–14. Irradiation growth in Zr0.1Sn and Zr1.5Sn at 553 K (280 °C) [118], (60×10^{24} ≈ 10dpa).

3.4.3.3. Iron (Fe). Iron is an alloying element in some zirconium alloys. For the Zr–1Nb alloys (E110, M5) the range is specified as 300–500 ppm, although early versions of E110 could have lower Fe concentrations. For the Zircaloy-type alloys the specified Fe concentration range is 2000–4000 ppm and for the ZrSnNb alloys the current range is 1000–4000 ppm. The effect on growth is substantial, Figs. 3–17 and Figs. 3–18 and further illustrated by the following examples:

- E110 (Zr–1Nb) undergoes accelerated growth for Fe concentrations less than about 400 ppm at > 20 dpa (about 1.3×10^{26} n/m^2 >1 MeV, PWR equivalent). Figs. 3–19 gives data for Fe concentrations and fluence [132].
- Zr-2.5Nb pressure tube material has lower axial growth when Fe concentration doubled to 1000 ppm, Figs. 3–20. The difference in growth increases with fluence [93].
- M5™ (≈400 ppm Fe) has only slightly higher growth than M5-Fe (1000 ppm Fe) at > 20 dpa, [133].
- Zircaloy-types have lower growth with higher Fe concentrations, Tables 3–4, [113]. The effect is largest at > 20 dpa.
- Yagnik et al. [113], also showed a reduction in growth for a variety of alloys having 100, 500, 1000 and 4000 ppm Fe additions, Figs. 3–17. Particularly susceptible was the Zr–1Sn alloy; smaller but consistent effects were observed for Zr–1Nb–1Sn

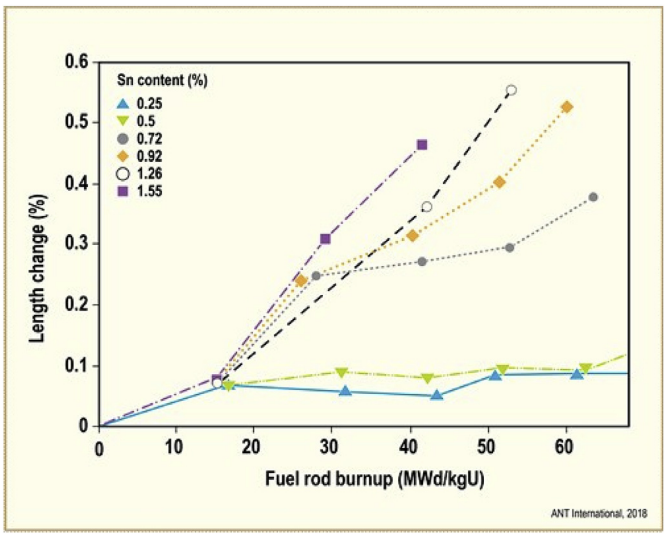

Fig. 3–15. Length change PWR fuel rods with Zr–Sn–FeCrV cladding having different Sn-concentrations, partial data from [Seibold & Garzarolli, [103]], (60 MWd/kg U ≈ 18 dpa).

and Zr–1Nb alloys, all having smaller growth for higher Fe additions.

Fe in zirconium alloys has a strong influence on diffusion processes, greatly enhancing Zr self-diffusion by lowering the migration energy of vacancies [134]. Fe is proposed to interact with vacancies and with interstitials even though the size factor is not favourable, [135]. Calculations indicate Fe may induce vacancy formation (or strongly attract vacancies) relative to the equilibrium number at a given temperature [136]. Ab initio or atomistic modelling computational approaches to understanding these phenomena are showing progress [137–139].

3.4.4. Cold work

As indicated in Figs. 3–1, cold work (CW) or cold work followed by stress relief anneal (SRA) has a large effect on the amount of growth and its rate. The early data are shown in Figs. 3–21 and Figs. 3–22 [130]. These data at low fluence indicate that growth increase is almost linearly related to percent cold work. (Although not specified in the figures, all specimens were given a stress relief anneal before irradiation). Holt [140] measured the dislocation density, ρ, of Adamson's Zircaloy-4 specimens and calculated that growth rate varied with $\rho^{0.82}$, the same as for Zr-2.5Nb pressure tubes shown earlier in Figs. 2–33.

Baty et al. [122] provided data for unstressed fuel rods, Figs. 3–23, confirming the trends of Adamson's results.

Garzarolli et al. [127] compared RXA, PRX (intermediate between RXA and SRA) and SRA (about 70% CW) Zircaloy-4, Figs. 3–24, at high fluence. Except for β-quenched material, it is clear that materials with similar textures, but different heat-treatment histories, have different growth behaviour.

Both Holt et al. [125] and Rogerson [118] report that growth rate for cold worked Zircaloy-2 pressure tubes increased slightly with fluence and attributed increase in growth rate to a measured increase in <c> component density with fluence.

A direct evaluation of the effect of cold work has been reported by Yagnik et al. [113], with materials being irradiated at 320 °C (593 K), Figs. 3–4 and Figs. 3–25. For Zircaloy-2 and ZIRLO™ alloys, the CW (cold worked) or SRA (cold worked plus stress relief anneal) materials grow at a high and almost constant rate, while the RXA material have the typical pre- and post-breakaway behaviour.

The growth curves for Zircaloy-2 and ZIRLO™ (Zr1Nb1Sn.1Fe) that had been cold worked are very similar, whereas the RXA materials have different post-breakaway growth rates, Figs. 3–4. Using the common assumption that <c>-component dislocations and loops are responsible for high growth rates, it appears that pre-irradiating cold worked material introduces the requisite c-dislocations in both alloys but in RXA materials an incubation fluence is required. See Section 4 of this report for more details on mechanisms. Figs. 3–25 illustrates that at 33 dpa the amounts of growth

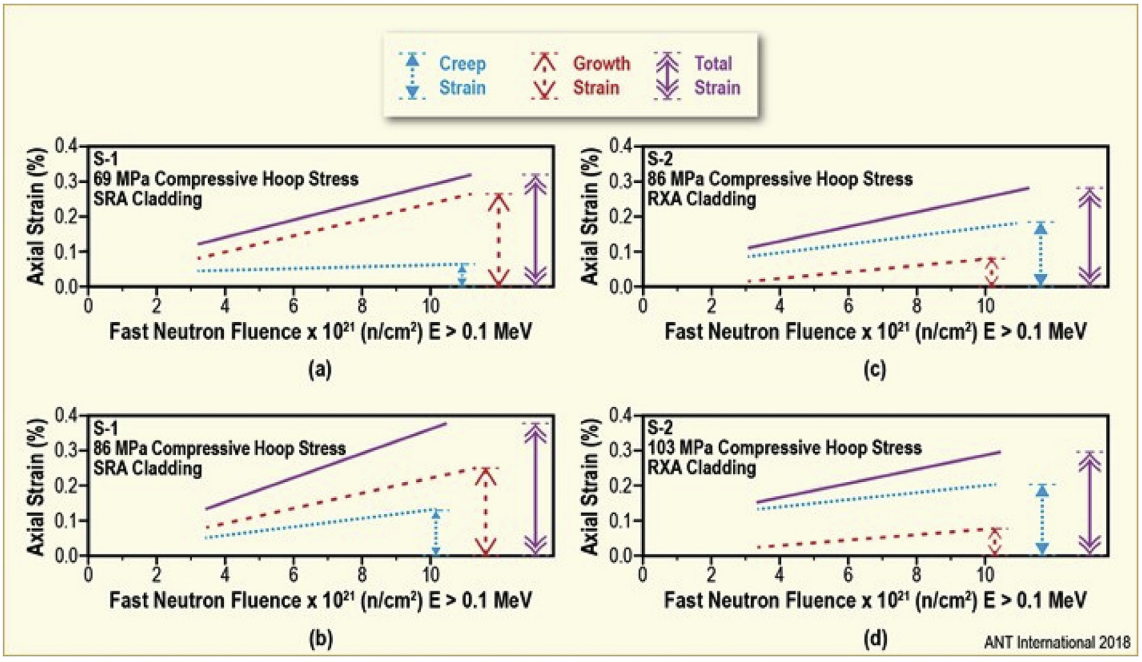

Fig. 3–16. Axial strain components of fuel rods as a function of fluence. Data from Baty et al., [122].

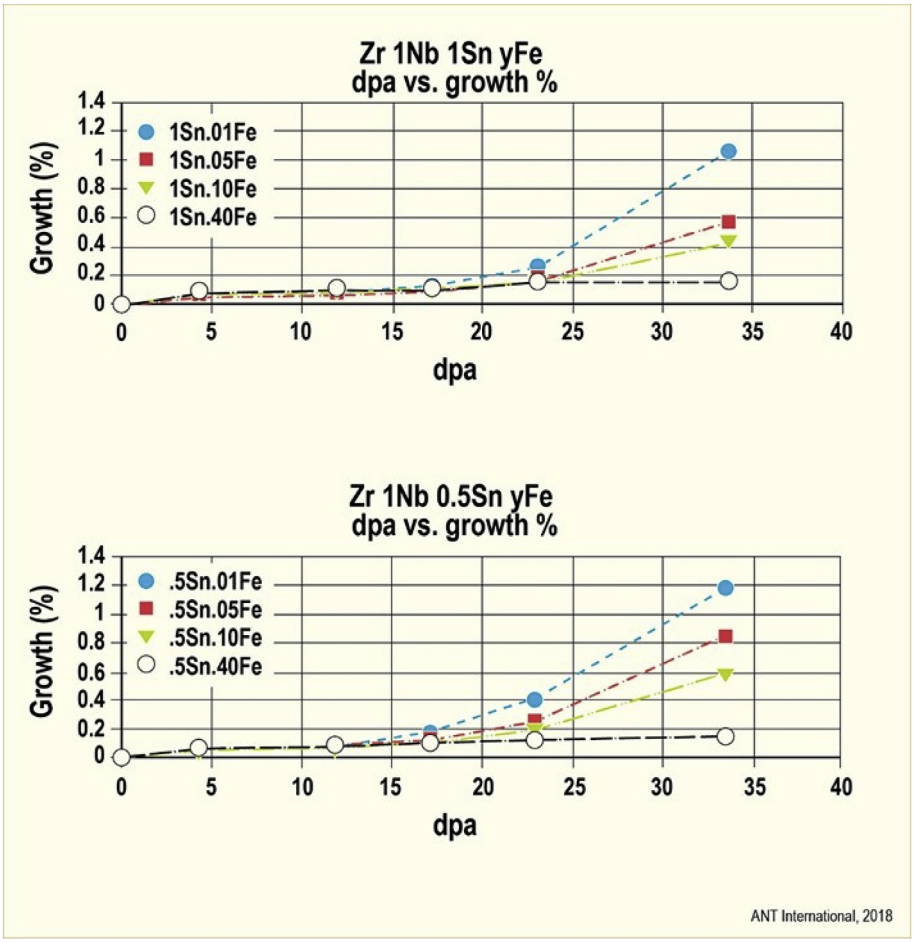

Fig. 3–17. Effect of Sn and Fe on growth of Zr–1Nb–SnFe alloys as a function of dpa [113113]. In the measurement direction, f ≈ 0.1.

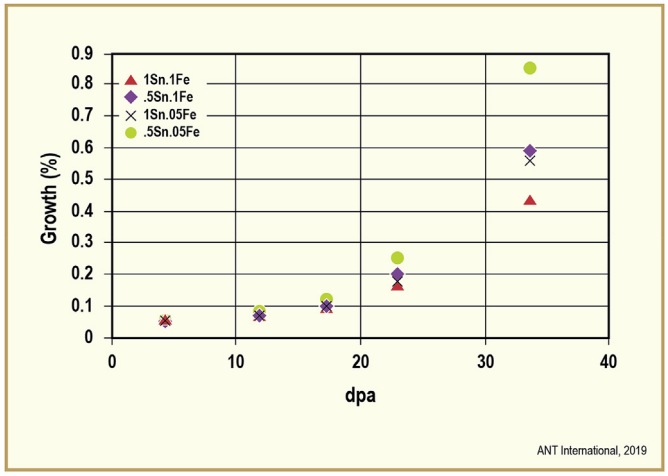

Fig. 3–18. Effect of Sn and Fe on growth of Zr–1Nb–SnFe alloys as a function of dpa [113].

of RXA and CW Zircaloy-2 are almost the same, but the growth rate of RXA materials appears to be higher. Unfortunately, the growth rate of CW materials at higher dpa is not known.

3.4.5. Temperature dependence

3.4.5.1. Zircaloy. Data on the temperature dependence of growth are available providing the overall trend for growth rate illustrated in Figs. 3–26 and Figs. 3–27 ("rate" is defined as the slope of the growth strain curve in the breakaway growth regime). For low fluences, in the pre-breakaway region for RXA material, growth strain appears to increase with temperature in the range of 70–300 °C (350–573 K). For RXA material, growth tends to decrease at higher temperatures; however, for CW or SRA material growth increases rapidly above about 377 °C (650 K), Figs. 3–28 At high fluences, above the fluence at breakaway, growth of both RXA and CW/SRA materials increase rapidly above about 377 °C (650 K), Figs. 3–26, Figs. 3–27, Figs. 3–29. High and low fluence seems to be divided arbitrarily above and below about 8 dpa (5×10^{25}, n/m^2, E > 1 MeV)

In the temperature range important for commercial reactors, 288 °C (561 K) to 350 °C (623 K), temperature dependence is weak. CW and RXA Zircaloys behave similarly. Reasons for this complicated behaviour are not clear; see growth mechanism Section 4.

3.5. Zr-2.5Nb

Zr-2.5Nb pressure tubes as used for CANDU reactors have two phase microstructure with flat α-grains elongated along the axial direction of the tube surrounded by a thin layer of partially decomposed β-phase. They are typically fabricated with a final cold work of about 27% followed by an SRA of 400 °C (673 K) for 24 h. Contrary to the Zircaloys, the temperature dependence of growth and growth rate is negative in the practical temperature range of

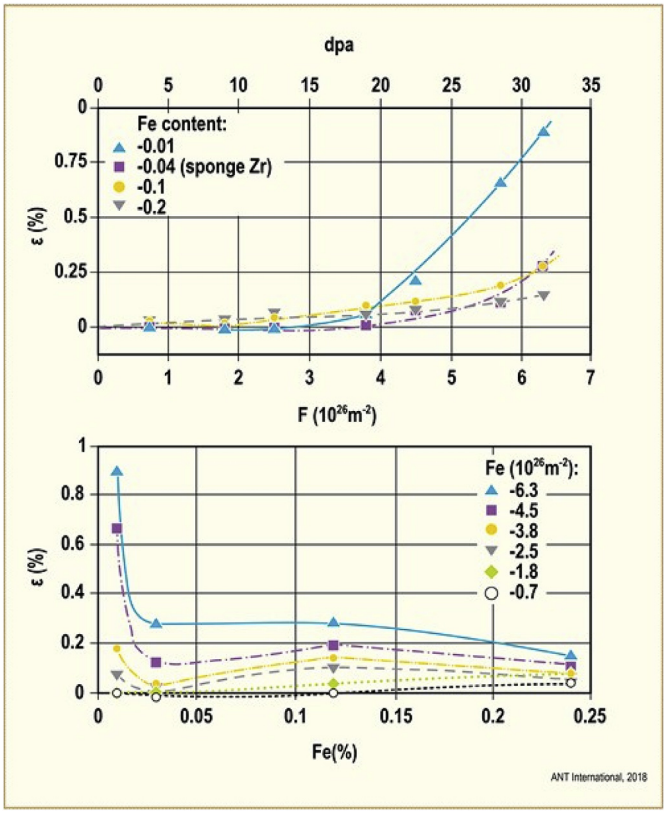

Fig. 3–19. Irradiation growth of RXA E110 type cladding tubes versus Fe concentration (BOR60) irradiation at 335 °C (608 K). f_d in measurement direction is 0.1 [132]. Fluence in figures is given as E > 0.1 MeV, then divided by 4 to get E > 1.0 MeV, (4×10^{26} n/m^2 ≈ 20 dpa).

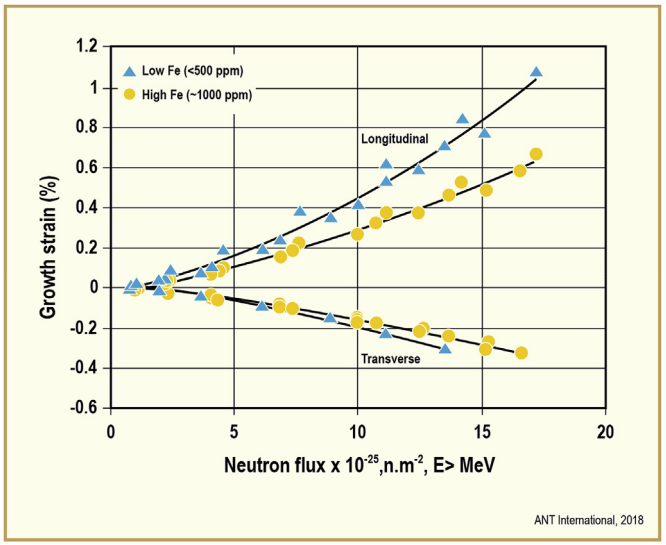

Fig. 3–20. Irradiation growth for cold worked Zr-2.5Nb pressure tube with different Fe concentrations at irradiation temperature of 280 °C (553 K) [33], (10×10^{25} n/m^2 ≈ 15 dpa).

250–320 °C (523–593 K), demonstrated by data of Figs. 3–30 and Figs. 3–31. See mechanism Section 4 for discussion of this behaviour.

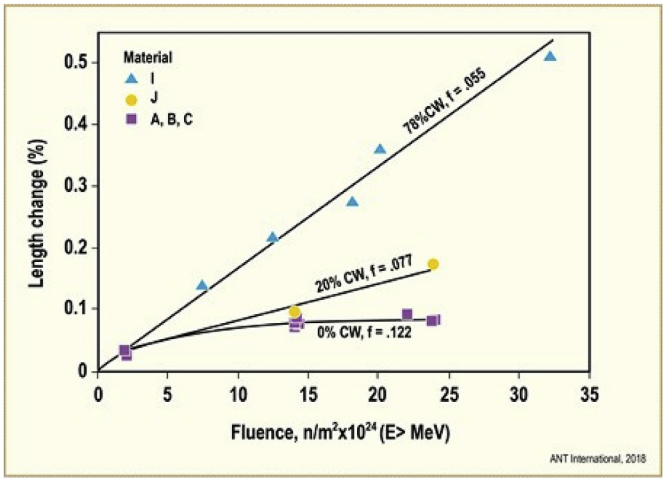

Fig. 3–21. Irradiation growth as a function of cold work and fluence for Zircaloy-4 irradiated near 282 °C (555 K) [130], (20×10^{24} n/m^2 ≈ 3 dpa). All measurements in the rolling direction of plates.

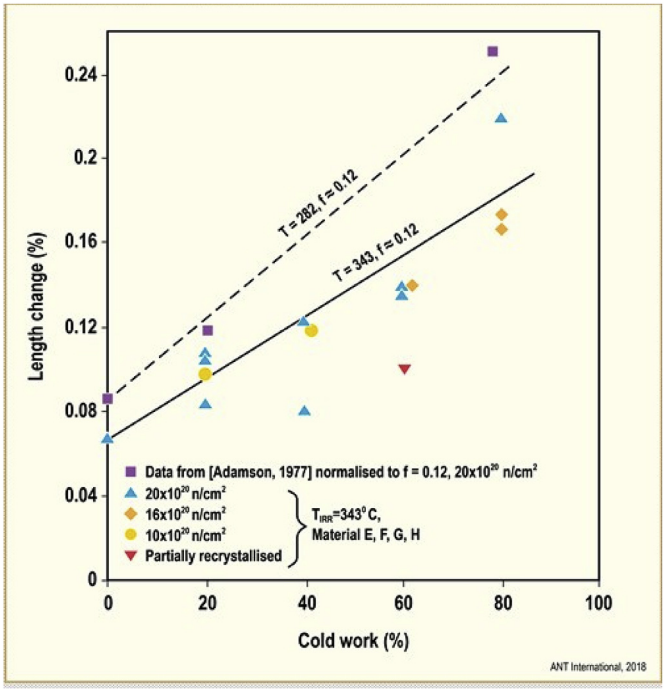

Fig. 3–22. Irradiation growth of Zircaloy-4 as a function of cold work [130].

3.4.6. Minor constituents

Minor constituents can have a measurable effect on growth. Most, for example Fe, H, and C, can be controlled during melting and fabrication steps. H (hydrogen) concentration in components invariably increases during in-reactor service through corrosion processes. Knowledge of the effects of the constituents is important for predicting the behaviour of core components during reactor operation.

3.4.6.1. Hydrogen. The effects of hydrogen (H) on irradiation growth is confounded by the volume swelling caused by H in solution and precipitates of ZrH hydrides; in addition, recent data show unequivocally that there is a synergistic effect of H in exacerbating the growth process itself. Figs. 3–32 gives dimensional

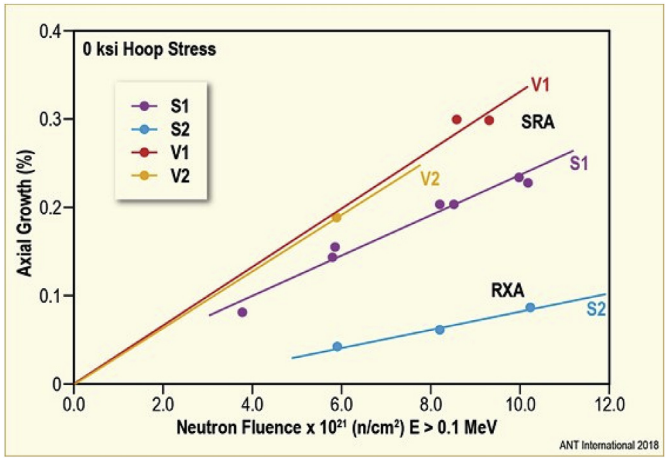

Fig. 3–23. Axial strain of unstressed fuel rods for SRA(V1,V2,S1) and RXA(S2) Zircaloy-4 at 307 °C (580 K) as a function of fluence [122], (10×10^{25} n/m^2 ≈ 8 dpa).

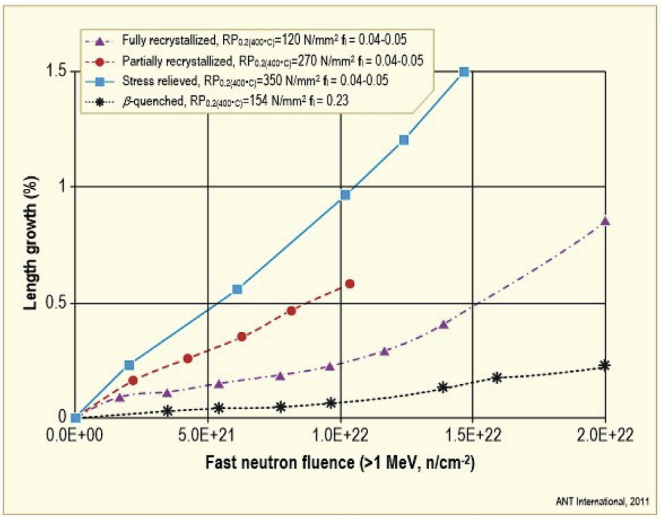

Fig. 3–24. Irradiation growth at 300 °C (573 K) for Zircaloy-4 with different yield strengths and textures. Data from Refs. [32,127], (1.0E+22 n/cm^2 ≈ 15 dpa).

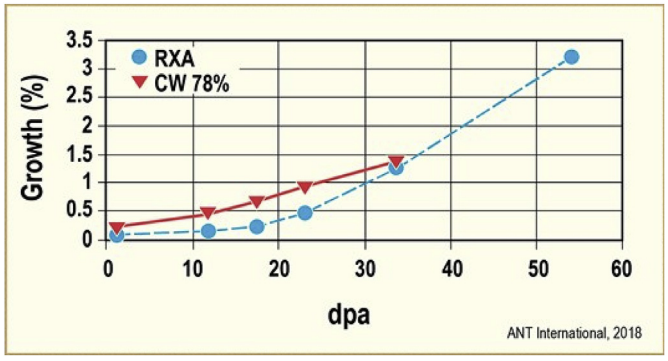

Fig. 3–25. Irradiation growth of RXA and CW Zircaloy-4 as a function of dpa. Temperature is 320 °C. Data extracted from [Yagnik et al., [113]].

changes at room temperature in unirradiated Zircaloy caused by concentrations of H. (Note: at room temperature all H is in the form of hydrides). Expansion is the same in axial and tangential directions and was not measured in the third orthogonal direction.

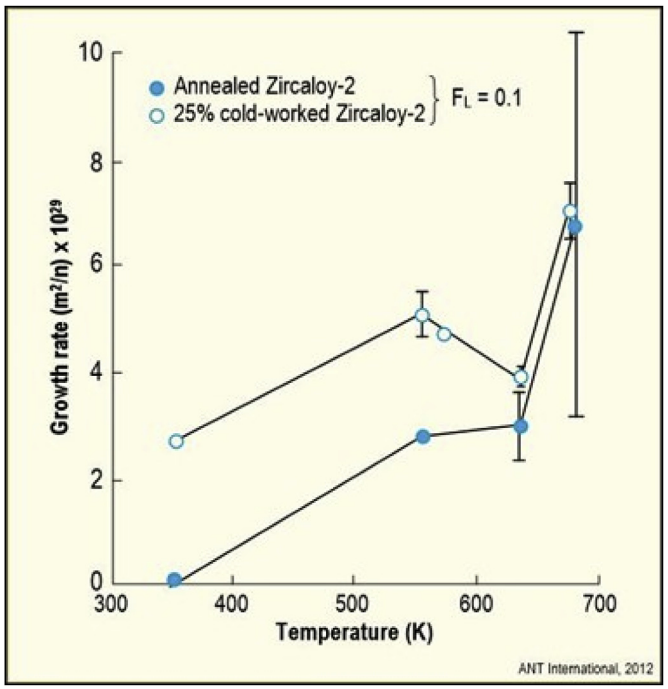

Fig. 3–26. Temperature dependence of growth rate of Zircaloy-2 at high fluence [118].

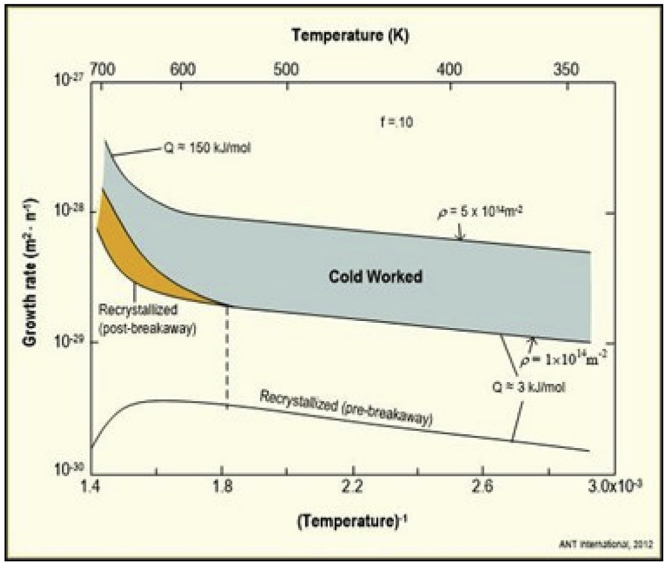

Fig. 3–27. Temperature dependence of irradiation growth rate of Zircaloys (generalized representation) [117].

For example, for 1000 ppm H, the dimensional increase in a zirconium alloy component could be about 0.3%. This increase would cause a 12 mm (0.47 inch) length change in a typical 4 m long fuel rod; such a change is detectable and measurable in a pool-side inspection.

Effects of H on the growth process have been reported by several investigators (including Shishov, [37]; McGrath and Yagnik, [70]; Mader et al., [144]; Foster et al., [60]), but the most definitive data are by Yagnik et al., [113]. Figs. 3–33 gives growth strain as a function of fluence for four alloys that have been hydrided before irradiation to H concentrations of 116, 335 and 718 ppm, all above the H solubility limit at the irradiation temperature of 320 °C

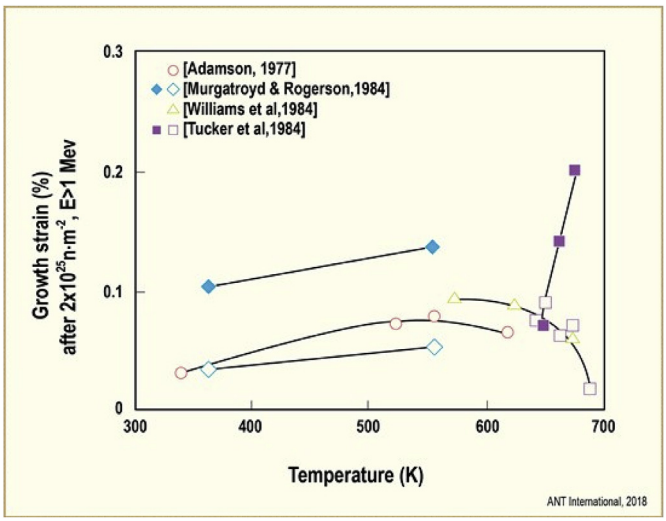

Fig. 3–28. Temperature dependence of growth of recrystallized and cold worked Zircaloy at low fluences. All results normalized to $f_L = 0.13$ and fast neutron fluence of 2×10^{21} n/cm.[2] Open symbols = recrystallized materials; filled symbols = cold worked materials [117].

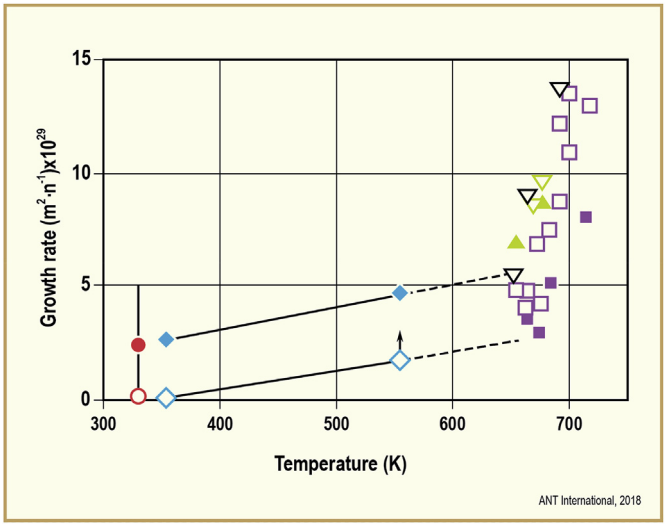

Fig. 3–29. Temperature dependence of growth rate of Zircaloy ($f_L = 0.1$) at high fluence ($>5 \times 10^{25}$ n/m^2 E > 1 MeV). Open symbols for recrystallized materials; filled symbols of 20–25% cold worked materials [117], ($>5 \times 10^{25}$ n/m^2 ≈ > 15 dpa).

(593 K). It is seen that each alloy has increased growth of various degrees relative to the reference material and independent of the amount of H added There is also some evidence that H (hydrides) causes an increase in the density of <c>-component dislocation loops formed during irradiation, which is generally related to growth magnitude [113,145], but more work is needed in this area.

Zircaloy-4 was tested in a PWR environment at 350 °C resulting in corrosion – thick oxides and a maximum value of 1600 ppm hydrogen; growth was measured at pool temperature, Figs. 3–34, Bossis et al., [115]. The downward arrow, not part of the original figure, adjusts the data for the expected volume swelling caused by the 1600 ppm hydrogen. Compared with the Mahmood Zircaloy-2 specimens containing only 85 ppm hydrogen, the Bossis material still has an unusually high growth, most likely associated with the effect indicated in Figs. 3–33. Note the large difference in Zircaloy-4 and M5, the latter containing Nb and having less than 100 ppm

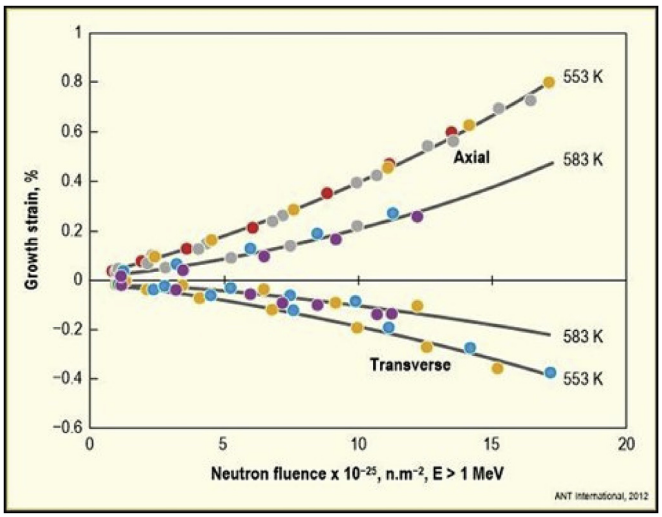

Fig. 3–30. Irradiation growth strain of cold worked Zr2.5Nb as a function of fluence [33,141], (10×10^{25} n/m^2 ≈ 17 dpa).

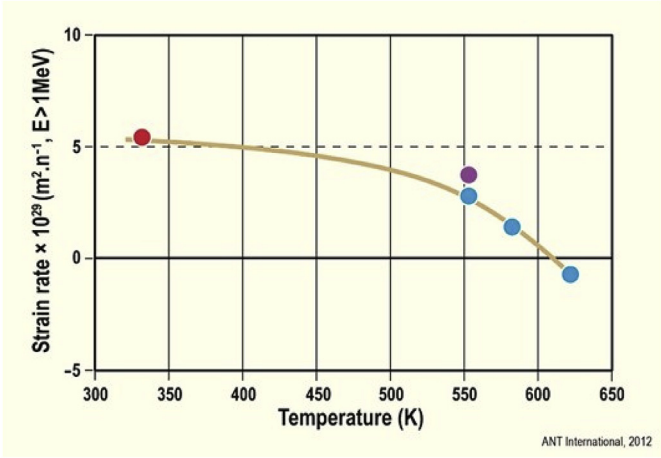

Fig. 3–31. Irradiation growth rate of cold worked Zr-2.5Nb in the axial direction of several standard pressure tubes as a function of irradiation temperature [33,142]. Fluence is greater than approximately 17 dpa.

hydrogen pick-up during corrosion.

Atomic scale modelling shows promise in describing the interaction of H with irradiation-produced defects and clusters, and the net effect on H-solubility and dimensions of zirconium alloys [138,139,146,147].

3.4.6.2. Carbon (C). Carbon is added to Zr during the Zircaloy ingot melting process to facilitate nucleation of a favourable arrangement of alpha grains. The ASTM specification is 270 ppm (maximum) and the solubility in the alpha phase is about 140 ppm by weight. Fuel providers generally aim for the range of 75–125 ppm. More data on the effect on irradiation growth is needed, but existing data indicate increased growth above the carbon solubility limit; for example, Figs. 3–35, [148]. Mardon's data are for SRA Zircaloy-4 fuel rods rather than pure irradiation-growth, but irradiation growth dominates the length changes for SRA PWR rods; see Section 3.4.3.2.

3.6.1. Grain size

Grains in most LWR RXA alloys are equiaxed and in the size

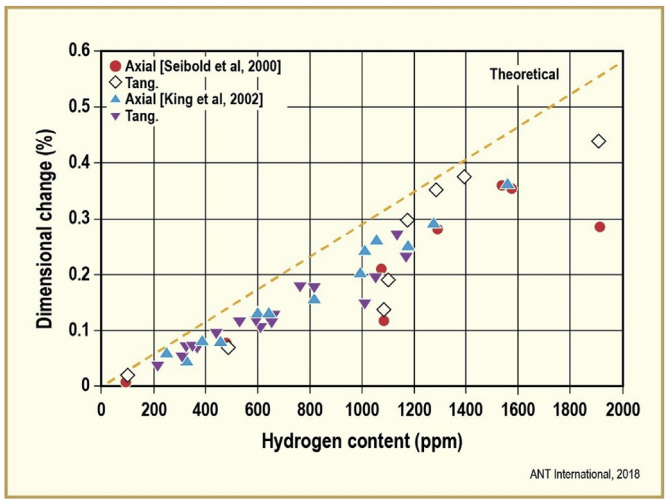

Fig. 3–32. Dimensional changes in unirradiated Zircaloy-4 at room temperature as a function of hydrogen concentration when the data of [King et al., [143]] and [Seibold et al., [103]] are combined. "Theoretical" is based on assumptions of 16 000 ppm of $ZrH_{1.5}$, a 17% volume increase on formation of hydride and an isotropic volume expansion for hydrides. [143].

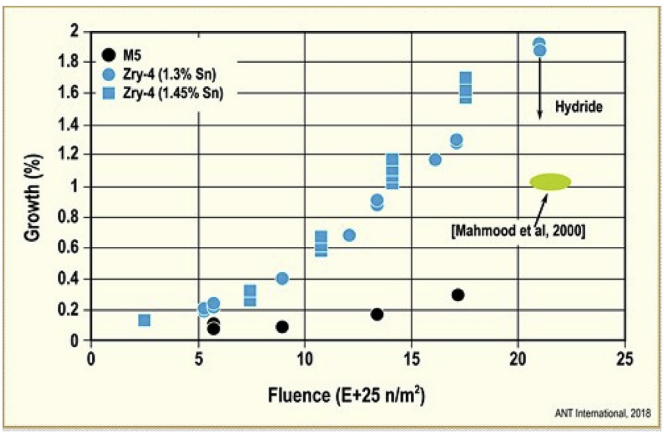

Fig. 3–34. Irradiation growth of Zircaloy-4 [115], (10×10^{25} n/m^2 ≈ 15 dpa).

range between 2 and 9 μm. Cold worked or SRA alloys have flattened grains and generally are reported to have grain size at the lower end of that range (often it is difficult to define grain size in cold worked or SRA material). Almost no data are available where grain size is a single variable. For instance, some data are taken from fuel rod length change where there are at least two variables causing the change: irradiation growth and anisotropic creep, [127]. Data, (Figs. 3–36), indicate only a small effect for RXA materials in the practical grain size range, but a larger effect for SRA materials, especially below a grain size of 2 μm.

For a temperature close to being relevant to BWRs and PWRs (260 °C) [118] has some data indicating large grain size decreases

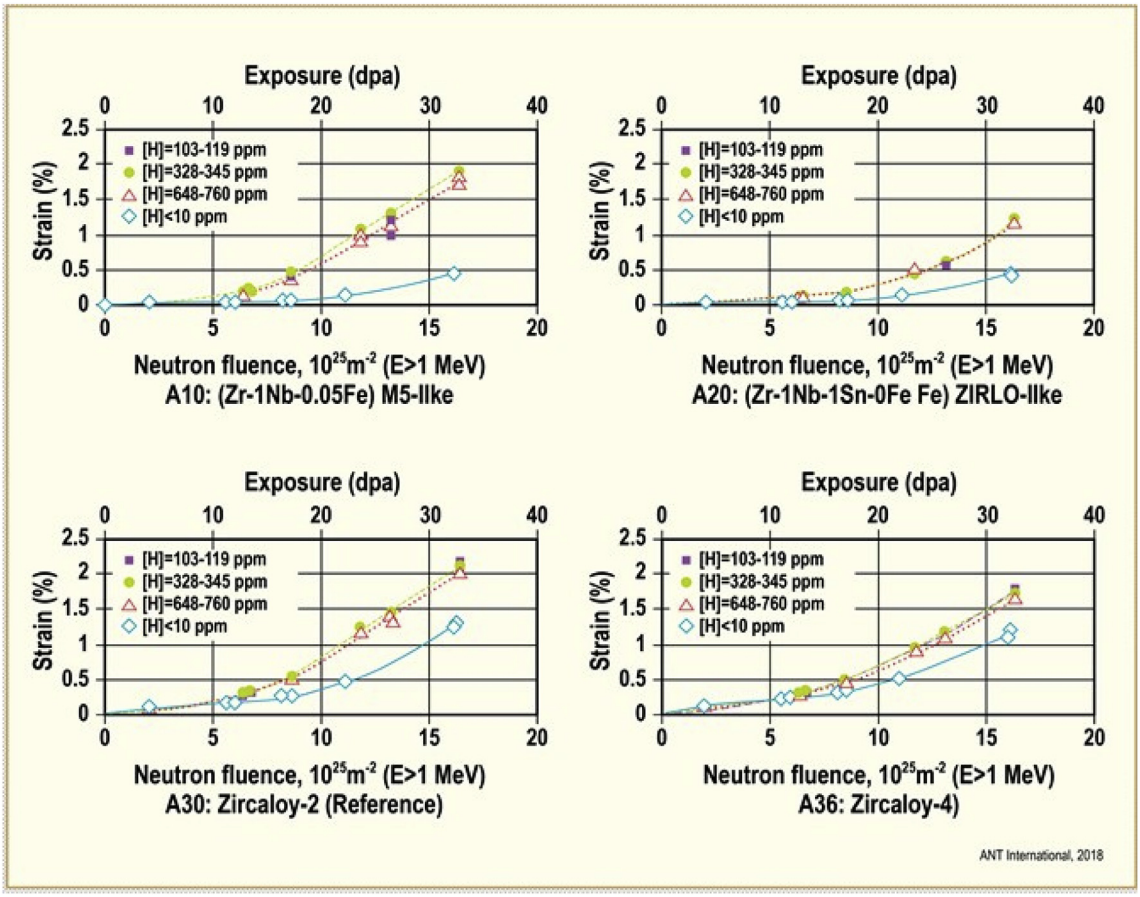

Fig. 3–33. Irradiation-induced growth strain (%) as a function of dpa for a) M5-like, b) ZIRLO™-like, c) Zircaloy-2 and d) Zircaloy-4, all with pre-irradiation concentrations of H: 116, 335 and 718 ppm [113].

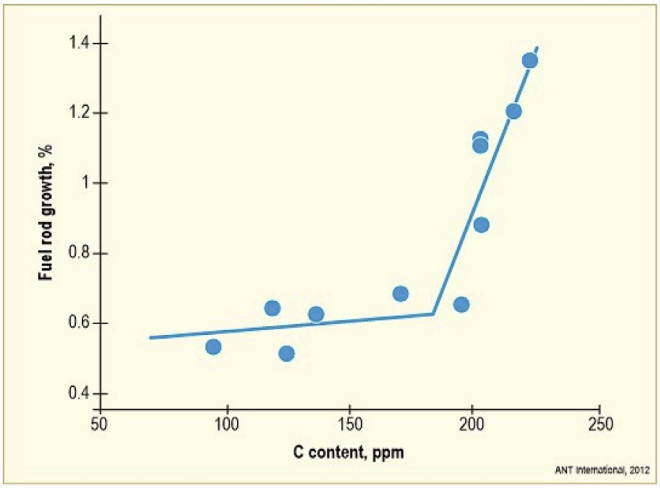

Fig. 3–35. Influence of carbon concentration on Zircaloy-4 SRA fuel rod length change at about 10 dpa and "normal PWR temperatures" (about 320 °C) [148].

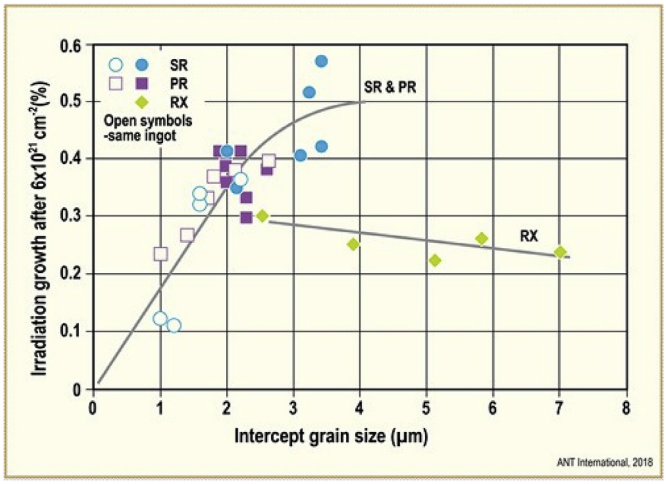

Fig. 3–36. Length change of PWR fuel rods with Zircaloy-4 cladding as a function of grain size at a fluence of 6×10^{25} n/m^2 (E > 1 MeV) [127], (6×10^{25} n/m$^2 \approx 9$ dpa).

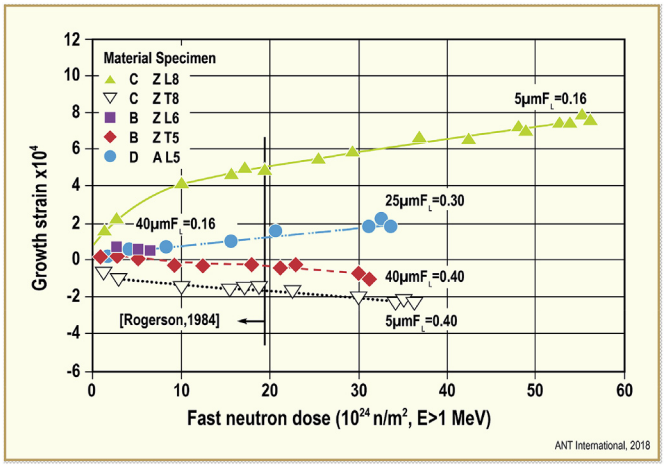

Fig. 3–37. Irradiation growth in annealed polycrystalline zirconium at 553 K (260 °C) [118] (a), (30×10^{24} n/m$^2 = 5$ dpa).

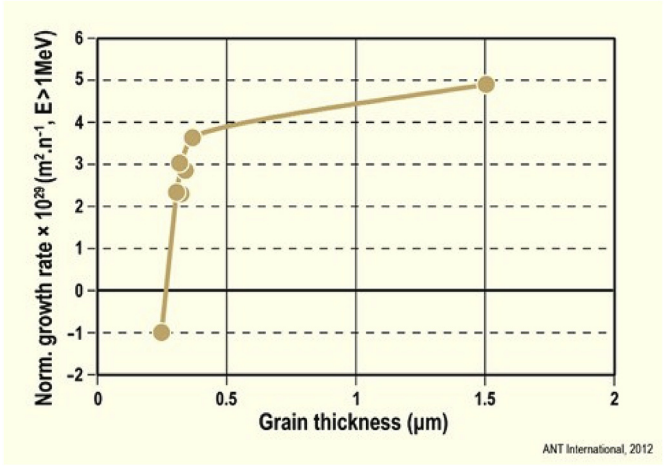

Fig. 3–38. Effect of grain thickness on growth rate of cold worked Zr-2.5Nb, normalized for several variables [33].

growth, Figs. 3–37. Comparing similar textured material, 40 μm grain size has much less growth than 5 μm grain size materials, at least during transient region at low fluence. (These materials have very low Fe concentration (170 ppm) and very high C (260 ppm), which could both increase growth).

Quantitative analysis of the grain size effect based on very limited data is unwarranted. It does appear that for zirconium alloys in the normal 2–8 μm grain size range the sensitivity to grain size is small, and above this range irradiation growth is decreased.

For pressure tubes made from Zr-2.5Nb, grain size is expressed as thickness of the elongated alpha-phase grains in the cold worked structure. Attempts have been made to determine the effect of grain thickness (Figs. 3–38), [93]. The results are similar to those in Figs. 3–36 for Zircaloy-4, with growth rates decreasing rapidly for small grain thickness. Holt does add the comment that other variables, such as the degree of transformation of the β-phase and the dislocation density, may be influencing the results.

Early work reported in Ref. [140] indicated little effect of "grain size" on growth of Zr-2.5Nb pressure tubes. Tubes with similar dislocation densities and a factor of two difference in grain size had similar growth rates. The method of grain size analysis was not reported.

3.4.8. vol and density change

It is generally assumed that irradiation growth occurs with little or no volume change; that is, dimensional increases in some directions are counter balanced by decreases in other directions. Experimentally, growth determinations are most often made in the longitudinal and transverse directions of component materials; for example, axial and circumferential directions in tubing or length and width directions in BWR channels. Since significant growth (often shrinkage) occurs in the radial or through-thickness directions, volume changes cannot be deduced experimentally from just two directions.

A volume increase (density decrease) at low fluence, in the pre-breakaway range, has often been predicted by theory or observed, being in the range 0.01–0.10%.

Carpenter et al. [123] report a volume increase for Zr single crystals of about 0.02% for irradiation temperature of 250 °C (523 K). Morize et al. [129] report a density decrease for polycrystalline Zircaloy-4 of <0.01% at 315 °C (588 K). Holt & Causey [149] report an initial volume increase for Zr-2.5Nb at 2×10^{24} n/m^2 of 0.05–0.10%, decreasing at higher fluence to <0.05%, at 250 °C

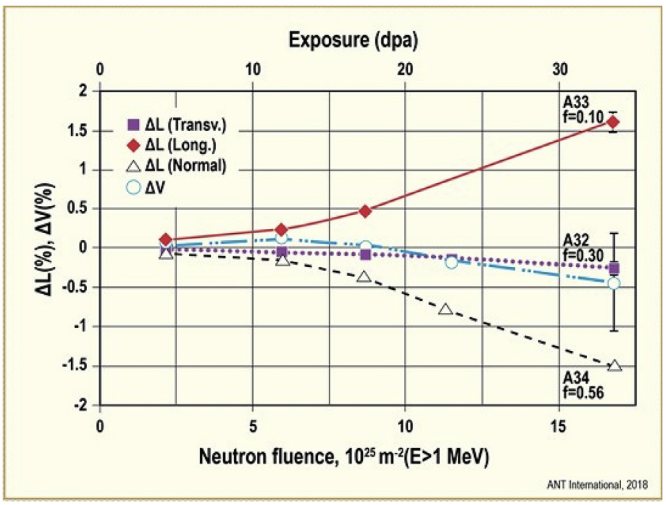

Fig. 3–39. Length change of Zircaloy-4 in three orthogonal directions having texture parameters "f", and calculated volume change as a function of neutron fluence and dpa. Irradiation temperature = 320 °C (593 K) in BOR 60 reactor [113].

(523 K). Harbottle & Herbillon [150] report density decreases for Zircaloy-2 in the range 0.03–0.10% at 300 °C (573 K) for low fluence.

Yagnik et al. [113] determined growth at 320 °C on three separate orthogonal specimens cut from a thick Zircaloy-4 plate having accurately measured textures, Figs. 3–39. Volume was calculated by summing the three values at five fluences. Results indicate a small (0.1%) volume increase at pre-breakaway fluence and a small (0.4%) volume decrease at very high fluence. Overall, the volume change is very nearly zero, within the scatter of the data. Density measurements on two specimens at damage dose of 33 dpa gave an average density increase (volume decrease) of 0.06 ± 0.2%, which covers the experimental range of volume change.

3.4.9. Single crystals

Testing single crystals of Zr gives data on the effect of absence of grain boundaries on growth, [118,123]. All the materials had impurities of <100 ppm Fe and <16 ppm H (by weight). Figs. 3–40 shows that the shape of the growth curve is similar to that for

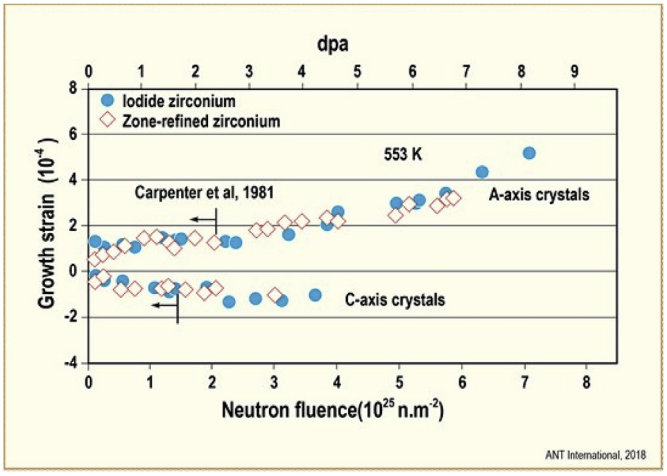

Fig. 3–40. Growth data for annealed Zr single crystals at 280 °C (553 K) as a function of fluence (Note that 1 dpa = 9×10^{24} n/cm^2 E > 1 MeV, which does not match well with more recent determinations given in, Section 1.1) [Carpenter et al., [118]]. and [Rogerson, [118]], (3×10^{25} n/m^2 = 5 dpa).

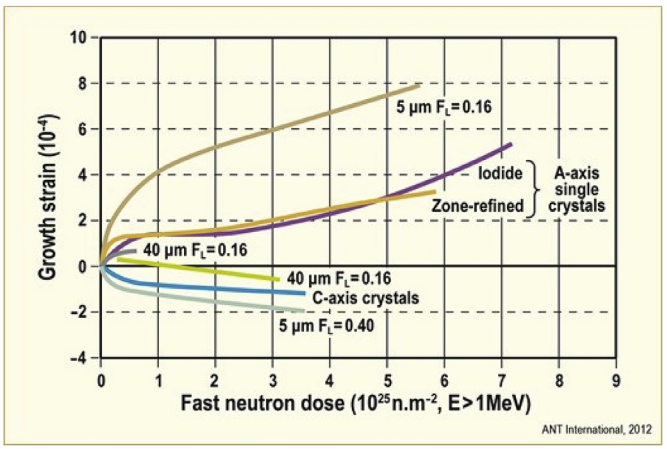

Fig. 3–41. Comparison of growth of annealed single crystals with polycrystalline iodide Zr at 280 °C (553 K) [123], (3×10^{25} n/m^2 = 5 dpa).

the Zircaloys:

- a-axis crystals ($f_L = 0$) grow and c-axis crystals ($f_L = 1$) shrink.
- breakaway growth occurs at moderate fluence.

Note that the pre-breakaway strain (≈0.015%) for the single crystal is a factor of 3–10 smaller than, for example, Zircaloy or ZrNb alloys. Adding grain boundaries, Figs. 3–41, adds more primary strain, but it is clear that grain boundaries are not required to produce transient growth or breakaway. More details are provided in Ref. [39].

3.4.10. Thermal stability

Data already presented identify several parameters that affect growth. This Section explores the effect of post-irradiation thermal annealing on recovery of growth and of the irradiation-produced microstructures. Annealing above about 400 °C (673 K) induces some recovery of growth strain and elimination of the small irradiation-produced <a>-component dislocation loops. Annealing above about 575 °C (848 K) eliminates the <c>-component dislocation loops, the extent of which depends on annealing time.

Only growth strain in the low growth-rate, pre-breakaway fluence range is recoverable. That is, growth strains for cold worked or stress-relieved (CW/SRA) material and for recrystallized (RXA) material beyond the breakaway fluence, growth is not recoverable beyond that which occurs for RXA material in the pre-breakaway regime. These facts indicate that there are at least two distinct growth mechanisms (one recoverable, one not) and implicate <c>-component dislocations as contributors.

The first report of recovery of irradiation-induced strain was for stress relaxation experiments on Zircaloy-4 (irradiation temperature near 310 °C, fluences near 2×10^{25} n/m^2 (E > 1 MeV), bent beam relaxation) [74]. Over 60% of the relaxation strain was recovered by anneals of 450 °C/10 h or 480 °C/1 h. The mechanisms of strain recovery were not explained or known at that time; later data would implicate annealing of <a>-component dislocation loops as a contributing factor.

One study by Adamson [130], described the recovery effect for irradiation growth of RXA and SRA Zircaloy-4 and -2 in the pre-breakaway regime where irradiation-produced <c> loops are not present. The data in Tables 3–5 give a sample of Adamson's data, indicating that the magnitude of growth recovery is approximately only that of the RXA material at low fluence, even though the magnitude of growth strain is larger for the SRA materials. Strain

Tables 3–4
Irradiation growth of similar alloys except for Fe concentration **[113]** (10×10^{25} n/m^2 = 20 dpa).

Exposure (dpa)		4	12	17	24	34
Alloy	Iron (%)	IIG (%)				
A30 reference Zircaloy-2	0.17	0.08	0.14	0.24	0.47	1.25
W8 Zircaloy-2	0.17	0.11	0.18	0.26	0.49	1.29
X6 Ziron alloy	0.25	0.11	0.16	0.22	0.35	0.87
V17 HiFi alloy	0.40	0.12	0.19	0.24	0.31	0.53

Note: IIG = irradiation-induced growth.

recovery was shown to begin at about 400 °C and was rapid at 500 °C. Figs. 3–42 gives recovery for isothermal and isochronal temperature/time anneals.

Recovery of stress-free growth of RXA Zircaloy-4 tubing above the fluence where breakaway growth occurs is shown also to consist of only the pre-breakaway growth component, Figs. 3–43 [127]. The annealing temperature was 500 °C, which is too low to affect <c>-loops.

Figs. 3–43 and Tables 3–5 clearly illustrate that growth recovery is independent of fluence for a post-irradiation anneal at 500 °C for 24–48 h. It was reported that <c>loops were observed at ≥ 9×10^{21} n/cm^2 on the fluence scale of Figs. 3–43.

Growth recovery and irradiation damage recovery are linked. Radiation damage as seen in transmission electron microscopy (TEM) are in the form of "black spots", which are known [151] to be <a>-component dislocation loops (<a> loops). It is seen in Figs. 3–44 that in the temperature range 400–550 °C the loop defect density decreases rapidly (as does the irradiation-induced hardness increment) and the loop size increases, [152,153]. It is noted from Figs. 3–42 and Figs. 3–44, that recovery temperatures for irradiation growth correlate well with those of <a>loop increment and hardness decrement.

Growth might be recovered at temperatures where it would be expected that <c>loops would be annealed out. From the data of Yang [154], Kruger [155], Yang & Adamson [156], Vizcaino et al. [157] and Hengstler-Eger et al. [158] it appears that annealing of <c>loops begins at about 560 °C, is well underway at 575–600 °C and is rapid at 625 °C. Data on recovery of growth and mechanical properties at those temperatures are not available.

More details of recovery experiments are available at Adamson et al., [39].

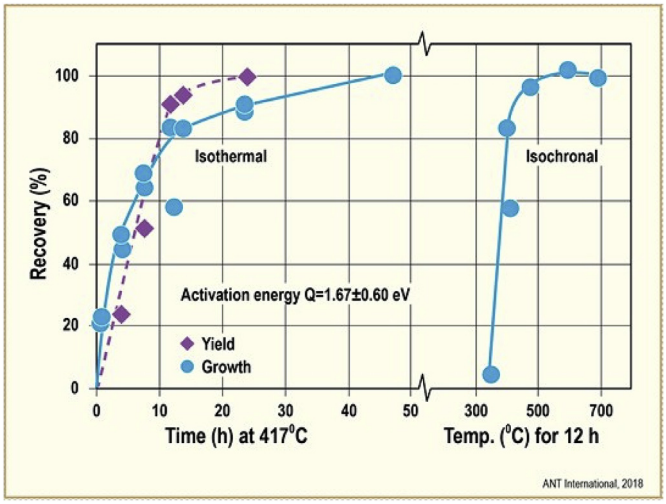

Fig. 3–42. Recovery of irradiation growth and yield strength by post-irradiation annealing. RXA Zircaloy-4 irradiated at 250 °C to 2×10^{25} n/m^2 (E > 1 MeV) [130], (dpa ≈ 2–3).

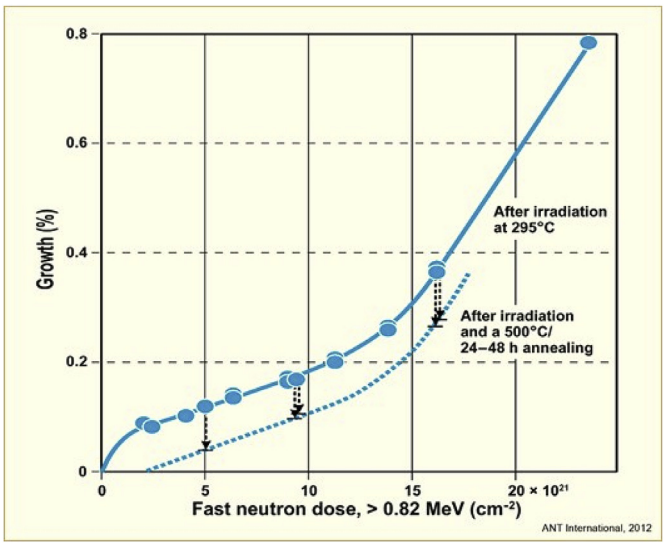

Fig. 3–43. . Effect of post-irradiation annealing at 500 °C for 24–48 h on the recovery of axial (f ≈ 0.05) growth. RXA Zircaloy-4 specimens [127], (10×10^{21} n/cm^2 (E > 0.0.82 MeV = 12 dpa).

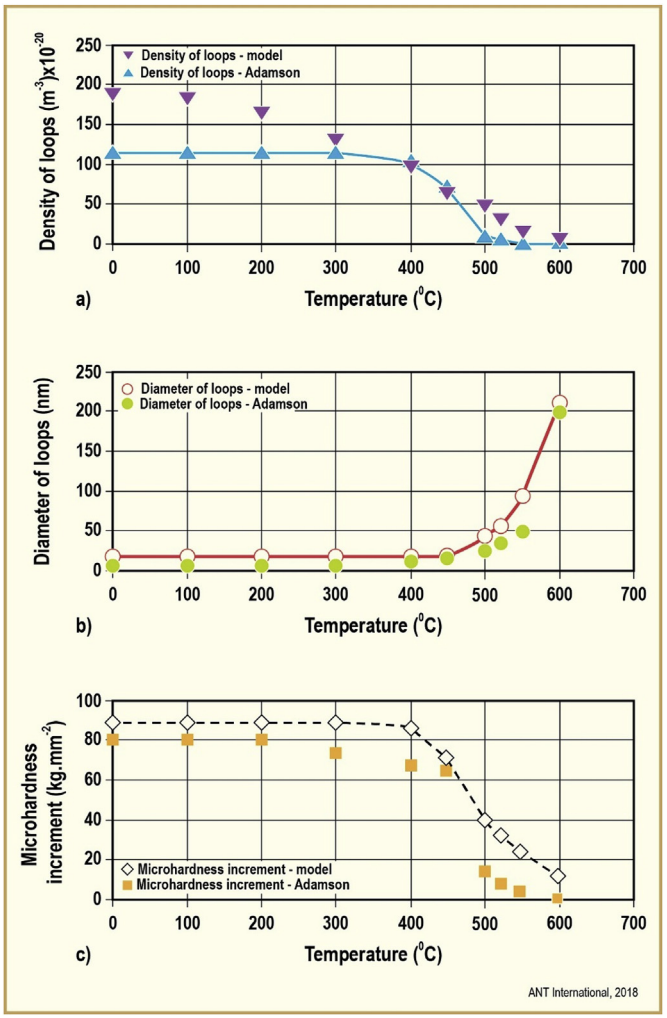

Fig. 3–44. Recovery of <a>loop size and density and hardness. Model (derived from data) [152]; comparison data [153]: annealing time = 1 h, irradiation temperature = 327 °C (600 K), irradiation dose ≈ 1 dpa.

3.4.11. Irradiation growth summary

Irradiation growth is strongly affected by fluence, cold work (CW), texture, irradiation temperature, and material composition (alloying and impurity elements). The shape of the fluence (or dpa) versus irradiation growth curve for a particular material is well defined. Growth in recrystallized (RXA) materials starts out slowly with texture-dependent strains in the long (longitudinal, axial) directions up to 0.10% in the first 5 dpa. At some critical incubation fluence range, which is influenced by temperature and alloy composition, the growth rate increases. It is in this "breakaway" growth regime where flux and fluence gradients can result in reactor component bowing. In cold worked stress-relieved (CW-SRA) materials the growth rate is continuously high starting at low fluences. At high fluence, post-breakaway, RXA materials may grow more rapidly than SRA materials. High growth rates are associated with the existence of microstructural features— for RXA the creation of an anisotropic distribution of radiation-induced dislocation loops lying on basal planes (<c>-component dislocation loops) and on prism planes (<a>-component dislocation loops), and for cold worked material the existence of <c>-component dislocations in the as-fabricated state plus the irradiation-induced <c>– and <a>-component loops. Alloy composition has a major influence on initiation of <c>-component loops; in particular, niobium (Nb) containing alloys can resist formation of <c>-component loops, therefore resisting breakaway growth until fluences approaching the design lifetime of many components.

Existing data suggests that design of a growth-resistant reactor component require consideration of many factors.

For a component for which texture can be varied, like a spacer grid or channel strip, a texture as close to f = 0.33 as possible in the direction of interest will limit growth. A uniform texture close to f = 0.33 will limit growth in all directions.

Additions of Nb can lower growth.

For Zr1Nb alloys, an Fe concentration greater than about 200 ppm is required to minimize growth. For other alloys, increasing the Fe concentration to as high as 4000 ppm results in decreased growth.

For most alloys, to minimize the effect of C on growth, its concentration should be maintained below the solubility limit, about 150 ppm.

Hydrogen in solution or as hydrides can increase growth but details are still unclear. If hydrogen concentrations approach the solubility limit of H at the operating temperature of the component, perturbation of the growth curve must be anticipated.

For any component design, awareness of the effects of cold work on growth is essential: even cold work less than about 2% may induce growth transients; cold work greater than about 10% will increase growth; 70% cold work will produce a very high growth rate. For component temperatures in the range 290–330 °C (563–603 K) the temperature dependence of growth rate is small (although the critical fluence for breakaway will decrease as temperature increases); at temperatures greater than 370 °C (643 K) growth rates for RXA and SRA become high and equal.

More exact mechanisms of growth are explored in Section 4. One key factor is the initiation of <c>-component dislocation loops lying on the basal plane. The correlation between <c>-loop initiation and the beginning of breakaway growth is firm, but the reasons behind the incubation fluence for <c>-loop initiation are not known. In particular, why does hydrogen decrease the incubation fluence and Nb increase the incubation fluence?

4. Mechanisms

Irradiation growth of Zr-alloys is determined by the intrinsic properties of the material (microstructure and chemistry) and the extrinsic influences of the irradiation damage (a function of the neutron flux) and temperature. We will therefore consider the effect of the various factors controlling irradiation growth in two parts: (i) microstructure and chemistry; and (ii) operating conditions (neutron flux, time and temperature).

4.1. Mechanisms of irradiation growth

4.1.1. Effects of microstructure and chemistry

Irradiation growth is a phenomenon that was first identified in uranium alloys. Much of the early effort on mechanisms and modelling of irradiation growth in Zr-alloys stemmed from experience gained from uranium. Metallic uranium has an orthorhombic crystal structure with lattice parameters: a [100] = 0.2852 nm; b, [010] = 0.5865 nm; and c, [001] = 0.4945 nm. Because of the single crystal anisotropy polycrystalline samples of highly textured uranium were found to exhibit anisotropic deformation (growth) in a radiation environment [159,160]. Buckley proposed a qualitative model for irradiation growth in uranium [160,161], based on the preferential condensation of point defects on particular crystallographic planes. Buckley's hypothesis was dependent on the anisotropy of thermal expansion and the stresses induced in the thermal spike of collision cascades. Buckley proposed that interstitial loops condensed on those close-packed planes perpendicular to the direction of lowest thermal expansion, i.e. (010), and vacancy loops condensed on those closed-packed planes with the lowest loop energies, i.e. {110} as opposed to (001), that are also inclined to directions of largest thermal expansion, [100]. The net effect after irradiation is for an expansion in directions perpendicular to (010) and a contraction in directions perpendicular to (100).

Buckley proposed that irradiation growth of Zr could be explained by a similar mechanism to that for U. Although qualitatively similar, the anisotropy of thermal expansion is less for Zr compared with U [160]. For Zr, Buckley proposed that interstitial loops would form preferentially on type-1 prism planes, $\{10\bar{1}0\}$, and vacancy loops would form preferentially on basal planes, (0001), due to the stresses induced by the thermal spike of collision cascades. Because thermal expansion is highest for the c-direction, Buckley argued that the deviatoric component of stress would be compressive along the c-axis [160]. Even though the stresses in the thermal spike may all be compressive (depending on the temperature in the thermal spike), the driving force in terms of work done when the loops form from a super-saturated solid solution would favour vacancy loops on (0001) and interstitial loops on $\{10\bar{1}0\}$, see Figs. 4–1.

To illustrate the Buckley concept one can build a simple model for irradiation growth in which there are only two types of point defect sinks; c-component dislocation loops on basal planes and a-type dislocation loops on prism planes. Such a model would apply to annealed, large-grained Zr-alloys in which the dominant sinks are dislocation loops created from radiation damage. So long as there is a bias causing a net accumulation of vacancy or interstitial point defects at sinks with differing orientations there is a mechanism for irradiation growth. Because we observe that basal plane loops are consistently vacancy in nature [151,162], it is reasonable to assume that there is a bias for interstitial absorption at a-type defects. The rate-theory equations describing irradiation growth for large-grained annealed Zr-alloys, containing a- and c-component dislocation loops with densities ρ_a and ρ_c respectively, can then be formulated using a bias parameter (b) to represent the probability that interstitial point defects will be absorbed at an a-type sink. The interstitiitial bias parameter may be a function of anisotropic diffusion [163], the elastic size-effect interaction [164,165], or both. The fluxes to sinks resulting in an a-axis strain and a c-axis strain

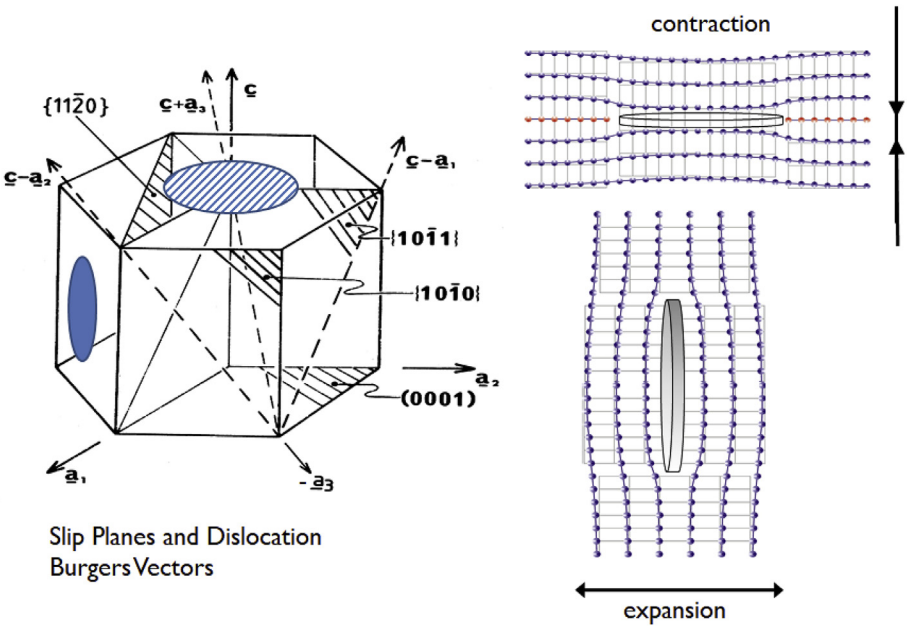

Fig. 4–1. Schematic showing irradiation growth in Zr proposed by Buckley [160]. Interstitial loops form on $\{10\bar{1}0\}$ planes and vacancy loops form on basal (0001) planes.

are given by:

$$J_a = \left[\frac{(1+b).\rho a}{(1+b).\rho a + \rho c} - \frac{\rho a}{\rho a + \rho c}\right] \cdot \Phi \tag{4.1}$$

$$J_c = \left[\frac{\rho c}{(1+b).\rho a + \rho c} - \frac{\rho c}{\rho a + \rho c}\right] \cdot \Phi \tag{4.2}$$

Where ρ_a is the a-type dislocation density, ρ_c is the c-type dislocation density and φ is the atomic displacement damage rate in dpa.s^{-1}. Equations (4.1) and (4.2) describe the point defect partitioning to sinks that produce strain either perpendicular or parallel to the c-axis. The c-axis is unique, but the strain in any given direction in the basal plane (perpendicular to the c-axis) will be dependent on the distribution of sinks within that plane. For a uniform distribution of a-type dislocations the strain in any given direction in the basal plane = $J_a/2$ (see Section 4.2.2).

Figs. 4–2 shows a simple rate-theory model output describing longitudinal strain for a grain with crystal orientation as shown where the main vacancy point defect sinks are basal plane dislocation loops and the main interstitial point defect sinks are prism plane dislocation loops. For an idealized fuel cladding texture with most basal poles oriented in the radial direction, the longitudinal growth rate is a maximum when the ratio of the vacancy and interstitial sink strengths is equal to $\sqrt{1+b}$, where b is the bias differential for interstitial point defect diffusion to prism plane loops due to a combination of elastic size-effect interaction and the DAD bias due to line orientation [163,165–167]. The DAD bias refers to the tendency for interstitial point defects to diffuse preferentially within the basal plane. Assuming that vacancy point defects diffuse isotropically, the net result is a drift of vacancies to sinks parallel to the basal plane and a net drift of interstitials to sinks perpendicular to the basal plane illustrated by the arrows for the point defect diffusion paths in Figs. 4–2. Although DAD was introduced to account for the observations of irradiation growth in annealed polycrystalline Zr where the a-type loops could be both vacancy and interstitial in nature [163], experimental evidence to support it is evident in observations of denuded zones and loop character near grain boundaries in neutron irradiated Zr [168] (see Fig. 5).

For many years after Buckley's original hypothesis [160] researchers looked for evidence of basal plane c-component loops in Zr-alloys. It was not sufficient that such loops were present in the

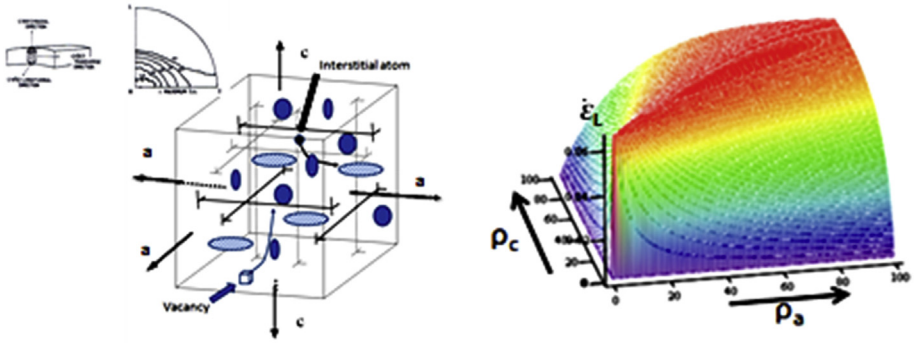

Fig. 4–2. Schematic and rate-theory output showing irradiation growth model results for the longitudinal direction of a large grained Zr-alloy as a function of the a (ρ_a) and c (ρ_c) dislocation densities. The strain rate per unit dpa ($\dot{\varepsilon}_L$) in the longitudinal direction (L) is a maximum when $\sqrt{1+b} \cdot \rho_a = \rho_c$, where b is governed by the size-effect interstitial bias for a-type dislocations and the DAD bias.

microstructure, they also had to be vacancy in nature to support Buckley's original theory. The first definitive evidence for the existence of vacancy basal plane loops came from work at Lucas Heights in Australia [169]. Jostsons et al. found vacancy basal plane dislocation loops in only three of five samples of zone-refined Zr, indicating that their existence was controlled by some factor linked to the purity of the different alloys as evidenced by hardness measurements. They found that the basal plane c-component loops were observed in samples with unusually high hardness values, suggestive of a high concentration of interstitial impurities. Since those early observations [169,170], similar observations have been made on the effect of impurities in material irradiated in EBR-II [162,171]. In the latter work vacancy basal loops were observed in sponge Zr but not crystal-bar Zr. There was clear evidence that the c-component loops tended to be segregated in layers parallel with the basal plane in the sponge Zr. Secondary precipitation/segregation of impurities was coincident with the high concentrations of c-component loops [162,172]. The association between impurities and c-component loop stability in sponge Zr compared with crystal bar Zr seems to be unequivocal given that all other variables are essentially the same in the two materials. However, there is some ambiguity concerning which impurities are promoting c-component loop formation in this case.

Six years after Jostsons et al. showed that c-component loops could form in neutron irradiated Zr, evidence appeared that Zircaloy-2 reactor components exhibiting unusually high rates of accelerated growth [173]. An examination of their samples showed that the acceleration in irradiation growth (breakaway) was coincident with the observation of c-component dislocations that were visible with a basal plane diffracting vector using transmission electron microscopy (TEM) [174]. There was still some ambiguity concerning the nature of these dislocations (prismatic loops or slip dislocations) and it was later shown that the c-component dislocations were, in fact, faulted basal plane vacancy loops viewed edge-on [162]. Although Buckley's model appeared to be valid, the fact that vacancy, basal plane c-component loops were also formed during electron irradiation [175], indicated that his model was only partially correct and that some factor other than stresses in collision cascades was responsible for the c-component loop formation.

It is now well established that breakaway growth occurs because there is an incubation period for the formation of vacancy basal plane c-component loops (Figs. 4–3). High irradiation growth rates are exhibited by some materials, such as EXCEL alloy or sponge Zr, that have a propensity for c-component loop formation (Figs. 4–4). It is noteworthy that the EXCEL alloy (Zr-3.5Sn–1Nb–1Mo-0.15Fe-0.1O) is similar in composition to ZIRLO (Zr–1Sn–1Nb-0.1Fe) and E635 (Zr-0.8Sn–1Nb-0.4Fe), except that the high Sn content in EXCEL (3.5 wt%) excludes Nb from solid solution in the α-phase [176]. Nb in solution appears to have a suppressing effect on accelerated growth, either through its effect on c-component loop formation or by reducing the number of freely-migrating point defects. Applying a simple rate theory model for irradiation growth one needs to apply a production efficiency factor of 1% for Zr–Nb alloys and 3% for Zr–Sn alloys [39].

The high rates of irradiation growth exhibited by materials containing high densities of basal plane vacancy loops is easily understood from rate theory when the effect of increasing the c-component loop density is that it becomes close to the a-type defect density (Figs. 4–2). At this time the mechanism by which vacancy basal plane loops are stabilized is not fully understood. There is some evidence that impurities are important [162,169–172], but there are other conflicting observations indicating that impurities such as Fe, for example, are responsible for low rates of growth [113]. Whereas Fe may be affecting the irradiation growth via a different mechanism, e.g. by promoting

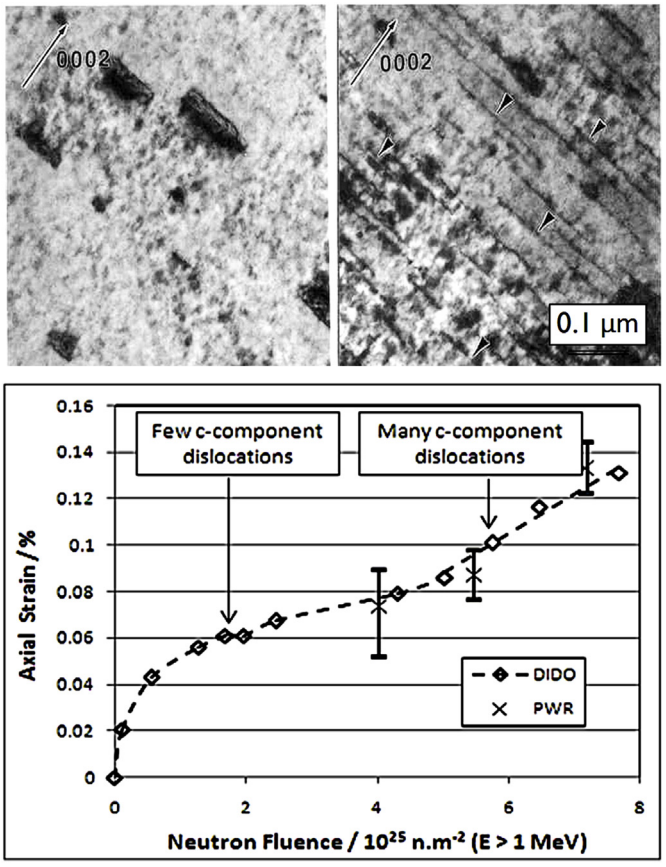

Fig. 4–3. rradiation growth in annealed (RXA) Zircaloy at 550 K–580 K, showing accelerating growth after a fluence of about 4×10^{25} nm^{-2} (E > 1 MeV). Modified from Holt and Gilbert [174] and Fidleris [18].

recombination, either directly [177] or indirectly by increasing the density of recombination sites [178], Fe appears to promote c-component loop formation in electron irradiated Zr doped with different levels of Fe [179]. Segregation of Fe at dislocation loops has also been observed in electron and proton irradiated Ti [180]. Other than any direct effect of Fe atoms on recombination [177], there are two other conceivable explanations to account for the neutron irradiation results of [113]: (i) high concentrations of Fe could promote the formation of high densities of a-type loops, thus increasing the ratio of a- and c-type sinks and thereby reducing irradiation growth (Figs. 4–2); (ii) high concentrations of Fe could produce large numbers of small Fe-rich precipitates, thus promoting recombination.

Although alloying elements and impurities can have a significant effect on irradiation growth (largely through their impact on point defect clustering), other factors important for irradiation growth are the as-fabricated microstructures: texture, dislocation density and grain structure (size and shape). The effects of microstructure can be accounted for using rate theory including those parameters, i.e. more than the simple case given by Equations (4.1) and (4.2). Such models can give a reasonable account of the observed behaviour [39]. Although the evolution of the dislocation structure during irradiation is important, the pre-existence of c-component dislocations in cold-worked materials precludes the need to form basal plane c-component loops in order to have a sink structure allowing the partitioning of interstitial and vacancy point defects to different sinks. In fact, in cold-worked material c-component loops evolve readily by helical climb on existing c-component screw dislocations [141,181–185]. There is therefore no

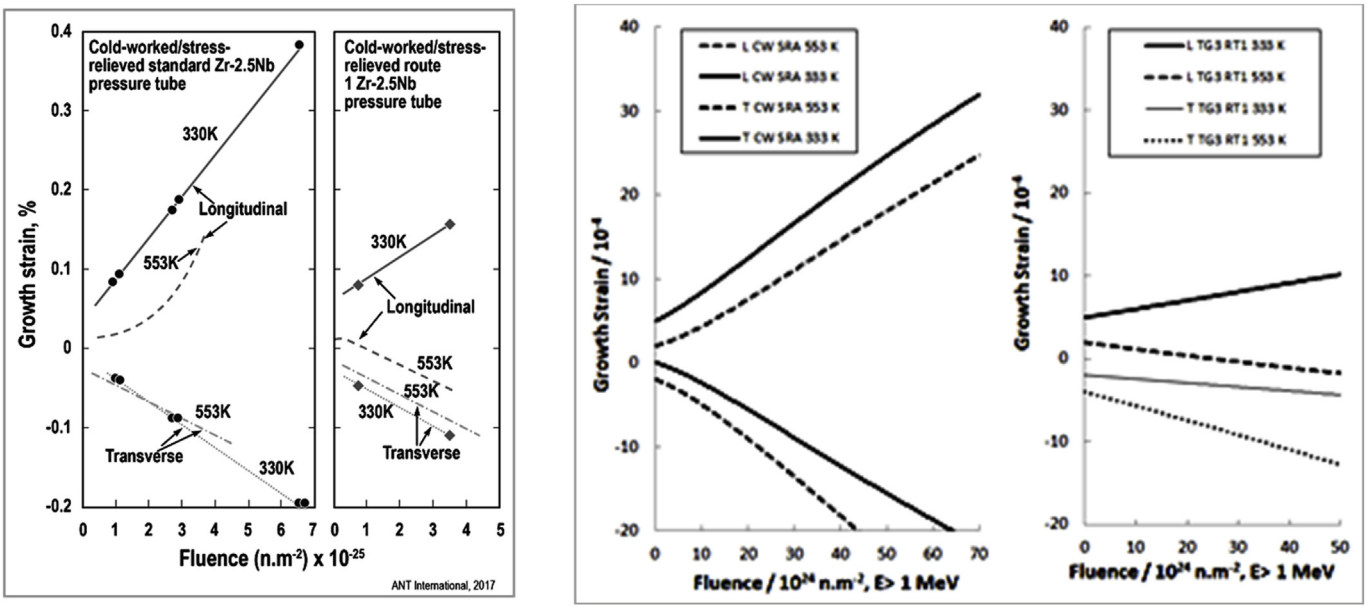

Fig. 4–4. Comparison of high temperature growth of iodine zirconium, Zircaloy-2, Zr-2.5Nb, and EXCEL alloy Adapted from Tucker et al. [126] and Griffiths et al., [187].

incubation period for accelerated growth in cold-worked materials because the requisite sink structure is already present. Rate-theory models should therefore include the original dislocation structure, grain shape and grain orientation (texture) with an additional provision for microstructure evolution. After taking into account the microstructures, rate theory models can account for the observed growth in Zr–Nb and Zr–Sn alloys using 1% and 3% point defect production efficiencies respectively [39]. It is noteworthy that Zircaloy-2 pressure tubes exhibit three times higher diametral creep compared with Zr-2.5Nb pressure tubes made by a similar manufacturing process [40]. The amount of cold-work and texture are similar in both cases, although the grains in the Zircaloy-2 pressure tubes are larger than those in Zr-2.5Nb tubing [172,184]. Unless the grain structure is responsible, one can hypothesize that the difference in the chemistry (Sn or Nb in solution) has an impact on damage production efficiency.

For the most part steady-state irradiation growth is largely assumed to be linear with neutron fluence, and independent of neutron flux, for a given microstructure. There are transients in irradiation growth that are associated with changes in the microstructure (evolution of a given sink structure, e.g. dislocation loops), or relaxation of residual inter-granular stresses or recovery and recrystallization effects, or both. For a given microstructure, in the absence of any transient effects, the main factor, other than dose, affecting irradiation growth is the irradiation temperature.

4.1.1. Temperature and flux dependence

4.1.1.1. Temperature. Zr and U are similar in that they exhibit irradiation growth that can be explained in terms of anisotropic crystal structures and properties. They differ in that the temperature dependence of irradiation growth is negative for U (higher in magnitude at lower temperatures) [160], and positive, for the most part, for Zr-alloys such as Zircaloy-2 and -4 (higher in magnitude at higher temperature), [18]. A large part of the positive temperature dependence for irradiation growth appears to be related to the propensity for basal plane c-component loop formation at higher temperatures, especially in large-grained, annealed materials [18,151]. However, axial irradiation growth of cold-worked Zr-2.5 Nb decreases with increasing temperature [188]. This may be because cold-worked Zr-2.5Nb is not sensitive to the same factors controlling c-component loop formation in annealed Zircaloys, c-component loop nucleation occurring on existing screw dislocations in cold-worked materials [172]. Also, the grain dimensions are small in Zr-2.5Nb pressure tubing and the sink strengths can be such that grain boundaries dominate the sink structure. The negative dependence of axial irradiation growth on temperature then follows from the effect of increasing DAD [39]. Given that the 1-3f dependence of irradiation growth arises directly from the partitioning of an excess of vacancies to basal plane sinks and an excess of interstitials to prism plane sinks, the more that grain boundaries affect the growth the more deviation from 1-3f one can expect. Coupled with that, if c-component loop nucleation increases with temperature, as appears to be the case, then bypassing that stage in the microstructure evolution by nucleation and growth on existing c+a screw network dislocations reduces the dependence on this rate-controlling component in the irradiation growth process [172,184].

Longitudinal irradiation growth of standard, cold-worked, pressure tubing exhibits a negative temperature dependence even before a basal plane c-component loop structure has time to evolve. One way in which a negative temperature dependence can be achieved in fine-grained materials such as Zr-2.5Nb pressure tubing (grains flattened in the radial direction and having a transverse basal texture) is if there is a reduction in anisotropic diffusion (DAD) at lower temperatures, i.e. an increase in DAD with increasing temperature [39]. The concept of DAD applied to irradiation growth of Zr alloys was originally proposed in Ref. [163]. Woo and then Tome et al. built on this phenomenon, developing models for irradiation growth [165,189–192], based primarily on dislocations. Woo [165] and also Holt and Fleck [188] developed treatments that included grain boundaries as biased sinks (due to anisotropic diffusion); the DAD concept was used to account for the unusual temperature dependence of irradiation growth for non-standard Zr-2.5Nb pressure tubing known as task group 3, route 1 (TG3 RT1) tubing [193]. The TG3 RT1 tubes exhibited negative axial irradiation growth compared to standard pressure tubes even though the textures were similar [194]. The TG3 RT1 tubes differed from the standard pressure tubing in having lower dislocation

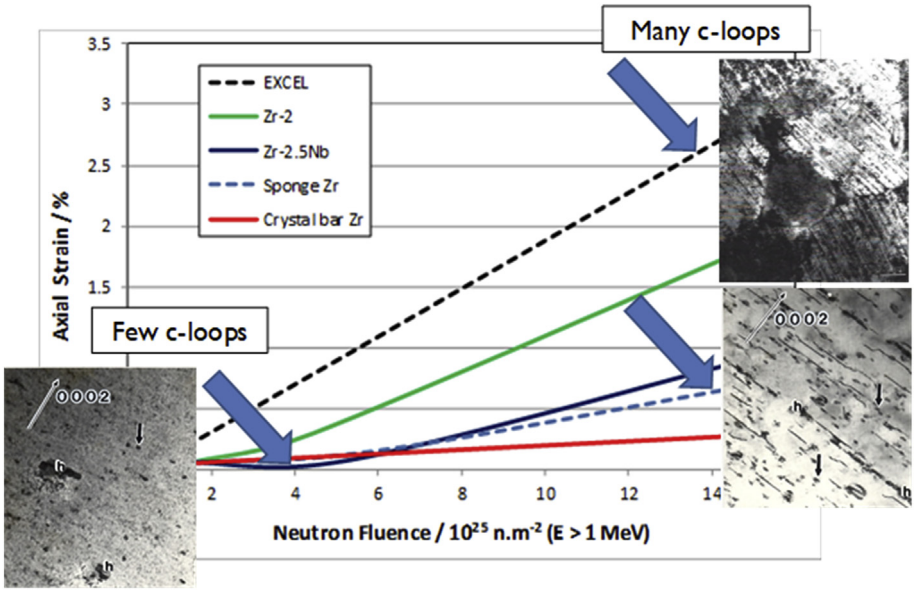

Fig. 4–5. Dependence of predicted longitudinal irradiation growth on DAD bias parameter in Zircaloy-2 with different grain structures. The dashed lines correspond to annealed material with a low dislocation density and the solid lines correspond to cold-worked material with a high dislocation density. The equiaxed grains have diameters of 5 μm and the platelet grains have dimensions of 0.1, 0.5 and 2 μm in the radial, transverse and longitudinal directions respectively. The texture is idealized with the c-axis in the transverse direction (see text).

densities and thinner grains [193,194]. The TG3 RT1 tubes were designed to have a low dislocation density to reduce growth; the grain size was also reduced in order to maintain strength because of the lower dislocation density. DAD could account for the negative temperature dependence of growth of both standard pressure tubing, and the change in sign of the growth for non-standard TG3 RT1 pressure tubing, if one assumed that the degree of anisotropic diffusion increased with increasing temperature [39,188].

In contrast to the negative temperature dependence of axial irradiation growth for cold-worked Zr-2.5Nb pressure tubing, cold-worked Zircaloy-2 exhibits the opposite temperature dependence in the absence of c-component loop formation [18,118]. Rogerson's results, in particular, showed that cold-worked Zircaloy-2 exhibited a decreasing growth rate with increasing temperatures in the range of 550 K and 600 K (277 °C–327 °C), and this trend was not exhibited by annealed Zircaloy-2. The most likely explanation for this behaviour is if there was recovery of the cold-worked dislocation structure. At temperatures greater than about 673 K (400 °C) Rogerson showed the irradiation growth increased but there was considerable variability. The increased growth could be attributed to the formation of c-component loops and reflects the variability in c-loop formation given that the post-breakaway irradiation growth rate is directly related to the c-component loop density [39,187].

A rate-theory formulation can be used to describe the irradiation growth behaviour of Zr-alloys as a function of microstructure [39]. The effect of the varying the DAD bias parameter on longitudinal elongation rate is shown in Figs. 4–5 for large-grained equiaxed and fine-grained platelet grain structures. The effect of increasing the DAD bias parameter on the axial (longitudinal) elongation rate (per dpa, assuming 1% freely-migrating point defects) is illustrated for pressure tubing with texture parameters of $f_R = 0.4$ and $f_T = 0.6$ and $f_L = 0$ and for platelet grains with dimensions of 0.1 μm, 0.5 μm, 2 μm in the radial, transverse and longitudinal directions respectively. The solid line shows the response for standard pressure tubing with $\rho_a = 4 \times 10^{14}\,m^{-2}$, $\rho_c = 1 \times 10^{14}\,m^{-2}$. The dotted line is the output maintaining the same dislocation structure but for equiaxed grains of 1 μm diameter. It is clear that the irradiation growth has a strong negative dependence on the DAD parameter for the flattened platelet grains, whereas there is a weak positive dependence for the equiaxed grains. The temperature dependence of irradiation growth that is observed may, in part, be related to the effect of temperature on DAD [163] but will also be affected by recovery of network dislocations or dislocation loop structures at high temperatures. Increasing temperature also increases the propensity for c-component loop formation [162,168,169,187] and there is also a potential synergy between increasing DAD and the likelihood of c-component loop formation at higher temperatures [195].

In production bias models the increasing irradiation growth at high temperatures has been attributed to an increase of freely migrating vacancy point defects that would otherwise have been tied up in small clusters formed in collision cascades [196–198].

The data for Figs. 4–5 were obtained using a model developed for Zr-alloys used to demonstrate the dependencies of irradiation growth on different microstructural parameters [39], see Section 4.2. The model output is compared with growth data in Figs. 4–6. The rate-theory model uses applicable microstructural parameters for Zr-2.5Nb pressure tubing and TG3 RT1 experimental tubing and employs a DAD interstitial bias that increases with increasing temperature. Qualitative agreement with experimental data is demonstrated.

Temperature dependencies for physical parameters such as anisotropic diffusion are confounded by the effect of temperature on microstructure, either because of recovery of dislocations or stabilization of c-component loops at higher temperatures. In general one observes lower a-type dislocation loop densities with increasing temperature (151, 184). Other explanations have been posited regarding the temperature dependence of irradiation growth, the most notable being the production-bias effect. The production bias model for Zr [198] assumes that vacancy clusters form in collision cascades from cascade collapse and are more stable at lower temperatures. The freely-migrating point defect population is then a function of temperature and this then drives

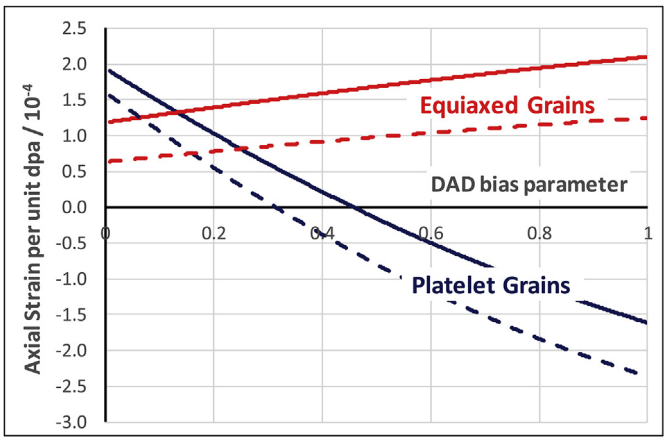

Fig. 4–6. Temperature dependence of irradiation growth of cold-worked/stress relieved and Route-1 Zr-2.5Nb pressure tube material: (a) experimental data [18]; (b) rate-theory model output. Note the change in direction of growth of Route-1 material longitudinal specimens with increasing temperature.

the response. If the vacancy basal plane loops are always potential vacancy sinks then a shift to more freely migrating vacancies could explain the rapid increase in growth (from c-loop formation) that is observed at temperatures >350 °C in the Zircaloys [118]. This could be an explanation for the evolution of the c-loops associated with accelerated growth at higher temperatures in the Zircaloys. Other hypotheses on the temperature dependence of accelerated growth are based on the effect of higher irradiation temperatures on the dispersal of impurities that promote c-loop formation and growth [187]. The positive temperature dependence observed for Zircaloy-2 at temperatures up to 400 °C [118] could also be due to the effect of recombination if the intrinsic vacancy migration energy (1.3 eV) applied [61,134]. For the vacancy migration energy less than 1 eV that is likely applicable to Zr-alloys [165,199–201], there will be no effect of recombination on reducing the point defect concentrations due to recombination for the temperature range of interest (>250 °C) [39].

It should be noted that, at the time of his 1962 report Buckley concluded that the irradiation growth of U and hexagonal close-packed metals such as Zn, Cd, Zr and Ti followed the same trend and actually decreased with increasing temperature. Buckley demonstrated that Cd, Zn, Zr and Ti elongated in the direction of smallest thermal expansion coefficient. In his conclusions he suggested that " …. the temperature dependence of growth rates in uranium and the hexagonal metals, and its disappearance above self-diffusion temperatures, could be a manifestation of thermal annealing of the defect clusters". The dependence of growth on cluster formation rather than point defect diffusion would account for the lack of an effect of cold-working on irradiation growth observed by Buckley, at least for U [160]. In fact, although Buckley dismissed cold-working as affecting the irradiation growth of U at low temperatures he later showed that his model of irradiation growth (dependent on thermal expansion anisotropy) at homologous temperatures between $0.2T_m$ and $0.33T_m$ only applied to metals that were annealed [202]. He also showed that irradiation growth also occurred in cubic materials with the positive expansion corresponding with the direction of cold-work [202].

In rate-theory modelling the temperature dependence of irradiation processes such as growth is intimately coupled with the damage rate dependence, which is proportional to the fast neutron flux. Neutron fluence is often regarded as a state variable when it comes to describing the fluence dependence of steady-state irradiation growth, i.e. after an initial transient. The displacement damage rate (neutron flux) will be important when it comes to time-dependent processes such as creep. For growth, however, the main effect of damage rate is whether one is in a sink-dominated or a recombination dominated regime and this is dependent on the temperature, vacancy migration energy and choice of recombination parameter. Given that for Zr the vacancy migration energy is somewhat uncertain [203], and so is the recombination parameter [204], one can best decide whether one is in a recombination- or sink-dominated regime simply by comparing growth behaviour for the same material at two different damage rates. Figs. 4–7 shows a rate-theory output for interstitial migration to dislocation sinks in a cold-worked Zr-alloy as a function of temperature for a high flux (OSIRIS) and low flux (NRU) reactor irradiation given a range of possible migration energies [177,203]. The plot shows that strong temperature dependencies could be expected depending on the point defect properties and that the growth rate decreases by orders of magnitude when one transits to the recombination regime. Given that temperature affects the microstructure, and thus growth to some extent, if one observes comparable growth rates at widely differing temperatures (say 60 °C and 300 °C) then it is likely that one is in a sink-dominated regime and any effect of temperature is determined by the effect on anisotropic diffusion and microstructure rather than the vacancy migration energy.

4.1.1.2. Neutron flux (damage rate). The rate theory output shown in Figs. 4–7 illustrates that a strong temperature dependence on irradiation growth can arise simply as a result of the transition from recombination- to sink-dominated reaction kinetics. Figs. 4–7 also shows that, for recombination-dominated effects, any temperature dependence is concurrent with a neutron flux dependence. In Figs. 4–7 the net interstitial flux to dislocations is shown for damage rates corresponding to high and low flux materials test reactors that are an order of magnitude different in damage rates, i.e. ATR and OSIRIS compared with DIDO and NRU. Although the fast neutron flux gives an approximate measure of the relative displacement damage rate, especially for Zr-alloys, spectral differences can be important. Many reactors have been characterized in terms of the dpa per unit fast neutron fluence [10,205]. It turns out that growth data from the DIDO reactor, which has been the source of many studies on irradiation growth of Zr-alloys, has been incorrectly characterized for two reasons: (i) the fast fluences were originally determined from the activation of Fe flux monitors based on the fission spectrum rather than the spectrum applicable to the irradiation site; (ii) the dpa calculations were performed using the estimated, not the adjusted, spectrum [206]. Many of the published growth data have been plotted as a function of fast neutron fluence and the growth behaviour in various reactors have, in the past, been compared assuming that the displacement damage ((rate) is roughly the same for a given fast fluence (flux). Conclusions have been reached regarding neutron flux dependencies for ATR relative to DIDO at about 50 °C [18], and OSIRIS relative to DIDO and NRU/CANDU at about 280 °C [93]. In the latter case an assessment of the relative dpa rate between OSIRIS, DIDO and NRU/CANDU was performed, and it was concluded, that fast flux was a reasonable measure of relative displacement damage provided the fast neutron fluence correction for fission spectrum in DIDO was not applied. The comparisons between DIDO and OSIRIS data were made over a very short fluence range ($<1 \times 10^{25}$ n.m^{-2}, E > 1 MeV) and were taken from early data reported by Murgatroyd and Rogerson [207] from the same, although slightly altered, data set later reported by Rogerson and Murgatroyd [118,120] also plotted in Figs. 4–8. It was concluded by Holt et al. [125], that the irradiation growth rates as a function of fast neutron fluence of Rogerson's cold-worked Zircaloy-2 material irradiated were not consistent when irradiated in DIDO and OSIRIS. When one corrects for the

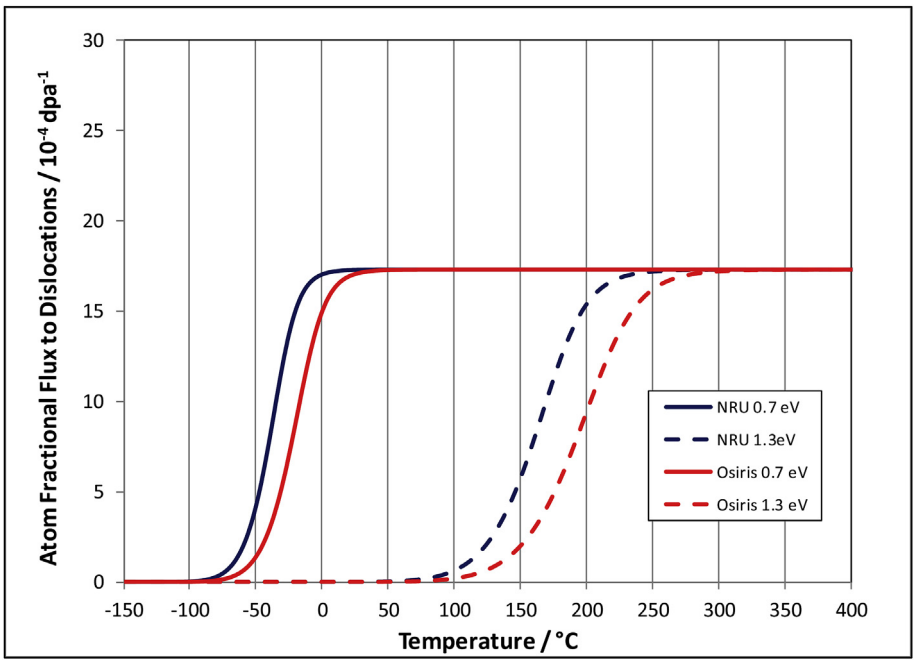

Fig. 4–7. Net flux of self-interstitials to dislocations in CW Zr as a function of temperature (assuming 3% damage efficiency on NRT calculations) for different damage rates. The damage rate is proportional to neutron fluence at temperatures >300 °C for all conceivable vacancy migration energies (E_v), 0.7 eV - 1.3 eV, and a recombination parameter, n = 10, after Heald and Speight [164].

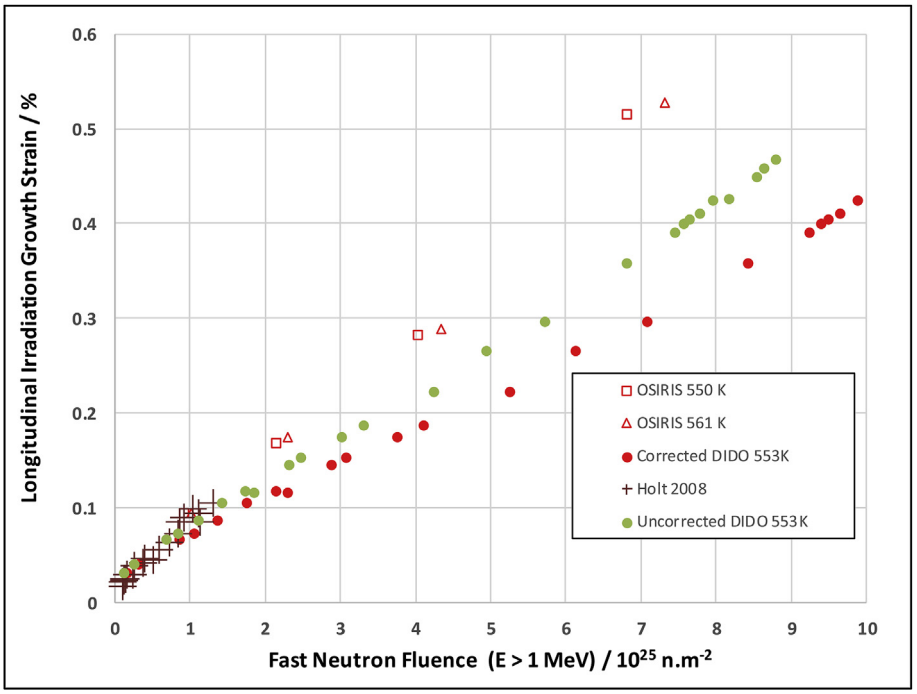

Fig. 4–8. Irradiation growth of 25% cold-worked Zircaloy-2 (SGHWR pressure tube manufactured by Chase Nuclear) as a function of fast fluence and irradiated in the OSIRIS, ATR and DIDO reactors at about 553 K (280 °C).

errors in fluence measurement and damage rate calculation in DIDO, the comparisons of irradiation growth as a function of dpa show a similar lack of alignment. Figs. 4–8 shows the DIDO growth data for the cold-worked Zircaloy-2 pressure tubing at about 60 °C and 280 °C [120] corrected for spectral effects (both fluence measurement and dpa calculation) and plotted with data for the same material from ATR [18] and OSIRIS [125]. The damage rates are approximately 8×10^{-8} dpa.s^{-1} for the DIDO case and 3×10^{-7} dpa.s^{-1} for ATR and OSIRIS. Although the higher damage rates are only about four times larger, it is clear that, at both high and low temperatures, the higher damage rates correspond with higher rates of irradiation growth per unit dpa and not lower rates as one

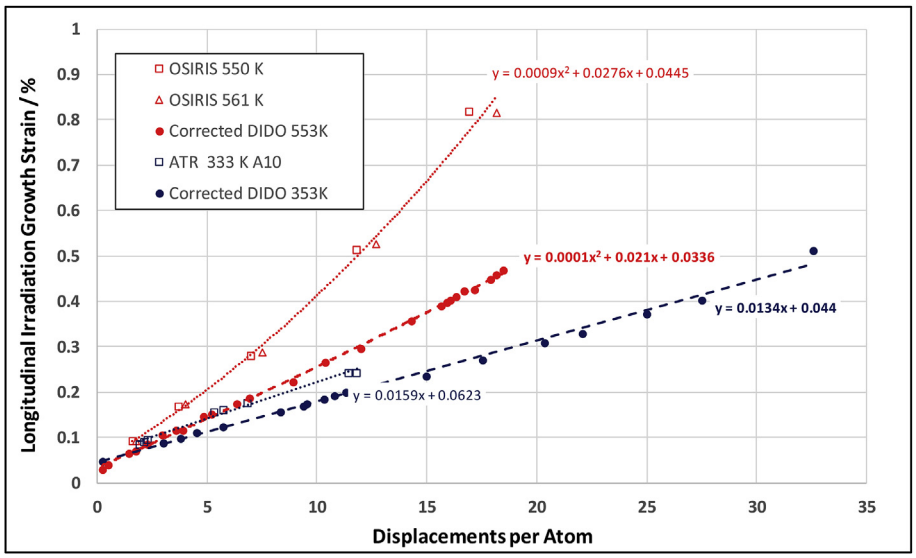

Fig. 4–9. Irradiation growth of 25% cold-worked Zircaloy-2 (SGHWR pressure tube manufactured by Chase Nuclear) as a function of dpa and irradiated in the OSIRIS, ATR and DIDO reactors.

might expect if recombination was dominant. Therefore, either irradiation growth is positively correlated with the dpa rate or the growth specimens, albeit from the same pressure tube, are different. One thing is clear, if the irradiation growth is dependent on dpa rate it is not because of recombination, because that would result in lower growth per unit dpa at higher fluxes (see Figs. 4–7), not higher growth per unit dpa as shown in Figs. 4–9.

Because of the discrepancies between irradiation growth rates in the different reactors some researchers have advocated adjusting for the differences based on characteristic growth specimens that were assumed to give the same growth per dpa in any reactor, i.e. each had identical microstructures [46,208]. However, comparisons of identical materials irradiated in different reactors [124] show internal inconsistencies. The shifts one would apply to match the growth curves for Rogerson cold-worked Zircaloy-2 the irradiation growth of cold-worked Zr-2.5Nb pressure tubing (Material A in Ref. [124]) go in different directions. For the Zr-2.5Nb pressure tube data (Material A) conversion to dpa shows that there is reasonable agreement OSIRIS and DIDO reactor irradiations, see Figs. 4–10. Ignoring the initial offset that could arise from the relaxation of inter-granular stresses, there may be a slightly higher rate of growth per unit dpa for the higher damage rate irradiation (OSIRIS) but the difference is not statistically significant. Figs. 4–10 also shows the transverse growth, which exhibits the same relative behaviour (higher negative rate for the higher damage rate). The differences in growth per unit dpa between the high flux and high flux datasets described here are quite small and within the range of variability normally exhibited by Zr-2.5Nb growth specimens [124]. In light of the fact that flux effects should result in less, not more, growth at the higher damage rates and the experimental data came from multiple specimens in a program designed to explore and control material variability one can conclude that, for the Zr-2.5Nb pressure tubing at least, the effect of dose rate at 280 °C is negligible. Given that the relative dose-rate behaviour is not consistent with what one might expect based on a consideration of recombination using reaction rate theory, one can conclude that either: (i) the Zircaloy-2 data are compromised by specimen variability; or (ii) Zircaloy-2 behaves differently with respect to damage rate compared with Zr-2.5Nb, which exhibits negligible difference in growth rates when comparing OSIRIS and DIDO as a function of dpa.

4.2. Modelling irradiation growth

There are two approaches to modelling irradiation-induced growth: empirical and mechanistic. Empirical models are distinct from mechanistic models in that they are simply designed to describe the phenomenon of interest in terms of the controlling variables by establishing statistical relationships from the data and are only applicable within the variable range used to derive the model parameters. Mechanistic models are designed to be accurate descriptions of the phenomenon that include the fundamental physical mechanisms contributing to the object of the model in question and are, in principle, applicable outside of the range of any available data. In the absence of operational experience many of the earliest models were either mechanistic or semi-empirical.

4.2.1. Empirical models of irradiation growth

The earliest empirical and semi-empirical models for irradiation growth in Zr-alloys up until 1980 were reported by Hesketh et al. [16], Harbottle [209], Harbottle and Cornell, [210]. and Bullough and Wood, [201]. A dearth of good quality data on irradiation growth meant that most researchers turned to mechanistic models.

Today researchers have had the benefit of an additional 40 years of operational data and a wealth of test data using many different research reactors that have been operating for over 50 years. Many of the research reactors have now shut down but new reactors (JHR for example) are being built to provide a resource for experimental testing while at the same time providing isotope production. Empirically derived models used in engineering models for reactor design and operation have been reviewed in Ref. [39].

The empirical correlations for the irradiation growth of zirconium alloys utilized in design and licensing analyses are generally of a power-law form given by Geelhood et al. [211,212] and Luscher et al., [213]. The equations are of the following general form:

$$\Delta\varepsilon = A \cdot G(\varphi \cdot \Delta t)^m \tag{4.3}$$

where A and G are material constants, A being determined by the alloy and its metallurgical state (cold-work or annealed, for example) and G is a growth parameter dependent on the Kearns texture parameter (f) and is (1-3f). This latter parameter has a mechanistic basis, see Section 4.2.2. The product of the neutron flux

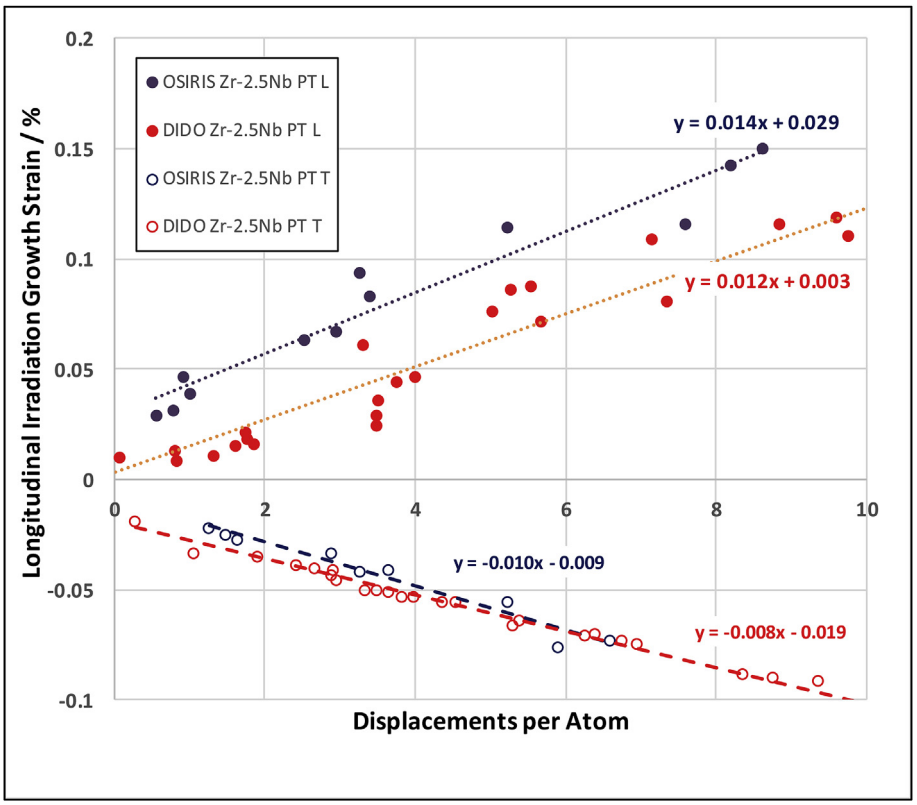

Fig. 4–10. Irradiation growth of the same material taken from a 27% cold-worked Zr-2.5Nb pressure tube (Material A in Fleck et al., [124]) as a function of dpa and irradiated in the OSIRIS and DIDO reactors.

(φ) and time (t) is a measure of the total neutron dose. The equations that have been developed are essentially a series of polynomials in fluence applied in terms of time increments during different stages of the growth. The total strain at any point during service is given by,

$$\varepsilon_{t+\Delta t} = \varepsilon_t + A \cdot G(\varphi \cdot \Delta t)^m \tag{4.4}$$

4.2.2. Mechanistic models of irradiation growth

Mechanistic models address the variables controlling growth in terms of the physical mechanisms affecting the strain. A number of different attempts have been made to model irradiation growth of Zr-alloys over many years, primarily, but not exclusively, based on a rate-theory approach. A number of notable models have been proposed [125,141,163,165,188–192,198,201,214–221]. Some of the early mechanistic models assumed that only interstitial loops formed during irradiation, [214]. Other models assumed that dislocations were net interstitial sinks and the growth occurred due to an excess of vacancies migrating to grain boundaries in grains of different shapes [215]. The observation of the co-existence of interstitial and vacancy a-type loops created some problems for modellers, but the possibility that the loops were primarily interstitial in nature at power reactor temperatures [222] allowed that assumption to be applied and grain boundaries were still considered as net vacancy sinks [201,216]. The very important concept of intrinsic interstitial anisotropic diffusion introduced by Woo and Gosele [163], provided a means of accounting for irradiation growth in the presence of a mixed population of vacancy and interstitial a-type loops. DAD also provided a means of having variable bias differentials according to the orientation of the sinks and thus provided for the possibility of having stable vacancy loops on the basal plane [125,165]. Once data were accumulated at higher fluences, transient behaviour became apparent and modelling efforts were directed at understanding the effects of grain interaction stresses on irradiation growth [167,189,219,223,224]. The observation of breakaway growth resurrected the possibility that high growth rates were driven primarily by the formation of basal plane vacancy loops. Even though the observations of neutron irradiation were the same during electron irradiation (the co-existence of vacancy and interstitial a-type loops and the formation of vacancy basal plane loops [151]) researchers still invoked cascade effects in modelling. The evolution of the production bias concept provided a mechanism to account for the increase in irradiation growth at high temperatures, as vacancy loop clusters created by cascade collapse disintegrated, freeing up vacancies to form basal plane vacancy loops [197,198]. Likewise, one-dimensionally diffusing interstitial clusters formed at the edges of collision cascades were invoked to account for irradiation growth in a manner similar to DAD [220,225].

Since irradiation growth in annealed poly-crystalline Zr is generally about ten times greater than for single crystal material [118,226,227], and increases with decreasing grain size [117], grain boundaries have been considered important sinks for point defects, especially in annealed Zr and Zr-alloys for which the only other type of sink is a-type dislocation loops. In single crystal material the growth quickly saturates at low fluences, $\approx 0.1 \times 10^{25}$ n.m^2 (E > 1 MeV). In annealed polycrystalline material, growth almost saturates at low fast neutron fluences but there is a smaller long term steady-state growth rate, proportional to the neutron fluence. If there were only a-type dislocations or dislocation loops present

in a material, grain boundaries provide an alternate sink. If one assumes that the a-type dislocations have a bias for interstitial absorption [164] then any long-term irradiation growth has to involve a net absorption of vacancies at grain boundaries. For annealed Zr-alloy materials, in particular, where a-type dislocation loops are the only dislocation sink observed [228], early models for irradiation growth considered grain boundaries to be net vacancy sinks [214]. Fidleris et al. [117] showed that irradiation growth is inversely dependent on grain size in annealed polycrystalline Zr for grains of 23 μm and 225 μm diameter irradiated at 330 K. There was a similar dependence for Zircaloy-2 with grains of 12 μm and 31 μm diameter irradiated at about 680 K, but this was reversed for irradiation of Zircaloy-2 at 330 K [18].

Hesketh et al., [16], proposed that irradiation growth of polycrystalline material could be described by a model in which atoms were transferred from basal to prism planes. Grain boundaries were assumed to be neutral sinks and interstitial point defects migrated to a-type dislocations and dislocation loops. Hesketh et al.'s model was based on the earlier hypothesis of Buckley [160], to account for irradiation growth in Zr. They related the irradiation growth to the texture through the parameter G = 1−3T where G is a growth coefficient and T is the basal pole texture coefficient in the growth direction, more widely known as the Kearns texture parameter, f [12]. The 1-3f relationship is a direct consequence of the Buckley model in which there is a net flux of vacancy point defects to basal plane sinks (dislocation loops) and a net flux of interstitial point defects to prism plane sinks (dislocation loops). The 1−3T (1-3f) model is equally applicable however, if there are an excess of prism plane interstitial dislocation loops with all other sinks randomly oriented, as in the Hesketh et al. model. The Hesketh et al. model could be considered applicable to the cases where vacancy basal plane loops are absent, e.g. in the early stages of irradiation growth when the a-loop population is evolving. The Hesketh et al. model could then be considered as applicable to the initial transient period of irradiation growth observed for annealed materials. In that case the irradiation growth strain increases rapidly with dose and then slows to zero or a very low rate coincident with the cessation of loop evolution, provided there was an excess of interstitial point defects accumulating at the a-type loops [229]. The a-type loop evolution is practically complete at low doses (<1 dpa or $<2 \times 10^{24}$ n.m^{-2}, E > 1 MeV) after which any further growth of annealed material has to be accounted for by a biased flow of interstitials to the a-type loops or by anisotropic diffusion to grain boundaries [163], or both. In the presence of an a-type dislocation network irradiation growth can be explained by a biased flow of interstitials to dislocations leaving and excess of vacancies to accumulate at grain boundaries [216]. The presence of c-component dislocations in the network adds to the sink anisotropy in the same way as adding c-component dislocation loops [151] leading to high rates of non-saturating growth. The question of why c-component defects on basal planes tend to attract vacancies can best be explained by anisotropic diffusion [163,167]. Accelerated irradiation growth of annealed material due to the formation of vacancy loops on basal planes is likely to be governed by the same mechanism that promotes high rates of irradiation growth in cold-worked materials, i.e. helical climb on existing c-component screw dislocations at temperatures between 60 °C and 400 °C [172,184].

Consider the 1-3f model in the context of the Buckley model. The 1-3f model is derived from the sum of the strain tensors from each individual grain resolved onto the specimen coordinate system. For a-type interstitial dislocation loops that are equally distributed on all prism planes and c-type vacancy loops on the basal plane, the strain tensor of individual grains referred to principle axes (corresponding to the principle crystallographic axes) is given by,

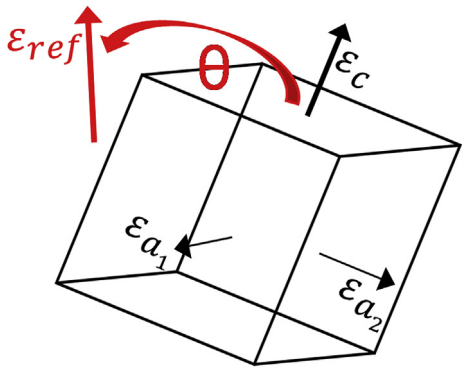

Fig. 4–11. Strains in Zr single crystal represented with respect to Cartesian axes.

$$\begin{bmatrix} \varepsilon_{11} & 0 & 0 \\ 0 & \varepsilon_{22} & 0 \\ 0 & 0 & \varepsilon_{33} \end{bmatrix} = \begin{bmatrix} \varepsilon_{a1} & 0 & 0 \\ 0 & \varepsilon_{a2} & 0 \\ 0 & 0 & \varepsilon_{c} \end{bmatrix} = A \cdot \begin{bmatrix} 1 & 0 & 0 \\ 0 & 1 & 0 \\ 0 & 0 & -2 \end{bmatrix} \tag{4.5}$$

where A is a constant. The crystal coordinates are shown in Figs. 4–11.

The resolved strain in the reference specimen coordinate system is given by,

$$\varepsilon(\theta)_{ref} = \varepsilon_c \cdot \cos^2\theta + \varepsilon_{a2} \cdot \sin^2\theta \tag{4.6}$$

where the angle between the reference direction and the basal plane = θ. For each grain (i) in a poly-crystal

$$\varepsilon(\theta_i)_{ref} = \varepsilon_c \cdot \cos^2\theta_i + \varepsilon_{a2} \cdot \left(1 - \cos^2\theta_i\right) \tag{4.7}$$

Summed over a poly-crystal:

$$\varepsilon_{ref} = \varepsilon_c \cdot \sum_i V_i \cdot \cos^2\theta_i + \varepsilon_{a2} \cdot \sum_i V_i \cdot \left(1 - \cos^2\theta_i\right) \tag{4.8}$$

$$\varepsilon_{ref} = -2 \cdot \varepsilon_a \cdot f_{ref} + \varepsilon_{a2} \cdot \left(1 - f_{ref}\right) = G \cdot \left(1 - 3 \cdot f_{ref}\right) \tag{4.9}$$

where f is the Kearns texture parameter.

The 1-3f relationship did not work well to explain the irradiation growth of materials with small, anisotropically shaped grains, i.e. when grain boundaries were dominant sinks. Holt and Ibrahim [216] introduced a modification to the growth anisotropy factor originally proposed by Hesketh et al., [16]. They proposed that irradiation growth was modified by the grain structure such that the growth factor $G = P_d/2 - 2A_d$, where A_d, is a grain boundary anisotropy factor for the direction, d and P_d is the resolved prism plane component of texture. The parameter A_d was defined as,

$$A_d = \frac{\frac{1}{d_d}}{\frac{1}{d_R} + \frac{1}{d_T} + \frac{1}{d_L}} \tag{4.10}$$

where d_d is the grain dimension in the direction d; likewise d_R , d_T and d_L are the grain dimensions in the radial (R), transverse (T) and longitudinal (L) directions of the component of interest. This growth factor (G) was later modified by Holt et al. [230], in terms of the basal pole texture parameter to be consistent with the anisotropy factor, $G = 1-3f_d$, where f_d is the basal pole texture parameter for the direction, d, as proposed by Hesketh et al. [16] and Tempest, [231]. The grain boundaries were considered to be unbiased vacancy sinks that absorbed the excess of vacancies due to the biased

absorption of interstitial point defects at network dislocations and dislocation loops.

As modelling efforts evolved it was soon realized that the irradiation growth could not be adequately accounted for in terms of the simple models based on isotropic diffusion of interstitial and vacancy point defects, i.e. where the net flux to dislocations was based on the interaction of the point defects and dislocation strain fields [164]. It was recognized that when grain shapes are anisotropic (as for cold-worked and stress-relief annealed (SRA) materials), a modification was needed to account for the effect of grain boundaries on the anisotropy of irradiation growth. Irradiation growth could be better explained by invoking anisotropic diffusion of interstitial point defects in the basal plane [163]. Woo, coined the acronym DAD (diffusional anisotropy difference) to describe the irradiation growth behaviour of Zr-alloys during irradiation. The inclusion of anisotropic diffusion then meant that grain boundaries would be biased sinks based on their orientation relative to the crystal structure of the grain]. Woo proposed a model for irradiation growth that included anisotropic diffusion [165]. In Woo's model the grain dimensions were for the first time explicitly included as biased sinks. This model was applied to account for the irradiation growth of Zr-2.5Nb pressure tubing by Holt and Fleck, [188]. Experimental observations to support the existence of DAD came from a rationalization of irradiation growth data and direct observations of cavity growth during electron irradiation in a HVEM [195].

Rate theory models have been developed that take into account the grain dimensions in relation to the relative orientation between the crystal structure and the grain boundary [58,167,190,191, 232 ,233]. Golubov et al.'s model relies on anisotropic diffusion based on one-dimensional interstitial cluster migration. By comparison, earlier established models included a grain boundary bias induced by the anisotropic diffusion of self-interstitial atoms, the so-called DAD effect [165,188]. Both approaches give essentially the same result. There is some question about how rate-theory models should be applied when one is essentially considering mobile species and there may be an inequality in interstitial and vacancies due to preferential clustering of one type over another in the collision cascade. The clustering of one species leads to more of the other species being available to migrate to sinks, the so-called production bias. One needs to then consider whether there are more interstitials clustering in collision cascades or more vacancies. Additional complications arise when one considers that some of these clusters may be mobile and themselves able to migrate to sinks [220]. In the case of vacancy clustering there will be a bias for the production of interstitials at low temperatures due to vacancy clustering but more vacancies will be available to migrate to sinks as the intra-cascade clusters become unstable at higher temperatures [198]. The intricacies, merits and limitations of the various proposed mechanisms governing point defect accumulation at sinks has been described and discussed in an excellent review by Woo [225]. With respect to the production bias Woo states that the bias does not originate from the reaction kinetics of the point-defects with the sinks and should not be confused with a sink bias such as the dislocation bias. He also notes that the interstitial clusters considered in the production bias model are immobile and any mobile interstitial clusters are effectively considered as part of the collection of the three-dimensional migrating interstitials annihilated at the sinks.

One of the best tools to illustrate how point defects partition to various sinks is through the use of rate-theory [165,167,220,221]. One can construct a set of balance equations that describes the point defect partitioning to various sinks based on bias parameters and sink densities. When modelling swelling in steels the directionality is not important and one simply needs to determine the excess biased flow of interstitials to dislocations in order to calculate what percentage of vacancies accumulate in cavities (three-dimensional sinks). For Zr-alloys void and cavity swelling is small and insignificant compared with irradiation growth and creep. Anisotropic strain, with and without an applied stress, is a big technological concern and to model that one needs to consider not just the net excess flow of one point defect over another but the direction of that flow. Rate theory models therefore need to accommodate the directional flow and the chance of interacting with various sinks, not only based on their density but also on their orientation. The resulting strain is anisotropic and can be demonstrated with a set of balance equations.

To illustrate and help understand how point defects migrate to different sinks thus producing strain one can construct a simple set of balance equations. If it is assumed that the sink orientation is biased for interstitial absorption following the DAD mechanism according to the bias parameter (p) indicating preferential diffusion in the basal plane, [163]. The dislocation bias for interstitials is denoted by the parameter, b, based on the size-effect interaction between dislocations and point defects [164]. The dislocation bias will also be modified by the DAD bias due to the line orientation [165] but for the sake of this treatment we will assume that any additional effects due to anisotropic diffusion and line orientation are subsumed into this dislocation bias term. The effect of stress can be incorporated as a bias parameter (s) resulting from elastodiffusion [166], if necessary. The model then becomes one for irradiation growth by setting $s = 0$. For simplicity only the growth model will be described here. Assuming that one is operating in a temperature regime where recombination and vacancy emission is insignificant, one can represent the net flux of interstitials and vacancies to sinks, resulting in strain in the radial (R), transverse (T) and longitudinal (L) directions of a given grain of dimensions $d_{R,T,L}$ by the following expressions:

$$J_R = \sum_R k_i^2 . D_i C_i - \sum_R k_v^2 . D_v C_v \tag{4.11}$$

$$J_T = \sum_T k_i^2 . D_i C_i - \sum_T k_v^2 . D_v C_v \tag{4.12}$$

$$J_L = \sum_L k_i^2 . D_i C_i - \sum_L k_v^2 . D_v C_v \tag{4.13}$$

Summing all sink strengths for sinks (s) internal to the grains,

$$\left(k_{i,v}^{gb}\right)^2 = \frac{k_{i,v}}{d_{R,T,L}} k_i = \sqrt{(1\ +b)\rho_a + \rho_c + \rho_N} k_v = \sqrt{\rho_a + \rho_c + \rho_N} \tag{4.14}$$

where the contributions from the a- and c-type network dislocations with densities ρ_a and ρ_c, and the dislocation loops, ρ_N (assumed neutral) to the total internal sink strength from which the grain boundary sink strength is derived [234] are assumed to be independent of the grain boundary orientation.

For a grain that has the c-axis parallel with the radial direction (Figs. 4–12) the sink strengths in the radial (R), transverse (T) and longitudinal (L) directions are, respectively:

$$k_i^2 = \rho_c + \frac{\rho_N}{3} k_v^2 = \rho_c + \frac{\rho_N}{3}\left(k_i^{gb}\right)^2 = \frac{k_i}{d_R}\left(k_v^{gb}\right)^2 = \frac{k_v}{d_R} \tag{4.15}$$

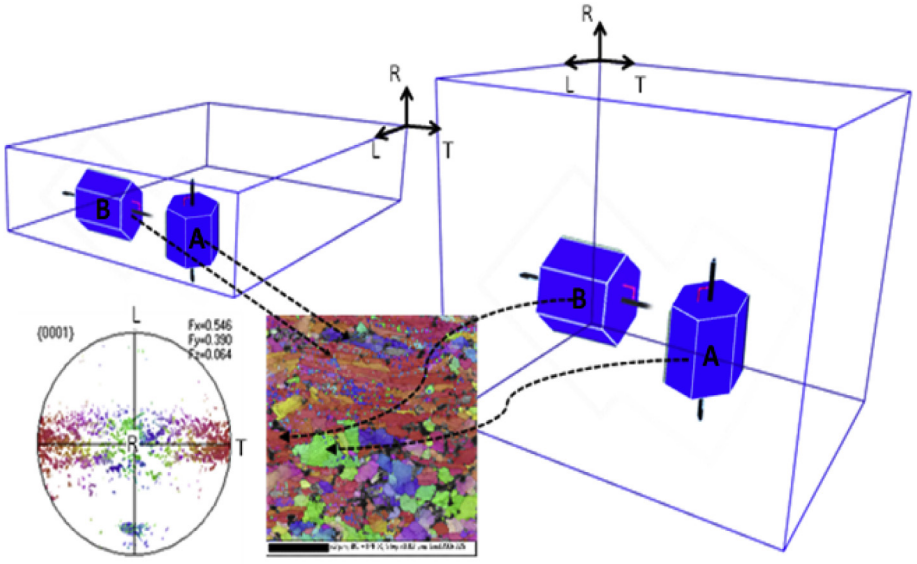

Fig. 4–12. Schematic diagram showing the possible combinations of grain shapes and crystallographic orientations in a cold-worked stress-relief annealed (SRA) material. Specimen of Zr-2.5 Nb pressure tubing: TEM, TKD and texture taken from (Bickel, 2013).

$$k_i^2 = (1+b).\frac{\rho_a}{2} + \frac{\rho_N}{3}k_v^2 = \frac{\rho_a}{2} + \frac{\rho_N}{3}\left(k_i^{gb}\right)^2 = \frac{(1+p).k_i}{d_T}\left(k_v^{gb}\right)^2 = \frac{k_v}{d_T} \tag{4.16}$$

$$k_i^2 = (1+b).\ \frac{\rho_a}{2} + \frac{\rho_N}{3}\ k_v^2 \ = \ \frac{\rho_a}{2} + \frac{\rho_N}{3}\ \left(k_i^{gb}\right)^2 = \ \frac{(1+p).k_i}{d_L}\left(k_v^{gb}\right)^2 \ = \ \frac{k_v}{d_L} \tag{4.17}$$

$$D_iC_i = \frac{\phi}{\sum_L k_i^2 + \sum_T k_i^2 + \sum_R k_i^2} \tag{4.18}$$

$$D_vC_v = \frac{\phi}{\sum_L k_v^2 + \sum_T k_v^2 + \sum_R k_v^2} \tag{4.19}$$

The results of this model, developed to describe irradiation growth in Zr-2.5Nb pressure tubing [39], is shown in Figs. 4–6. This model is similar to, but not as complex as, the model described in Ref. [165]. Both models were developed for Zr-2.5Nb pressure tubing but are generally applicable to all Zr-alloys. In the case of Zr-2.5Nb pressure tubing the grain structure is important because the grain dimensions are sub-micrometer and have sink strengths comparable with the network dislocations. The best way to construct a model to describe the behaviour is to use idealized structures where grains are considered as rectangular prisms with idealized orientations, as shown in Figs. 4–12. The relative contributions from each idealized combination of grain shape and orientation can be incorporated into the model based on the Kearns' texture parameters f_R, f_T, and f_L. The output of the model shows how grain dimensions affect the longitudinal irradiation growth for different idealized textures [39], Figs. 4–13. The grain aspect ratio becomes important when the grain dimensions are small, i.e. when the grain sink strength becomes comparable with the sink strength of network dislocations and dislocation loops. In this example only one grain dimension has been altered (radial). In practice it is the relative densities of all sinks of all types (dislocations and surfaces) producing strains in different directions that are taken into account.

4.2.2. Primary irradiation growth strain and grain interaction stresses

The initial transient that is often observed in irradiation growth is likely to be due to either the result of the formation of point defect clusters such as dislocation loops (especially for annealed materials) or relaxation of residual stresses. There is ample evidence that the initial transient corresponds with the evolution of the a-type loop structure, which increases rapidly at the beginning of irradiation and then reaches a constant state after a fluence of about 2×10^{24} n.m^{-2}, E > 1 MeV. Perhaps the best example illustrating the primary growth transient for comes from the work of Rogerson and Murgatroyd on annealed and cold-worked Zircaloy-2 irradiated at 353 K (80 °C) and 553 K (280 °C) in the DIDO reactor [131]. Their results show that the transient is complete at low fluences (<2×10^{24} n.m^{-2}) at both temperatures. The high temperature data, at the very least, are consistent with the saturation in a-type dislocation density at a dose <2×10^{24} n.m^{-2} for annealed Zircaloy-4 irradiated at about 280 °C [184]. There is a longer duration evolution in c-component loop structure [184] that correlates well with the long term secondary or "steady-state" irradiation growth rate. Measurements on the strain from a-type loops (~2×10^{-4}) that coincide with the primary growth transient indicates that they can only contribute a small fraction of the measured strain [229] even assuming that all the a-loops were interstitial in nature. The strain from small clusters has been modelled in Ref. [138] and also shows a small effect (<5×10^{-4}). For these reasons many researchers focussed on studying the effect of residual inter-granular stresses on the transient, primary growth.

At the time that DAD was introduced as a means of accounting for the irradiation growth of Zr-alloys it was recognised that grain interactions could have a significant modifying effect on irradiation growth. Experimental evidence indicated that inter-granular stresses introduced by thermo-mechanical treatment had a profound effect on the initial irradiation growth of Zr-alloys [18,219,223,224]. Models based on stress relaxation of inter-granular stresses were developed to account for the transients in

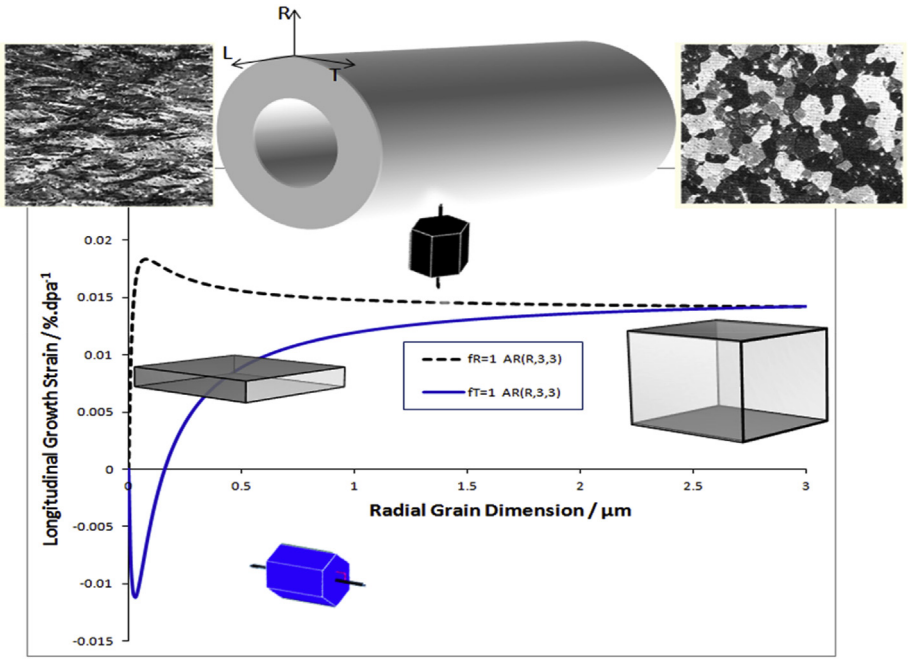

Fig. 4–13. Atom fractional flux (strain) to sinks in the longitudinal direction as a function of radial grain dimension in μm. Grain dimensions fixed by aspect ratio (AR) in the radial, transverse and longitudinal directions (R,T,L). Plot shows two cases for which R varies and T = L = 3 μm: (i) radial c-axis grain (dashed black lines); (ii) transverse c-axis grain (solid blue lines). Cold-worked structure, $\rho_a = 4 \times 10^{14}$ and $\rho_c = 1 \times 10^{14}$. Assumes 1% damage efficiency.

irradiation growth in both cold-worked and annealed materials [223,224]. Ostensibly, such models could account for the very long transients in irradiation growth (between 5 and 10×10^{25} n.m^{-2}) observed during low temperature irradiations in ATR [18]. Although the prior thermo-mechanical treatment had a profound effect on the magnitude and sign of the initial transient strain, there is no indication that the duration of the transient is in any way affected by residual inter-granular stresses, being the same for annealed, cold-worked and stress-relieved materials. In other data [236,237] showed that the irradiation growth of Zr-0.1Sn and Zr-1.5Sn alloys irradiated in DIDO exhibited transients that were up to an order of magnitude shorter than the Zircaloy-2 material irradiated in ATR. The shorter transient corresponded with the lower radiation damage rates in DIDO indicating that the transient may be time dependent and therefore a thermal creep phenomenon. Irradiation growth transients at any temperature are typically <0.1% strain [18] and are therefore not a significant contributors to irradiation growth in Zr-alloys at high fluences.

It has long been known that inter-granular stresses introduced by thermal cycling give rise to deformation of Zr in the absence of an applied external stress [238]. Relaxation of inter-granular stresses introduced by thermo-mechanical treatment at the start of irradiation is therefore hardly surprising. Whereas the relaxation by creep of the inter-granular stresses seemed to be the best and most appropriate method of accounting for the initial strain transients observed in irradiated materials, it is not certain that the steady-state growth behaviour is significantly affected by interaction stresses induced by the irradiation growth differential between neighbouring grains. Differences in strain rate between adjacent grains in any given direction may be expected to be manifested as an interaction stress. However, the magnitude of such stresses will be limited by the feedback that would exist affecting the strain rate of individual grains.

Once the material has hardened and the material exhibits pseudo-steady-state growth (because the c-component dislocation structure may still be evolving) one can hypothesise that the intrinsic diffusional behaviour of the material, governed by DAD, is modified by grain interaction stresses. This extrinsic diffusion anisotropy could have a noticeable modifying effect on the irradiation growth magnitude and anisotropy. The driving force for the irradiation growth process is still diffusional mass transport, and one can expect that the irradiation growth will be qualitatively similar to the case where the grains are assumed to deform independently; the so-called lower-bound case [189,190,239,265]. In the assessment of the effects of inter-granular stresses Woo concluded that the growth anisotropy is reduced by about 20% [189,190]. Woo's model assumes that the creep relaxation of inter-granular stresses is by dislocation slip. However, any slip will be exhausted eventually and is unlikely to play a major role in modifying the long-term, post-transient growth behaviour.

Existing irradiation growth models incorporating grain boundary sinks [39,58,165,188,233,240,240] do not include the effect of grain interaction stresses. Also many cases of irradiation growth involve annealed material and accelerated growth in cases where c-component loops are formed. In such circumstances one cannot invoke creep due to dislocation slip as a mechanism to modify the growth because there are no network dislocations to slip; the c-component loops are also sessile. Even in cold-worked material slip of c+a screw dislocations is likely to be suppressed due to climb, the c-component network is also mostly sessile [241]. The reader is reminded that irradiation enhancement of slip or stress-induced climb and glide can only apply to pure edge dislocations. Screw dislocations are simply locked by absorption of point defects. Also, unlike dislocations created by shear, prismatic dislocation loops do not add to the strain by glide. The only influence that gliding dislocation loops can have on the strain exhibited by an irradiated material is by their removal from the matrix, thus creating more space for new loop evolution from point defect clustering and climb.

It is a common misconception that gliding dislocation loops can contribute to creep strain through slip on their glide cylinders. Once a loop has formed the strain is manifested in the material and any

slip toward the edge of the grain or surface simply concentrates the strain over a smaller area. There is no change in the overall bulk strain. Also, many c-component dislocations exist in sessile junctions [241] and any climb of glissile c-component screw dislocations inhibits their glide [97,172,184,185]. In the absence of any conceivable slip mechanism to relax the stresses when climb is the main strain producing step, the growth behaviour is best described using a rate theory approach. Grain interaction stresses will modify the growth strain but a lower bound estimate of the strain (assuming no grain interaction stresses) is likely to be sufficient to explore the effects of material variables using rate theory models. This is especially true for annealed materials exhibiting accelerated growth due to c-component loop formation at high fluences when the relaxation mechanism is unlikely to involve dislocation slip.

5. Mechanisms of irradiation creep

Zirconium alloys are unique in comparison to most other engineering alloys in that they deform anisotropically during irradiation in the absence of an applied stress. An applied stress modifies the deformation and the response is now described as irradiation creep.

5.1. Review of mechanisms

5.1.1. Historical perspective

The history of the development of irradiation creep concepts until 1984 has been described and discussed in detail in Ref. [30]. Figs. 5–1 is a reproduction of the timeline given by Franklin et al. that describes the evolution of the main irradiation creep concepts up until 1980. The main contributors to the evolution in modelling irradiation creep deformation of zirconium alloys up to that time were Dollins, Gittus, Schoek, Hesketh, Mosedale, Piercy and Nichols [201,242–259]. More recent reviews of irradiation creep mechanisms in Refs. [225,260] indicates how mechanistic understanding has evolved. Stress induced preferred nucleation (SIPN) and Stress induced preferred absorption (SIPA) have been largely dismissed as major contributors to irradiation creep [91,165,239], leaving stress induced climb and glide (SICG) and simple mass transport as the more prominent mechanisms in recent years. Whereas stress-induced climb and glide was the mainstay of earlier modelling efforts on creep, a straightforward effect of stress on the diffusion tensor [165,167]) is probably more realistic, especially given the large amount of evidence in recent years showing the large effect that grain structure has on irradiation creep when the grain sink strengths are large [58,107,108,233,261]. That diffusion plays a major role in irradiation creep is hardly surprising when one considers that the stress exponent is 1 (see section 2).

One of the central tenets of irradiation deformation that has existed throughout the history of the study of dimensional stability of Zr-alloys is that irradiation creep and growth are separate and additive [17,216,217]. This is an assumption that is a reasonable simplification to distinguish between the deformation that is observed with and without applied stress. However, the assumption can only be correct if the mechanisms of creep and growth are separate and do not interfere with one another. Many theories of irradiation creep of Zr-alloys presume that the strain step is from the glide of network dislocations [93,216,247,255]. More recent data are showing that the mechanisms of irradiation creep include the direct accumulation of strain from diffusional mass transport as well as dislocation glide, the relative proportion of each being dependent on the neutron flux, fluence and irradiation

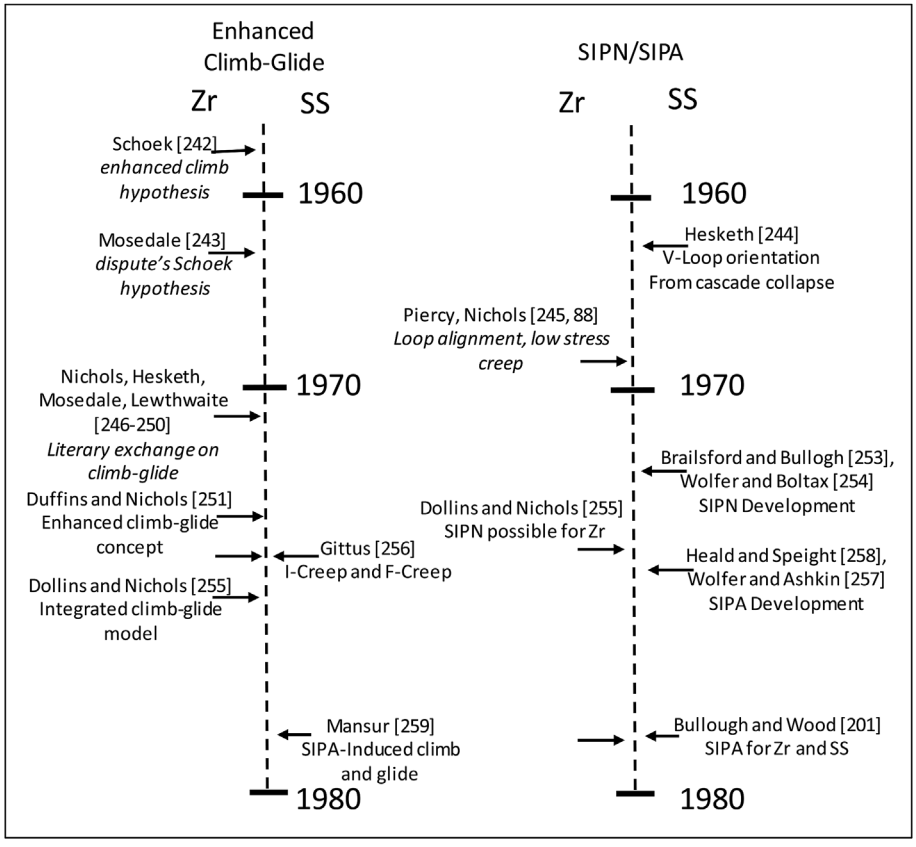

Fig. 5–1. Evolution of irradiation creep concepts up until 1980, modified from Franklin et al., [30].

temperature [61,97,233,262]. Irradiation creep has a different anisotropy to thermal creep occurring by dislocation slip. The difference in anisotropy response to a given stress state is probably because irradiation creep and thermal creep are dominated by different mechanisms. Whereas thermal creep in the temperature and stress ranges of interest is clearly dependent on dislocation slip, there is strong evidence that irradiation suppresses dislocation slip [61,97,233,262]. Although the stress-induced climb and glide mechanism assumes that climb of dislocations over obstacles more than compensates for the hardening effect of irradiation, there are few data to indicate whether this is the dominant mechanism in most power reactor conditions. At low fluences, high temperatures or high stresses one might expect slip to be dominant. In the reactor core, one must assume that dislocation slip and diffusional mass transport are both potential mechanisms for irradiation creep, the important question is how much of each contributes to the observed strain and under what circumstances. Clearly at the beginning of irradiation one can expect thermal creep to start out the same as in the laboratory for unirradiated material, quickly transitioning to secondary irradiation creep as the material hardens from the accumulation of radiation damage. Likewise, with increasing temperature the material is increasingly less influenced by the effects of irradiation and more of a contribution to the creep strain due to thermal creep by dislocation slip can be expected, unless the temperature is so high that other diffusional creep mechanisms start to be important. In the middle ground, where most reactors operate, it is difficult to determine exactly what mechanisms are operating. However, one can infer which mechanisms are the most applicable from the data in many cases.

Irradiation creep has a different anisotropy to thermal creep due to dislocation slip and this is likely due to the effect of stress on the intrinsic anisotropic diffusion of irradiation-induced point defects, the effect of so-called elasto-diffusion [166]. Once one incorporates the effect of stress on mass transport one effectively links the processes of irradiation creep and growth, the transition from growth to creep being a continuous evolution as a function of stress [61]. It could be argued that the mechanisms of irradiation creep are applicable to deformation even in the absence of an applied stress due to: (i) the grain interaction stresses that exist from fabrication, (ii) stresses that are induced by the intrinsic irradiation growth in individual grain of a textured poly-crystal. However, especially for high irradiation growth rates, the irradiation deformation in the absence of an applied stress can be understood simply based on the intrinsic deformation of the material (irradiation growth). Irradiation creep then represents the extrinsic effect of the applied stress on the growth behaviour.

Up until the 1980's most irradiation creep models were centred on dislocations or dislocation loops and the associated inhomogeneity interactions between dislocations and point defects. Grain boundaries were largely assumed to be neutral sinks. Since that time concepts such as anisotropic diffusion [163] and elasto-diffusion [166] have provided the means to treat grain boundaries as biased sinks, the bias being due to their orientation relative to the crystal structure of the grain or the imposed stress tensor. For the most part mechanistic modelling has focussed on the steady-state irradiation creep because over long periods of reactor operation this is the main strain producing component of in-reactor deformation. However, under some circumstances (creep during power transients and stress relaxation) the primary creep strain is important also. Most of the theoretical work relating to transient behaviour has been directed at the transients for irradiation growth. In many cases primary irradiation growth has been attributed to the relaxation of inter-granular stresses and, as such, is a creep mechanism. It is noteworthy that primary creep is not detectable in high flux irradiations of cold-worked material, but is observable in zero or low flux irradiations [61]. The creep models developed to address primary irradiation growth due to inter-granular stress relaxation have been discussed in Section 4.2.2. They are based largely, and justifiably, on dislocation slip because the deformation is often occurring in the early stages of irradiation before the material has hardened appreciably. Other than the application to primary irradiation growth there has been little theoretical work addressing mechanisms of primary irradiation creep other than by treating the creep by conventional (slip-based) modelling. Before addressing the mechanisms and modelling of steady-state irradiation creep, primary irradiation creep will be discussed briefly.

5.1.2. Primary irradiation creep

Primary irradiation creep is important for stress relaxation (discussed in Section 4.2.2) and in power transients affecting the interaction of fuel cladding with fuel described in Section 2. Models addressing fuel cladding creep have been largely empirical and have been discussed extensively by Garzarolli in Ref. [24] and Patterson in Ref. [39]. Mechanistically, one of the more interesting observations to do with primary creep in the past twenty years involves the work on the effect of sulphur first reported by Soniak et al., [23]. Soniak et al. demonstrated that the primary irradiation creep of Zr–1Nb M5 cladding was sensitive to the presence of as little as 10 ppm sulphur. Soniak showed how the sulphur effect on primary creep was consistent with the effect of sulphur in reducing thermal creep laboratory tests [148]. It is noteworthy that Soniak et al.'s data showed that only primary creep was affected with little apparent effect on steady state creep behaviour (Figs. 5–2). Later, data presented by Rebeyrolle et al. [104], seemed to indicate that both primary and secondary creep rates were affected by sulphur. However, examination of Rebeyrolle's in-reactor creep data, which were plotted as a function of time, shows that it is likely the same data as that presented by Soniak et al., plotted as a function of fast neutron fluence, with some adjustments in the strain values. Rebeyrolle et al. [104], showed that the steady-state creep rate of the low sulphur material was higher than the high sulphur material (containing 10 wt ppm S). However, Rebeyrolle et al. fitted their trend lines by including the strain point at zero time. Whereas this fit would not affect the slope when there is no transient, as in the case of the high S material, fitting in this way introduces a bias in the slope when there is a substantial transient, as in the case of the low S material. Considering that the transient will interfere with the steady-state strain rate calculated in this way, the best one can do is to compare rates as far away as possible from the transient. Rebeyrolle's data are re-produced in Figs. 5–3. It is clear that, long after the transient has ended, the slopes of the creep curve are very similar for low S and high S materials (Figs. 5–3) and are consistent with the data of Soniak et al. (Figs. 5–2), showing similar rates of steady-state creep for high and low sulphur material.

The French work demonstrated two important things: (i) that sulphur is an important element in reducing primary creep; (ii) that the effect of sulphur is not apparent in the steady-state irradiation creep regime. One can understand this behaviour if one assumes that primary creep is governed by dislocation slip. The effect of sulphur appears to be one where it segregates to dislocation cores and thus reduces dislocation mobility, which is apparent in laboratory tests and also during primary creep. One can understand these results if one considers that primary creep likely represents the thermal creep behaviour of a given material and is governed by dislocation slip. As the material hardens from the accumulation of radiation damage the slip-based creep is suppressed and there is then a transition to the secondary irradiation creep regime. In steady-state irradiation creep there is little apparent effect of sulphur and which probably supports the conclusion that

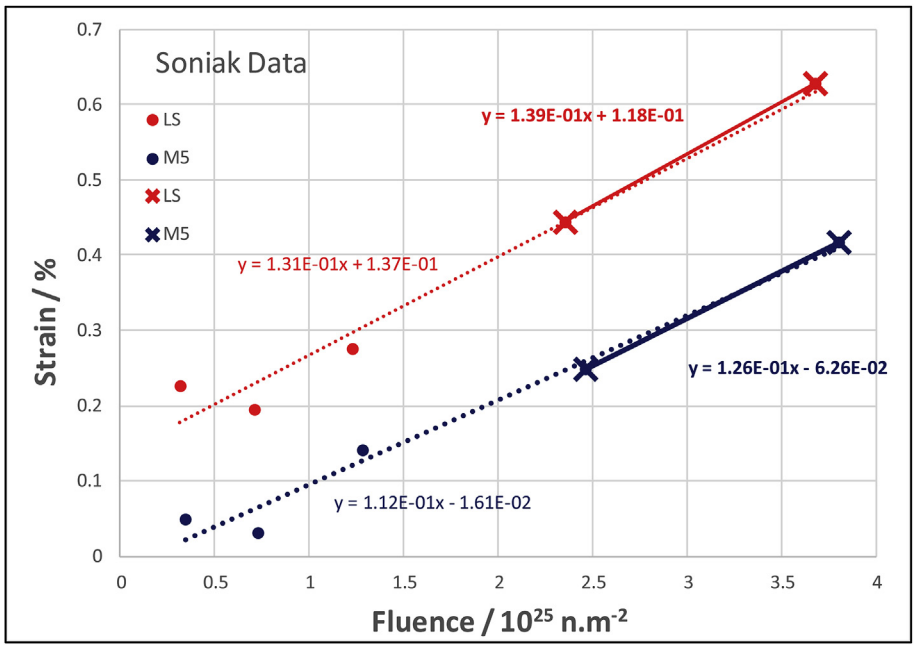

Fig. 5–2. Irradiation creep of low suplur (LS) and M5 alloy (containing 10 wt ppm S) from Soniak et al., [23].

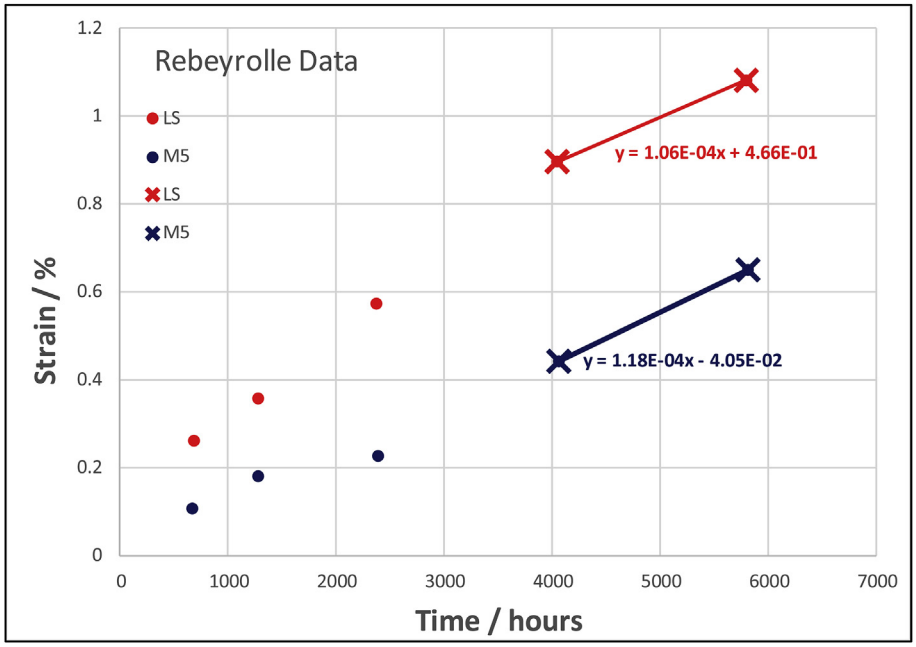

Figs. 5–3. Irradiation creep of low suplur (LS) and M5 alloy (containing 10 wt ppm S) from Rebeyrolle et al., [104].

irradiation creep in the steady-state is not governed by dislocation slip.

The effect of accumulated dose on the transition to lower steady-state creep rates was also addressed in Soniak's report [23]. In that case the attention was on the effect of high dose irradiation on thermal creep at high temperatures (350 °C) and stresses (445 MPa) during dry storage. Soniak's results showed that the hardening effect of irradiation on post-irradiation thermal creep persisted up until fluences of about 9×10^{25} n.m^{-2} for PWR fuel cladding (cold-worked and stress-relief annealed material). The strong creep suppression has been attributed to high density of irradiation defects that harden the material [263], Figs. 2–12. At temperatures in the range of 560 K–580 K (287 °C–307 °C), the a-type loop structure saturates at low fluences (<2×10^{24} n.m^{-2}) [184], but the c-component loop structure evolves over a much larger dose range and is very apparent for cold-worked material, Figs. 5–4. The thermal creep hardening behaviour reported by Soniak et al. [23], extending to high fluences is likely because of the effect of the higher irradiation temperature (350 °C) on the evolution of the a-type loop structure or c-component loop structure, or both.

The creep rate is dependent on the microstructure of the

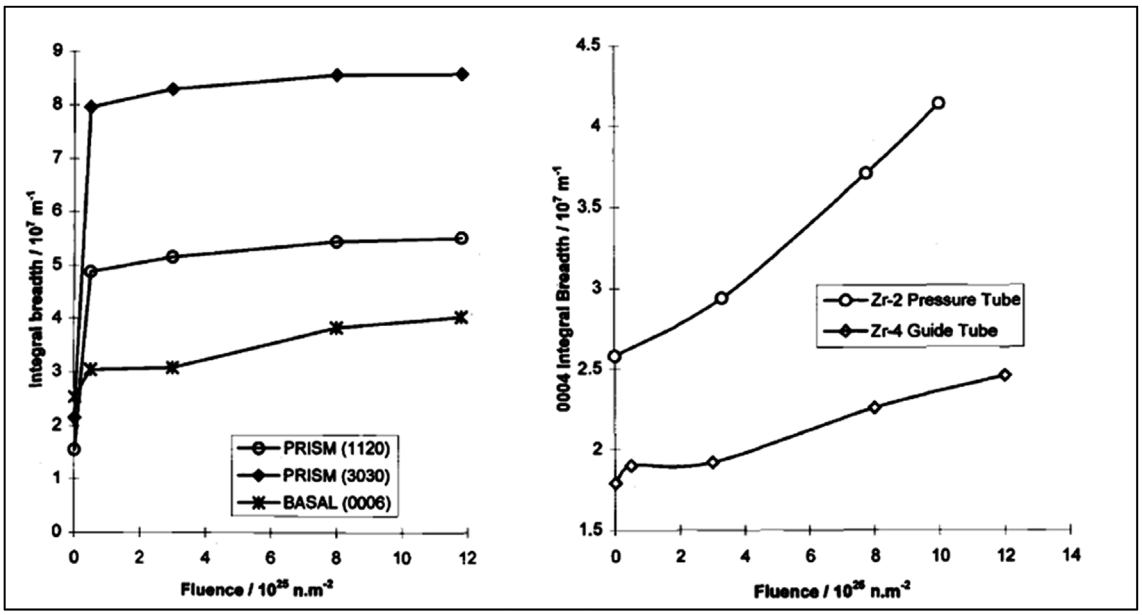

Fig. 5–4. (a) Variation in integral breadths as a function of fast neutron fluence (E > 1 MeV) for Zircaloy-4 guide tubes irradiated at 560–580 K (287 °C–307 °C). The prism line breadths reflect changes in the a-type loop density and the basal line breadths reflect changes in the c-component loop density; (b) Variation in basal line broadening as a function of neutron fluence at about 570 K (300 °C)for annealed Zircaloy-4 guide tubes and cold-worked Zircaloy-2 pressure tubes (similar to SRA fuel cladding).

material and the creep rate therefore varies as the microstructure evolves. The effect of dislocation loops, both by inhibiting glide and as sinks for point defects, is an obvious factor to consider but in addition there are hardening effects that are not restricted to dislocation loop evolution, at least any observable or detectable dislocation loop evolution [97,262]. Plotted as a function of time, a range of different creep curves are observed for different neutron fluxes (Figs. 2–20). A high primary creep strain rate is observed in each case that then changes into a slower pseudo-steady-state rate after an irradiation time of a few thousand hours. The transition from the high primary rate to lower secondary rate is a function of both the fast neutron flux and fluence. The secondary rate is a minimum for a flux of about 2×10^{15} n.m^{-2}.s^{-1} and shows up as a creep suppression region just outside of the reactor core where the flux is dropping rapidly (Figs. 5–5). At lower fluxes the creep rate begins to rise again until it approaches thermal behaviour when the flux is too low to have any affect [97,262]. The secondary rate is lower but not constant and changes as the microstructure evolves. A plot of the creep rate per neutron fluence against fluence for different neutron fluxes illustrates how the irradiation creep response changes as a function of flux and also fluence (Figs. 5–6). The irradiation creep rate is constantly changing as a function of fluence until a fluence where the microstructure has achieved a steady-state condition (about 2×10^{24} n.m^{-2} in this case). When the a-type loop structure has reached a steady-state condition the creep rate per neutron fluence approaches a minimum value (Figs. 5–7). This rate still corresponds to a high creep rate as a function of time.

It is clear that the primary creep strain is complex. Early on there are at least two possibilities. The creep rate per unit time at relatively low neutron fluxes is suppressed for fluences before there is any visible detectable effect of the irradiation on the microstructure [97,262]. One can only assume that the hardening effect is related to either small sub-microscopic clusters, or helical climb of the screw components of the network dislocations, or both. Also the strain rate per unit fluence is high at low fluences and drops to a steady-state value at fluences corresponding to the saturation in the a-type dislocation loop evolution (by about 2×10^{24} n.m^{-2}). This next stage of creep is itself not necessarily constant but changes to a lower rate as the c-component dislocation structure evolves. The changes that are observed as a function of fast neutron flux and fluence can be understood in terms of the suppression of thermal creep (dislocation slip) and a transition to a different creep mechanism, one governed by diffusional mass transport.

5.1.3. Secondary steady-state irradiation creep

The main mechanism that has been considered in the past to explain the steady-state irradiation creep of cold-worked materials such as Zr-2.5Nb pressure tubing is stress-induced climb and glide (SICG). A number of the early models included this mechanism implicitly to account for irradiation creep, i.e. it was the dislocation density structure and the anisotropy of dislocation slip, albeit possibly modified during irradiation, that governed the creep process [46,91,192,239,264,265]. In more recent years data have increasingly been accumulated indicating that grain boundary sinks are very important, especially when the grain dimensions are sub-micrometer. A weak dependence on dislocation density has been known for some time [102]. More recent analyses have shown that the dependence is either weak or even negative depending on the strain direction [58,233], Figs. 5–8. One recent study shows that the amount of cold-work can have a pronounced effect on irradiation creep, there being higher rates of diametral creep exhibited by Zr-2.5Nb creep capsules cold-worked to 27% compared with 12% [61]. This observation would imply that there is a positive dependence of irradiation creep on dislocation density in those cases. The data correspond to low fluences where thermal creep by slip may be operating. The data also show that at the lowest temperature tested (280 °C) the difference in steady-state creep rate between 12% and 27% cold-work materials disappears with increasing fluence (see Section 5.3) and can be attributed to the hardening effect of irradiation damage by impeding dislocation slip. The creep rate and creep mechanism is constantly evolving as discussed in section 5.1.2. One can still identify pseudo-stages in behaviour. For most observations there is a high strain rate (as a function of time)

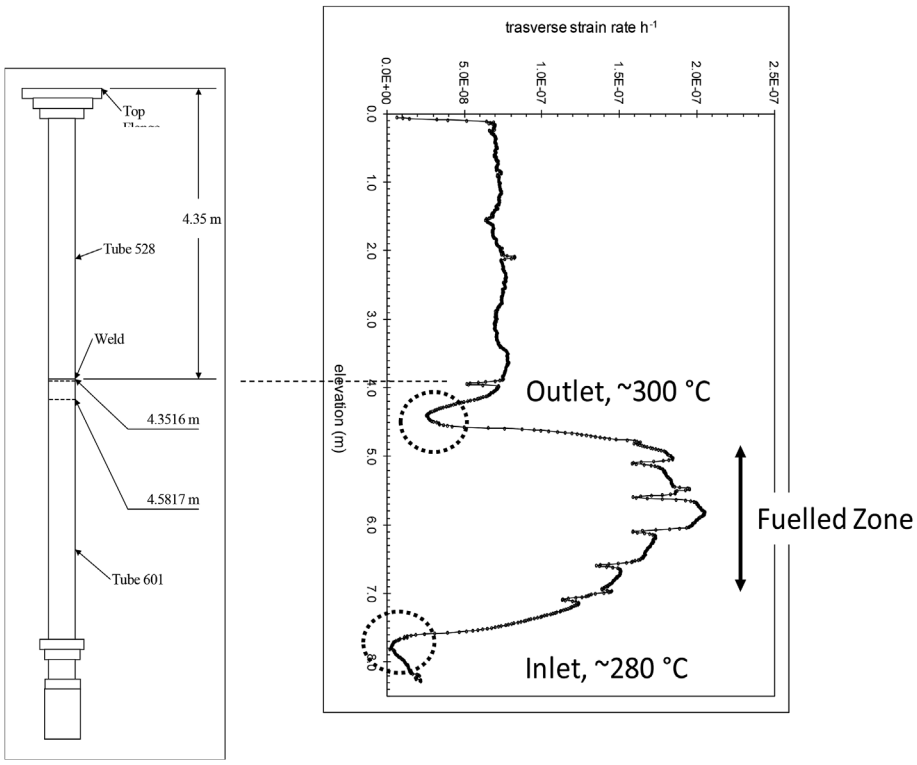

Fig. 5–5. Diametral strain rates for Zr-2.5Nb pressure tube assembly 50206 irradiated in NRU at 280°C-300 °C. The creep suppression zones that occur at neutron fluxes of about 2×10^{15} n.m^{-2}.s^{-1} are circled.

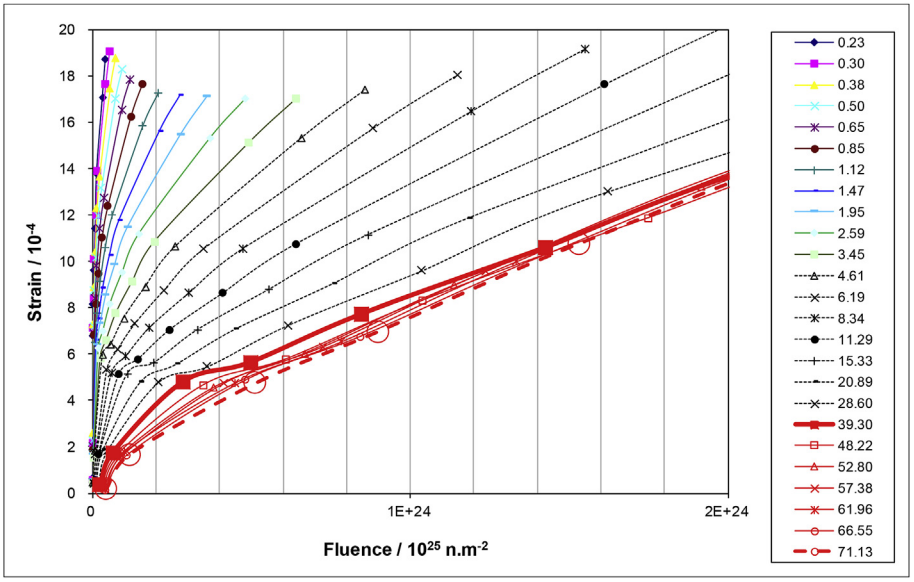

Fig. 5–6. Diametral strain for Zr-2.5Nb pressure tube assembly 50206 in the vicinity of the creep suppression zone at the outlet (300 °C). The strain data correspond to diameter gaugings between 170 and 51 570 h of operation. Each curve corresponds to a different neutron flux, given in the legend in units of 10^{15} n.m^{-2}.s^{-1}.

primary stage that is complete after about 3000 h, i.e. primary thermal creep. The time for this stage appears to be insensitive to neutron flux $<10^{17}$ n.m^{-2} and is manifested as an almost instantaneous jump in strain at the beginning of irradiation. This transient appears to be non-existent at high fluxes (see, for example, strain per unit time for OSIRIS in Figs. 2–13) and this is presumably because the high damage rate quickly suppresses the thermal creep at high neutron fluxes. Note that the axial laboratory test data for unirradiated and pre-irradiated material were initially negative indicating a problem with the measurement and the apparent offset appeared to be an artefact.

The second stage involves slowing down of the creep as the dislocation loop density increases and is more-or-less complete when the a-loops have stopped evolving at a fluence of about 10^{24} n.m^{-2}, except any continued evolution of the c-component microstructure will also have an effect on the creep rate per unit

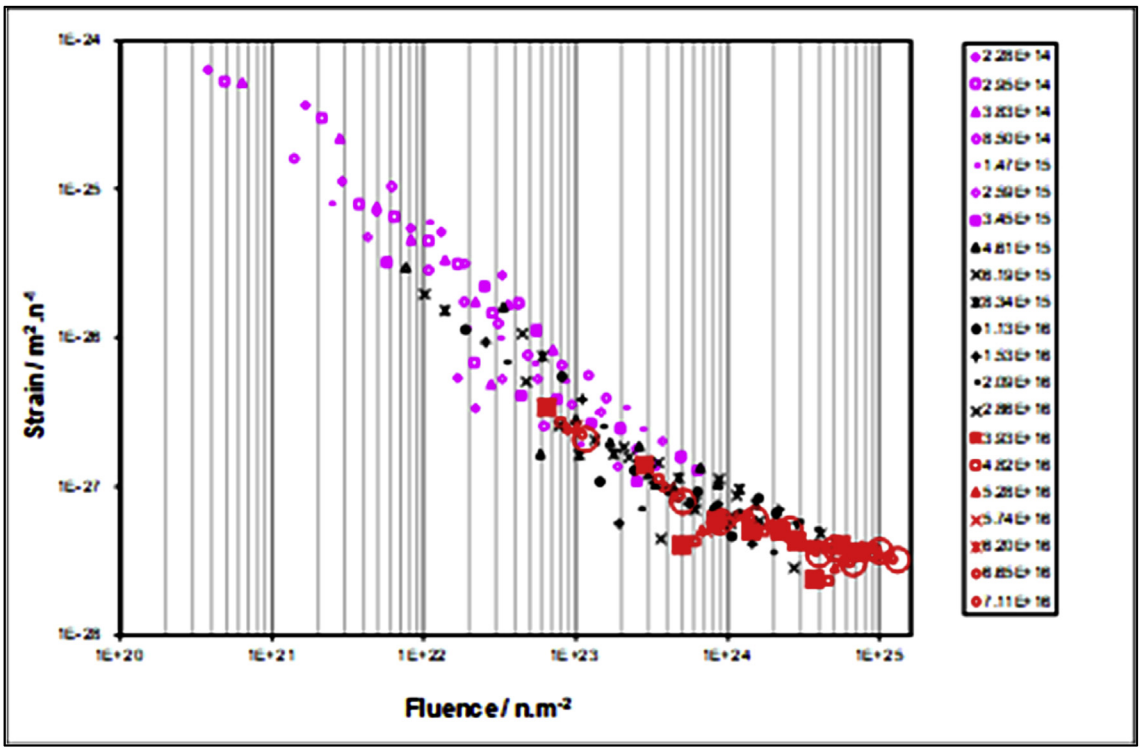

Fig. 5–7. Diametral strain rates per unit neutron fluence for Zr-2.5Nb pressure tube assembly 50206 in the vicinity of the creep suppression zone at the outlet (300 °C). The data correspond to diameter gaugings between 170 and 51 570 h of operation. Each curve corresponds to a different neutron flux, given in the legend in units of $n.m^{-2}.s^{-1}$.

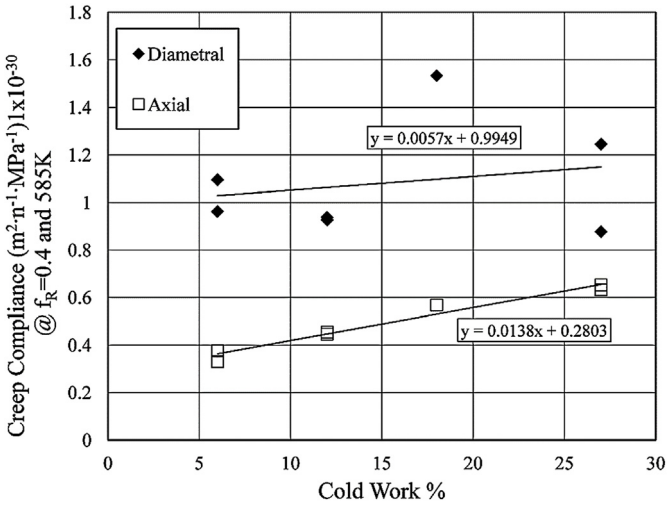

Fig. 5–8. Creep compliance of cold-worked Zr-2.5Nb creep capsules normalized to a temperature of 585 K and a texture of $f_R = 0.4$ versus % cold-work [58].

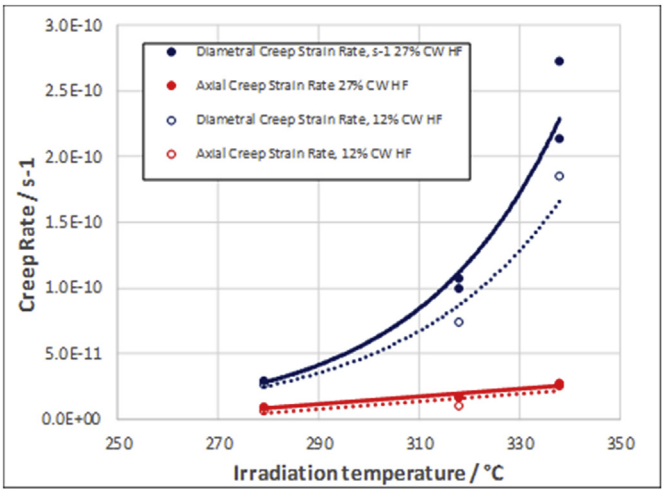

Fig. 5–9. Axial and diametral creep rates for 12% and 27% cold-worked pressurised creep capsules irradiated in the NRU reactor at temperatures from 280 °C to 340 °C. Data reported by DeAbreu et al. [61] for a fast neutron flux is $1.52–1.63 \times 10^{17}$ $n.m^{-2}.s^{-1}$ and a hoop stress ~125 MPa and for fluences between about 10^{23} $n.m^{-2}$ and 10^{25} $n.m^{-2}$.

fluence. The diametral and axial steady-state creep rate data from pressurised creep capsules reported in Ref. [61] for the "high flux" case, i.e. 2×10^{17} $n.m^{-2}.s^{-1}$, are plotted in Figs. 5–9. One can see that at low temperatures (280 °C) there is little apparent effect of cold-work, but differences are readily apparent in the response for diametral creep at higher temperatures (340 °C).

Comparing the NRU data with those obtained from irradiation of similar creep capsules in OSIRIS reactor at a much larger fast neutron flux, i.e. about 2×10^{18} $n.m^{-2}.s^{-1}$, the effect of temperature and cold-work is very much the same. In OSIRIS the temperature dependence of diametral creep is much stronger compared with the axial creep (Figs. 2–38). In addition, the dependence of both axial and diametral creep on cold-work is weak at an irradiation temperature of 585 K, i.e. ≈310 °C (Figs. 5–9). This latter observation is consistent with earlier observations of a weak dependence of creep on dislocation density [102,140]. If slip was a dominant mechanism for irradiation creep one would expect that the creep rate would at least be proportional to the dislocation density, but it is not. Also, the fact that the creep anisotropy changes with temperature, and there is only a weak dependence of creep on

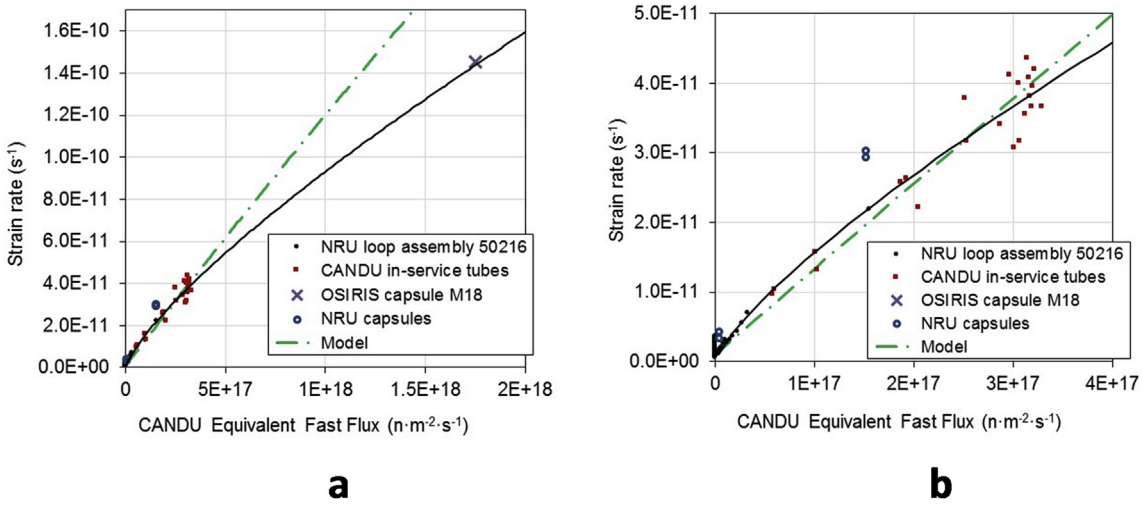

Fig. 5–10. . Diametral steady-state creep strain rates (s-1) for Zr-2.5Nb pressure tubing as a function of fast neutron flux irradiated in NRU, CANDU and Osiris reactors. All rates compared at 285 °C and a hoop stress between about 120 and 130 MPa. The solid line is the result of a power law fit for flux > 3 × 1015 n·m-2·s-1. The plots are shown as (a) linear-linear and (b) log to illustrate the non-linear nature of the creep rate as a function of fast neutron flux [61].

dislocation density, implies that dislocation slip is not a dominant strain producing mechanism at temperatures of about 310 °C in OSIRIS. The strong effect of temperature on diametral creep, as opposed to axial creep, is an indication that the temperature dependence of irradiation creep is anisotropic. This anisotropy and temperature dependence of creep could best be explained if the effect of stress on point defect diffusion, elasto-diffusion, was also temperature dependent just as the positive temperature dependence of DAD could account for the effect of temperature in reducing axial irradiation growth in the case of pressure tubing (see Figs. 4–6). It is worth reminding the reader that irradiation creep models based on slip assume that the creep deformation anisotropy does not change with temperature [46].

It could be argued that the negative temperature dependence of irradiation growth [142,188] is consistent with the positive temperature dependence of diametral creep; the high transverse basal texture would mean that lower growth (less negative strain) would result in more positive diametral strain at higher temperatures. Such an effect would also show up in the axial direction and there is no evidence that there is a strong effect of temperature on axial creep (Figs. 2–38). Elasto-diffusion may increase with increasing temperature because the elastic modulus decreases and is in the denominator of the expression for elasto-diffusion [166], but there have been no studies on the stress sensitivity due to this effect. The weak dependence on temperature for axial strain of creep capsules is consistent with the temperature dependency for irradiation creep exhibited by stress relaxation specimens from Zr-2.5Nb pressure tubing between 280 °C and 340 °C [266]. Normally irradiation processes in the sink-dominated regime should be independent of temperature (provided the microstructure is constant). When the microstructure is constant (unaffected by temperature) one might consider that temperature dependencies for irradiation processes are an indication of transiting from a recombination to sink-dominated regime [39]. This mechanism would be particularly true at low temperatures (<300 °C) while at higher temperatures (>300 °C) one could anticipate other thermal process, i.e. dislocation slip, to be dominant. All the evidence indicates that the vacancy migration energy is too low in Zr-alloys for point defect recombination to have an effect on the temperature dependence of creep [61]. It is more likely that the temperature affects the radiation damage density, which has an effect both on dislocation slip and mass transport because of a changing sink density. Even if there were equal numbers of vacancy and interstitial dislocation loops and they were, in effect, neutral sinks, a higher density of a-type loops at lower temperatures would effectively enhance recombination by annihilating more interstitial and vacancy point defects. Also, any effect of temperature on the evolution of the c-component loop structure, coming from helical climb on network dislocations even at low doses [186], would alter the point defect balance and the observed creep. For the samples corresponding with Figs. 5–10 and 5-11, further work to measure and compare the a-type and c-type radiation damage density is required to understand why the irradiation creep anisotropy changes with temperatures.

The role of dislocations, either as sinks resulting in climb, or as vehicles for glide deformation, remains somewhat ambiguous in

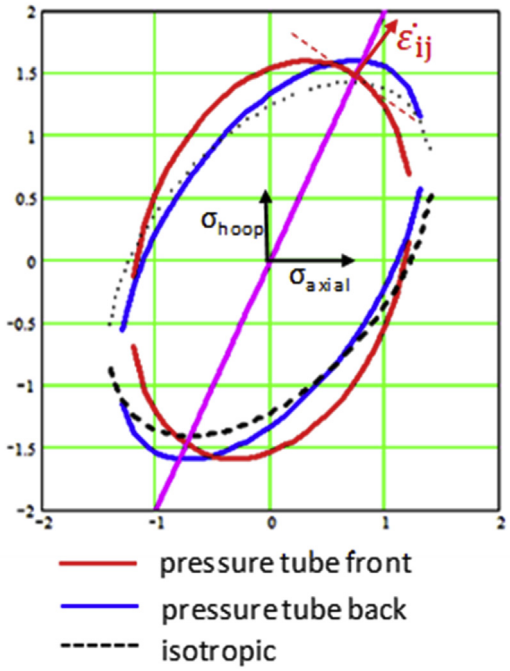

Fig. 5–11. Strain response surface for irradiation creep based on anisotropy parameters, F, G and H corresponding with the average of the front and back ends of Zr-2.5Nb pressure tubes taken from Christodoulou et al. and DeAbreu et al., [46,61].

the context of irradiation creep. The fact that there is a weak dependence of irradiation creep on dislocation density [58,102,140] implies that dislocation slip cannot be the main strain-producing mechanism, as it is in thermal creep. One could argue that irradiation suppresses dislocation slip, even when the point defect flux is elevated to enhance climb over obstacles to glide. Logically the glide motion of screw dislocations, in particular, can only be suppressed by irradiation with no chance for enhancement by climb. In fact, only perfect edge dislocations can be candidates for an enhanced climb and glide process, so it is hardly surprising that evidence for slip-based deformation during irradiation is weak. Moreover, for cold-worked Zr-2.5Nb pressure tubing with a strong basal texture in the hoop direction, the slip systems that must operate to produce the observed strain are c+a on pyramidal planes, i.e. $<11\bar{2}3>\{10\bar{1}\bar{1}\}$, [91]. Most c-component dislocations in Zr-2.5Nb pressure tubing are either locked in sessile junctions or in a screw orientation, neither of which is conducive to slip during irradiation [241]. In addition, post-irradiation annealing shows that the original dislocation network structure is retained after high doses in ex-service pressure tubing [267]. Any slip-based deformation is unlikely to have occurred from the glide of existing dislocations, otherwise the network dislocation density would be seen to reduce with creep during irradiation. Any slip-based deformation will exhaust the dislocation structure eventually. In submicrometre grain size pressure tubing the distance that a dislocation can travel before encountering a grain boundary and therefore ceasing to participate in the strain producing process, even if mobility was possible, is < 1 μm. For the c-component dislocation densities present in pressure tubing ($\approx 1 \times 10^{14}\,m^{-2}$), diametral strains <0.5% only are possible if all the dislocations slipped as far as they could. The fact that non-saturating strains up to 5% have been observed in many pressure tubes is a good indication that dislocation slip is not the dominant mechanism contributing to the irradiation creep in those cases. Unless irradiation creep involves the creation of dislocations by yielding (as proposed by Hesketh, [268]), one has to conclude that irradiation creep occurs primarily by mass transport. Creep models that are based on dislocation slip are still valid under certain circumstances, e.g. during primary creep before radiation hardening has suppressed slip or when the temperature is high and the radiation damage density is low, or at high stresses when yielding occurs thus clearing out the radiation damage [263].

5.2. Modelling of irradiation creep

Creep can be divided into two categories: (i) high stress creep, involving yielding and a stress exponent >1; (ii) low stress creep, with no yielding and a stress exponent of 1, or close to 1. Irradiation creep is typically applied to the deformation of components in nuclear reactors at low operating stresses, and occurring over long time scales, months and years. The mechanisms and modelling of irradiation creep will therefore be restricted to considering low stress creep, i.e. the non-yielding case, except in those cases where modellers have speculated that localised (intra-granular) stresses could exceed the yield stress even when the macroscopic applied stress was below the yield point. This review is restricted to power reactor components during normal operation so high stress creep involving yielding (generation of new dislocations) is not considered.

There are two ways in which anisotropic irradiation creep in Zr-alloys can be addressed: empirically and mechanistically. There are also, so-called, semi-empirical models where some mechanistic reasoning is applied to construct an equation combining different mechanisms [93].

$f''(M,\ \Phi, T)$

5.2.1. Empirical models of irradiation creep

Many in-reactor creep models assume that long-term, steady-state plastic deformation consists of separable, additive components from thermal creep, irradiation creep and irradiation growth. The deformation behaviour can be described empirically by,

$$\dot{\varepsilon}_d = \dot{\varepsilon}_d^{\text{thermal creep}} + \dot{\varepsilon}_d = \dot{\varepsilon}_d^{\text{irrad'n creep}} + \dot{\varepsilon}_d^{\text{irrad'n growth}} \quad f(M,\ \sigma, T)\, f'(M,\ \sigma, \Phi, T)\, f''(M,\ \Phi, T) \tag{5.1}$$

where f, f' and f'' are functions of the material and operating conditions. The operating conditions are stress (σ) temperature (T) and neutron flux (Φ). The response to these external constraints is dependent on the material or microstructure (M), which is dependent on fabrication and irradiation history.

With this assumption the role of irradiation growth can be separated from creep by evaluating strain data at zero stress. The thermal, in-reactor, creep contribution is that of an irradiated material subjected to a neutron flux and will differ from the creep behaviour of either unirradiated or pre-irradiated material tested out of flux. Assuming that the out-reactor creep of pre-irradiated material represents the in-reactor thermal creep contribution, at power reactor temperatures (below 350 °C) the contribution is small, at least for the moderate stresses of interest for long time behaviour of fuel components and pressure tubes [97,262]. Thermal creep at such low temperatures is often assumed to be dominated by dislocation slip. If irradiation creep is also dictated by dislocation slip it is reasonable to assume that irradiation creep is simply enhanced thermal creep. There are no data to show that irradiation and thermal creep are governed by the same physical mechanism, although elements of thermal creep, i.e. dislocation glide, do seem to be operating at lower neutron fluxes and fluences and high temperatures [61]. From this perspective primary creep may be regarded as the transition from thermal creep of unirradiated material to irradiation creep of irradiated material as the material hardens due to radiation damage at the beginning of irradiation. The transition from thermal to steady-state irradiation creep is often represented as an offset (or intercept) strain at time zero in empirical models. Irrespective of whether irradiation creep is determined by dislocation slip, or mass transport, or a combination of both, it is not possible to differentiate between thermal and irradiation creep in the analysis of the in-reactor creep data in the temperature range from 60 °C to 400 °C unless one has already assumed the value of one or other from a mechanistic model. Thus, empirical models for steady-state in-reactor creep implicitly contain the combined effect of irradiation and thermal creep, the latter being subsumed into the former.

The time (t) dependency of irradiation creep deformation in a neutron flux (φ) at stresses below yield stress (ε) is usually described by a primary strain (ε_0) and a steady state creep rate $\dot{\varepsilon}$ (dε/dt):

$$\varepsilon = \dot{\varepsilon} \cdot dt + \varepsilon_0 \tag{5.2}$$

The other concept to describe the time dependency of creep deformation is a power law:

$$\varepsilon \approx t^k \text{ or } \varepsilon \approx (\varphi \cdot t)^k \tag{5.3}$$

The creep mechanisms have been reviewed by Franklin et al. [30], Matthew & Finnis [260], Holt [93], Adamson et al. [24] and Murty, [269].

From a functional perspective, the steady-state strain rate in a direction (d) due to irradiation creep has been expressed by

relationships of the form Luscher & Geelhood [213],

$$\dot{\varepsilon}_d = A \cdot f(T) \cdot \bar{\sigma}^n \cdot \varphi^p \tag{5.4}$$

where, A = creep rate coefficient (dependent on factors such as material composition, metallurgical state and orientation), f(T) = weak function of temperature (0.72–1.47 for 300–350 °C), n = stress exponent (1.0), p = flux exponent (0.85), and $\bar{\sigma}$ is the effective stress. This form is analogous to the conventional expressions for plastic flow when the effective stress is based on a yield criterion and the direction of strain is dictated by the normal to the yield surface in a conventional tensor representation of the creep compliance.

Simple models such as that described above have been developed for fuel cladding applications. More complicated models have been developed to apply to the large range of stress states, neutron fluxes and temperatures that apply to pressure tubing in CANDU reactors. The model proposed in Ref. [46] is semi-empirical in that there are some parameters (the compliance tensor for example) that are derived from a mechanistic base. Primary creep is empirically derived to best match available data and it is assumed that there are three components to the steady-state creep rate, as outlined in Equation (5.1). The thermal creep component (Equation (5.5)) is that which applies to radiation hardened material in the creep suppression zone for the pressure tube [61]. Creep suppression is observed at very low fast neutron fluxes (between 10^{14} and 10^{16} n.m^{-2}.s^{-1}, E > 1 MeV) at the edges of the reactor core [97,262]. In this flux range the diametral creep rate as a function of time is an order of magnitude lower than either out-reactor creep of unirradiated material, or in-reactor creep of the same material.

$$\dot{\varepsilon}_d^{\text{thermal creep}} = \left[K_1 C_1^d \sigma_1 + K_2 C_2^d \sigma_2^2\right] \exp(-Q_1/T) + K_3 C_1^d \sigma_1 \exp(-Q_3/T) \tag{5.5}$$

The parameters K and Q are based on best fits to available data. The anisotropy factors are different for each direction, d, denoting directionality; σ_i are effective stresses for thermal creep.

The irradiation creep component (Equations (5) and (6)) is given by an expression similar in form to Equations (5–4) derived for fuel cladding. The creep anisotropy factor, $C_1^d(x)$, varies as a function of axial location in response to changes in the texture. An additional axial correction factor, $K_4(x)$, is added to account for non-texture dependent effects that affect the creep along the pressure tube.

$$\dot{\varepsilon}_d^{\text{irrad'n creep}} = K_c K_4(x) C_1^d x) \sigma(x) \varphi [\exp(-Q_4/T) + K5] \tag{5.6}$$

The irradiation growth component (Equations (5–7)) is given by an expression similar to Equations (5) and (6), except for the absence of a stress term. The growth anisotropy factor, $K_6(x,\varphi t)$, is a function of axial location and fluence to take into account changes in the microstructure during irradiation that are believed to affect growth but not creep.

$$\dot{\varepsilon}_d^{\text{irrad'n growth}} = K_g K_6(x, \varphi t) \varphi \exp(-Q_6/T) \tag{5.7}$$

This model appears complicated and includes parameters derived from many different sources, but ultimately it is adjusted using empirical parameters to fit available experimental data for the direction of interest. It should therefore be considered empirical. Despite its complexity the model does not attempt to account for the non-linear flux dependence of irradiation creep; the flux dependence is assumed to be linear. The model output as a function of fast neutron flux has been compared with recent measurements [61]. Figs. 5–10 shows the model output compared with measurements as a function of fast neutron flux for a narrow range of parameters applicable to CANDU reactor operation. There is a minimum in the data corresponding to the creep suppression observed for neutron fluxes between 10^{15} and 10^{16} n.m^{-2}, E > 1 MeV, [97,262]. It is clear that the model does not predict the creep rate well at high and low fluxes but gives reasonable agreement for fluxes of about 3×10^{17} n.m^{-2}, i.e. corresponding to the main body of pressure tube for CANDU reactor operation. The model is therefore adequate for applications to pressure tubing at fluxes of about 3×10^{17} n.m^{-2}. Another area where recent data are showing disagreement is in the prediction of anisotropy. The model anisotropy was validated against creep data mostly coming from creep capsules in the Osiris reactor, see Fig. 13 in Ref. [92]. In the model the irradiation creep anisotropy is independent of temperature. The model predicts that the ratio of axial to transverse irradiation creep rates (compliance) for a CANDU pressure tube with Kearns texture parameters, f_T-$f_R \approx 0.25$–0.3, is about 1. For the Osiris creep capsules, f_T-$f_R \approx 0.23$, the ratio was about 0.6 at 280 °C and 0.7 at 310 °C. However, for similar creep capsules, 27% cold-worked material with f_T-$f_R \approx 0.21$–0.26 and irradiated in NRU at 125 MPa, the ratio of axial to transverse creep rates is ~0.3 at 280 °C, dropping to ≈0.1 at temperatures 340 °C [61], see Figs. 5–9. Part of the discrepancy may arise because of the inability to separate thermal creep from irradiation creep. The model assumes that both contribute, but in the assessment [92], it is assumed that irradiation creep is dominant. Whereas this assumption is reasonable for Osiris data, it is not clear how the CANDU pressure tube data cited in Ref. [92] could possibly be included in the same validation plot. The ratio of the creep compliance reported is about 1 (equal diametral and axial strain rates) and refers to another paper [45]. But in that paper, the only tabulated ratio that is close to 1 is the axial/maximum diametral strain rates for full length pressure tubes for a flux of 3.6×10^{17} n.m^{-2}.s^{-1}, a stress of 120 MPa and a temperature varying from 239 °C (inlet) to 311 °C (outlet). The axial creep rate is the average over the length of the fuel channel and the maximum diametral creep rate corresponds to that (unspecified) location where the combined effect of flux, temperature and material properties gives the maximum creep rate.

The Zr-2.5Nb pressure tubes of a CANDU reactor have a length of about 6 m, an inner diameter of 104 mm and a wall thickness of 4.2 mm. During service, they operate with fast-neutron fluxes up to about 4×10^{17} n·m^{-2}·s^{-1} (E > 1 MeV), with coolant temperatures between 250 °C and 310 °C and coolant pressures up to 11.5 MPa, resulting in initial hoop stresses of about 140 MPa. The tubes expand subject to the stress, fast neutron flux, temperature and variable material creep rate, all of which vary along the length of the pressure tubes [94,270]. A large amount of gauging data are available for in-service Zr-2.5Nb pressure tubing and can be correlated with microstructural data from pressure tube offcuts with the application of a suitable normalisation model for the operating conditions [271]. The application of an empirical model that accounts for stress, fast neutron flux and temperature has made it possible to assess the effects of microstructural variables on diametral creep and axial elongation. The microstructure variables (grain dimensions, crystallographic orientation and dislocation structure) were included in an empirical model for material variability and the results showed that grain dimensions were important in addition to texture and dislocation density [233]. The results showed that the high diametral creep and low elongation exhibited by TG3 RT1 pressure tubing in service could be attributed to the fact that these experimental tubes had smaller grain dimensions and a lower dislocation density compared to the average standard pressure tube [233]. The TG3 RT1 tubes were originally fabricated to have a reduced dislocation density to minimise in-reactor elongation and were fabricated with a smaller grain structure to maintain strength [124]. Although the negative transverse growth rate of the TG3 RT1 tubing is about half

that of standard pressure tubing [188], and the difference in growth could contribute to the observation that diametral creep of in-service pressure tubes is higher for TG3 RT1 compared to other tubes [233], the irradiation growth differential is insufficient to account for the observations, see Section 5.3. The in-service diametral strain of TG3 RT1 pressure tubing in a CANDU reactor is about double that of standard pressure tubing at a fluence of about 8×10^{25} n.m^{-2} and 280 °C, i.e. about 2% compared with 1% [272]. But the growth difference at the same fluence and temperature is <0.1% [142]. The behaviour of the TG3 RT1 tubing illustrates that microstructure has a profound effect on not just irradiation growth but also on irradiation creep. The effect of varying the microstructure on irradiation creep has been assessed using rate-theory modelling in Ref. [233] and will be described in the next section.

5.2.2. Mechanistic models of irradiation creep

Whereas some creep models used to describe the deformation for a given direction under a given state of stress are derived empirically, constitutive models describe the strain behaviour consistently in three dimensions. Therefore, most mechanistic models are constitutive in nature. The irradiation creep models developed for Zr-alloys described here apply to low stresses and temperatures and to power reactor operating conditions and therefore to conditions and mechanisms that do not involve yielding. However, some of the concepts that apply to yielding in anisotropic materials, such as Hill's yield criterion [14], are equally applicable for creep. Hill's formula defines a yield surface that can also be represented by a compliance tensor, which is similar to that used to describe the elastic strain response of a material to applied stress through a compliance tensor [273]. The radius-normal property relates strain rate to stress [274]. For brevity the stress is referred to principal axes here (no shear terms) and only the first three (non-zero) terms of the compliance tensor need to be shown. For treatments involving dislocation glide and applied shear stresses the full, uncontracted compliance tensor needs to be considered and the reader is referred to the work of Woo [165], and Tomé et al. [192] for details.

The equation describing Hill's yield criterion is also a representation quadric for the tensor relating strain rate to stress and is given by,

$$F(\sigma 1-\sigma 2)^2+G(\sigma 2-\sigma 3)^2+H(\sigma 3-\sigma 1)^2=k \tag{5.8}$$

In terms of a tensor equation for creep strain rate the formal definition of the compliance (referred to the principal axes of stress) is,

$$\begin{pmatrix} \dot{\varepsilon}_1 \\ \dot{\varepsilon}_2 \\ \dot{\varepsilon}_3 \end{pmatrix} = f(M,\Phi,T)\cdot \begin{pmatrix} G+H & -G & -H \\ -G & G+F & -F \\ -H & -F & H+F \end{pmatrix} \cdot \begin{pmatrix} \sigma_1 \\ \sigma_2 \\ \sigma_3 \end{pmatrix} \tag{5.9}$$

The yield criterion developed by Hill can be represented as a creep compliance tensor relating the strain rate to the stress state. In this form the expression for the strain is essentially a balance equation where the choice of anisotropy parameters, F, G and H, dictates the observed anisotropy. Equation (5.8) shows a standard expression for yielding developed by Hill [273]. Hill's equation is essentially the representation quadric of the creep compliance tensor. Equation (5.9) is the corresponding tensor equation that relates the strain rate to the stress state. The stress is referred to principle axes (no shear terms) for simplicity. The tensor equation represented in this way will give a strain state that is balanced and the strains add up to zero (no volume change). The quadric can be scaled to correspond with the creep behaviour for a given magnitude of stress, i.e. defining where the stress locus intersects the quadric surface (determined by the stress locus and k in equation (5.8)). The intersection with the compliance tensor surface is essentially the same as the point at which yielding would occur if the compliance represented a yield surface. But, of course, the representation of the actual yield surface does not necessarily correspond with the surface representing irradiation creep although it might in some special circumstances, e.g. if the irradiation creep was dominated entirely by the slip of dislocations generated by yielding. The strain vectors are given by the radius-normal [274], which is illustrated graphically in two dimensions for the case of a biaxial stress in a pressurised thin-walled tube in Figs. 5–11. Although the radial stress is finite, it is assumed zero for the sake of this illustration, which is a cut through the yield surface in the plane normal to the radial direction of the tube, i.e. a plane-stress condition. The stress locus for increasing pressurisation in a closed-end tube is shown by the solid line. The creep anisotropy is defined by the normal to the surface where the stress locus intersects the quadric surface. The radius-normal is a fundamental tensor property defining any vector or tensor derived from the tensor relation shown in Equation (5.9). The direction of the creep strain rate vector (assumes principal strain components) is shown for the front-end case by the normal to the surface at the point where the biaxial stress locus for a closed-end pressurised tube intersects the surface. The parameters, F, G and H for Figs. 5–11 correspond with the values for Zr-2.5Nb pressure tubing for average front-end and back-end textures [91].

Many of the early irradiation creep models did not attempt to capture the anisotropy of the deformation. Rather they were empirical expressions derived to describe the strain in a given direction subject to a given stress state.

Ultimately, all one really needs in an empirical model is to set up the compliance equation as shown in Equation (5.9) and choose the right set of F, G and H that describes the response for the stress state in question. If one assumes that the anisotropy is unaffected by temperature, damage rate and stress magnitude, one can simply combine these parameters into the scaling factor, (M, σ, Φ, T). One can scale the stress provided the stress exponent is 1. When the stress exponent is > 1 (as it is for high stresses and yielding) there is a complication affecting the compliance tensor itself because different slip systems are activated according to the resolved shear stress on the different slip planes [275]. The resolved shear stress is responsible for slip and the magnitude of the shear stress in the slip direction is obtained by transformation of the applied stress tensor onto the applicable co-ordinate system. For irradiation creep it is reasonable to assume that the stress dependence is linear [165,167] because of the experimental data [18,92]. Although a stress exponent = 1 is generally an indication of a creep process controlled by diffusion, there are a number of irradiation creep models that are based on the I-creep mechanism proposed by Gittus [256] in which the strain rate and anisotropy are governed by slip of network dislocations [30]. Gittus considered two modes of creep to be expected in materials containing a three-dimensional network of dislocations that absorb interstitials ('I-creep') or interstitials plus vacancies 'F-creep'.

5.2.2.1. Slip-based mechanisms. One steady-state irradiation creep model based on the original I-creep mechanism proposed by Gittus [256] was further developed by Woo [165,167]. The role of dislocation creep due to residual stresses in controlling the transients of irradiation growth were reported by Tome et al. [224]. Woo's polycrystalline model was a general polycrystalline model that was based on a single crystal compliance that itself was formulated by combining contributions from various base tensors representing modes of deformation that would allow the material to deform

homogeneously, i.e. five independent shears to produce an arbitrary volume-conserving deformation and one dilatational strain. It should be noted that the different slip systems tend to interact, forming sessile attractive junctions [241]. Woo [167] pointed out that these base tensors could be applied generally, representing any creep deformation mechanism. In the analysis in Ref. [91] the basis tensors were applied assuming the I-creep mechanism [30,256], there being insufficient experimental data to support a SIPA mechanism [265]. The polycrystalline model developed by Woo [165,167,190,191] was applied to Zr-2.5Nb pressure tubes under power reactor conditions and it was assumed that irradiation deformation consisted of additive components of irradiation creep by slip and irradiation growth driven by diffusional mass transport [46,91]. The same type of polycrystalline model has also been applied to the study of transients in irradiation growth that are the result of relaxation of residual stresses [223,224].

In Woo's formalism [165,167,189,191], the basis tensor, $b^{(1)}$ (Appendix A), which is the compliance tensor representing pyramidal slip, has the same form (and sign) as the strain tensor representing irradiation growth (see Equation (4.5)). The slip (Schmid) tensor, [276], corresponding with this deformation mode comprises equal slip on pairs of pyramidal planes sharing a common a-direction zone axis, and with all six pyramidal planes equally active. The reconciliation of a slip based model and a stress exponent of 1 is presumably justified by the rate-determining, slip-enabling, step coming from radiation-enhanced climb of dislocations over barriers [255,256].

In deriving a slip-based creep model the essence of the problem is to equate the strain arising from slip on a given slip plane in a given grain onto a coordinate system that applies to the component. The shear stress on the slip system of interest for a given stress state applicable to the poly-crystal (specimen) coordinates, and the resolution of the resultant shear strain back into the specimen coordinates on which the applied stress is defined, are related through the Schmid tensor [277], and is illustrated in Figs. 5–12. The creep can then be expressed by a standard expression relating strain rate to stress state through a compliance tensor [165,167,273–275],

$$\dot{\varepsilon}^c_{ij} = k^c_{ijkl}\sigma^c_{kl} \ (i,j,k \ and \ l = 1,2,3) \tag{5.10}$$

where $\dot{\varepsilon}^c_{ij}$ is the 2nd rank strain rate tensor in a single crystal; k^c_{ijkl} is the 4th rank single crystal creep compliance; σ^c_{kl} is the 2nd rank stress tensor in the single crystal (c).

At the single crystal level the components of strain can be assigned to different slip systems using the standard Schmid tensor formula, but for a stress exponent = 1 [165,275],

$$k^c_{ijkl} = \sum_s \dot{\gamma}^s_0 \frac{m^s_{ij} m^s_{kl}}{\tau_s} \tag{5.11}$$

where $\dot{\gamma}^s_0$ is a reference (measured or calculated) shear strain of a slip system, s; τ_s is the critical resolved shear stress (measured or calculated) of the slip system, s; and m^s is the 2nd rank Schmid tensor characterizing the slip system (Figs. 5–12) in single crystal coordinates. In combining equations (5.10) and (5.11), the term $m^s_{kl}\sigma^c_{kl}$ is the inner product of the Schmid and stress tensors referred to the same coordinate system, i.e. it is the sum of the product of the terms in m^s_{kl} with the terms in σ^c_{kl} having the same indices [91]). The inner product is a shorthand formula taking into account the tensor transformations needed to extract the shear stress on the slip system (shown on the left in red in Fig. 5.12) for a given stress state σ^c_{kl} in the crystal coordinate system. The shear stress on the slip system of interest then represents a scaling factor which, combined with the reference strain rate ($\dot{\gamma}^s_0$) and shear stress (τ_s) in equation (5.11) and applied to the Schmid tensor (m^s_{ij}), which transforms the shear strain rate on the slip system back into the crystal coordinates, gives the strain rate tensor in crystal coordinates from slip on the slip system, s. The 6×6 compliance tensor is defined by the outer produce ($m^s_{ij}m^s_{kl}$) as described by Hutshinson, [275].

Once one has constructed a model of this type to describe the single crystal response during irradiation the polycrystalline behaviour can be calculated by resolving the combined strains from each grain according to their volume fraction. Such a summation would give a so-called lower-bound result where each grain is allowed to deform according to the activated slip systems [216]. Many models adopt the more realistic approach by allowing for grain-to-grain incompatibility. This situation can be achieved by allowing each grain to deform equally in a so-called upper-bound treatment where the stress is allowed to vary from grain-to-grain [219,223]. With the additional constraint that some grains may deform differently than others, self-consistent models have evolved

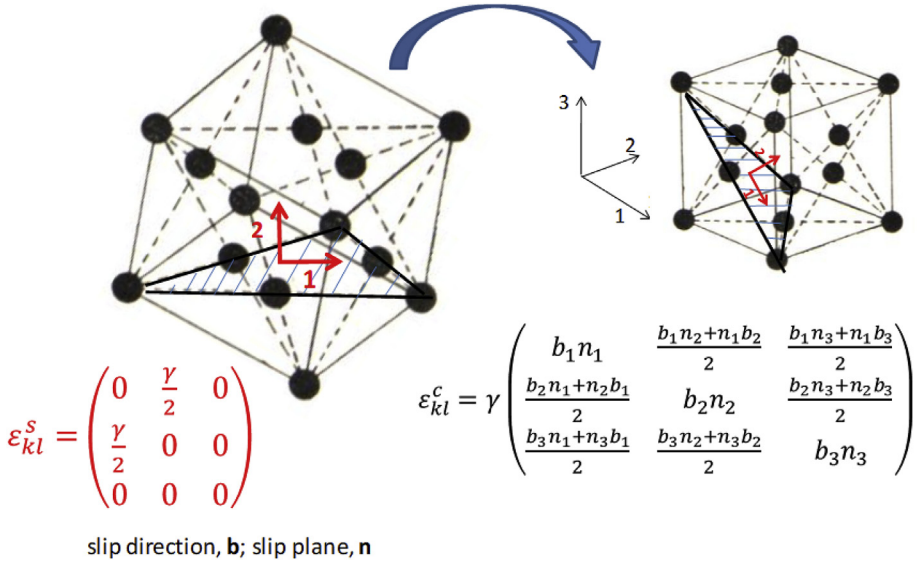

Fig. 5–12. . Relationship between the shear strain tensor for a given slip plane and the corresponding strain tesnor (the Schmid tensor) in the single crystal coordinate system.

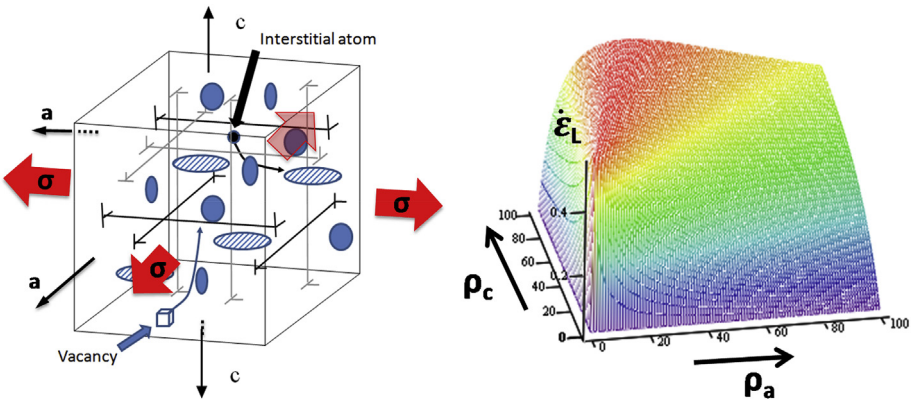

Fig. 5–13. Schematic and rate-theory output showing irradiation growth model results for the longitudinal direction of a large grained Zr-alloy as a function of the a (ρ_a) and c (ρ_c) dislocation densities. The strain rate per unit dpa ($\dot{\varepsilon}_L$) in the longitudinal direction (L) is a maximum when $\sqrt{1+b+s}\cdot\rho_a = \rho_c$, where p is the interstitial bias for a-type dislocations.

[165,167,189,191,224].

The main shortcomings of models that assume I-creep, where dislocation slip is the dominant deformation mechanism, are: (i) slip may not be the dominant mechanism; (ii) there is no provision for diffusional mass transport to contribute to the strain other than through enhancing climb of dislocations over obstacles. If the irradiation creep was dominated by slip one would eventually expect to see two characteristics in the observed deformation behaviour: (i) the creep would eventually cease as the mobile dislocations are exhausted at grain boundaries or at large obstacles (large inclusions, precipitates or voids for example), and (ii) the total creep and the creep rate would be smaller in small-grained material as the dislocation travel shorter distances before running into boundaries. Neither of these characteristics are demonstrated by irradiated Zr-alloys. In the absence of evidence for irradiation creep cessation in Zr-alloys, and given that irradiation creep increases with decreasing grain size [58,233], the evidence suggests that other mechanisms and models are more applicable. There are other reasons why there are shortcomings with slip-based models and this stems from the need to separate the strain arising directly from diffusional mass transport and the strain arising from slip.

5.2.2.2. Diffusion-based mechanisms. Rate theory models for irradiation creep involving diffusional mass transport have been developed in Refs. [165,167] based on DAD [163] and elasto-diffusion [166]. The effect of these two features of diffusion anisotropy can be illustrated for the modified case of the Buckley model described in Equations (4.1) and (4.2) and illustrated previously in Figs. 4–2. One can consider that the stress has an extrinsic effect on the diffusion (elasto-diffusion) thus modifying the intrinsic diffusion properties of the material. For the simple case of microstructure consisting primarily of basal plane vacancy loops and prism plane interstitial loops, the rate-theory expression describing the point defect flow to the different sinks in a biaxial stress field is given by,

$$J_a\left[\frac{(1+b+s).\rho a}{(1+b+s).\rho a+\rho c}-\frac{\rho a}{\rho a+\rho c}\cdot\Phi\right. \tag{5.12}$$

$$J_c=\left[\frac{\rho c}{(1+b+s).\rho a+\rho c}-\frac{\rho c}{\rho a+\rho c}\right]\cdot\Phi \tag{5.13}$$

where ρ_a is the a-type dislocation density, ρ_c is the c-type dislocation density and φ is the atomic displacement damage rate in dpa.s^{-1}. The intrinsic interstitial bias parameter, b, which can exist either because of elastic interactions or anisotropic diffusion or both [165], is modified by the effect of stress given by the bias factor, s. The effect of the stress-induced bias is to modify the axial strain behaviour so that the peak strain is now dictated by a different ratio of c-type and a-type sinks than for the zero stress situation, compare Figs. 4–2 with Figs. 5–13.

Rate theory models of this simple type can be used to explore the effects of microstructural variables that, in addition to dislocations, can have an effect on irradiation creep. For Zr alloys, models can be constructed with a mixture of idealised grains, cubes or platelets, whose axes are aligned with the crystallographic axes of the grain interior [39,165], for example see Figs. 4–12 and 4-13. Following this idealisation of the grain structure the effect of stress can be incorporated as a stress-dependent interstitial bias parameter. In that case the vacancy sink strengths in equations (4.15) to (4.17) stay the same but the interstitial sink strengths are modified by an elasto-diffusion term.

For the case of a grain with a c-axis in the transverse direction in an internally pressurised closed-end tube, the principal stress vector referred to principal axes [274] is given by s(0,2,1), and corresponds with radial, transverse and longitudinal axes (R,T,L). Following the treatment of Heald and Harbottle [234], the grain boundary sink strengths are given by:

$$\left(k_{i,v}^{gb}\right)^2=\frac{2\cdot k_{i,v}}{d_{R,T,L}}.k_i=\sqrt{(1+b)\rho_a+\rho_c+\rho_N}k_v=\sqrt{\rho_a+\rho_c+\rho_N} \tag{5.14}$$

The sink strengths from the a- and c-type network dislocations with densities ρ_a and ρ_c, and the dislocation loops, ρ_N (assumed neutral) for the strain in different directions are dependent on the crystal orientation, but the totals used in Heald and Harbottle expression for grain boundary sink strengths are assumed to be independent of orientation for simplicity.

Restricting all biases to interstitials, for a grain that has the c-axis parallel with the transverse direction (grain B in Figs. 4–12), the interstitial sink strengths in the radial (R), transverse (T) and longitudinal (L) directions are:

$$k_i^2=(1+b).\frac{\rho_a}{2}+\frac{\rho_N}{3}\left(k_i^{gb}\right)^2=\frac{2\cdot(1+p)\cdot k_i}{d_R} \tag{5.15}$$

$$k_i^2=(1+2\cdot s)\cdot\rho_c+\frac{\rho_N}{3}\left(k_i^{gb}\right)^2=\frac{2\cdot(1+2\cdot s).k_i}{d_T} \tag{5.16}$$

$$k_i^2=(1+b+s).\frac{\rho_a}{2}+\frac{\rho_N}{3}\left(k_i^{gb}\right)^2=\frac{2\cdot(1+p+s).k_i}{d_L} \tag{5.17}$$

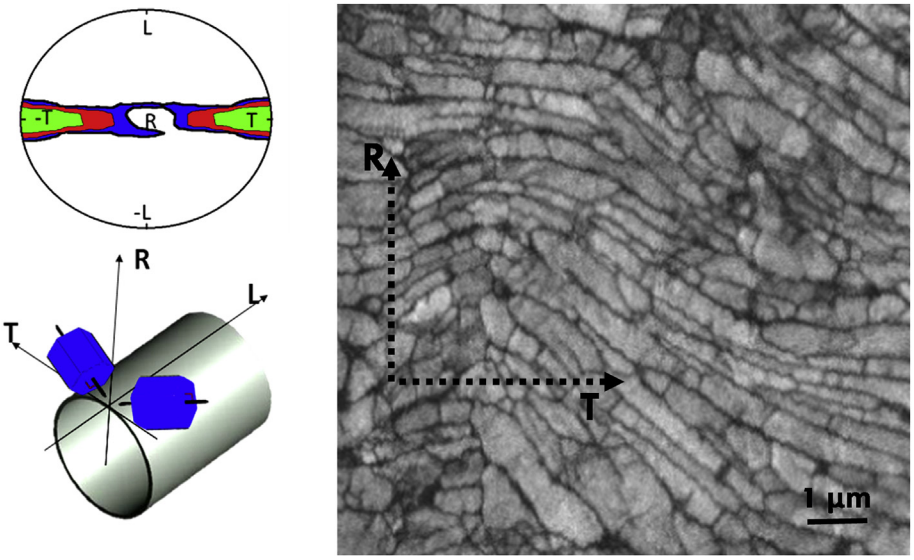

Fig. 5–14. Schematic diagram and pole figure showing grain textures in Zr-2.5Nb pressure tubing and Transmission Kikuchi Diffraction (TKD) band contrast image showing typical grain structure in Zr-2.5Nb pressure tubing. The grain boundary densities in the radial (R) and transverse (T) directions are derived from the intercepts along the lines shown [233].

For Zr-2.5Nb pressure tubing the net flux of point defects to sinks, resulting in strain in the radial (R), transverse (T) and longitudinal (L) directions are obtained by substituting these interstitial sink strengths into the generic balance equations described in Equations (4.11) to (4.19). The interstitial dislocation bias arising from the elastic inhomogeneity (b) will be different in this case as it will involve some SIPA or DAD modification. The DAD bias to grain boundary sinks is given by p, and the bias from elasto-diffusion is given by s, both are orientation dependent, either with respect to the crystal structure or with respect to the stress tensor.

Alternatively, balance equations can be constructed to reflect the varying orientation of grain boundaries relative to both the crystal structure of the grain (Figs. 5–14) and its orientation relative to the specimen/stress axes [58]. Applied to Zr-2.5Nb pressure tubing one can represent the net flux of point defects to sinks, resulting in strain in the radial (R), transverse (T) and longitudinal (L) directions of a pressure tube, by the following balance equations:

$$J_R = [(1 + (1 - f_R).p).D_iC_i - D_vC_v] .(GB_R + \rho_R) \quad (5.18)$$

$$J_T = [(1 + f_R.p + 2s)D_iC_i - D_vC_v].(GB_T + \rho_T) \quad (5.19)$$

$$J_L = [(1 + p + s). D_iC_i - D_vC_v] .(GB_L + \rho_L) \quad (5.20)$$

where

$$D_iC_i = \frac{\phi}{(1 + (1 - f_R).p).(GB_R + \rho_R) + (1 + f_R.p + 2s).(GB_T + \rho_T) + (1 + p + s).(GB_L + \rho_L)} \quad (5.21)$$

$$D_vC_v = \frac{\phi}{(GB_R + \rho_R) + (GB_T + \rho_T) + (GB_L + \rho_L)} \quad (5.22)$$

The grain boundary and dislocation sink densities corresponding with each direction R, T and L are given by GB_m and ρ_m, where the orientation, m = R, T and L. In this model the interstitial bias factor, p, is assumed to be a function of sink orientation and determined by interstitial diffusional anisotropy. The bias parameter is therefore modified by the basal pole orientation parameter, f_R, in order to capture the effect of the diffusional anisotropy difference of interstitial point defects along the a and c- axes [163]. The bias factor due to stress, s, is applied to interstitial diffusion based on the concept of the influence of stress on diffusion and developed as the "elasto-diffusion" model for creep in Ref. [166]. The sink densities, GB_m and ρ_m, can be separated with appropriate changes of bias factors to account for strain-field interactions, if necessary.

One can model the grain boundary sinks as idealised or equivalent grains with dimensions aligned with the crystal axes as shown in Figs. 4–12 [39] or as the probability of a point defect diffusing in a particular direction interacting with a grain boundary or other sink to produce strain in that direction as shown in Figs. 5–14. The results are essentially the same when it comes to demonstrating the strong dependence of irradiation creep on grain structure when the grain dimensions are comparable with the dislocation spacing, see Figs. 5–15 [233]. Apart from the α-phase grain structure, the contribution of the second (beta) phase has also been studied [240].

5.3. Flux and fluence dependence of irradiation creep

One of the main issues concerning the mechanisms of irradiation creep and growth revolves around the question of whether they are separable. In this context one has to also consider whether irradiation creep and thermal creep are separable.

If one considers that irradiation creep contains an element of diffusional mass transport it is difficult to see how irradiation creep and growth can be separated mechanistically; a point defect does not know that it should contribute to creep or growth, it only

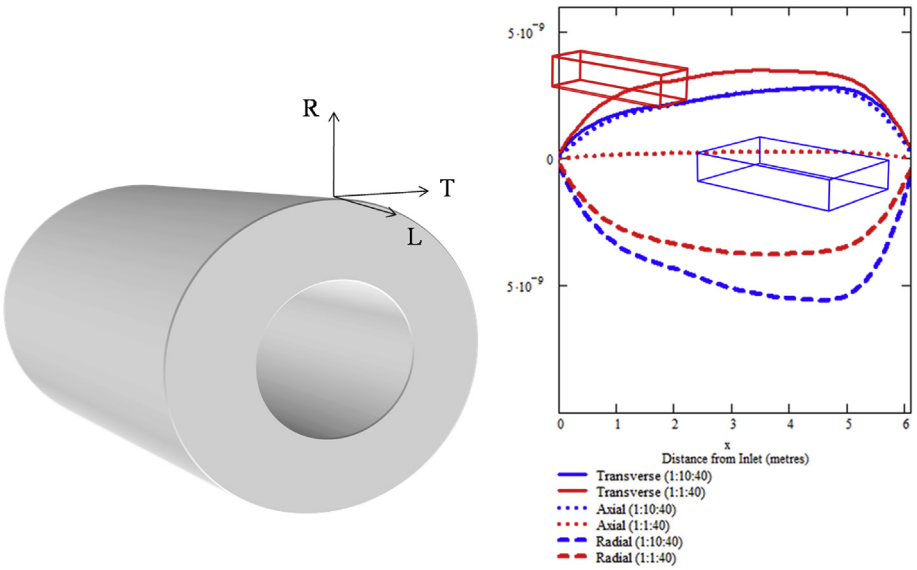

Fig. 5–15. Effect of different grain shapes on strain calculated as a function of axial location for CANDU pressure tubing using a rate-theory model containing grain dimensions. The elongation can be minimised with a grain having smaller transverse dimensions but at the expense of a higher diametral strain [233].

responds to its surroundings and how these are altered by the imposition of a stress. In empirical models the two can be separated. In an empirical model one can define an equation that gives a finite strain rate (per unit fluence or dpa) at zero stress (growth) and an additive component that is a function of stress. Likewise, if one considers creep to consist of separate thermal and irradiation components one can define a thermal creep rate at zero neutron flux (dpa rate) and the creep during irradiation is additive to this base.

Mechanistically, the only way that irradiation creep can be separated from irradiation growth is if creep is dependent on different physical processes from irradiation growth. If, in addition, creep during irradiation is deemed to consist of two components (thermal creep and irradiation creep), it is difficult to understand how they can be governed by the same mechanism and have different anisotropies (texture dependence) as represented in some models [88,91,247]. If irradiation creep was dependent solely on dislocation slip (by the same mechanism that applies out-reactor, in the laboratory) then that would be a case where the two can be treated separately, even if there is an enhancement of slip due to enhanced climb of the network dislocations by an elevation of the steady-state point defect concentration during irradiation. In reality, all of the evidence indicates that irradiation suppresses dislocation slip, which is evident from the creep suppression observed at low fluences where mass transport is only a small direct contribution to the strain [61,97,262]. As the radiation damage rate increases, one sees an increase in creep rate as a function of time but a decrease in creep rate as a function of dpa or neutron fluence. Figs. 5–16 shows the secondary irradiation creep data for Zr-2.5Nb pressure tubing as a function of fast neutron fluence. Results from low flux irradiations of creep capsules in the NRU reactor [61], are combined with low-to-intermediate flux irradiations of pressure tubes in CANDU reactors [233,235,261] and high flux irradiations of creep capsules in OSIRIS. Fluences have been normalised to CANDU-equivalent values so that OSIRIS data and CANDU/NRU data can be plotted on the same graph [10,61]. The OSIRIS capsules were manufactured by the same route as those irradiated in NRU [58] and were intended to be representative of CANDU reactor pressure tubing. All samples were subject to a biaxial stress with hoop stresses of 125 MPa at temperatures of about 280 °C. The data shown in Figs. 5–16 correspond with the

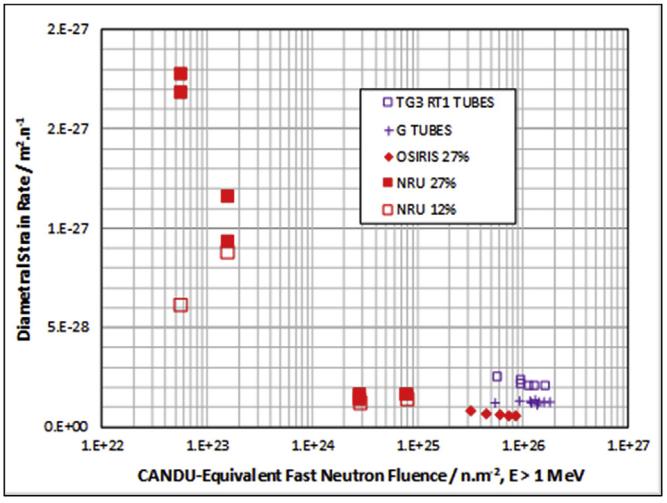

Fig. 5–16. Irradiation creep and growth rates (per unit fluence) as a function of CANDU-equivalent fast neutron fluence for Zr-2.5Nb having similar textures but made by different manufacturing routes and therefore having different dislocation and grain structures.

slope of strain against fluence at various fluences after the primary creep transient, i.e. at times >2000 h. The creep strain as a function of time for the NRU data are shown in Figs. 5–17. There are a number of interesting features demonstrated by the data shown in Figs. 5–16: (i) the secondary creep rate per unit fluence decreases with increasing fluence up to a fluence of about 2×10^{24} n.m^{-2}, E > 1 MeV; (ii) the creep of 12% cold-worked material is less than the 27% cold-worked material at low fluences, but not at fluences > 2×10^{24} n.m^{-2}, E > 1 MeV; (iii) the creep rate per unit fluence is more-or less constant for fluences between about 2×10^{24} n.m^{-2} and 2×10^{26} n.m^{-2}, E > 1 MeV; (iv) at high fluences there is a gradual decreases in creep with increasing fluence. All the creep capsules irradiated in OSIRIS and NRU have similar microstructures. The pressure tubing data comprises two different batches of tubes manufactured by different routes, one is a non-standard route, designated task group three route 1 (TG3 RT1) and the other is by a standard manufacturing route [193]. At high fluences the diametral

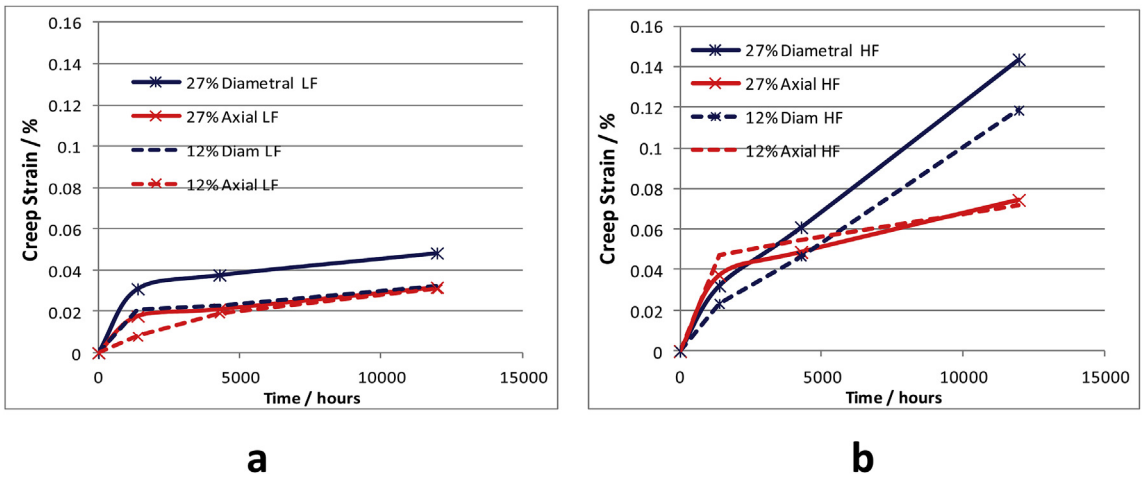

Fig. 5–17. Creep strain as a function of time in the NRU reactor in (a) low-flux (LF) and (b) high-flux (HF) locations. Temperature about 280 °C and hoop stress about 125 MPa. Comparison of 12% cold-worked material with 27% cold-worked material [61].

creep rates can be ranked in order prototype pressure tubing (TG3 RT1) > standard pressure tubing (STD PT) > Creep Capsules.

The observed behaviour can best be understood in terms of variations in microstructure; the decrease up until 2×10^{24} n.m^{-2} corresponds with a rapid increase in a-type loop density, thus hardening the material and slowing down thermal (slip-based) creep. The longer trend with increasing neutron fluence can be accounted for by the continued slow evolution of the c-component loop structure [61,185]. The microstructure evolution can be tracked using X-ray diffraction line broadening. Figs. 5–18 shows how the a-type and c-component loop structure evolves with increasing neutron fluence for OSIRIS creep capsules. This trend is also illustrated by pressure tubing [184] and is independent of the neutron flux, i.e. whether the irradiation is in the CANDU reactors or in OSIRIS. The overlap between the microstructure evolution data is illustrated for the a-type dislocation structure in Figs. 5–19. Because there is no clear influence of damage rate on microstructure (Figs. 5–19) one must conclude that the lower creep rate for the creep capsules in OSIRIS shown in Figs. 5–16 reflects the material variability arising from manufacturing of the creep capsules; there appears to be a continuation of the trend from capsules irradiated in the NRU reactor at lower fluences.

The pressure tube data can be separated into two distinct groups of tubes that reflect different manufacturing routes. In this case the G-tubes represent the majority behaviour for tubes in a particular CANDU reactor; the TG3 RT1 tubes represent the behaviour of prototype tubes installed in the same reactor. The TG3 RT1 tubes were specifically manufactured to have a low dislocation density and were designed also to have smaller grains to make up for the lower dislocation density compared with conventional pressure tubes [193].

The important point to note is that the TG3 RT1 tubes exhibit diametral creep rates that are 50%–100% higher than other tubes whereas they have lower dislocation densities. The higher creep rate is related to the smaller grain size and this is another indication that dislocation slip is not a dominant mechanism for creep at high

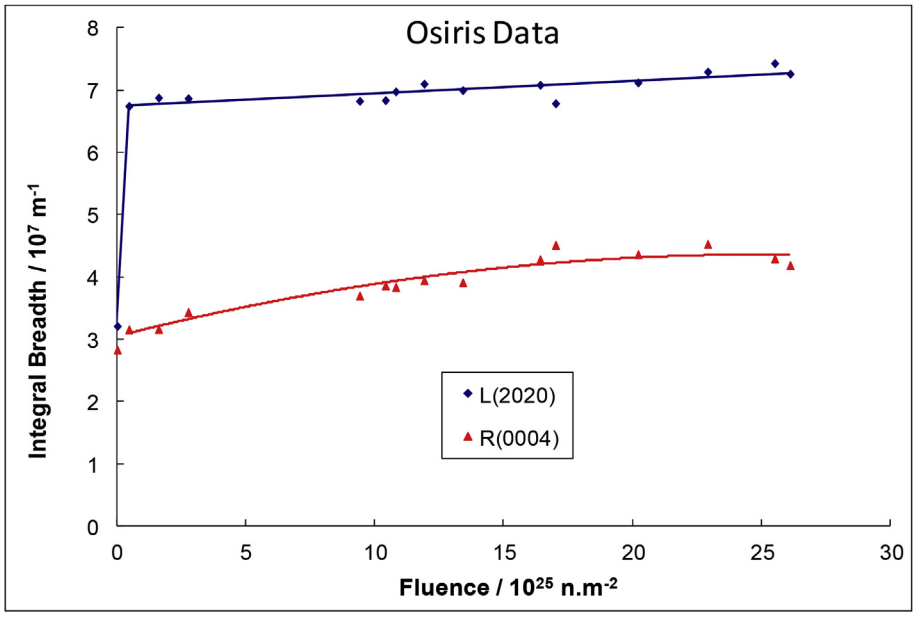

Fig. 5–18. Dislocation densities (a- and c-type) for CANDU pressure tubing irradiated in the OSIRIS reactor, represented by prism and basal plane X-ray diffraction line broadening respectively, as functions of fast neutron fluence, E > 1 MeV, at 250 °C, adapted from Pan et al., [208].

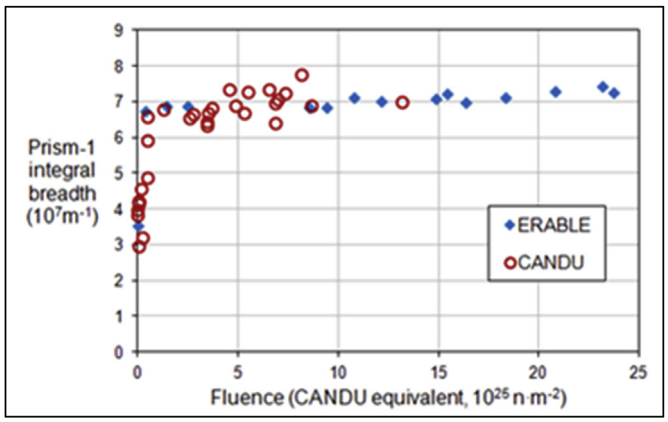

Fig. 5–19. Radiation damage for pressure tubes from CANDU reactors and samples of CANDU pressure tubing irradiated in the Osiris reactor, represented by prism plane X-ray diffraction line broadening, as functions of fast neutron fluence, E > 1 MeV, at 250 °C [94].

fluences. The differences in creep rates as a function of fluence are not the result of differences in irradiation growth. Figs. 5–20 shows the creep and growth strain rates determined from incremental sequential measurements for the creep capsule, standard pressure tubing (RT4) and the experimental pressure tubing (RT3). It is clear that the transverse growth rates of RT3 and RT4 are small and similar and could not account for the differences in creep strain of these tubes at 125 MPa, should creep and growth be additive. To reduce errors due to the small numbers the strain rates fitted to all the data rather than sequential values (inset) are also included The growth of the creep capsules is more negative compared with pressure tubing material and also exhibits the same downward trend with increasing fluence exhibited by the creep capsules. The creep capsules have textures that are similar to CANDU pressure tubes. The TG3 RT1 tubes have a radial basal texture, f_R, that is at the high end of the range for CANDU pressure tubing [61] but is unlikely to be the cause of the higher diametral deformation based on an examination of texture variability for creep in OSIRIS irradiations based on creep capsule data [58]. The creep and growth are correlated to some extent because the same microstructural features responsible for the more negative trend in transverse growth rate with increasing fluence also affects the creep strain. The microstructural feature that is responsible for the negative correlation between strain rate per unit fluence with fluence is the evolution of the c-component loop structure; an increase in c-loop density gives a negative contribution to the strain along the c-axis, whether or not there is an applied stress. The effect of increasing the c-dislocation density can be demonstrated using the model described in equations (5.14) to (5.17). Figs. 5–21 shows the model output for the TG3 RT1 and a standard pressure tube (STD PT) as a function of c-dislocation density increasing with dose. The upper curve shows the creep strain rate for TG3 RT1 tubing with a nominal grain thickness of 0.1 μm and an initial a-type and c-type network dislocation density of 1×10^{14} m^{-2} and 0.1×10^{14} m^{-2} respectively, and a radial basal texture parameter = 0.4. The lower curve shows the output for a standard Zr-2.5Nb pressure tube with a nominal grain thickness of 0.4 μm and an initial a-type and c-type network dislocation density of 4×10^{14} m^{-2} and 1×10^{14} m^{-2} respectively, and a radial basal texture parameter = 0.32. Both microstructures have aspect ratios of 1:5:20 in the radial:transverse:longitudinal directions respectively. The model shows how the TG3 RT1 material has a higher strain rate than the standard pressure tube and the decrease in strain rate with increasing dose occurs as the c-dislocation density increases, consistent with the data shown in Figs. 5–16 and 5-18. This model shows that higher creep is expected for pressure tubing with a lower dislocation density and smaller grain size, opposite to what one might expect from a slip based mechanism but consistent with the observations (Figs. 5–16).

One can still think of irradiation growth as intrinsic response of the material that is modified by the application of a stress. The fact that the both the creep and growth rates of the capsules are more negative relative to pressure tubing in both the CANDU and DIDO reactors is an indication that the difference in both creep and growth is because of some microstructural differences rather than a flux effect; a flux effect would reduce the magnitude of both creep and growth.

The transition to more-or-less constant secondary creep rate

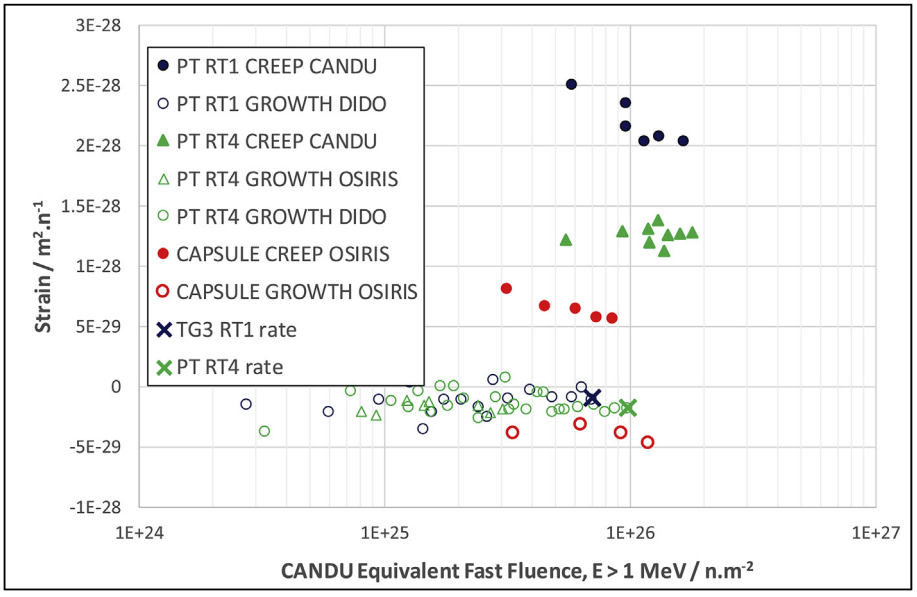

Fig. 5–20. Irradiation creep and growth rates (per unit fluence) as a function of CANDU-equivalent fast neutron fluence for Zr-2.5Nb having similar textures but made by different manufacturing routes and therefore having different dislocation and grain structures. Rates are derived for each incremental measurement. The irradiation growth rates corresponding with a fit to all the data shown in the inset are illustrated by crosses.

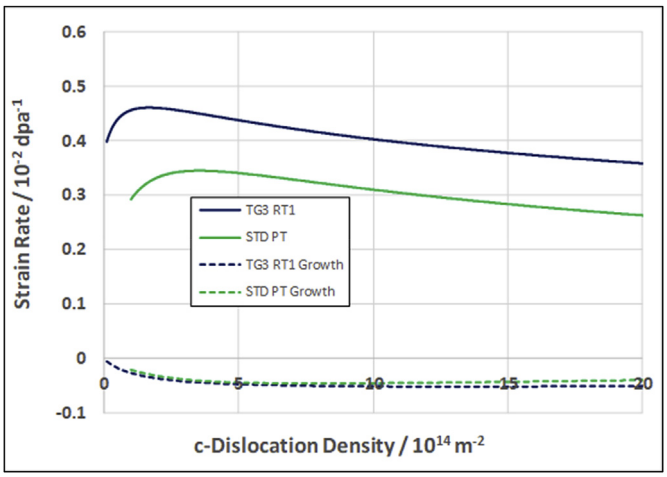

Fig. 5–21. Predicted Irradiation creep and growth rates (per dpa) as a function of c-dislocation desnity for Zr-2.5Nb TG3 RT1 and STD pressure tubing having similar textures but made by different manufacturing routes and therefore having different dislocation and grain structures.

with increasing fluence (Figs. 5–16) reflects a transition in mechanisms from slip-dominated deformation (thermal creep) to irradiation deformation, with little or no slip, at high fluences. The slight downward trend in diametral creep rate with increasing fluence can be attributed to c-component loop formation (or helical climb on existing screw network dislocations) that gives a negative contribution to the diametral strain for all tubes, which have a basal plane texture that is highest in the transverse direction. Another possibility would be the exhaustion of any mobile dislocations if slip was a significant contributor to the strain. This should be detectable as a reduction in network dislocation density (distinct from dislocation loops).

Although many of the cold-worked dislocations are locked in sessile junctions [241], some dislocations will be mobile and these could then potentially contribute to creep strain from slip. Post-irradiation annealing of Zr-2.5Nb pressure tubing irradiated to fluences of 8×10^{25} n.m^{-2} removes the radiation damage to reveal a microstructure that is close to the original cold-worked structure [267] indicating that little, if any, of the mobile network dislocations have moved, otherwise there would be a visible reduction in dislocation density as the mobile dislocations annihilate at grain boundaries. In Figs. 5–16 the data showing higher creep rates at low fluences $<1 \times 10^{24}$ n.m^{-2} indicates that the contribution from slip is being shut down (from radiation damage hardening) as the a-type loop structure evolves (Figs. 5–18). One can conclude that the negative trend in strain at higher fluence is not due to the exhaustion of mobile slip dislocations, rather it is likely due to the evolution of the c-component dislocation loop structure (Figs. 5–18 and 5-16).

5.4. Summary of models and mechanisms

Mechanistically one should not separate irradiation creep from irradiation growth, although the growth will be reflected in the observed creep strain because one is starting from a condition of zero stress and the material then responds to the effects of increasing stress. Creep and growth should be separate if they were governed by different mechanisms (e.g. slip and diffusional mass transport). Based on the available evidence one can conclude that irradiation creep is not dominated by dislocation slip, i.e. irradiation creep is not governed primarily by a climb-and-glide type mechanism. In the theoretical analysis of polycrystalline creep in Ref. [265] the creep due to elasto-diffusion was determined to be an order of magnitude lower than creep by slip [265]. concluded that either the slip-based polycrystalline model [91] was dominant, or the model parameters for diffusion were incorrect. Grain boundaries were not included in their analysis and it is hardly surprising that the amount of strain one can obtain from dislocation slip turned out to be more than the strain possible from dislocation climb, as they concluded. When grain boundaries are incorporated in a rate-theory model, as outlined in equations 5–14 to 5.17, it is relatively easy to show that one can account for the relative behaviour of the materials exhibited in Figs. 5–15 by selecting appropriate bias parameters (equivalent to anisotropy factors). Even the parameters in the slip-based models at the single crystal level are adjusted so that the polycrystalline output fits the experimental data. In the case of creep capsules and pressure tubing shown in Figs. 5–15, all of the creep giving a c-axis strain is attributed to pyramidal slip [91]. However, there is no evidence for dislocation mobility or that there are even sufficient mobile c-component dislocations to generate the necessary strain to match the data. Most of the c-component dislocations in Zr-2.5Nb pressure tubing are locked in sessile junctions [241] and it is hard to imagine how many, or any, of these dislocations are able to unlock and glide, especially in an irradiated material. In fact there is no evidence that the cold-worked dislocations in ex-service, crept pressure tubes have changed from their original as-fabricated configuration [267]. It should be emphasised that prismatic dislocation loops cannot provide a source for mobile dislocations that can contribute to creep strain by slip even if they have evolved by climb into a coarse network [239]; the strain resulting from a dislocation loop is the same whether or not it has moved along its glide cylinder, or even if it tilts. Irradiation creep appears to be primarily governed by the same processes that control is an intrinsic response of the material to neutron irradiation that is then modified by the imposition of a stress to produce the extrinsic effect that we call irradiation creep. Dislocation slip is important at low fluences, either during primary creep or at low fluxes when the contribution from mass transport is small. Dislocation slip also appears to be important when the radiation damage density is low and there is increased thermal activation of slip at high irradiation temperatures [61]. Dislocation slip will also dominate at stresses high enough that yielding occurs. When considering irradiation creep at moderate reactor operating temperatures (250 °C–350 °C) and stresses (100 MPa–150 MPa), one must consider that the mechanism is dominated by diffusional mass transport, i.e. a modification of irradiation growth by the stress.

6. Perspective

Strains in core components arising from operation in nuclear reactors come from many sources. These include thermal expansion strains, stress-induced elastic and plastic strains (for example, those from pellet-cladding interaction (PCMI), fuel swelling or zirconium oxidation) and hydriding strains. In addition are the strains from irradiation creep and growth. Strain magnitudes are strongly dependent on component design, stress, temperature, fluence and metallurgical and crystallographic variables.

Both creep and growth are dependent on microstructure evolving with fluence (dpa or Φt); for example, creation of a high density of irradiation-induced point defects, clusters and dislocation loops, dissolution of second phase particles, formation of new precipitates and alteration of the matrix chemistry Quantitative comparisons between strains induced by irradiation creep or growth, or between any two sets of in-reactor data, must be based on the total damage produced, dpa. Comparisons using neutron fluence from reactors having different neutron energy spectra can

be misleading unless one has applied a correction factor to ensure the data are compared against the same equivalent fluence.

The large number of relevant parameters highlights why predictions of reactor-component strains are complex.

Flux and flux-induced microstructure changes affect both creep and growth. <a> component dislocation loop density tends to saturate with increasing fluence (dpa) for all zirconium alloys, resulting in decreasing strain rates for both creep and growth at low fluences. Creep at higher fluences then becomes a near linear function of damage rate (ϕ or dpa/s). Thermal creep, which is deemed to be independent of irradiation fluence but is reduced in an irradiation environment because of radiation hardening, may be negligible at normal power reactor operating conditions but will be increasingly important during abnormal, high temperature, operation. For growth, in the post-breakaway region associated with <c>-component loop formation, the growth rate is a linear function of the total irradiation damage (dpa) but does not appear to be a direct function of the neutron flux or damage rate.

Cold-work-induced microstructural changes increase both creep and growth rates, although not necessarily in the absence of neutron radiation. Creep is less sensitive to dislocation density than is growth.

Fabrication-induced texture strongly affects both creep and growth. Strains are usually lower in component directions that have high basal f-parameter values.

Irradiation temperature affects both creep and growth in complicated ways. For Zircaloy and light water reactor alloys, strains tend to increase with increasing temperature, particularly when temperature exceeds about 350 °C (623 K), where mechanisms are changing. However, for Zr-2.5Nb pressure tubes, growth rate decreases with increasing temperature in the operating range of CANDU reactors.

The presence of hydrogen, or perhaps hydrides, or both, increases irradiation growth rates but appears not to affect irradiation creep.

Niobium (Nb) in solution decreases strain for both creep and growth. Iron (Fe) in irradiation-induced solution lowers growth. Tin (Sn) in solution decreases creep.

The common assumptions that creep and growth strains are additive and independent of each other, analyzed and disputed in Section 5, is often used empirically to predict total strain from independent creep and growth data sets. Mechanisms for creep and growth are closely linked, each depending on creation and diffusion of a population of radiation-produced defects. Growth in this view is thought of as an intrinsic response of the material to irradiation. In the reactor operating conditions of interest, strain from dislocation motion is much restricted and the creep strain is probably dominated by mass transport, leading to the concept that creep is growth modified by the application of stress.

Acknowledgements

The authors are grateful to Cathy Den Bleyker for significant help with organizing the manuscript and to Judith Coleman for assistance in editing. Peter Rudling and ANT International contributed drafting of many of the figures.

Appendix A. Determination of the Creep Anisotropy Factors, F, G and H

As outlined in section 5.2.2, irradiation creep can be represented by the Hill's compliance tensor that, when referred to principal axes of stress, is given by equations (5.8) and (5.9). These equations are equivalent in defining the creep compliance tensor. The tensor relates the deformation (creep rate) with applied stress. Another way to think of the compliance tensor is as a set of balance equations describing the response of the material to an imposed stress state. In this case it does not matter what controls the anisotropy, rather that there are a set of parameters, F, G and H,that describe the response of the material to an imposed stress. There may be a number of different physical processes that govern the response but, ultimately, one needs only define F,G and H to be able to describe the response of a given material to a given stress state. F, G and H will change as the microstructure changes and are likely to be most sensitive to dislocation structure, grain structure and crystallographic texture. In the case of thermal creep the dislocation structure and texture are most important with the grain boundaries acting as sinks for gliding dislocations thus aiding thermal creep cessation as the gliding dislocations are exhausted. For irradiation creep, grain structure is very important and that is largely due to the effect of the grain boundaries as sinks for point defects. The dependence of creep on mass transport is the most likely reason why there is a linear stress dependence of irradiation creep – diffusional creep is linear in stress and has an inverse relationship with grain dimensions. There are two ways in which the compliance tensor for irradiation creep can be obtained: (i) by measurement; (ii) by using a polycrystalline model.

A.1 Determination of F, G and H by measurement

Just as one can determine the yield anisotropy of a given material by measuring the yield stress in three orthogonal directions, or three directions sufficiently different to sample the yield surface adequately, one can, in principle, determine the creep anisotropy by measuring the creep strain rate for two different stress states, effectively defining the radius-normal to the compliance tensor surface for each stress locus thus allowing one to extract the F, G and H parameters defining that surface, see Figs. 4–6.

Given that the irradiation creep response can be described by an equation of the form described in Equation (5.1), one can design an experiment that allows one to determine F, G and H. A number of different examples of tests that one could conduct to derive F, G and H have been described by Woo et al., [239]. Ideally one should measure the strain rate of tensile specimens under a constant stress in at least three directions. Assuming that the stress exponent = 1, if one is able to obtain creep specimens from three orthogonal directions corresponding with the axes defining the compliance tensor, the strain rates will be proportional to $(G + H)\sigma$, $(G + F)\sigma$ and $(H + F)\sigma$ thus enabling one to determine F, G and H. The sum of the diagonals, $2(G + F + H)$ is a tensor invariant and is constant.

However, the nuclear reactor core components for which irradiation creep is most important are internally-pressurised tubes. In the case of a thin-walled tube one cannot obtain a simple tensile response in a direction that is sufficiently inclined to the surface of the tube that would provide nough information from which to extract the anisotropy factors. However, if one can measure both the strain along the axis of the tensile specimen and perpendicular to the gauge at the same time then one could deduce F, G and H. Perhaps the simplest creep experiment that can be practically achieved in a reactor environment is the stress relaxation test. A stress relaxation test provides a measure of the creep compliance for a given strain direction for a tensile stress state [75].

If one conducts tensile or stress relaxation tests with specimens cut from the axial and transverse directions of the tube of interest (Fig. A-1), the strain rate in the axial and transverse directions is defined by the normal to the yield surface at the point where the stress locus intersects the yield surface, as shown in Fig. A-2.

For bent beam stress-relaxation tests the strains are those determined in the outer fibre of the bent beam with appropriate fiducial markings on the surface from which to determine the strain

rates in the two orthogonal directions corresponding with the principal axes of stress and strain.

At the intersection of the stress locus with the creep compliance (yield) surface one can deduce F, G and H as follows:

$$\begin{pmatrix} \cdot & \cdot & \cdot \\ \varepsilon_R \varepsilon_T \varepsilon_A \end{pmatrix}^A = f(M,\Phi,T)\cdot \begin{pmatrix} G+H & -G & -H \\ -G & G+F & -F \\ -H & -F & H+F \end{pmatrix} \cdot \begin{pmatrix} 0 \\ 0 \\ \sigma \end{pmatrix} \tag{A1.1}$$

$$\begin{pmatrix} \cdot & \cdot & \cdot \\ \varepsilon_R \varepsilon_T \varepsilon_A \end{pmatrix}^T = f(M,\Phi,T)\cdot \begin{pmatrix} G+H & -G & -H \\ -G & G+F & -F \\ -H & -F & H+F \end{pmatrix} \cdot \begin{pmatrix} 0 \\ \sigma \\ 0 \end{pmatrix} \tag{A1.2}$$

$$\dot{\varepsilon}_R^A = -f(M,\Phi,T)\cdot\sigma\cdot H;\ \dot{\varepsilon}_T^A = -f(M,\Phi,T)\cdot\sigma\cdot F;\ \dot{\varepsilon}_A^A = f(M,\Phi,T)\cdot\sigma\cdot[H+F] \tag{A1.3}$$

$$\dot{\varepsilon}_R^T = -f(M,\Phi,T)\cdot\sigma\cdot G;\ \dot{\varepsilon}_T^T = f(M,\Phi,T)\cdot\sigma\cdot[G+F];\ \dot{\varepsilon}_A^T = -f(M,\Phi,T)\cdot\sigma\cdot F \tag{A1.4}$$

Solving for F, G and H,

$$G = \left(\dot{\varepsilon}_T^T + \dot{\varepsilon}_A^T\right) \Big/ f(M,\Phi,T)\cdot\sigma \tag{A1.5}$$

$$H = \left(\dot{\varepsilon}_T^A + \dot{\varepsilon}_A^A\right) \Big/ f(M,\Phi,T)\cdot\sigma \tag{A1.6}$$

$$F = \dot{\varepsilon}_A^T \Big/ f(M,\Phi,T)\cdot\sigma = \dot{\varepsilon}_T^A \Big/ f(M,\Phi,T)\cdot\sigma \tag{A1.7}$$

It is clear that absolute values of the constants F, G and H are dependent on the material constant, $f(M,\Phi,T)$. When comparing the anisotropy of different materials it is customary to compare the ratio of the strains in different directions for a given stress state (see Section 2.4.1). It is also customary to arbitrarily scale the material constant, $f(M,\Phi,T)$, so that F + G + H = 1.5 to facilitate comparisons between different materials. It should be emphasized that there is no reason for F, G and H to be scaled in this way except for ease of comparison between different materials. Naturally, for isotropic materials F = G = H = 0.5 [15].

A.2 Determination of F, G and H using a polycrystalline model

It is difficult to determine the creep anisotropy coefficients by measurement, especially in reactor, and one would need to determine a new set of coefficients each time the material changes. For reactor components such as CANDU pressure tubing the microstructure varies along the length and also circumferentially around the tube; the anisotropy varies accordingly. One can, in principle, determine the polycrystalline response from an agglomeration of single crystals (grains). If one can thus define how the single crystal responds to a given stress state one can determine the polycrystalline response for any combination of single crystals described by the texture. By generating theoretical data for different textures using the single crystal compliance as the input one can thus determine the anisotropy of the polycrystalline aggregate (F, G and H) as a function of texture. Such an approach would allow for the determination of the creep response for any texture without the need to do measurements in each case. It should be noted that the interactions between the individual grains will have a modifying effect on the bulk response and a self-consistent model is needed that takes into account how the stress state is modified within each grain because of the incompatibility with surrounding grains. Such a model has been developed for Zr-2.5Nb pressure tubing and has been described by Christo. et al. [46] using a single crystal creep compliance tensor derived by fitting the model output to experimental data [91,146].

In a very general sense, and borrowing from the elastic compliance tensor representation described by Nye [273], with a stress exponent n = 1 the single crystal deformation can be represented in Ref. [275]:

$$\dot{\varepsilon}_{ij}^c = k_{ijkl}^c \sigma_{kl}^c \ (i,j,k \text{ and } l = 1,2,3) \tag{A1.8}$$

where.

$\dot{\varepsilon}_{ij}^c$ is the 2nd rank strain rate tensor in a single crystal;
k_{ijkl}^c is the 4th rank single crystal creep compliance;
σ_{kl}^c is the 2nd rank stress tensor in a single crystal.

In expanded form, Eq. (A1.6) is expressed as.

$$\begin{pmatrix} \dot{\varepsilon}_{11}^c \\ \dot{\varepsilon}_{12}^c \\ \dot{\varepsilon}_{13}^c \\ \dot{\varepsilon}_{21}^c \\ \dot{\varepsilon}_{22}^c \\ \dot{\varepsilon}_{23}^c \\ \dot{\varepsilon}_{31}^c \\ \dot{\varepsilon}_{32}^c \\ \dot{\varepsilon}_{33}^c \end{pmatrix} = [\mathrm{fx}]$$

The compliance tensor, k_{ijkl}^c, can be represented as a 6 × 6 matrix following the convention described by Nye [273]. Assuming orthorhombic symmetry this tensor becomes, in matrix form:

$$\begin{pmatrix} \dot{\varepsilon}_1^c \\ \dot{\varepsilon}_2^c \\ \dot{\varepsilon}_3^c \\ \dot{\varepsilon}_4^c \\ \dot{\varepsilon}_5^c \\ \dot{\varepsilon}_6^c \end{pmatrix} = \begin{pmatrix} k_{11}^c & k_{12}^c & k_{13}^c & 0 & 0 & 0 \\ k_{21}^c & k_{22}^c & k_{23}^c & 0 & 0 & 0 \\ k_{31}^c & k_{32}^c & k_{33}^c & 0 & 0 & 0 \\ 0 & 0 & 0 & k_{44}^c & 0 & 0 \\ 0 & 0 & 0 & 0 & k_{55}^c & 0 \\ 0 & 0 & 0 & 0 & 0 & k_{66}^c \end{pmatrix} \begin{pmatrix} \sigma_1^c \\ \sigma_2^c \\ \sigma_3^c \\ \sigma_4^c \\ \sigma_5^c \\ \sigma_6^c \end{pmatrix}$$

where the suffixes are [273],

tensor notation 11, 22, 33, 23, 32, 31, 13, 12, 21
matrix notation 1, 2, 3, 4, 5, 6

Although often referred to as Hill's creep compliance tensor, the compliance represented in this way is strictly speaking a matrix and, despite having two suffixes, the k_{ij} are not the, components, and do not transform like the components, of a second rank tensor, see page 135 in Ref. [273]. The upper left quadrant, however, corresponds to the tensor representation of creep compliance given in equation (5.9) when referred to the principal axes of stress (no shear terms). In that case the compliance can be treated as a second rank tensor, see chapter 3 in Ref. [274], and it has a representation quadric that is equivalent to Hill's yield criterion (equation (5.8)).

Woo's treatment of irradiation creep [167], follows the methodology adopted by Groves and Kelly [276] to represent the strain from slip on individual slip systems in the single crystal coordinate system. In Woo's treatment the single crystal creep compliance tensor is obtained from the sum of the compliances derived from the slip or Schmid tensors for individual active slip systems, each weighted by a factor determined from experimental data. The

compliance for each slip system is equivalent to the "tensor of creep compliances" described by Hutchinson [275], setting the stress exponent n = 1. The basis tensors described in Ref. [167], $\mathbf{b}^{\lambda}$, are similar to the slip or Schmid tensors corresponding with the fundamental strain tensors characterizing each slip system described in [276]. The basis tensors represent the five independent slip systems necessary to describe an arbitrary volume-conserving deformation as outlined in [277].

Although formulated and interpreted from a consideration of the strains arising from slip, Woo points out that these basis tensors can also be used to describe deformation by any mechanism [165]. In fact the same set of basis tensors were employed to model irradiation creep based on diffusional mass transport [265]. Although they represent the strains due to slip on each slip system transformed into the crystal coordinates they can also be used as the orthonormal basis on which to partition the contributions to the total strain of the single crystal where the strain arises from the elasto-diffusion tensor [265]. The basis tensors are as follows:

$$\mathrm{b}^1 = \frac{1}{\sqrt{6}}\begin{pmatrix}1&0&0\\0&1&0\\0&0&-2\end{pmatrix},\ b^2 = \frac{1}{\sqrt{2}}\begin{pmatrix}0&0&0\\0&0&1\\0&1&0\end{pmatrix},\ b^3 = \frac{1}{\sqrt{2}}\begin{pmatrix}1&0&0\\0&-1&0\\0&0&0\end{pmatrix}, b^4 = \frac{1}{\sqrt{2}}\begin{pmatrix}0&0&1\\0&0&0\\1&0&0\end{pmatrix}, b^5 = \frac{1}{\sqrt{2}}\begin{pmatrix}1&0&0\\0&1&0\\0&0&0\end{pmatrix},\ \text{and } b^6 = \frac{1}{\sqrt{3}}\begin{pmatrix}1&0&0\\0&1&0\\0&0&1\end{pmatrix}$$

If one was to assign these basis tensors to slip the Schmid tensors would be as follows.

Schmid Tensors
$b^{(1)}$ - represents <c+a> slip on $\{10\bar{1}1\}$
$b^{(2)}$ and $b^{(5)}$ - represent <a> slip on $\{10\bar{1}0\}$
$b^{(3)}$ and $b^{(4)}$ - represent <a> slip on (0001)

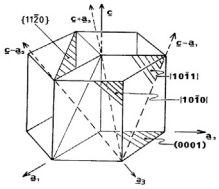

The single crystal compliance ($\mathbf{K}^{c}$) is given by,

$$\mathbf{K}^{c}_{ijkl} = = \ k_{\alpha} \cdot \mathbf{b}^{\alpha}_{ij} \cdot \mathbf{b}^{\alpha}_{kl} \tag{A1.9}$$

and the single crystal strain is then given by,

$$\dot{\varepsilon}^{c}_{ij} = \sum_{c} \sigma_{\alpha} \mathbf{K}^{c}_{ijkl}\, \mathbf{b}^{\alpha}_{kl} \tag{A1.10}$$

where σ_{α} and k_{α} are eigenvalues derived for the applicable stress and microstructure [91]. In the model described in Ref. [91] these equations are similar in nature to the Schmid tensor described in Figs. 4–7 and they represent the resolved strain in the crystal coordinates due to slip on various slip systems. The k_{α} are essentially adjustable (fitting) parameters for the relative amount of slip on different slip systems that would be necessary in the model in order to account for the observed anisotropy. The parameter, k_1, in particular, accounts for all of the c-axis strain and is derived from <c+a> slip on pyramidal planes. It is a critical element in deciding whether the model is applicable to any particular material and condition. For Zr-2.5Nb pressure tubing at power reactor operating temperatures there is no evidence to show that <c+a> slip is active because the network dislocation structure appears to be the same both before and after service [267] and, perhaps more importantly, there are insufficient c-component network dislocations to account for the large diametral strains that are typical for Zr-2.5Nb pressure tubing (see Section 5.1.3).

As with the compliance tensor for the bulk material the basis tensors simply represent modes of deformation that one must invoke in order to maintain grain-to-grain compatibility within the polycrystalline agglomerate [165,167,264,265]. The polycrystalline strain is derived by summing the contributions from individual crystals (Fig. A-3). The incompatabilities in the strains of each individual grain compared with the average results in grain interaction stresses that can be taken into account when calculating the stress states as they evolve during creep in an iterative routine. The bulk applied stress, combined with the stress from strain incompatability, translates into different stress states in each grain. The resultant stress and strain evolution during creep is determined in a self-consistent manner [192].

Having developed a polycrystalline model, the creep subjected to given stress state can be calculated taking into account the effects of grain interaction stresses and, from those results, the anisotropy factors, F, G and H can be derived from the calculated strain rates in exactly the same fashion as described for the experimental derivation of F, G and H. Of course, the anisotropy factors F, G and H can equally be derived from the predicted deformation using the diffusion-based or slip-based models described in Section 4.2.2. The difference is that, in the slip-based models described in Section 4.2.2, it is assumed that creep during irradiation is a combination of irradiation growth, thermal creep and irradiation creep, each with their own anisotropy [46]. The anisotropic factors deduced from the mass transport model described in Section 4.2.2.2 comprise the total deformation resulting from diffusion. When slip is occurring to any large extent (in primary creep, or secondary creep at low fluences and/or high temperatures) additional mechanisms come into play and the contributions must be separated.

In the model described in Ref. [46] the irradiation creep deformation is assumed to be by slip only and is therefore dependent on dislocation structure and texture only; it is assumed that the grain structure does not affect the deformation anisotropy. Such an approach would be an elegant and efficient way to describe the creep anisotropy, provided that the anisotropy is only dictated by the texture, i.e. dislocation slip, and provided one could conduct the right experiment to determine the single crystal creep compliance tensor. The best way to determine whether the polycrystalline model is valid, i.e. that the single crystal compliance is accurate and the anisotropy is only dictated by texture, is to compare with experiment. However, even that is difficult when the deformation model is comprised of different contributions other than irradiation creep for which one wants to derive the anisotropy factors: F, G and H.

In the context of the pressure tube deformation equation, it is assumed that the in-reactor deformation is comprised of three parts, irradiation growth, thermal creep and irradiation creep (see Equations (5.5), (5.6) and (5.7)). Whereas the creep compliance in any given direction for a given stress state can be deduced from the slope of the creep rate as a function of stress, both thermal creep and irradiation creep are contributing and one has no idea how much of a contribution comes from thermal creep. The best that one can do is either subtract an estimate of thermal creep or assume that it is negligible. With this caveat, the data on creep rate can then be used to establish a single crystal creep compliance in the context of the polycrystalline model described in Ref. [46]. The validation of the creep anisotropy factors described in Ref. [46] has

been performed by Causey et al., [92]. It was claimed that the model works well [93], however it is not clear whether some of the validation data cited, reference [17] in Ref. [92], is itself valid [45].

The polycrystalline model outlined in Ref. [46] shows reasonable agreement with the OSIRIS data for a narrow range of textures corresponding to the OSIRIS creep capsules (f_T-f_R ~ 0.2), see Section 2.4.1. However, it is assumed that the anisotropy is only dependent on the texture. This assumption is largely based on the further assumption that the irradiation creep is dominated by dislocation slip. We know from irradiation growth that grain structure changes the anisotropy, so it would be hardly surprising if grain structure did not also affect the creep anisotropy. For the pressure tube deformation equation, Christodoulou et al. [46], attempted to include the effect of grain size through the inclusion of the $K_4(x)$ parameter, which is meant to capture variations in microstructure other than texture along the pressure tube length. However, $K_4(x)$ was derived in order to fit experimental data after applying the anisotropy parameters obtained from the polycrystalline model. This means that $K_4(x)$ also accounts for any variation in texture not adequately accounted for by the polycrystalline model. In effect, $K_4(x)$ renders the anisotropy factors redundant and one is left with, essentially, an empirical model. Clearly further work is needed using polycrystalline models for irradiation creep involving slip. Such models should include both mass transport and grain structure as integral components.

Appendix D. Supplementary data

Supplementary data related to this article can be found at https://doi.org/10.1016/j.jnucmat.2019.04.021.

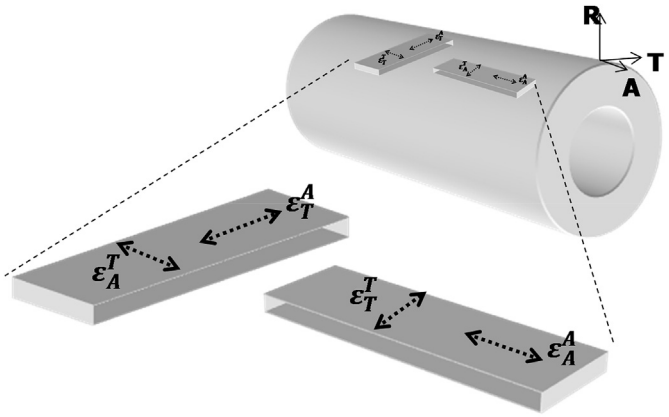

Fig.A-1. Orientation of specimens and measurement directions of bent beam stress-relaxation specimens. The subscript defines the orientation with respect to the material of interest (tube), the superscipt defines the orientation with respect to the bent beam and ε is the strain rate.

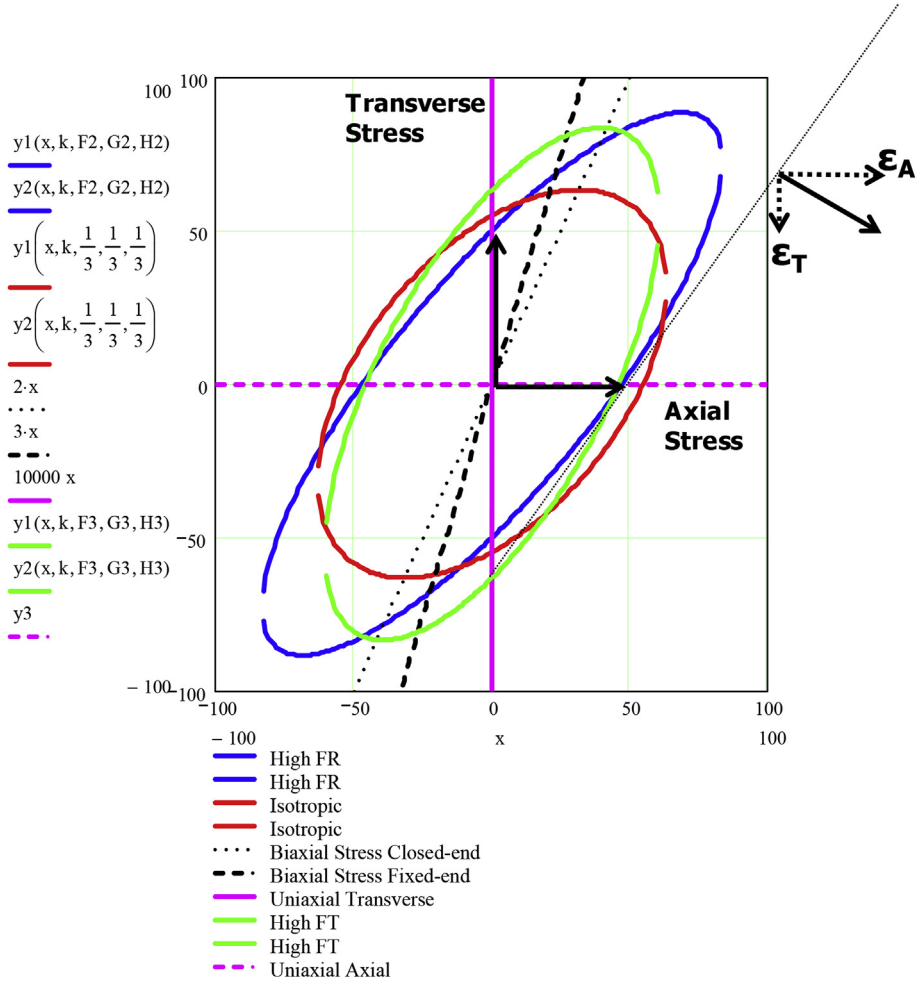

Fig.A-2. Example of stress loci and yield surfaces defined by the creep compliance tensor in the plane of a tube for a range of different anisotropy factors. An example is given for the strain rate vector (ε), defined by the normal to the surface at the intersection with an axial tensile stress for an axial tensile specimen and has components ε_A and ε_T corresponding with the axial and transverse directions respectively; ε is the strain rate.

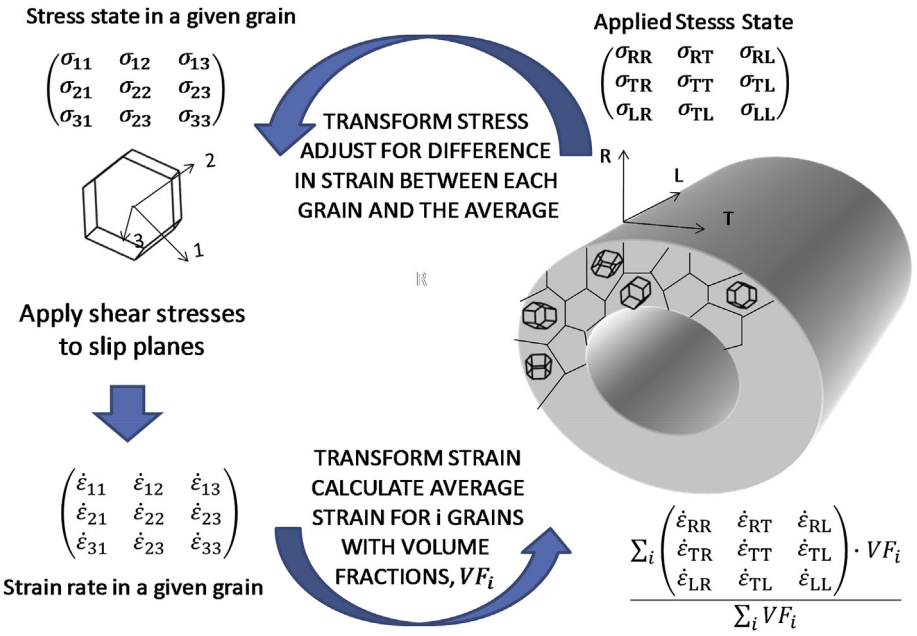

Fig.A-3. Determination of creep strain in a polycrystalline aggregate. The single crystal coordinates are represented by numerical suffixes and the component (bulk) coordinates are represented by alphabetical suffixes.

References

[1] B. Lustman, Zirconium technology – twenty years of evolution, zirconium in the nuclear Industry: 4th symposium, American society for testing and materials, ASTM STP 681 (1979) 5–18.

[2] H.G. Rickover, in: R.B. Adamson (Ed.), The Decision to Use Zirconium in Nuclear Reactors, Zirconium Production and Technology: the Kroll Medal Papers 1975-2010, ASTM International, RPS2, 2010, pp. 9–17.

[3] E8/E8M-15, ASTM Standard Test Methods for Tension Testing of Metallic Materials, ASTM International, Approved 2015. ASTM Standard test methods for elevated temperature tension tests of metallic materials, ASTM International, E21-17 (Approved 2017).

[4] F. Garzarolli, R.B. Adamson, P. Rudling, A. Strasser, BWR Fuel Channel Distortion, ZIRAT16/IZNA11 Special Topical Report,ANT International, Mölnlycke, Sweden, 2011.

[5] S.T. Mahmood, Y.P. Lin, M.A. Dubecky, K. Edsinger, E. V Mader, Channel bow in boiling water reactors – hot cell examination results and correlation to measured bow, in: Proc. International Meeting LWR Fuel Performance, American Nuclear Society, San Francisco, CA, USA, 2007, pp. 124–133. Paper 1061.

[6] D.G. Franklin, R.B. Adamson, Implications of Zircaloy creep and growth to light water reactor performance, J. Nucl. Mater. 159 (1988) 12–21.

[7] G.J. Field, Problems caused by irradiation deformation in CANDU reactors, J. Nucl. Mater. 159 (1988) 3–11.

[8] M.J. Norgett, M.T. Robinson, I.M. Torrens, A proposed method of calculating displacement dose rates, Nucl. Eng. Des. 33 (1975) 50–54.

[9] A. Ya Rogozyanov, A.V. Smirnov, B.A. Kanashov, V.S. Polenok, A.A. Nuzhdov, Use of the irradiation- thermal creep model of Zr-1% Nb alloy cladding tubes to describe dimensional changes on VVER fuel rods, J. ASTM Int. (JAI) (2005) 2. Paper JAI 12426.

[10] L. Walters, S.R. Douglas, M. Griffiths, Equivalent radiation damage in zirconium irradiated in various reactors, in: R.J. Comstock, A.T. Motta (Eds.), Zirconium in the Nuclear Industry: 18th International Symposium, ASTM International, West Conshohocken, PA, 2018, pp. 676–690. ASTM STP 1597.

[11] E. Tenckhoff, Review of deformation mechanisms, texture and mechanical anisotropy in zirconium and zirconium base alloys, J. ASTM Int. (JAI) 2 (2005). Paper ID JAI 12945.

[12] J.J. Kearns, Thermal Expansion and Preferred Orientation in Zircaloy, Bettis Atomic Power Laboratory, West Mifflin PA, 1965, p. 472. Report WAPD-TM.

[13] J.G. Merkle, An Engineering Approach to Multiaxial Plasticity, Oak Ridge National Laboratory Report, 1967. ORNL-4138.

[14] R. Hill, The Mathematical Theory of Plasticity, Oxford Univ. Press, London, 1954.

[15] P.A. Ross-Ross, V. Fidleris, D.E. Fraser, Anisotropic creep behaviour of zirconium alloys in a fast neutron flux, Can. Met. Quart. 11 (1972) 101–111.

[16] R.V. Hesketh, J.E. Harbottle, N.A. Waterman, R.C. Lobb, Irradiation Growth and Creep in Zircaloy-2, Symposium on Radiation Damage in Reactor Materials, vol. 1, IAEA, Vienna, 1969, pp. 365–383.

[17] W.K. Alexander, V. Fidleris, R.A. Holt, Zircaloy-2 pressure tube elongation at the Hanford N Reactor, in: Zirconium in the Nuclear Industry: 3rd International Symposium, American Society for Testing and Materials, vol. 633, ASTM STP, Philadelphia, 1977, pp. 344–364.

[18] V. Fidleris, The irradiation creep and growth phenomena, J. Nucl. Mater. 159 (1988) 22–42.

[19] R. Adamson, K. Coleman, T. Mahmood, P. Rudling, Mechanical Testing of Zirconium Alloys, Volume I, ZIRAT18/IZNA13, Special Topics Report, ANT International, Mölnlycke, Sweden, 2013.

[20] J. Romero, M. Preuss, J. Quinta da Fonseca, R.J. Comstock, M. Dahlbäck, L. Hallstadius, Texture evolution of Zircaloy-2 during beta-quenching: effect of process variables, J. ASTM Int. (JAI) 7 (2010). Paper ID JAI 103014.

[21] C.E. Coleman, Tertiary creep in cold-worked Zircaloy-2, J. Nucl. Mater. 42 (1972) 180–190.

[22] N.E. Dowling, Mechanical Behavior of Materials, second ed., Prentice Hall, 1999, ISBN 0-13-905720-X.

[23] A. Soniak, N. L'Hullier, J.-P. Mardon, V. Rebeyrolle, P. Bouffloux, C. Bernaudat, Irradiation creep behaviour of Zr-base alloys, in: G.D. Moan, P. Rudling (Eds.), Zirconium in the Nuclear Industry: 13th Int'l Symposium, vol. 1423, ASTM STP, 2002, pp. 837–862.

[24] R. Adamson, F. Garzarolli, P. Patterson, In-reactor Creep of Zirconium Alloys, ZIRAT 14 Special Topic Report, A.N.T. International, Skultuna, Sweden, 2009.

[25] V. Fidleris, Uniaxial in-reactor creep of zirconium alloys, J. Nucl. Mater. 26 (1968) 51–76.

[26] M.R. Cundy, P. von der Hardt, R.H. Loelgen (Eds.), Proceedings of international conference on measurement of irradiation-enhanced creep in nuclear materials, petten, 65, 1977. May 1976, J. Nucl. Mater.

[27] G.J.C. Carpenter, C.E. Coleman, S.R. MacEwen (Eds.), Proceedings of the International Conference on Fundamental Mechanisms of Radiation Induced Creep and Growth, Chalk River, May 8-10, 1979, vol. 90, J. Nucl. Mater., 1980.

[28] Proceedings of the international conference on fundamental mechanisms of radiation-induced creep and growth, Hecla Island, Manitoba, Canada, June 22-25, 1987, in: C.H. Woo, R.J. McElroy (Eds.), J. Nucl. Mater. 159 (1988).

[29] V. Fidleris, Summary of experimental results on in-reactor creep and irradiation growth of zirconium alloys, Atom. Energy Rev. 13 (1975) 51–80.

[30] D.G. Franklin, G.E. Lucas, A.L. Bement, Creep of Zirconium Alloys in Nuclear Reactors, ASTM STP 815, ASTM, Philadelphia, PA, 1983.

[31] F.A. Nichols, Mechanistic modeling of Zircaloy deformation and fracture in fuel element analysis, in: R.B. Adamson, L.F.P. Van Swam (Eds.), Zirconium in the Nuclear Industry: 7th International Symposium, vol. 939, ASTM STP, Philadelphia, 1987, pp. 5–22. American Society for Testing and Materials.

[32] F. Garzarolli, H. Stehle, E. Steinberg, Behavior and properties of Zircaloys in power reactors: a short review of pertinent aspects in LWR fuel, Zirconium in the Nuclear Industry: 11th Int'l Symposium 1295, ASTM STP, 1996, pp. 12–32.

[33] R.B. Adamson, Effects of neutron irradiation on microstructure and properties of Zircaloy, in: Zirconium in the Nuclear Industry; 12th International Symposium, American Society for Testing and Materials, vol. 1354, ASTM STP, West Conshohocken, PA, 2000, pp. 15–31.

[34] R.A. Holt, In-reactor Deformation of Zirconium Alloy Components, vol. 5, J. ASTM International, 2008. Paper ID JAI 101354.

[35] M. Griffiths, Microstructure evolution in Zr alloys during irradiation: dose, rate and impurity dependence, J. ASTM Int. (JAI) 5 (2007). Paper ID JAI 1011046.
[36] R.B. Adamson (Ed.), Zirconium Production and Technology: the Kroll Medal Papers 1975-2010, ASTM International, RPS2, 2010.
[37] V.N. Shishov, The evolution of microstructure and deformation stability in Zr-Nb-(Sn, Fe) alloys under neutron irradiation, J. ASTM Int. (JAI) 7 (2010). Paper ID JAI 103005.
[38] B.A. Cheadle, The development of Zr-2.5Nb pressure tubes for CANDU reactors, J. ASTM Int. (JAI) 7 (2010). Paper ID JAI 103057.
[39] R. Adamson, M. Griffiths, C. Patterson, Irradiation Growth of Zirconium Alloys, ZIRAT 22 Special Topic Report, A.N.T. International, Tollered, Sweden, 2017.
[40] P.A. Ross-Ross, C.E.L. Hunt, The in-reactor creep of cold-worked Zircaloy-2 and Zirconium-2.5wt.% Niobium pressure tubes, J. Nucl. Mater. 26 (1968) 2–17.
[41] M. Koike, T. Asada, Irradiation creep and growth of pressure tubes in HWR Fugen, J. Nucl. Mater. 159 (1988) 62–74.
[42] P.A. Platonov, A.N. Ivanov, I.A. Frolov, E.P. Riazantsev, B.S. Rodchenkov, YuO. Zakharzhevsky, V.G. Kiselev, Creep of the RBMK pressure tubes from Zr-2.5Nb alloy, Mater. Sci. Nov. Mater. 36 (1990) 22–33.
[43] R. Gunn, G. Van Drunen, W.R. Mayo, D. Kalenchuk, fuel channel inspection with AFCIS (AECL fuel channel inspection system), in: 7th Technical Committee Meeting on Exchange of Operational Safety Experiences of Pressurized Heavy Water Reactors, IAEA J8-TC-2000.14, Haiyan, China, 2002 (Available as AECL Report AECL-CONF 1276).
[44] C.E. Coleman, B.A. Cheadle, A.R. Causey, P.C.K. Chow, P.H. Davies, M.D. McManus, D.K. Rodgers, S. Sagat, G. Van Drunen, Evaluation of Zircaloy-2 pressure tubes from NPD, in: L.F.P. Van Swam, C.M. Eucken (Eds.), Zirconium in the Nuclear Industry: 8th International Symposium vol. 1023, ASTM STP, Philadelphia, 1989, pp. 35–49. American Society for Testing and Materials.
[45] A.R. Causey, V. Fidleris, S.R. MacEwen, C.W. Schulte, In-reactor Deformation of Zr-2.5 Wt% Nb Pressure Tubes, Influence of Radiation on Material Properties: 13th International Symposium, Part II, in: F.A. Garner, C.H. Henager Jr., N. Igata (Eds.), American Society for Testing and Materials, vol. 956, ASTM STP, Philadelphia, 1987, pp. 54–68.
[46] N. Christodoulou, A.R. Causey, R.A. Holt, C.N. Tomé, N. Badie, R.J. Klassen, R. Sauvé, C.H. Woo, Modeling in-reactor deformation of Zr-2.5Nb pressure tubes in CANDU power reactors, in: E.R. Bradley, G.P. Sabol (Eds.), Zirconium in the Nuclear Industry: 11th International Symposium vol. 1295, ASTM STP, 1996, pp. 518–537. American Society for Testing and Materials.
[47] C.E. Coleman, M. Griffiths, V. Grigoriev, V. Kiseliov, B. Rodchenkov, V. Markelov, Mechanical properties of Zr-2.5Nb pressure tubes made from electrolytic powder, J. ASTM Int. (JAI) 4 (2007). Paper ID JAI 101111.
[48] C.K. Chow, C.E. Coleman, M.H. Koike, A.R. Causey, C.E. Ells, R.R. Hosbons, S. Sagat, V.F. Urbanic, D.K. Rodgers, Properties of an irradiated heat-treated Zr-2.5Nb pressure tube removed from the NPD reactor, in: E.R. Bradley, G.P. Sabol (Eds.), Zirconium in the Nuclear Industry: 11th International Symposium, ASTM STP 1295 vol. 1295, ASTM STP, West Conshohocken, PA, 1996, pp. 468–491. American Society for Testing and Materials.
[49] E.F. Ibrahim, In-reactor Creep of Zr-2.5Nb Tubes at 570 K, Zirconium in Nuclear Applications, vol. 551, American Society for Testing and Materials, ASTM STP, 1974, pp. 249–262.
[50] E.F. Ibrahim, Deformation of cold-drawn tubes of Zr-2.5 wt.% Nb after 7 years in-reactor, J. Nucl. Mater. 118 (1983) 260–268.
[51] E.F. Ibrahim, J.E. Winegar, Development of an air gauge for measuring in-reactor creep of tubular specimens, J. Phys. E Sci. Instrum. 6 (1973) 884–888.
[52] E.F. Ibrahim, In reactor deformation of internally pressurized Zr-2.5 wt.% Nb tubes at 570 K, J. Nucl. Mater. 102 (1981) 214–219.
[53] D.S. Wood, High Deformation Creep Behaviour of 0.6-in.-diameter Zirconium Alloy Tubes under Irradiation, Zirconium in Nuclear Applications, vol. 551, American Society for Testing and Materials, ASTM STP, 1974, pp. 274–291.
[54] R.S. Matfield, Neutron-Radiography Services in Research Reactor Division at Harwell, 1971. AERE-R 6372.
[55] E.F. Ibrahim, Creep ductility of cold-worked Zr-2.5 wt.% Nb and Zircaloy-2 tubes in-reactor, J. Nucl. Mater. 96 (1981) 297–304.
[56] A.R. Causey, R.A. Holt, N. Christodoulou, E.T.C. Ho, Irradiation-enhanced deformation of Zr-2.5Nb tubes at high neutron fluences, Zirconium in the Nuclear Industry: 12th International Symposium, in: G.P. Sabol, G.D. Moan (Eds.), ASTM, vol. 1354, ASTM STP, West Conshohocken, PA, 2000, pp. 74–85.
[57] D. Gilbon, A. Soniak, S. Doriot, J.P. Mardon, Irradiation creep and growth behavior, and microstructural evolution of advanced Zr-base alloys, Zirconium in the Nuclear Industry, 12th International Symposium, in: G.P. Sabol, G.D. Moan (Eds.), ASTM, vol. 1354, ASTM STP, West Conshohocken, PA, 2000, pp. 51–73.
[58] L. Walters, G.A. Bickel, M. Griffiths, The effects of microstructure and operating conditions on irradiation creep of Zr-2.5Nb pressure tubing, Zirconium in the Nuclear Industry: 17th International Symposium, in: R.J. Comstock, P. Barberis (Eds.), ASTM International, vol. 1543, ASTM STP, West Conshohocken, PA, 2015, pp. 693–725.
[59] J.P. Foster, R. Baranwal, ZIRLO irradiation creep stress dependence in compression and tension, J. ASTM Int. (JAI) 8 (2011). Paper ID JAI 103297.
[60] J.P. Foster, G. Pan, L. Cai, A.R. Atwood, Effect of hydrogen on irradiation creep and growth for ZIRLO™ alloy and Zr-1.0Nb, Zirconium in the Nuclear Industry, 18th International Symposium, in: R.J. Comstock, A.T. Motta (Eds.), ASTM International, vol. 1597, ASTM STP, West Conshohocken, PA, 2018, pp. 725–747.
[61] R.F. DeAbreu, G.A. Bickel, A.W. Buyers, S.A. Donahue, K. Dunn, M. Griffiths, L. Walters, Temperature and flux dependence of in-reactor creep for cold-worked Zr-2.5Nb, Zirconium in the Nuclear Industry: 18th Int'l Symposium, in: R.J. Comstock, A.T. Motta (Eds.), ASTM International, ASTM STP1597, West Conshohocken, PA, 2018, pp. 938–964.
[62] V. Fidleris, The Zircaloy-2 In-Pile Creep Measurements at Chalk River, Presented at ASME Winter Annual Meeting, New York, 1962. Paper Number 62-WA-325. (Available as AECL Report: AECL-2054).
[63] V. Fidleris, I.R. Emmerton, R.D. Delaney, An in-reactor creep machine for high flux application, J. Phys. E Sci. Instrum. 5 (1972) 442–444.
[64] J. Pefhany, Pneumatic gauges for in-pile measurements, Nucl. Eng. 6 (1961) 77–79.
[65] V. Fidleris, C.D. Williams, in: J.P. Pemsler, E.C.W. Perryman, W.W. Smeltzer (Eds.), Influence of Neutron Irradiation on the Creep of Zircaloy-2 at 300 °C, Zirconium and its Alloys, vol. 4, Electrochemical Tech, 1966, pp. 258–267.
[66] V. Fidleris, The effect of texture and strain aging on creep of Zircaloy-2, Applications-Related Phenomena for Zirconium and its Alloys, Am. Soc. Test. Mater, ASTM STP 458 (1969) 1–17.
[67] B. Watkins, D.S. Wood, The significance of irradiation-induced creep on reactor performance of Zircaloy-2 pressure tubes, Applications-Related Phenomena for Zirconium and its Alloys, American Am. Soc. Test. Mater, ASTM STP 458 (1969) 226–240.
[68] D.S. Wood, B. Watkins, A creep limit approach to the design of Zircaloy-2 reactor pressure tubes at 275 °C, J. Nucl. Mater. 41 (1971) 327–340.
[69] R.W. Kozar, A.W. Jaworski, T.W. Webb, R.W. Smith, In situ monitored in-pile creep testing of zirconium alloys, J. Nucl. Mater. 444 (2014) 14–22.
[70] M.A. McGrath, S.Y. Yagnik, Experimental investigation of irradiation creep and growth of recrystallized Zircaloy-4 guide tubes pre-irradiated in PWR, J. ASTM Int. (JAI) 8 (2011). Paper ID JAI 103770.
[71] J.P. Foster, T.M. Karlsen, in: J.T. Busby, G. Ilevbare, P.L. Andresen (Eds.), Irradiation Creep and Irradiation Stress Relaxation of 316 and 304l Stainless Steels in Thermal and Fast Neutron Spectrum Reactors, 15th International Conference on Environmental Degradation, The Minerals, Metals & Materials Society, TMS, 2011, pp. 1339–1354.
[72] A.R. Causey, In-reactor stress relaxation of zirconium alloys, in: Zirconium in Nuclear Applications, vol. 551, American Society for Testing and Materials, ASTM STP, 1974, pp. 263–273.
[73] D.E. Fraser, Stress relaxation testing of small bent beams: an evaluation of some out-of-pile tests, Atomic Energy Can. Ltd. Rep. (1971). AECL-3782.
[74] P.H. Kreyns, M. W Burkhart, Radiation enhanced relaxation in Zircaloy-4 and Zr/2.5wt%Nb/0.5 wt.% Cu alloys, J. Nucl. Mater. 26 (1968) 87–104.
[75] D.E. Fraser, P.A. Ross-Ross, A.R. Causey, The relation between stress-relaxation and creep for some alloys during neutron irradiation, J. Nucl. Mater. 46 (1973) 281–292.
[76] C.E. Coleman, A.R. Causey, V. Fidleris, In-reactor creep of zirconium-2.5 wt% niobium at 570 K, J. Nucl. Mater. 60 (1976) 185–194.
[77] A.R. Causey, Thermally induced strain recovery in irradiated and unirradiated zirconium alloy stress-relaxation specimens, J. Nucl. Mater. 6 (1976) 71–78.
[78] T.A. Kenfield, H.J. Busboom, W.K. Appleby, In-reactor stress relaxation in bending of 20% cold-worked 316 stainless steel, J. Nucl. Mater. 65 (1977) 238–243.
[79] A.R. Causey, G.J.C. Carpenter, S.R. MacEwen, In-reactor stress relaxation of selected metals and alloys at low temperatures, J. Nucl. Mater. 90 (1980) 216–223.
[80] A.R. Causey, V. Fidleris, R.A. Holt, Acceleration of creep and growth of annealed Zircaloy-4 by pre-irradiation to high fluences, J. Nucl. Mater. 139 (1986) 277–278.
[81] A.R. Causey, F.J. Butcher, S.A. Donohue, Measurement of irradiation creep of zirconium alloys using stress relaxation, J. Nucl. Mater. 159 (1988) 101–113.
[82] S. Carassou, C. Duguay, P. Yvon, F. Rozenblum, J.M. Cloué, V. Chabretou, C. Bernaudat, B. Levasse, A. Maurice, P. Bouffioux, K. Audic, REFLET Experiment in OSIRIS: relaxation under flux as a method for determining creep behavior of Zircaloy assembly components, in: P. Barbéris, M. Limbäck (Eds.), Zirconium in the Nuclear Industry: 16th ASTM International Symposium, vol. 1529, ASTM STP, 2010, pp. 899–928.
[83] L.M. Howe, W.R. Thomas, The effect of neutron irradiation on the tensile properties of Zircaloy-2, J. Nucl. Mater. 2 (1960) 248–260.
[84] C.E. Coleman, Private Communication, Atomic Energy of Canada Limited, Chalk River Laboratories, Ontario, 1989.
[85] A.C. Roberts, A.H. Cottrell, Creep of alpha uranium during irradiation with neutrons, Phil. Mag. LXXII (1956) 711–717.
[86] R.V. Hesketh, A transient irradiation creep in nonfissile metals, Phil. Mag. 8 (1963) 1321–1333.
[87] R.H. Fillnow, Private Communication, Bettis Atomic Power Laboratory, West Mifflin, PA, 1968.
[88] F.A. Nichols, Theory of the creep of Zircaloy during neutron irradiation, J. Nucl. Mater. 30 (1969) 249–270.
[89] J.J. Holmes, J.A. Williams, D.H. Nyman, J.C. Tobin, in: In-reactor Creep of Cold-Worked Zircaloy-2, Flow and Fracture of Metals and Alloys in Nuclear Environments, vol. 380, American Society for Testing and Materials, Philadelphia, 1965, pp. 385–394. ASTM STP.

[90] W.J. Dowis, Basis of Design - Hanford New Production Reactor (NPR), Report HW-SA-2981, HAPO, 1963. March.

[91] N. Christodoulou, A.R. Causey, C.H. Woo, C.N. Tomé, R.J. Klassen, R.A. Holt, in: A.S. Kumar, D.S. Gelles, R.K. Nanstad, E.A. Little (Eds.), Modelling the Effect of Texture and Dislocation Structure on Irradiation Creep of Zirconium Alloys, Effects of Radiation on Materials: 16th International Symposium vol. 1175, ASTM STP, Philadelphia, 1993, pp. 1111–1128. American Society for Testing and Materials.

[92] A.R. Causey, J.E. Elder, R.A. Holt, R.G. Fleck, On the anisotropy of in-reactor creep of Zr-2.5Nb tubes, in: A.M. Garde, E.R. Bradley (Eds.), Zirconium in the Nuclear Industry: 10th ASTM International Symposium, vol. 1245, ASTM STP, 1994, pp. 202–220.

[93] R.A. Holt, In-reactor deformation of cold-worked Zr–2.5Nb pressure tubes, J. Nucl. Mater. 372 (2008) 182–214.

[94] D.K. Rodgers, M. Griffiths, G. Bickel, A. Buyers, C.E. Coleman, H.M. Nordin, S. St Lawrence, Performance of pressure tubes in CANDU reactors, CNL Nuclear Review 5 (2016) 1–15.

[95] C.E. Coleman, A.R. Causey, V. Fidleris, In-reactor creep of zirconium-2.5 wt% niobium at 570 K, J. Nucl. Mater. 60 (1976) 185–194.

[96] C.C. Dollins, Irradiation creep associated with dislocation climb, Radiat. Eff. 11 (1971) 123–131.

[97] M. Griffiths, N. Christodoulou, S.A. Donohue, Damage dependence of irradiation deformation of Zr-2.5Nb pressure tubes, J. ASTM Int. (JAI) 2 (2005). Paper ID JAI 12432.

[98] F. Tinti, Uniaxial in-reactor creep of Zry-2: stress, flux, and temperature dependency, Nucl. Tech. 60 (1983) 104–113.

[99] C.K. Chow, R.A. Holt, C.H. Woo, C.B. So, Deformation of zirconium irradiated by 4.4 MeV protons at 347 K, J. Nucl. Mater. 328 (2004) 1–10.

[100] O.J.V. Chapman, R.J. McElroy, B.E. Sheldon, Irradiation creep and growth during proton and neutron bombardment of Zircaloy plate, in: Zirconium in the Nuclear Industry, 6th International Symposium, vol. 824, American Society for Testing and Materials, Philadelphia, 1984, pp. 343–375. ASTM STP.

[101] A.R. Causey, R.A. Holt, S.R. MacEwen, in: D.G. Franklin, R.B. Adamson (Eds.), In-reactor Creep of Zr-2.5Nb, Zirconium in the Nuclear Industry: 6th International Symposium vol. 824, ASTM STP, Philadelphia, Pa, 1984, pp. 269–288. American Society for Testing and Materials.

[102] R.A. Holt, Effect of microstructure on irradiation creep and growth of Zircaloy pressure tubes in power reactors, J. Nucl. Mater. 82 (1979) 419–429.

[103] A. Seibold, F. Garzarolli, Influence of composition and condition on behavior of Zr-Sn-FeCrV alloys, in: G.D. Moan, P. Rudling (Eds.), Zirconium in the Nuclear Industry: 13th International Symposium vol. 1423, ASTM STP, West Conshohocken, PA, 2002, pp. 743–757. American Society for Testing and Materials.

[104] V. Rebeyrolle, J.-P. Mardon, D. Charquet, A. Soniak, L. Robert, P. Bouffioux, Influence of sulfur addition on irradiation creep of M5 alloy, (poster) Zirconium in the Nuclear Industry: 14th International Symposium, Stockholm, Sweden, June 2004.

[105] F. Ferrer, A. Barbu, T. Bretheau, J. Crépin, F. Willaime, D.L. Charquet, The effect of small concentration of sulfur on the plasticity of zirconium alloys at intermediate temperatures, Zirconium in the Nuclear Industry: 13th International Symposium, in: G.D. Moan, P. Rudling (Eds.), ASTM International, vol. 1423, ASTM STP, West Conshohocken, PA, 2002, pp. 863–887.

[106] D. Charquet, Microstructure and properties of zirconium alloys in the absence of irradiation, in: G.P. Sabol, G.D. Moan (Eds.), Zirconium in the Nuclear Industry, 12th International Symposium, vol. 1354, ASTM STP, West Conshohocken, PA, 2000, pp. 3–14. American Society for Testing and Materials.

[107] M. Griffiths, P.H. Davies, W.G. Davies, S. Sagat S, Predicting the in-reactor mechanical behavior of Zr-2.5Nb pressure tubes from post-irradiation microstructural examination data, in: G.D. Moan, P. Rudling (Eds.), 13th Int. Symposium on Zirconium in the Nucl. Ind., 2002, pp. 507–523. ASTM-STP-1423.

[108] M. Griffiths, W.G. Davies, A.R. Causey, G.D. Moan, R.A. Holt, S.A. Aldridge, Variability of in-reactor diametral deformation for Zr-2.5Nb pressure tubing, in: Zirconium in the Nuclear Industry: 13th International Symposium, vol. 1423, ASTM International, West Conshohocken, PA, 2002, pp. 796–810. ASTM STP.

[109] R.B. Adamson, B. Cox, Impact of Irradiation on Material Performance, ZIRAT10/IZNA5 Special Topics Report, ANT International, Mölnlycke, Sweden, 2005/2006.

[110] W.A. McInteer, D.L. Baty, K.O. Stein, The influence of tin content on the thermal creep of Zircaloy-4, in: L.F.P. Van Swam, C.M. Eucken (Eds.), Zirconium in the Nuclear Industry: 8th International Symposium, vol. 1023, ASTM STP, Philadelphia, 1989, pp. 621–640. American Society for Testing and Materials.

[111] J.P. Foster, H. Ken Yueh, R.J. Comstock, ZIRLO cladding improvement, in: B. Kammezind, M. Limbäck (Eds.), Zirconium in the Nuclear Industry, 15th International Symposium, vol. 1505, ASTM International, West Conshohocken, PA, 2009, pp. 457–470. ASTM STP.

[112] A.M. Garde, P.G. Smerd, F. Garzarolli, R. Manzel, Influence of metallurgical condition on the in-reactor dimensional changes of Zircaloy fuel rods, in: D.G. Franklin, R.B. Adamson (Eds.), Zirconium in the Nuclear Industry: 6th International Symposium, vol. 824, ASTM STP, 1984, pp. 289–305. American Society for Testing and Materials.

[113] S. Yagnik, R.B. Adamson, G. Kobylyansky, J.-H. Chen, D. Gilbon, S. Ishimoto, T. Fukuda, L. Hallstadius, A. Obukhov, Effect of alloying elements, cold work, and hydrogen on the irradiation-induced growth behavior of zirconium alloy variants, in: R.J. Comstock, A.T. Motta (Eds.), Zirconium in the Nuclear Industry, 18th International Symposium, ASTM International, West Conshohocken, PA, 2018, pp. 748–795. ASTM STP 1597.

[114] G.P. Kobylyansky, A.E. Novoselov, Z.E. Ostrovsky, A.V. Obukhov, V. Shishin, V.N. Shishov, A.V. Nikulina, M.M. Peregud, S.T. Mahmood, D. White, Y.-P. Lin, M. Dubecky, Irradiation-induced growth and microstructure of recrystallized, cold worked and quenched Zircaloy-2, NSF and E635 Alloys, in: B. Kammenzind, M. Limback (Eds.), Zirconium in the Nuclear Industry: 15th International Symposium, vol. 1505, ASTM STP, 2009, pp. 564–582. American Society for Testing and Materials.

[115] P. Bossis, B. Verhaeghe, S. Doriot, D. Gilbon, V. Chabretou, A. Dalmais, J.-P. Mardon, M. Blat, A. Miquet, PWR comprehensive study of high burn-up corrosion and growth behaviour of M5 and recrystallised low-tin Zircaloy-4, in: B. Kammenzind, M. Limback (Eds.), 15th ASTM International Symposium: Zirconium in the Nuclear Industry, vol. 1505, ASTM International, West Conshohocken, PA, 2009, pp. 430–456. ASTM, STP.

[116] A.M. Garde, R.J. Comstock, G. Pan, R. Baranwal, L. Hallstadius, T. Cook, F. Carrera, Advanced zirconium alloy for PWR application, J. ASTM Int. (JAI) 7 (2010). Paper ID JAI 103030.

[117] V. Fidleris, R. P Tucker, R.B. Adamson, An overview of microstructural and experimental factors that affect the irradiation growth behaviour of zirconium alloys, in: R.B. Adamson, L.F.P. Van Swam (Eds.), Zirconium in the Nuclear Industry: 7th International Symposium vol. 939, ASTM STP, 1987, pp. 49–85. American Society for Testing and Materials.

[118] A. Rogerson, Irradiation growth in zirconium and its alloys, J. Nucl. Mater. 159 (1988) 43–61.

[119] S.I. Choi, J.H. Kim, Radiation-induced dislocation and growth behaviour of zirconium and zirconium alloys – a Review, Nucl. Eng. Tech. 45 (2013) 385–392.

[120] A. Rogerson, R.A. Murgatroyd, Long-term irradiation growth in zirconium alloys, in: R.J. Comstock, A.T. Motta (Eds.), Zirconium in the Nuclear Industry: 18th International Symposium, vol. 1597, ASTM International, West Conshohocken, PA, 2018, pp. 1–18. ASTM STP.

[121] S.T. Mahmood, C. Patterson, P. Rudling, Hot Cell Post-irradiation Examination Techniques for LWR Fuels, ZIRAT 19 Special Topic Report, ANT International, Molnlyske, Sweden, 2014.

[122] D.L. Baty, W.A. Pavinich, M.R. Dietrich, G.S. Clevinger, T.P. Papazoglou, Deformation characteristics of cold-worked and recrystallized Zircaloy-4 cladding, in: D.G. Franklin, R.B. Adamson (Eds.), Zirconium in the Nuclear Industry: 6th International Symposium, vol. 824, ASTM STP, 1984, pp. 306–339. American Society for Testing and Materials.

[123] G.J.C. Carpenter, R.H. Zee, A. Rogerson, Irradiation growth of zirconium single crystals - a Review, J. Nucl. Mater. 159 (1988) 86–100.

[124] R.G. Fleck, J.E. Elder, A.R. Causey, R.A. Holt, Variability of irradiation growth in Zr-2.5Nb pressure tubes, in: A.M. Garde, E.R. Bradley (Eds.), Zirconium in the Nuclear Industry: 10th International Symposium, vol. 1245, ASTM STP, Philadelphia, 1994, pp. 168–182. American Society for Testing and Materials.

[125] R.A. Holt, A.R. Causey, N. Christodoulou, M. Griffiths, E.T.C. Ho, C.H. Woo, Non-linear irradiation growth of cold-worked Zircaloy-2, in: E.R. Bradley, G.P. Sabol (Eds.), Zirconium in the Nuclear Industry: 11th International Symposium, vol. 1295, ASTM STP, 1996, pp. 623–637. American Society for Testing and Materials.

[126] R.P. Tucker, V. Fidleris, R.B. Adamson, High-fluence irradiation growth of zirconium alloys at 644 K to 725 K, in: R.B. Adamson, D.G. Franklin (Eds.), Zirconium in the Nuclear Industry: 6th International Symposium, vol. 824, ASTM STP, Philadelphia, 1984, pp. 427–451. American Society for Testing and Materials.

[127] F. Garzarolli, P. Dewes, G. Maussner, H.-H. Basso, Effects of high neutron fluences on microstructure and growth of Zircaloy-4, in: L.F.P. Van Swam, C.M. Eucken (Eds.), Zirconium in the Nuclear Industry: 8th International Symposium, vol. 1023, ASTM International, West Conshohocken, PA, 1989, pp. 641–657. ASTM STP.

[128] S.T. Mahmood, D.M. Farkas, R.B. Adamson, Y. Etoh, Post irradiation characterization of ultra-high-fluence Zircaloy-2 plate, in: G.P. Sabol, G.D. Moan (Eds.), Zirconium in the Nuclear Industry: 12th International Symposium, American Society for Testing and Materials, vol. 1354, ASTM STP, West Conshohocken, PA, 2000, pp. 139–169.

[129] P. Morize, J. Baicry, J.P. Mardon, Effect of irradiation at 588 K on mechanical properties and deformation behaviour of zirconium alloy strip, in: R.B. Adamson, L.F.P. Van Swam (Eds.), Zirconium in the Nuclear Industry: 7th International Symposium, vol. 939, ASTM STP, Philadelphia, 1987, pp. 101–119. American Society for Testing and Materials.

[130] R.B. Adamson, Irradiation growth of Zircaloy, in: A.L. Lowe Jr., G.W. Parry (Eds.), Zirconium in the Nuclear Industry: 3rd Conference, vol. 633, ASTM STP, Philadelphia, 1977, pp. 326–343. American Society for Testing and Materials.

[131] A. Rogerson, R.H. Zee, Irradiation growth in Zr-Sn alloys at 353 K and 553 K, J. Nucl. Mater. 152 (1988) 220–224.

[132] V.N. Shishov, The evolution of microstructure and deformation stability in Zr-Nb-(Sn, Fe) alloys under neutron irradiation, in: M. Limbäck, P. Barbéris (Eds.), Zirconium in the Nuclear Industry: 16th International Symposium, vol. 1529, ASTM International, West Conshohocken, PA, 2011, pp. 37–66. ASTM STP.

[133] D. Kaczorowski, J.P. Mardon, P. Barberis, R.B. Hoffmann, J. Stevens, in: R.J. Comstock, P. Barbéris (Eds.), Impact of Iron in M5^{TM}, Zirconium in the Nuclear Industry: 17th International Symposium, vol. 1543, ASTM International, West Conshohocken, PA, 2015, pp. 159–183. STP.
[134] G.M. Hood, The anomalous self-diffusion in α-Zr, J. Nucl. Mater. 135 (1985) 292–295.
[135] G.M. Hood, T. Laursen, J.A. Jackman, R. Belec, R.J. Schultz, J.L. Whitton, Solute Diffusion in alpha-Zr: rutherford backscattering and secondary-ion mass spectrometry study, Phil. Mag. A 63 (1991) 937–947.
[136] R.A. Pérez, M. Weissmann, Ab-initio approach to the effect of Fe on the diffusion in hcp Zr, J. Nucl. Mater. 374 (2008) 95–100.
[137] R.C. Pasianot, R.A. Pérez, V.P. Ramunni, M. Weissmann, Ab-initio approach to the effect of Fe on the diffusion in hcp Zr II: the energy barriers, J. Nucl. Mater. 392 (2009) 100–104.
[138] M. Christensen, W. Wolf, C. Freeman, E. Wimmer, R.B. Adamson, L. Hallstadius, P. Cantonwine, E.V. Mader, Effect of hydrogen on dimensional changes of zirconium and the influence of alloying elements: first principles and classic simulations of point defects, dislocation loops and hydrides, in: R.J. Comstock, P. Barberis (Eds.), Zirconium in the Nuclear Industry: 17th International Symposium, vol. 1543, ASTM STP, West Conshohocken, PA, 2015, pp. 55–92. ASTM International.
[139] M. Christensen, W. Wolf, C. Freeman, E. Wimmer, R.B. Adamson, L. Hallstadius, P. Cantonwine, E.V. Mader, Understanding irradiation growth through atomistic simulations: defect diffusion and clustering, and the influence of alloying elements, in: R.J. Comstock, A.T. Motta (Eds.), Zirconium in the Nuclear Industry: 18th International Symposium on Zirconium in the Nuclear Industry, vol. 1597, ASTM STP, West Conshohocken, PA, 2018, pp. 645–675. ASTM International.
[140] R.A. Holt, Microstructure dependence of irradiation creep and growth of zirconium alloys, J. Nucl. Mater. 90 (1980) 193–204.
[141] R.A. Holt, A.R. Causey, M. Griffiths, E.T.C. Ho, High fluence irradiation growth of cold-worked Zr-2.5Nb, in: G.P. Sabol, G.D. Moan (Eds.), Zirconium in the Nuclear Industry; 12th International Symposium, vol. 1354, ASTM STP, West Conshohocken, PA, 2000, pp. 86–104. ASTM International.
[142] R.A. Holt, R.G. Fleck, The contribution of irradiation growth to pressure tube deformation, in: C.M. Eucken, A.M. Garde (Eds.), Zirconium in the Nuclear Industry; 9th International Symposium, vol. 1132, ASTM STP, Philadelphia, PA, 1991, pp. 218–229. American Society for Testing and Materials.
[143] S.J. King, R.L. Kesterson, K.H. Hyueh, R.J. Comstock, W.M. Herwig, S.D. Ferguson, in: G.D. Moan, P. Rudling (Eds.), Impact of Hydrogen on Dimensional Stability of ZIRLO™ Fuel Assemblies, Zirconium in the Nuclear Industry: 13th International Symposium, vol. 1423, ASTM STP, West Conshohocken, PA, 2002, pp. 471–489. ASTM.
[144] E.V. Mader, M. Reitmeyer, P. Garcia Sedano, J. Morris, P. Cantonwine, L. Hallstadius, G. Potts, H.R. Peters, W. Li, EPRI BWR Channel Distortion Program, Water Reactor Fuel Performance Meeting, Chengdu, China, 2011. Paper Track #2-001.
[145] L. Tournadre, F. Onimus, J.-L. Béchade, D. Gilbon, J.-M. Cloué, J.-P. Mardon, X. Feaugas, Toward a better understanding of the hydrogen impact on the radiation induced growth of zirconium alloys, J. Nucl. Mater. 441 (2013) 222–231.
[146] M. Christensen, W. Wolf, C. Freeman, E. Wimmer, R.B. Adamson, L. Hallstadius, P.E. Cantonwine, E.V. Mader, H in α-Zr and in zirconium hydrides: solubility, effect on dimensional changes and the role of defects, J. Phys. Condens. Matter 27 (1–12) (2015), 025402.
[147] M. Christensen, W. Wolf, C. Freeman, E. Wimmer, R.B. Adamson, L. Hallstadius, P.E. Cantonwine, E.V. Mader, Diffusion of point defects, nucleation of dislocation loops, and effect of hydrogen in hcp-Zr : ab initio and classical simulations, J. Nucl. Mater. 460 (2015) 82–96.
[148] J.P. Mardon, D. Charquet, J. Senevat, Development of new zirconium alloys for PWR fuel rod cladding, in: Proc. ANS Int. Topical Meeting on LWR Fuel Performance, West Palm Beach, Florida, 1994, pp. 643–649.
[149] R.A. Holt, A.R. Causey, Volume conservation during irradiation growth of Zr-2.5Nb, J. Nucl. Mater. 335 (2004) 529–533.
[150] J.E. Harbottle, F. Herbillon, Shape and volume changes during irradiation growth of Zircaloy-2, J. Nucl. Mater. 90 (1980) 249–255.
[151] M. Griffiths, A review of microstructure evolution in zirconium alloys during irradiation, J. Nucl. Mater. 159 (1988) 190–218.
[152] J. Ribis, F. Onimus, J.-L. Béchade, S. Doriot, C. Cappelaere, C. Lemaignan, A. Barbu, O. Rabouille, Experimental and modelling approach of irradiation defects recovery in zirconium alloys: impact of an applied stress, J. ASTM Int. (JAI) 5 (2008). Paper ID JAI 101118.
[153] R.B. Adamson, W.L. Bell, in: Haicheng Gu, Jiawen He (Eds.), Effects of Neutron Irradiation and Oxygen Content on the Microstructure and Mechanical Properties of Zircaloy, Proc. International Symposium: Microstructure and Mechanical Behaviour of Materials, Chinese Mechanical Engineering Society, 1986, pp. 237–246.
[154] W.J.S. Yang, Microstructural development in neutron irradiated Zircaloy-4, in: N.H. Packan, R.E. Stoller, A.S. Kumar (Eds.), Effects of Radiation on Materials: 14th International Symposium, vol. 1, ASTM STP, Philadelphia, 1989, pp. 442–456. American Society for Testing and Materials.
[155] R.M. Kruger, Precipitate Stability in Zircaloy-2, 1990. EPRI NP 6845-D.
[156] W.J.S. Yang, R.B. Adamson, Beta-quenched Zircaloy-4: effects of thermal aging and neutron irradiation, in: L.F.P. Van Swam, C.M. Eucken (Eds.), Zirconium in the Nuclear Industry, 8th International Symposium, vol. 1023, Philadelphia ASTM STP, 1989, pp. 451–477. American Society for Testing and Materials.
[157] P. Vizcaino, Hydride formation in neutron irradiated material under in-reactor conditions, 2nd RCM of spar III, charlotte, NC, USA, may14-18, in: Included in: Spent Fuel Performance Assessment and Research, 2012, pp. 176–178. IAEA-TEDOC-1771 (2015).
[158] R.M. Hengstler-Eger, P. Baldo, L. Beck, J. Dorner, K. Ertl, P.B. Hoffmann, C. Hugenschmidt, M.A. Kirk, W. Petry, P. Pikart, A. Rempel, Heavy ion irradiation induced dislocation loops in AREVA's M5 alloy, J. Nucl. Mater. 423 (2012) 170–182.
[159] J.H. Kittel, S.H. Paine, Effects of high burnup on natural uranium, Nucl. Sci. Eng. 3 (1958) 250–268.
[160] S.N. Buckley, Irradiation growth, atomic energy research establishment report, Harwell, England, AERE R 3674 (1962).
[161] S.N. Buckley, Irradiation growth in uranium, atomic energy research establishment report, Harwell, England, AERE R 5262 (1966).
[162] M. Griffiths, R.W. Gilbert, The formation of c-component defects in zirconium alloys during neutron irradiation, J. Nucl. Mater. 150 (1987) 169–181.
[163] C.H. Woo, U. Gosele, Dislocation bias in an anisotropic diffusive medium and irradiation growth, J. Nucl. Mater. 119 (1983) 219–228.
[164] P.T. Heald, M.V. Speight, Point defect behaviour in irradiated materials, Acta Metall. 23 (1975) 1389–1399.
[165] C.H. Woo, Theory of irradiation deformation in non-cubic metals: effects of anisotropic diffusion, J. Nucl. Mater. 159 (1988) 237–256.
[166] C.H. Woo, Irradiation creep due to elastodiffusion, J. Nucl. Mater. 120 (1984) 55–64.
[167] C.H. Woo, Polycrystalline effects on irradiation creep and growth in textured zirconium, J. Nucl. Mater. 131 (1985) 105–117.
[168] M. Griffiths, R.W. Gilbert, C.E. Coleman, Grain boundary sinks in neutron-irradiated Zr and Zr-alloys, J. Nucl. Mater. 159 (1988) 405–416.
[169] A. Jostsons, P.M. Kelly, R.G. Blake, K. Farrell, in: J.A. Sprague, D. Kramer (Eds.), Neutron Irradiation-Induced Defect Structures in Zirconium, Effects of Radiation on Structural Materials, vol. 683, American Society for Testing and Materials, ASTM STP, 1979, pp. 46–61.
[170] A. Jostsons, R.G. Blake, J.G. Napier, P.M. Kelly, K. Farrell, Faulted loops in neutron-irradiated zirconium, J. Nucl. Mater. 68 (1977) 267–276.
[171] M. Griffiths, R.W. Gilbert, V. Fidleris, R.B. Adamson, R.P. Tucker, Neutron damage in zirconium alloys irradiated at 644 to 710 K, J. Nucl. Mater. 150 (1987) 159–168.
[172] M. Griffiths, R.A. Holt, A. Rogerson, Microstructural aspects of accelerated deformation of Zircaloy nuclear reactor components during service, J. Nucl. Mater. 225 (1995) 245–258.
[173] A. Rogerson, R.A. Murgatroyd, 'Breakaway' growth in annealed Zircaloy-2 at 353 K and 553 K, J. Nucl. Mater. 113 (1983) 256–259.
[174] R.A. Holt, R.W. Gilbert, c> component dislocations in annealed Zircaloy irradiated at about 570 K, J. Nucl. Mater. 137 (1986) 185–189.
[175] M. Griffiths, M.H. Loretto, R.E. Smallman, Anisotropic distribution of dislocation loops in HVEM-irradiated Zr, Phil. Mag. A49 (1984) 613–624.
[176] A. Harte, M. Griffiths, M. Preuss, The characterisation of second phases in the Zr-Nb and Zr-Nb-Sn-Fe alloys: a critical review, J. Nucl. Mater. 505 (2018) 1–13.
[177] G.M. Hood, Point Defect Properties of α-Zr and Their Influence on Irradiation Behaviour of Zr-Alloys, Atomic Energy of Canada Limited Report, 1977. AECL-5692.
[178] A. Adrych-Brunning, M.R. Gilbert, J.-Ch Sublet, A. Harte, C.P. Race, Modelling the interaction of primary irradiation damage and precipitates: implications for experimental irradiation of zirconium alloys, J. Nucl. Mater. 498 (2018) 282–289.
[179] Y. de Carlan, C. Regnard, M. Griffiths, D. Gilbon, C. Lemaignan, Influence of iron on the nucleation of <c> component dislocation loops in irradiated Zircaloy-4, in: E. Bradley, G. Sabol (Eds.), Zirconium in the Nuclear Industry: 11th International Symposium, American Society for Testing and Materials, vol. 1295, ASTM STP, 1996, pp. 638–653.
[180] M. Griffiths, J. White, M.H. Loretto, R.E. Smallman, Radiation damage in Zr and Ti, in: J.-I. Takamura, M. Doyama, M. Kiritani (Eds.), Proc. Yamada Conf. V on Point Defects and Defect Interactions in Metals, University of Tokyo Press, 1982, pp. 880–883.
[181] M. Griffiths, Evolution of microstructure in HCP metals during irradiation, J. Nucl. Mater. 205 (1993) 225–241.
[182] M. Griffiths, D. Gilbon, C. Regnard, C. Lemaignan, HVEM study of the effects of alloying elements and impurities on radiation damage in Zr-alloys, J. Nucl. Mater. 205 (1993) 273–283.
[183] M. Griffiths, R.C. Styles, C.H. Woo, F. Phillipp, W. Frank, Study of point defect mobilities in zirconium during electron irradiation in a high-voltage electron microscope, J. Nucl. Mater. 208 (1994) 324–334.
[184] M. Griffiths, J.F. Mecke, J.E. Winegar, Evolution of microstructure in zirconium alloys during irradiation, in: E.R. Bradley, G.P. Sabol (Eds.), Zirconium in the Nuclear Industry: 11th International Symposium, vol. 1295, ASTM STP, 1996, pp. 580–602. American Society for Testing and Materials.
[185] R.R. Hosbons, P.H. Davies, M. Griffiths, S. Sagat, C.E. Coleman, Effect of long-term irradiation on the fracture properties of Zr-2.5Nb pressure tubes, in: G.P. Sabol, G.D. Moan (Eds.), Zirconium in the Nuclear Industry: 12th International Symposium, vol. 1354, ASTM STP, West Conshohocken, PA, 2000, pp. 122–138. American Society for Testing and Materials.
[186] M. Griffiths, C.K. Chow, C.E. Coleman, R.A. Holt, S. Sagat, V.F. Urbanic,

Evolution of microstructure in zirconium alloy core components of nuclear reactors during service, in: A.S. Kumar, D.S. Gelles, R.K. Nanstad, E.A. Little (Eds.), Effects of Radiation on Materials: 16th International Symposium, vol. 1175, ASTM STP, Philadelphia, 1993, pp. 1077–1110. American Society for Testing and Materials.
[187] M. Griffiths, R.W. Gilbert, V. Fidleris, Accelerated irradiation growth of zirconium alloys, in: Zirconium in the Nuclear Industry: 8th International Symposium, American Society for Testing and Materials, vol. 1023, ASTM STP, 1989, pp. 658–677.
[188] R.A. Holt, R.G. Fleck, The effect of temperature on the irradiation growth of cold-worked Zr-2.5 Nb, in: L.F.P. Van Swam, C.M. Eucken (Eds.), Zirconium in the Nuclear Industry: 8th International Symposium, vol. 1023, ASTM STP, Philadelphia, 1989, pp. 705–721. American Society for Testing and Materials.
[189] C.H. Woo, Effect of intergranular interaction in the anisotropy of irradiation creep and growth in zirconium, in: Materials for Nuclear Reactor Core Applications, vol. 1, BNES, London, 1987, pp. 65–71.
[190] C.H. Woo, Effects of anisotropic diffusion on irradiation deformation, in: Radiation-Induced Changes in Microstructure: 13th International Symposium (Part 1), vol. 955, American Society for Testing and Materials ASTM STP, 1987, pp. 70–89.
[191] C.H. Woo, Modeling irradiation growth of zirconium and its alloys, Radiat. Eff. Defect Solid 144 (1998) 145–169.
[192] C.N. Tomé, C.B. So, C.H. Woo, Self-consistent calculation of steady-state creep and growth in textured zirconium, Phil. Mag. A 67 (1993) 917–930.
[193] R.G. Fleck, E.G. Price, B.A. Cheadle, Pressure tube development for CANDU reactors, in: D.G. Franklin, R.B. Adamson (Eds.), Zirconium in the Nuclear Industry: 6th International Symposium, vol. 824, ASTM STP, 1984, pp. 88–105. American Society for Testing and Materials.
[194] J.D. Parker, V. Perovic, M. Léger, R.G. Fleck, Microstructural effects on the irradiation growth of Zr2.5Nb, American society for testing and materials, ASTM STP 939 (1987) 86–100.
[195] C.H. Woo, R.A. Holt, M. Griffiths, Anisotropic diffusion of point defects: effects on irradiation-induced deformation and microstructure, in: C.A. English, J.R. Matthews, H. Rauh, A. M Stoneham, R. Thetford (Eds.), Symposium on Materials Modeling: from Theory to Technology, Institute of Physics Publishing, Bristol and Philadelphia, 1991, pp. 55–60.
[196] C.H. Woo, B.N. Singh, The concept of production bias and its possible role in defect accumulation under cascade damage conditions, Phys. Stat. Sol. B 159 (1990) 609–616.
[197] C.H. Woo, B.N. Singh, Production bias due to clustering of point defects in irradiation-induced cascades, Phil. Mag. A 65 (1992) 889–912.
[198] R.A. Holt, C.H. Woo, C.K. Chow, Production bias - a potential driving force for irradiation growth, J. Nucl. Mater. 205 (1993) 293–300.
[199] S.N. Buckley, S.A. Manthorpe, Dislocation loop nucleation and growth in Zirconium-2.5 Wt% Niobium alloy during 1 MeV electron irradiation, J. Nucl. Mater. 90 (1980) 169–174.
[200] S.N. Buckley, R. Bullough, M.R. Hayns, The direct observation of irradiation damage in zirconium and its alloys, J. Nucl. Mater. 89 (1980) 283–295.
[201] R. Bullough, M.H. Wood, Mechanisms of radiation induced creep and growth, J. Nucl. Mater. 90 (1980) 1–21.
[202] S.N. Buckley, in: B.L Eyre Harwell (Ed.), Proc. Symposium: the Interaction between Dislocations and Point Defects, Part III: Dislocation Climb, 1968, pp. 547–565. AERE-R-5944, 2.
[203] G.M. Hood, Point defect diffusion in α-Zr, J. Nucl. Mater. 159 (1988) 149–175.
[204] D.R. Olander, Fundamental Aspects of Nuclear Reactor Fuel Elements, TID 26711-Part 1, 1976.
[205] M. Griffiths, L. Walters, L.R. Greenwood, F.A. Garner, Accelerated materials evaluation for nuclear applications, J. Nucl. Mater. 488 (2017) 46–62.
[206] S.T. Mahmood, M. Griffiths, R.B. Adamson, C. Lemaignan, Material Test Reactors and Other Irradiation Facilities, ZIRAT 23 Special Topic Report, ANT International, Molnlyske, Sweden, 2019.
[207] R.A. Murgatroyd, A. Rogerson, Irradiation growth in cold-worked Zircaloy-2, in: J.H. Schemel, T.P. Papazoglou (Eds.), Zirconium in the Nuclear Industry: 4th International Conference, vol. 681, ASTM STP, 1979, pp. 213–226. American Society for Testing and Materials.
[208] Z.L. Pan, S. St Lawrence, P.H. Davies, M. Griffiths, S. Sagat, Effect of irradiation on the fracture properties of Zr-2.5Nb pressure tubes after irradiation to the end of design life, in: P. Rudling, B. Kammenzind (Eds.), Zirconium in the Nuclear Industry: 14th International Symposium vol. 1467, ASTM STP, 2004, pp. 759–782. American Society for Testing and Materials.
[209] J.E. Harbottle, in: A.L. Bement (Ed.), The Temperature and Neutron Dose Dependence of Irradiation Growth in Zircaloy-2, Irradiation Effects on Structural Alloys for Nuclear Reactor Applications, vol. 484, ASTM STP, Philadelphia, PA, 1970, pp. 287–299. American Society for Testing and Materials.
[210] J.E. Harbottle, R.M. Cornell, Analysis of pressurized water reactor fuel pin length changes, in: J.H. Schemel, T.P. Papazoglou (Eds.), Zirconium in the Nuclear Industry: 4th International Conference, vol. 681, ASTM STP, Philadelphia, PA, 1979, pp. 202–212. American Society for Testing and Materials.
[211] K. Geelhood, C. Beyer, W. Luscher, New release of fuel performance codes, FRAPCON-3.4 and FRAPTRAN 1.4, Proc. Top Fuel (2009) 233–244. Paris, France, (2009) Paper 2067.
[212] K. Geelhood, W. Luscher, P. Raynaud, I. Porter, FRAPCON-4.0: A Computer Code for the Calculation of Steady-State, Thermal-Mechanical Behavior of Oxide Fuel Rods for High Burnup, Pacific Northwest National Laboratory for the Division of System Analysis, Office of Nuclear Regulatory Research, U.S. Nuclear Regulatory Commission, Richland, Washington, USA, 2015.
[213] W. Luscher, K. Geelhood, I. Porter, Material Property Correlations: Comparisons between FRAPCON-4.0, FRAPTRAN-2.0, and MATPRO, Pacific Northwest National Laboratory for the Division of System Analysis, Office of Nuclear Regulatory Research, U.S. Nuclear Regulatory Commission, Richland, Washington, USA, 2015.
[214] C.C. Dollins, In-pile dimensional changes in neutron irradiated zirconium base alloys, J. Nucl. Mater. 59 (1976) 61–76.
[215] D. Fainstein-Pedraza, E.J. Savino, A.J. Pedraza, Irradiation-growth of zirconium-base alloys, Part I, J. Nucl. Mater. 73 (1978) 151–168.
[216] R.A. Holt, E.F. Ibrahim, Factors affecting the anisotropy of irradiation creep and growth of zirconium alloys, Acta Metall. 27 (1979) 1319–1328.
[217] F.A. Nichols, Radiation damage in non-fissile metallic alloys, Prog. Nucl. Energy 7 (1981) 11–45.
[218] M. Fuse, Analysis of irradiation growth in zirconium-base alloy, J. Nucl. Mater. 140 (1986) 131–139.
[219] R.A. Holt, A.R. Causey, The effects of intergranular constraints on irradiation growth of Zircaloy-2 at 320 K, J. Nucl. Mater. 150 (1987) 306–318.
[220] S.I. Golubov, A.V. Barashev, R.E. Stollar, B.N. Singh, Breakthrough in understanding radiation growth of zirconium, Zirconium in the Nuclear Industry: 17th International Symposium, in: R.J. Comstock, P. Barberis (Eds.), ASTM International, West Conshohocken, PA. ASTM STP, vol. 1543, 2015, pp. 729–758.
[221] A. Patra, C.N. Tomé, S.I. Golubov, Crystal plasticity modeling of irradiation growth in Zircaloy-2, Phil. Mag. 97 (2017) 2018–2051.
[222] D.O. Northwood, Irradiation damage in zirconium and its alloys, Atom. Energy Rev. 15 (1977) 547–610.
[223] A.R. Causey, C.H. Woo, R.A. Holt, The effects of intergranular stresses on the texture dependence of irradiation growth in zirconium, J. Nucl. Mater. 159 (1988) 225–236.
[224] C.N. Tomé, N. Christodoulou, P.A. Turner, M.A. Miller, C.H. Woo, J. Root, T.N. Holden, Role of internal stresses in the transient irradiation growth of Zircaloy-2, J. Nucl. Mater. 227 (1996) 237–250.
[225] C.H. Woo, in: W. Andreoni, S. Yip (Eds.), Modeling Irradiation Damage Accumulation in Crystals, Handbook of Materials Modeling, Springer International Publishing AG, part of Springer Nature, 2018, pp. 959–986.
[226] G.J.C. Carpenter, R.A. Murgatroyd, A. Rogerson, J.F. Watters, Irradiation growth of zirconium single crystals, J. Nucl. Mater. 101 (1981) 28–37.
[227] R.A. Murgatroyd, A. Rogerson, Irradiation growth in zirconium and its alloys, in: Proc. BNES Conference on Dimensional Stability and Mechanical Behaviour of Irradiated Metals and Alloys, London, vol. 2, 1984, pp. 93–96. Paper 36.
[228] D.O. Northwood, R.W. Gilbert, L.E. Bahen, P.M. Kelly, R.G. Blake, A. Jostsons, P.K. Madden, D. Faulkner, W. Bell, R.B. Adamson, Characterisation of neutron irradiation damage in zirconium alloys - an international round-robin experiment, J. Nucl. Mater. 79 (1979) 379–394.
[229] G.J.C. Carpenter, D.O. Northwood, Contribution of dislocation loops to radiation growth and creep of Zircaloy-2, J. Nucl. Mater. 56 (1975) 260–266.
[230] R.A. Holt, R.W. Gilbert, V. Fidleris, Dislocation substructure in zirconium irradiated in EBR-II, in: H.R. Brager, J.S. Perrin (Eds.), Effects of Radiation on Materials; 11th Conference, vol. 782, ASTM STP, 1982, pp. 234–250. American Society for Testing and Materials.
[231] P.A. Tempest, Preferred orientation and its effect on bulk physical properties of hexagonal polycrystalline materials, J. Nucl. Mater. 92 (1980) 191–200.
[232] R.A. Holt, Mechanisms of irradiation growth of alpha-zirconium alloys, J. Nucl. Mater. 159 (1988) 310–338.
[233] M. Griffiths, G.A. Bickel, R. DeAbreu, W. Li, in: I. Charit, Y.T. Zhu, S.A. Maloy, P.K. Liaw (Eds.), Irradiation Creep of Zr-Alloys, Mechanical and Creep Behavior of Advanced Materials, the Minerals, Metals & Materials Society, 2017, pp. 165–182.
[234] P.T. Heald, J.E. Harbottle, Irradiation creep due to dislocation climb and glide, J. Nucl. Mater. 67 (1977) 229–233.
[235] G.A. Bickel, Status and Plans for Work on Pressure Tube Creep at AECL Research Coordination Meeting for CRP on: Prediction of Axial and Radial Creep in HWR Pressure Tubes, 2013. www.iaea.org/inis/collection/NCLCollectionStore/_Public/45/017/45017242.pdf.
[236] R.H. Zee, A. Rogerson, G.J.C. Carpenter, J.R. Watters, Effect of tin on the irradiation growth of polycrystalline zirconium, J. Nucl. Mater. 120 (1984) 223–229.
[237] R.H. Zee, G.J.C. Carpenter, A. Rogerson, J.F. Watters, Irradiation growth in deformed zirconium, J. Nucl. Mater. 150 (1988) 319–330.
[238] I. Aitchison, R.W.K. Honeycombe, R.H. Johnson, The thermal cycling of zirconium, in: D.J. Littler (Ed.), Proc. Int. Conf. On Properties of Reactor Materials and the Effects of Radiation Damage, Butterworths, London, 1962, pp. 430–439.
[239] C.H. Woo, A.R. Causey, R.A. Holt, Methods of analysis and measurement of irradiation creep in non-cubic metals, Phil. Mag. A 79 (1999) 59–84.
[240] D.X. Du, C.H. Woo, Effect of grain-structure topology in modelling aggregate irradiation creep behaviour of two-phase alloys, Comput. Mater. Sci. 23 (2002) 260–269.
[241] R.A. Holt, M. Griffiths, R.W. Gilbert, c-component dislocations in Zr-2.5 wt% Nb alloy, J. Nucl. Mater. 149 (1987) 51–56.
[242] G. Schoeck, in: J.E. Dorn (Ed.), Theories of Creep, Mechanical Behavior of Materials at Elevated Temperatures, McGraw-Hill, New York, 1961,

pp. 79–107.
[243] D. Mosedale, Influence of irradiation on creep, J. Appl. Phys. 33 (1962) 3142–3143.
[244] R.V. Hesketh, in: D.J. Littler (Ed.), Strain Relaxation by Irradiation, Properties of Reactor Materials and the Effects of Radiation Damage, Butterworths, London, 1962, pp. 231–232.
[245] G.R. Piercy, Mechanisms for the in-reactor creep of zirconium alloys, J. Nucl. Mater. 26 (1968) 18–50.
[246] R.V. Hesketh, Diffusion creep under neutron irradiation, J. Nucl. Mater. 29 (1969) 217–222.
[247] F.A. Nichols, On the mechanisms of irradiation creep in zirconium-base alloys, J. Nucl. Mater. 37 (1970) 59–70.
[248] D. Mosedale, Dislocation climb and irradiation, J. Nucl. Mater. 35 (1970) 250.
[249] F.A. Nichols, Reply to Mosedale's note on dislocation climb and irradiation, J. Nucl. Mater. 35 (1970) 251–252.
[250] R.V. Hesketh, Dislocation climb: first catch your Poisson, J. Nucl. Mater. 35 (1970) 253.
[251] W.J. Duffin, F.A. Nichols, The Effect of Irradiation on Diffusion Controlled Creep Processes, Bettis Atomic Power Laboratories, WAPD-T-2412, 1972.
[252] G.W. Lewthwaite, The acceleration of climb controlled creep by neutron irradiation, J. Nucl. Mater. 38 (1971) 118–120.
[253] A.D. Brailsford, R. Bullough, Irradiation creep due to the growth of interstitial loops, Phil. Mag. 27 (1973) 49–64.
[254] W.G. Wolfer, A. Boltax, Stress Induced Deformation of Metals during Fast Neutron Irradiation, European Conference on Irradiation Embrittlement and Creep in Fuel Cladding and Core Components, British Nuclear Energy Society, London, 1972. Paper 31.
[255] C.C. Dollins, F.A. Nichols, Mechanisms of irradiation creep in zirconium-base alloys, in: J.H. Schemel, H.S. Rosenbaum (Eds.), Zirconium in Nuclear Applications vol. 551, ASTM STP, 1974, pp. 229–248. American Society for Testing and Materials.
[256] J.H. Gittus, Theory of dislocation creep for a material subjected to bombardment by energetic particles, role of thermal diffusion, Phil. Mag. 29 (1974) 751–764.
[257] W.G. Wolfer, M. Ashkin, Stress induced diffusion of point defects to spherical sinks, J. Appl. Phys. 46 (1975) 547–557.
[258] P.T. Heald, M.V. Speight, Steady state irradiation creep, Phil. Mag. 29 (1974) 1075–1080.
[259] L.K. Mansur, Irradiation Creep by Climb Enabled Glide of Dislocations Resulting from Preferred Absorption of Point Defects, Oak Ridge National Laboratory, 1978. ORNL TM-6443.
[260] J.R. Matthews, M.W. Finnis, Irradiation creep models – an overview, J. Nucl. Mater. 159 (1988) 257–285.
[261] G.A. Bickel, M. Griffiths, A. Douchant, S. Douglas, O.T. Woo, A. Buyers, Improved Zr-2.5Nb pressure tubes for reduced diametral strain in advanced CANDU reactors, in: P. Barbéris, M. Limbäck (Eds.), Zirconium in the Nuclear Industry: 16th International Symposium, vol. 1529, ASTM STP, 2010, pp. 327–348. American Society for Testing and Materials.
[262] M. Griffiths, N. Wang, A. Buyers, S.A. Donohue, Effect of irradiation damage on the deformation properties of Zr-2.5Nb pressure tubes, in: B. Kammenzind, M. Linbäck (Eds.), Zirconium in the Nuclear Industry: 15th International Symposium, vol. 1505, ASTM STP, 2007, pp. 541–549. American Society for Testing and Materials.
[263] F. Onimus, J.L. Béchade, in: R. Konings (Ed.), Radiation Effects in Zirconium Alloys, Comprehensive Nuclear Materials, vol. 4, 2012, pp. 1–31.
[264] C.N. Tomé, C.B. So, C.H. Woo, Self-consistent calculation of steady-state creep and growth in textured zirconium, Phil. Mag. A 67 (1993) 917–930.
[265] C.H. Woo, C.B. So, Effect of stress on point defect diffusion in HCP metals and irradiation creep, Phil. Mag. A 80 (2000) 1299–1318.
[266] R.A. Holt, A.R. Causey, V. Fidleris, Correlation of creep and growth of pressure tubes with operating variables and microstructure, in: Dimensional Stability and Mechanical Behavior of Irradiated Metal and Alloys, vol. 1, Proceeding, British Nuclear Energy Society, 1983, pp. 175–178. Paper 35.
[267] C.E. Coleman, P.C.K. Chow, C.E. Ells, M. Griffiths, E.F. Ibrahim, S. Sagat, in: R.E. Stoller, A.S. Kumar, D.S. Gelles (Eds.), Rejuvenation of Fracture Properties of Irradiated Zr-2.5 Nb by Heat-Treatment, Effects of Irradiation on Materials: 15th International Symposium, vol. 1125, ASTM STP, Philadelphia, 1992, pp. 318–336. American Society for Testing and Materials.
[268] R.V. Hesketh, Application of the generalised theory of yielding creep to irradiation creep in zirconium alloys, J. Nucl. Mater. 26 (1968) 77–86.
[269] K.L. Murty, An Introduction to Nuclear Materials: Fundamentals and Applications, first ed., Wiley-VCH, 2013, 13: 978-3527407675.
[270] D.K. Rodgers, C.E. Coleman, M. Griffiths, G.A. Bickel, J.R. Theaker, I. Muir, A.A. Bahurmuz, S. St Lawrence, M. Resta Levi, In-reactor performance of pressure tubes in CANDU reactors, J. Nucl. Mater. 383 (2008) 22–27.
[271] M.I. Jyrkhama, G.A. Bickel, M.D. Pandey, Statistical analysis and modelling of in-reactor diametral creep of Zr-2.5Nb pressure tubes, Nucl. Eng. Des. 300 (2016) 241–248.
[272] G.A. Bickel, Private Communication, Canadian Nuclear Laboratories, 2018.
[273] J.F. Nye, Physical properties of crystals, in: Their Representation by Tensors and Matrices, Oxford University press, 1957, ISBN 9780198511656.
[274] W.A. Backofen, Deformation Processing, Addison-Wesley Pub. Co., 1972, p. 37.
[275] J.W. Hutchinson, Bounds and self-consistent estimates for creep of polycrystalline materials, Proc. Roy. Soc. Lond. A. 348 (1976) 101–127.
[276] G.W. Groves, A. Kelly, Independent slip systems in crystals, Phil. Mag. 8 (89) (1963) 877–887.
[277] A.F. Kelly, K.M. Knowles, Crystallography and Crystal Defects, Wiley, 2012.

Dr. Ron Adamsonretired from GE Nuclear Energy in 2000, where he was the manager of Materials Technology at the Vallecitos Nuclear Center. Earlier he graduated from the University of Wisconsin with a B.S. in Mechanical Engineering, an M.S. in Nuclear Engineering and a PhD in Metallurgy. Post-doctoral work on irradiation effects was conducted at AERE, Harwell, England. After 4 years at GE Knolls Atomic Power Laboratory, he moved to the GE Vallecitos Nuclear Center and led research, development and testing programs for reactor core materials, with special emphasis on zirconium alloys.

During his 31 years with GE, Dr. Adamson was actively involved with utilities and the technical community worldwide. He holds 17 patents, has published over 100 technical papers involving nuclear materials technology, and has received several important awards, including the Outstanding Technical Contribution Award from GE Industrial Power Systems, the Mishima Award from the American Nuclear Society, and the Kroll Medal from the ASTM/Kroll Institute. Zirconium alloy areas in which Dr. Adamson has particular interest and experience include: in-reactor dimensional stability; in-reactor corrosion performance and mechanisms; microstructure evolution due to reactor irradiation; mechanical properties of irradiated material; high burnup performance; failure mechanisms and remedies; and fabrication technology. Since retirement he has been actively associated with A.N.T. International, EPRI and others as a consultant in zirconium technology.